

IN VITRO HEPATIC METABOLISM OF CURCUMIN DIETHYL DISUCCINATE IN DIFFERENT
ANIMAL SPECIES



A Dissertation Submitted in Partial Fulfillment of the Requirements
for the Degree of Doctor of Philosophy in Pharmaceutical Chemistry and Natural Products
Department of Food and Pharmaceutical Chemistry
FACULTY OF PHARMACEUTICAL SCIENCES
Chulalongkorn University
Academic Year 2019
Copyright of Chulalongkorn University

เมแทบอลิซึมในหลอดทดลองของเคอร์คิวมินไดเอทิลไดซัคซิเนตโดยตับของสัตว์ต่างชนิด



วิทยานิพนธ์นี้เป็นส่วนหนึ่งของการศึกษาตามหลักสูตรปริญญาวิทยาศาสตรดุษฎีบัณฑิต
สาขาวิชาเภสัชเคมีและผลิตภัณฑ์ธรรมชาติ ภาควิชาอาหารและเภสัชเคมี
คณะเภสัชศาสตร์ จุฬาลงกรณ์มหาวิทยาลัย
ปีการศึกษา 2562
ลิขสิทธิ์ของจุฬาลงกรณ์มหาวิทยาลัย

พรสิรี จิตรถเวช : เมแทบอลิซึมในหลอดทดลองของเคอร์คิวมินไดเอทิลไดซัคซิเนตโดยตับของสัตว์
ต่างชนิด. (*IN VITRO* HEPATIC METABOLISM OF CURCUMIN DIETHYL DISUCCINATE IN
DIFFERENT ANIMAL SPECIES) อ.ที่ปรึกษาหลัก : รศ. ภก. ดร.พรชัย โรจนสีหิศักดิ์

เคอร์คิวมินไดเอทิลไดซัคซิเนต (CDD) เป็นโปรตีนของสารออกฤทธิ์เคอร์คิวมิน CDD ถูกพัฒนาให้มีความคงตัวทางเคมี และมีการซึมผ่านลำไส้มากกว่าเคอร์คิวมิน CDD มีฤทธิ์ทางชีวภาพที่มากกว่าเคอร์คิวมิน การศึกษานี้มีวัตถุประสงค์เพื่อที่จะตรวจสอบความเหมาะสมของส่วนประกอบเอส 9 จากตับ (LS9) ในการศึกษาเมแทบอลิซึมของโปรไฟล์ซึ่งเป็นแหล่งเอนไซม์จากสัตว์ที่เกี่ยวข้องกับความเป็นไปได้ของการแปลผลจากหลอดทดลองไปสู่การศึกษาทางคลินิก ได้มีการตรวจวัดหาเมแทบอลิซึม จลนศาสตร์ในหลอดทดลอง และเอสเทอร์เอนไซม์ที่เกี่ยวข้องกับการเกิดไฮโดรไลซิสของ CDD ด้วย LS9 ของคน ลิง สุนัข และหนูแรท การวิเคราะห์ด้วยวิธีไฮเปอร์ฟอร์แมนซ์ลิควิดโครมาโตกราฟีเชื่อมต่อกับไฮเรสโซลูชันแมสสเปกโตรเมทรีพบว่า CDD เกิดไฮโดรไลซิสเป็นเคอร์คิวมินผ่านสารมัธยันต์โมโนเอทิลซัคซินิลเคอร์คิวมิน การวิเคราะห์ด้วยอัลตราไฮเปอร์ฟอร์แมนซ์ลิควิดโครมาโตกราฟีเพื่อใช้ในการหาค่าพารามิเตอร์จลนศาสตร์ได้แก่ค่าคงที่อัตราการสลายตัว ค่าครึ่งชีวิต และค่าความสามารถของตับในการกำจัดยา พบว่าไฮโดรไลซิสโปรไฟล์ของ CDD ในทุกสัตว์ทดสอบคล้ายกัน เป็นปฏิกิริยาการสลายตัวที่เป็นไปตามจลนศาสตร์อันดับหนึ่งเทียมแบบต่อเนื่องสองขั้นตอนและไม่ผันกลับ CDD ถูกเมแทบอลิซึมอย่างรวดเร็วใน LS9 ของทุกสัตว์ทดสอบ โดยลำดับค่าคงที่อัตราการสลายตัวของ CDD จากมากไปน้อยคือ คน สุนัข ลิง และหนูแรท ลำดับค่าการคาดการณ์ของการกำจัดยาออกจากตับจากมากไปน้อยคือ สุนัข ลิง หนูแรท และคน การบ่งชี้เอนไซม์ที่ไฮโดรไลซ์ CDD ใน LS9 จากคน ลิง สุนัข และ หนู ศึกษาได้จากผลกระทบของสารยับยั้งที่เฉพาะเจาะจงต่อเอนไซม์เอสเทอร์เอนไซม์คาร์บอกซิลเอสเทอร์เอนไซม์หลัก บิวทิลโคลิเนเอสเตอเรสเป็นเอนไซม์ถัดมาที่เกี่ยวข้องกับการเกิดไฮโดรไลซิสของ CDD ใน LS9 ของสัตว์ทดสอบทั้งสี่ชนิด ผลการศึกษาเมแทบอลิซึมของตับในหลอดทดลองนี้มีประโยชน์ต่อการแปลผลการศึกษาในสิ่งมีชีวิต และการศึกษาทางคลินิกของสารเอสเทอร์โปรตีน CDD

จุฬาลงกรณ์มหาวิทยาลัย
CHULALONGKORN UNIVERSITY

สาขาวิชา เภสัชเคมีและผลิตภัณฑ์ธรรมชาติ ลายมือชื่อนิสิต

ปีการศึกษา 2562 ลายมือชื่อ อ.ที่ปรึกษาหลัก

5876454033 : MAJOR PHARMACEUTICAL CHEMISTRY AND NATURAL PRODUCTS

KEYWORD: Curcumin, Curcumin diethyl disuccinate, In vitro metabolism, Liver S9, monoethylsuccinyl curcumin

Curcumin diethyl disuccinate (CDD) is an ester prodrug of the active compound, curcumin. CDD has been improved chemical stability and intestinal permeability more than curcumin. CDD demonstrated biological activity higher than curcumin. The aim of this study is to investigate a suitability of using liver S9 fraction (LS9) in drug metabolism profiling as function of animal sources of enzyme regarding possible translation of *in vitro* outcome to clinical study. The metabolites, *in vitro* kinetics and esterase enzyme involved in CDD hydrolysis by LS9 of human, monkey, dog and rat were determined. The high-performance liquid chromatography conjugated with high-resolution mass spectrometry-based methodologies indicated that CDD was hydrolysed to curcumin through the monoethylsuccinyl curcumin. Ultra-high-performance liquid chromatography analysis was used to determine kinetic parameters, including degradation rate constants, half-lives and hepatic intrinsic clearances. The hydrolysis profile of CDD was similar in all test species and showed a two-step, consecutive, pseudo-first-order irreversible reaction. CDD was rapidly metabolized in LS9 of all test species and ranked as human > dog > monkey > rat. The predicted clearance of CDD in liver might be ranked as dog > monkey > rat > human. The identification of CDD hydrolyzing enzymes from HLS9, MLS9, DLS9 and RLS9 evaluated by the effect of specific esterase inhibitor. Carboxylesterase was identified as the major hepatic enzyme responsible for CDD hydrolysis in LS9 of four species, followed by butyrylcholinesterase. The *in vitro* hepatic metabolism outcomes would be of benefit to future *in vivo* studies and the clinical translation of the ester CDD prodrug.

Field of Study: Pharmaceutical Chemistry and Student's Signature

Natural Products

Academic Year: 2019 Advisor's Signature

ACKNOWLEDGEMENTS

I would like to express my sincere gratitude to my dissertation advisor, Associate Professor Dr. Pornchai Rojsitthisak, for his expert guidance, valuable suggestions and constant encouragement throughout this research. His invaluable support helped me to move forward and accomplish this project.

I would also like to thank my thesis committee; Professor Dr. Somboon Tanasuptawat as the committee chairperson, Assistant Professor Dr. Boonsri Ongpipattanukul, Associate professor Dr. Vorasit Vongsutilers and Assistant Professor Dr. Rossarin Tansawat as committee members, and Dr. Rawiwan Maniratanachote for being the external committee member for investing time and providing valuable advices in this research.

I am deeply grateful to the Department of Food and Pharmaceutical Chemistry and the Pharmaceutical Research Instrument Center, Faculty of Pharmaceutical Sciences, Chulalongkorn University and the Medical Research Center of Faculty of Medicine at Chulalongkorn University for providing the chemicals, reagents and analytical instruments I need to execute this study.

I would like to extend my sincere thanks to all my research team for their motivation, time, and support during my study. I want to thank the staff at Chulalongkorn University and Bruker (Thailand) who would always help and train me in using the instruments.

I would like to express my appreciation to my parents, sisters, relative and friends, for their love, patience, understanding and support. Thank you for your kindness and consistent encouragement and good suggestion throughout this journey.

This work would not have been possible without the financial support of the Graduate School, Chulalongkorn University, the 100th Anniversary Chulalongkorn University Fund for Doctoral Scholarship and the 90th Anniversary Chulalongkorn University Fund (Ratchadaphiseksomphot Endowment Fund, No. GCUGR1125613043D).

Ponsiree Jithavech

TABLE OF CONTENTS

	Page
.....	iii
ABSTRACT (THAI).....	iii
.....	iv
ABSTRACT (ENGLISH).....	iv
ACKNOWLEDGEMENTS.....	v
TABLE OF CONTENTS.....	vi
LIST OF TABLES.....	ix
LIST OF FIGURES.....	x
LIST OF ABBREVIATION.....	1
CHAPTER I INTRODUCTION.....	3
CHAPTER II LITERATURE REVIEW.....	7
2.1. Turmeric and bioactive compounds.....	7
2.2. Prodrugs.....	15
2.3. Curcumin diethyl disuccinate.....	15
2.4. Enzymes involved in prodrug metabolism.....	18
2.4.1. Carboxylesterases.....	18
2.4.2. Acetylcholinesterase.....	26
2.4.3. Butyrylcholinesterase.....	27
2.4.4. Carboxymethylenebutenolidase.....	27
2.4.5. Paraoxonase.....	30
2.5. Enzymes inhibitors.....	31

2.6. <i>In vitro</i> metabolism.....	32
2.6.1. System of <i>in vitro</i> metabolism study	32
2.6.2. <i>In vitro</i> subcellular hepatic metabolism of curcumin.....	36
2.7. <i>In vitro</i> metabolism of prodrug	39
2.7.1. Metabolic stability	40
2.7.2. Metabolite identification	41
2.7.3. Enzyme identification.....	42
2.7.4. Interspecies	43
CHAPTER III MATERIALS AND METHODS	45
3.1. Materials.....	45
3.1.1. Equipment and instruments.....	45
3.1.2. Chemicals and Reagents	46
3.2. Methods	47
3.2.1. Esterase activity of LS9.....	47
3.2.2. Metabolite identification of CDD in LS9	48
3.2.3. <i>In vitro</i> metabolic stability of CDD in LS9.....	50
3.2.4. Enzyme identification of CDD hydrolysis in LS9.....	53
3.2.4.1. Optimization of condition for enzyme identification in LS9	53
3.2.4.2. Effect of esterase inhibitors on CDD hydrolysis in LS9.....	54
CHAPTER IV RESULTS	57
4.1. Esterase activity in LS9.....	57
4.2. Metabolite identification of CDD in LS9	57
4.3. <i>In vitro</i> metabolic stability of CDD in LS9	65
4.4. Enzyme identification of CDD hydrolysis in LS9	71

4.4.1. Optimization of condition for enzyme identification in LS9	71
4.4.2. Effect of esterase inhibitors on CDD hydrolysis in LS9	72
CHAPTER V DISCUSSION AND CONCLUSION	75
REFERENCES	81
APPENDIX A Supporting document for materials.....	97
APPENDIX B Preparation of solutions for enzyme activity study of LS9	111
APPENDIX C Preparation solutions for <i>in vitro</i> metabolism study	113
APPENDIX D Standard curve and sample preparation for enzyme activity study	119
APPENDIX E Standard and sample preparation for <i>in vitro</i> metabolism study	124
APPENDIX F Proposed five metabolites structure	133
APPENDIX G UV spectrum.....	134
APPENDIX H Kinetics reaction and raw data for metabolic stability.....	136
APPENDIX I Kinetics reaction and optimization condition for enzyme identification.	154
APPENDIX J Esterase inhibitor structure.....	168
APPENDIX K Esterase Activity in LS9	169
APPENDIX L Effect of nine esterase inhibitors on CDD metabolism in LS9.....	184
APPENDIX M Acceptance on an analytical run criterion	185
VITA.....	215

LIST OF TABLES

	Page
Table 1. Molecular properties of CES1 and CES2.....	20
Table 2. Interspecies differences in tissue expression of carboxylesterases.	23
Table 3. Interspecies different CES isoform in tissue distribution and multi-isoform of CES1 and CES2 in Rat.....	24
Table 4. The homology of carboxylesterase isozyme and CMBL in rat, dog and monkey with a human	24
Table 5. Hydrolase inhibitors to screen responsive enzyme for in vitro metabolism study.....	32
Table 6. Enzymes in liver subcellular fractions.....	34
Table 7. Cofactors used for enzymatic reaction in liver subcellular fractions.	37
Table 8. Specific activity of 0.5 mM p-nitrophenyl acetate and p-nitrophenyl caprylate hydrolysis in HLS9, MLS9, DLS9 and RLS9 ($\mu\text{mole min}^{-1} \text{mg}^{-1}$).	57
Table 9. LC-QTOF-MS/MS data of CDD, M1 and M2 after incubation in HLS9, MLS9, DLS9 and RLS9.	60
Table 10. Kinetic parameters for hepatic metabolism of CDD and MSCUR in the LS9 of human, monkey, dog and rat.....	70
Table 11. Purity of CDD, curcumin, MSCUR and DMC standard	98
Table 12. Effect of esterase inhibitors on CDD metabolism in LS9 of human monkey, dog and rat.....	184

LIST OF FIGURES

	Page
Figure 1. Structures of curcumin, desmethoxycurcumin and bisdesmethoxycurcumin	7
Figure 2. Tautomers of curcumin (1a) keto form (1b) enol form (69, 71).	8
Figure 3. The degradation products of curcumin through alkaline hydrolysis, autoxidation, and radiation with UV-light (70, 71, 77).....	10
Figure 4. Metabolism of curcumin by reduction, conjugation, and autoxidation. ADH, alcohol dehydrogenase; UGT, UDP-glucuronosyltransferase; SULT, sulfotransferase; GST, glutathione S-transferase; LOX, lipoxygenase; COX, cyclooxygenase; gluc, glucuronide; sulf, sulfate, GS; glutathionyl (60, 70).	13
Figure 5. Microbiota metabolism. CurA, NADPH-dependent curcumin/dihydro- curcumin reductase; MT, methyltransferase (101).	14
Figure 6. Structure of CDD	16
Figure 7. Hydrolysis by carboxylesterases (55).....	19
Figure 8. Cellular location of CES and UGT in hepatocytes (51).....	20
Figure 9. Proposed catalytic mechanism of carboxylesterases (50, 51, 107).....	21
Figure 10. Western blot analysis of CMBL expressions in tissue of mouse, rat, monkey dog and human (112).	28
Figure 11. Proposed catalytic mechanism in dienelactone hydrolase of Carboxymethylenebutenolidase (124, 125).....	29
Figure 12. Proposed catalytic mechanism in carboxylic ester hydrolase of Carboxymethylenebutenolidase (124, 126).	30
Figure 13. The proposed mechanism of PON1 (128).	31
Figure 14. Preparation of liver subcellular fraction.....	35

Figure 15. Structure of (A) MSCUR and (B) DMC.....	47
Figure 16. Extracted-ion chromatograms of CDD (625.2280), M1 (369.1333) and M2 (497.1806) after CDD at 10 μ M incubation in (A) HLS9, (B) MLS9, (C) DLS9 and (D) RLS9 for 0.5 min.....	58
Figure 17. Extracted-ion chromatograms of CDD (625.2280), M1 (369.1333) and M2 (497.1806) after incubation without CDD in (A) HLS9, (B) MLS9, (C) DLS9 and (D) RLS9 for 0.5 min.....	59
Figure 18. MS/MS spectrum of M1 in (A) HLS9, (B) MLS9, (C) DLS9 and (D) RLS9.....	61
Figure 19. MS/MS spectrum of M2 in (A) HLS9, (B) MLS9, (C) DLS9 and (D) RLS9.....	62
Figure 20. Extracted-ion chromatograms of (A) CDD (m/z 625.2280), (B) curcumin (m/z 369.1333) and (C) MSCUR (m/z 497.1806) standard.....	63
Figure 21. MS/MS spectrum of (A) CDD, (B) curcumin and (C) MSCUR standard.....	64
Figure 22. Proposed fragmentation of (A) CDD, (B) curcumin and (C) MSCUR.....	65
Figure 23. Representative chromatograms of CDD and metabolites in (A) HLS9, (B) MLS9, (C) DLS9, and (D) RLS9. After incubation CDD with HLS9, MLS9, DLS9 and RLS9 at 37°C, Aliquots were taken at 0.5, 1, 2, 3, 4, 5, 10, 15, 30, 45, 60, 90, 120 min and analyzed for concentration of CDD, M1 and M2. Peak: 1 = M1.....	66
Figure 24. Representative chromatograms of blank: (A) HLS9, (B) MLS9, (C) DLS9 and (D) RLS9. After incubating HLS9, MLS9, DLS9 and RLS9 without CDD at 37°C for 120 min and analyzed by HPLC. The chromatogram of each blank LS9 appeared prior to 2 min and had no metabolites in blank.....	67
Figure 25. Representative (A) chromatogram of CDD after incubation with HLS9 at 37 °C for 0.5 min (B) chromatogram of standard CDD, curcumin, MSCUR and DMC (IS) with each concentration at 0.15 μ M.	68
Figure 26. Percent CDD and its metabolites-time profiles in (A) HLS9, (B) MLS9, (C) DLS9 and (D) RLS9 as a function of incubation time. The incubation mixtures contained CDD and HLS9, MLS9, DLS9 and RLS9 at 37 °C	69

Figure 27. Percent curcumin formation rate of control (% of Control) in present of inhibitors. CDD (3 μ M) was incubated with (A) HLS9, (B) MLS9, (C) DLS9 and (D) RLS9 (0.02 mg/mL) in the presence of nine inhibitors. Control was prepared by using diluent with less than 2% organic solvent and without inhibitors. Data are expressed as the mean \pm SD (n = 3). One-way ANOVA analysis with Dunnett's post hoc test was used to indicate the statistical difference. ND = not detected since the curcumin concentration was below the limit of quantification; statistical significance, * p < 0.001 (vs. control).....	74
Figure 28. The chromatogram of CDD standard at 10 μ M.....	97
Figure 29. The chromatogram of curcumin standard at 10 μ M.....	98
Figure 30. The chromatogram of MSCUR standard at 10 μ M.....	98
Figure 31. The chromatogram of DMC standard at 10 μ M.	98
Figure 32. Proposed metabolite structure of CDD metabolism	133
Figure 33. UV spectrum of CDD 10 μ g/mL in 0.1%formic acid in acetonitrile-0.1%formic acid in water (50:50, (v/v); λ_{\max} = 400 nm	134
Figure 34. UV spectrum of curcumin 10 μ g/mL in 0.1%formic acid in acetonitrile-0.1%formic acid in water (50:50, (v/v); λ_{\max} = 427 nm	134
Figure 35. UV spectrum of MSCUR 10 μ g/mL in 0.1%formic acid in acetonitrile-0.1%formic acid in water (50:50, (v/v); λ_{\max} = 418 nm	135
Figure 36. UV spectrum of DMC 10 μ g/mL in 0.1%formic acid in acetonitrile-0.1%formic acid in water (50:50, (v/v); λ_{\max} = 421 nm	135
Figure 37. Ln [%Remaining] of CDD in HLS9 plotted against incubation time. CDD at 3 μ M were incubated in triplicate with HLS9 1 mg/mL.....	137
Figure 38. Ln [%Remaining] of CDD in MLS9 plotted against incubation time. CDD at 3 μ M were incubated in triplicate with MLS9 1 mg/mL.	137
Figure 39. Ln [%Remaining] of CDD in DLS9 plotted against incubation time. CDD at 3 μ M were incubated in triplicate with DLS9 1 mg/mL.....	138

Figure 40. Ln [%Remaining] of CDD in RLS9 plotted against incubation time. CDD at 3 μ M were incubated in triplicate with RLS9 1 mg/mL.	138
Figure 41. Formation of curcumin in HLS9 plotted against time. CDD at 3 μ M were incubated in duplicate with various concentration of each LS9 (0.01, 0.02, 0.05 and 0.1 mg/mL).....	157
Figure 42. Formation of curcumin in HLS9 plotted against enzyme concentration. CDD at 3 μ M were incubated in duplicate with various concentration of HLS9 (0.01, 0.02, 0.05 and 0.1 mg/mL) at 1 min.	157
Figure 43. Formation of curcumin in MLS9 plotted against time. CDD at 3 μ M were incubated in duplicate with various concentration of each LS9 (0.01, 0.02, 0.05 and 0.1 mg/mL).....	160
Figure 44. Formation of curcumin in MLS9 plotted against enzyme concentration. CDD at 3 μ M were incubated in duplicate with various concentration of MLS9 (0.01, 0.02, 0.05 and 0.1 mg/mL) at 0.5 min.	160
Figure 45. Formation of curcumin in DLS9 plotted against time. CDD at 3 μ M were incubated in duplicate with various concentration of each LS9 (0.01, 0.02, 0.05 and 0.1 mg/mL).....	163
Figure 46. Formation of curcumin in DLS9 plotted against enzyme concentration. CDD at 3 μ M were incubated in duplicate with various concentration of DLS9 (0.01, 0.02, 0.05 and 0.1 mg/mL) at 0.5 min	163
Figure 47. Formation of curcumin in RLS9 plotted against time. CDD at 3 μ M were incubated in duplicate with various concentration of each LS9 (0.01, 0.02, 0.05 and 0.1 mg/mL).....	166
Figure 48. Formation of curcumin in RLS9 plotted against enzyme concentration. CDD at 3 μ M were incubated in duplicate with various concentration of each LS9 (0.01, 0.02, 0.05 and 0.1 mg/mL) at 1 min.	166
Figure 49. Structure of esterase inhibitors.....	168

Figure 50. Structure of (A) p-nitrophenyl acetate, (B) p-nitrophenyl caprylate and (C) p-nitrophenol	169
Figure 51. UV spectrum of p-nitrophenol	169



LIST OF ABBREVIATION

AChE	Acetylcholinesterase
CDD	Curcumin diethyl disuccinate
CES	Carbosylesterase
°C	Degree Celcius
BChE	Butyrylcholinesterase
BNPP	Bis (4-nitrophenyl) phosphate
BW284c51	1,5-bis (4-allyldimethylammoniumphenyl) pentan-3-one dibromide
CMBL	Carboxymethylencebutenolidase
CL _{int}	Intrinsic clearance
DLS9	Dog liver S9 fraction
DMC	Dimethylcurcumin
DTNB	5,5' (dithiobis (2-nitrobenzoic acid)
EDTA	Ethylenediaminetetraacetic acid
ESI	Electrospray ionization
g	Gram
g	Relative centrifugal force
HLS9	Human liver S9 fraction
Hz	Hertz
IS	Internal standard
Iso-OMPA	Tetra (monoisopropyl) pyrophosphortetramide
k	Rate constant
Kg	Kilogram
kV	Kilovolt
L	Lite
LC-QTOF-MS	Liquid chromatography quadrupole time-of-flight mass spectrometry
LS9	Liver S9 fraction
mg	Milligram

min	Minute
mL	Milliliter
mm	Millimeter
mM	Millimolar
MLS9	Monkey liver S9 fraction
MSCUR	Monoethylsuccinyl curcumin
m/z	Mass-to-charge ratio
nm	nanometer
nmol	Nanomole
PCMB	4-(hydroxymercurio) benzoic acid sodium salt
PMSF	Phenylmethylsulfonyl fluoride
PNP	p-nitrophenol
PNPC	p-nitrophenyl caprylate
PNPA	p-nitrophenyl acetate
PON	Paraoxonase
rpm	Revolution per minute
RLS9	Rat liver S9 fraction
r^2	coefficient of determination
$t_{1/2}$	Half-lives
UHPLC	Ultra high-performance liquid chromatography
μL	Microlite
μm	Micron
μM	Micromolar
V	Volume
V	Volt
v/v	Volume-by volume
%	Percent

CHAPTER I

INTRODUCTION

Curcumin is a polyphenol compound possessing a variety of biological activities such as antioxidant (1, 2), anti-inflammatory (3-5), antiviral (6) antitumor (7-9) and anti-psoriatic (10). Several biological activities and low toxicity of curcumin make this compound more attractive for drug development (11-17). However, its poor chemical and metabolic stability, low solubility in water and poor absorption, hinder its successful therapeutic applications (18-21).

To overcome these limitations, many strategies have been applied to improve the solubility, increase stability and oral bioavailability of curcumin, including nanoparticle formulation (10, 22, 23), conjugated polymeric synthesis (24) and prodrug approach (25, 26). The succinate ester prodrug of curcumin, named curcumin diethyl disuccinate (CDD). CDD was found to be more stable in phosphate buffer pH 7.4 than curcumin (25) and can be converted to its active metabolite in plasma (25, 27, 28). However, CDD is rapidly eliminated from the bloodstream after oral and intravenous administration (19), which likely reflect the action of plasma esterases by hydrolyzing CDD in rats. CDD is also reported to be rapidly hydrolyzed in dog and human plasma (27).

CDD showed good *in vitro* and *in vivo* antitumor (8, 9, 25), antioxidant (29) and antinociceptive properties (30). Besides the free form of CDD, encapsulation in chitosan-alginate nanoparticles were developed (31-33). The nanoparticles showed sustained releases over at least 72 h (33), higher cellular uptake (31) and cytotoxicity in human breast adenocarcinoma MDA-MB-231 cells (32). Thus, the overall benefits of CDD demonstrate its potential to further develop as chemotherapeutic and analgesic agents.

In the drug discovery process, early *in vitro* absorption, distribution, metabolism and excretion (ADME) screening and *in vivo* pharmacokinetic profiling provide a basis for choosing new molecular entities (NMEs) and lead compounds that

have desirable drug metabolism, necessary for drug candidate selection and preclinical and clinical development. The ADME properties of a candidate drug allow the researcher to understand and predict not only drug behavior in *in vivo* metabolism but the safety and efficacy data also (34, 35). Regarding the liver size and its high-level of drug-metabolizing enzyme, the liver is the main organ responsible for drug metabolism (36, 37). Therefore, the *in vitro* hepatic drug metabolism studies is necessary for predicting the hepatic clearance, bioavailability, potential toxicity, and drug-drug interactions (38, 39). Several systems including recombinant enzymes, liver microsomes, liver cytosol, liver S9 fractions (LS9s), and hepatocytes are commonly used as *in vitro* drug metabolism models (37, 40). LS9 is a useful system for investigating *in vitro* hepatic drug metabolism studies because it contains both phase I and II metabolic enzymes, including microsomal and cytosol enzymes, representing all metabolizing enzymes in the liver (40, 41). It also low cost to produce and has a long storage time (41).

The recent studies indicated that LS9 is a robust *in vitro* system (41-45). LS9 and hepatocytes were found to perform equally well in predicting the metabolic stability of drugs, whereas microsomes might not present accurate metabolite profiles (41). Likewise, the use of human LS9 (HLS9) could reduce the prediction bias in high clearance prodrugs compared to human hepatocytes, and LS9 was especially applicable for predicting the metabolism of prodrugs (45). The LS9 contains several esterase enzymes, including carboxylesterase (CES), butyrylcholinesterase (BChE), acetylcholinesterase (AChE), carboxymethylenebuteno-lidase (CMBL) and paraoxonase (PON) (41, 46-48). The CESs play the main role in the hydrolysis of ester prodrugs in liver, such as sofosbuvir, sacubitril, tenofovir alafenamide, selexipag, telotristat ethyl, baloxavir marboxil. (49). The expression of CESs in each mammal species is different, in terms of the isoform distribution, enzyme activity and substrate specificity (50-52). As a result, the differences in CES-mediated hydrolytic

reactions and response towards CES inhibitors were observed among various species in liver sub-fraction (53, 54).

Prodrug are inactive drugs and then metabolized into an active drug in the body (55). Hydrolysis plays an essential role in metabolic activation of prodrugs. The prodrug hydrolysis in various tissue, and the extent of prodrug hydrolysis considerably affects the pharmacological and toxicological properties of prodrugs (49, 56, 57). The previous studies demonstrated that carboxylesterase hydrolysis of prodrug is faster than cytochrome P450 (CYP450), glucuronosyltransferase (UGTs) and sulfotransferase (SULTs)-mediated activity in liver subfraction (58, 59). The hydrolysis metabolites are produced prior to the oxidative, glucuronide and sulfate metabolites (58, 59). Several studies researched on species differences in the metabolism of ester prodrug using LS9 system to assessment of *in vitro* metabolism and *in vitro-in vivo* extrapolation such as perindopril, oseltamivir and ritobegron (45, 58).

In metabolic analysis of CDD, curcumin generated from CDD hydrolysis may undergo metabolic pathways including reduction, glucuronidation and sulfation conjugation as previously reported for curcumin (60-62). Previous study reported that the rate of ester-prodrug hydrolysis appeared 1000 times faster than glucuronide and sulfate conjugation formation rate in LS9 of the various animal species (58). It is likely that CDD hydrolysis might faster than curcumin reduction and conjugation in LS9 (58, 61). Therefore, this study interested in hydrolysis metabolism of CDD in LS9 of different animal species.

The LS9 system can be used for direct interspecies comparison of the metabolic activity and pathways of ester prodrugs. This aids the selection of appropriate preclinical species for *in vivo* experiments such as pharmacokinetics and toxicity studies (42). The use of LS9 system reduces the cost, time, and number of animals used in drug development. The knowledge of drug-metabolizing enzymes involving in the biotransformation of a test compound helps to forecast drug-drug interaction studies. Oseltamivir is metabolized by CES1, but the hydrolysis of

oseltamivir can be reduced by clopidogrel which has also shown to be the substrate of CES1 (63). Evaluating the hepatic metabolism of CDD using the LS9 from several preclinical species and human is predicted to facilitate the development of CDD for clinical applications.

In this study, the *in vitro* metabolism of CDD in LS9 preparations from four mammalian species (rat, dog, monkey and human) in terms of the metabolite profile, the metabolism rate and hepatic esterases involved the hydrolysis of CDD were evaluated. The hypothesis is that the metabolite formed, the degradation rate and participating esterases of CDD metabolism might differ in accordance with the LS9 of four test species. This implied that the therapeutic effect of curcumin and the active metabolite of CDD, may be a species dependence. Therefore, The interpretation of animal metabolism outcome for human clinical evaluation should careful justification.

The objectives of the study

1. To identify metabolites, metabolite profiles, metabolic pathways in LS9 of human, monkey, dog and rat.
2. To investigate kinetic parameters including degradation rate constants, *in vitro/in vivo* intrinsic clearances, and half-lives of CDD metabolism in LS9 of human, monkey, dog and rat.
3. To determine the enzyme responsible for the metabolism of CDD in LS9 of human, monkey, dog and rat.
4. To evaluate the differences in the *in vitro* metabolism of CDD in LS9 among four animal species.
5. To investigate the LS9 in drug metabolism as function of animal sources of enzyme regarding possible extrapolation of *in vitro* outcome to clinical study.

CHAPTER II

LITERATURE REVIEW

2.1. Turmeric and bioactive compounds

Curcuma longa L. (turmeric) is a member of family Zingiberaceae. The yellow powder derived from rhizomes of turmeric has been used in Asian cooking and traditional medicine for thousands of years. In present, turmeric has been indicated as safe by US-FDA. It has been used by the food industry as an additive, flavoring, preservative and coloring agent (13). The chemical composition of turmeric includes carbohydrates (69.4%), protein (6.3%), fat (5.1%), minerals (3.5%) moisture (13.1%) and essential oil (5.8%). The phytochemicals commonly found in turmeric powder are curcuminoids. Curcuminoids are a mixture of polyphenolic compounds including curcumin (52-63%), demethoxycurcumin (19-27%) and bisdemethoxycurcumin (18-28%) (64, 65) (**Figure 1**).

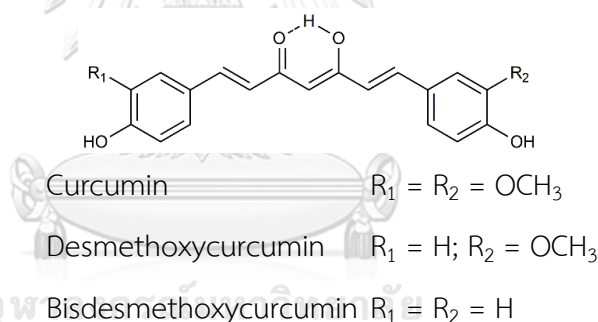


Figure 1. Structures of curcumin, desmethoxycurcumin and bisdesmethoxycurcumin

Curcumin (bis- α , β -unsaturated β -diketone) was first extracted in an impure form in 1815 by Vogel and Pelletier. In 1870, it was prepared in a pure and crystalline form by Daube. The first article related to the use of curcumin in a biliary disease was published in *The Lancet* in 1973. Only in the last ten years, curcumin has entered clinical trials at the phase I and II (13). Curcumin exhibits a variety of pharmacological activities including antioxidant (1), anti-inflammatory (66), antimutagenic (67), anticancer (7) and antimicrobial activities (68).

Curcumin displays a keto-enol tautomerism, which the enol tautomer is the dominant form of curcumin (90%) in all solvent (69-72) (**Figure 2**). The keto-enol

tautomers of curcumin could be confirmed by NMR (73), IR (74), and liquid chromatography conjugated with time-of-flight mass spectrometry (75, 76). The ratio of diketo/enol of curcumin is 0.08, 0.03 and 0.01 when dissolved in water, ethanol and acetonitrile, respectively depended on the solvent (69). The trans-diketo and closed cis-enol are the most stable isomers and the enol form coexists in two equivalent tautomers (69, 71). The preference for enol form leads to a planar, intramolecularly hydrogen-bonded structure, both in solution and in powder form (71). The solvent effects on the acidic property of curcumin that the hydrogen of the enolic hydroxyl group is more acidic in ethanol and water, whereas the hydrogen of the phenolic hydroxyl group is more acidic in other solvents including acetonitrile, acetone, n-octanol, DMSO, chloroform and benzene. However, the radical obtained from the phenolic hydroxyl group is more stable than the radical obtained from the enolic hydroxyl group (69).

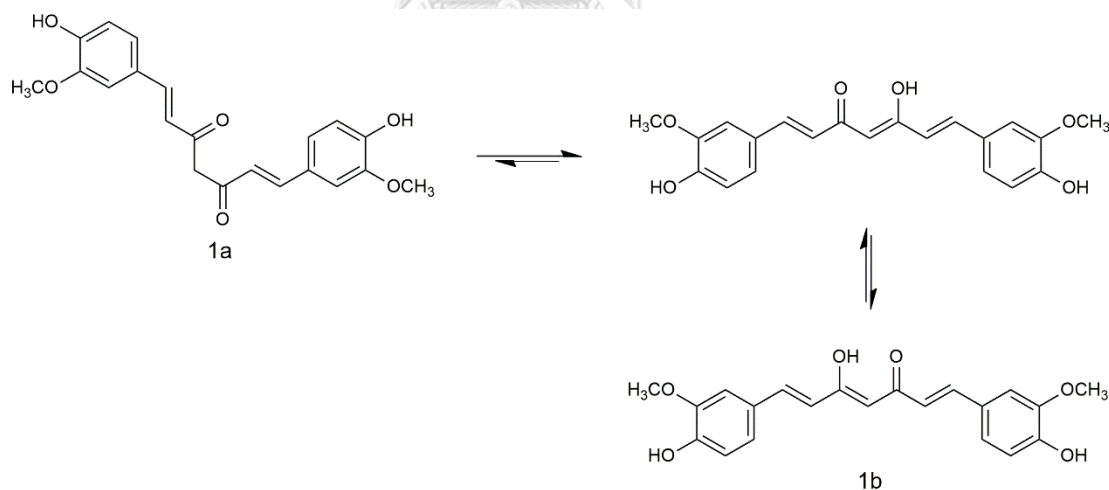


Figure 2. Tautomers of curcumin (1a) keto form (1b) enol form (69, 71).

Curcumin is an unstable compound that it is excessively affected by alkaline solution, oxygen and ultraviolet and visible light as show in **Figure 3**. Curcumin decomposed rapidly in neutral to alkaline solutions with a half-life of only about 10 min, but more stable in cell culture medium containing fetal bovine serum and in

human blood, which about 50% of curcumin is remained after incubation for 8 h (77). The degradation products of curcumin include Trans-6-(4'-hydroxy-3'-methoxyphenyl)-2,4-dioxo-5-hexenal, ferulic acid, feruloylmethane, and vanillin were found. The increasing incubation time lead to enhance the vanillin formation, major degradation product.

According to a recent study, ferulic acid, feruloylmethane and vanillin are the minor degradation products of curcumin, while the most abundant product is bicyclopentadione in an alkaline solution and cell culture media (70, 72, 78-80) (**Figure. 3**). The formation of bicyclopentadione is generated from curcumin by autoxidation (80). Co-addition of cyclooxygenases (81) and lipoxygenases (82) accelerated degradation of curcumin into autoxidation products. These products represent degradation products and metabolites. The addition of serum or antioxidants can stabilize the oxidation of curcumin (81).

Curcumin is unstable when irradiated with light (**Figure 3**). The photochemical degradation of crystalline curcumin exposed to UV-light produced vanillin, ferulic aldehyde, vanillic acid, and ferulic acid. The same degradation pattern is observed in organic solvents, including methanol, isopropanol, and chloroform after the dissolved curcumin was exposed to light. Moreover, curcumin dissolved in isopropanol leads to form additional metabolite, guaiacol derivative. However, the light-induced degradation can protect using curcumin for pharmaceutical coatings (70, 71, 79, 83).

$\mu\text{g/mL}$ was detected at time 0.83 h (87). In contrast of rat, when curcumin was given at a dose of 2g/kg to human, the low serum concentration of 0.006 $\mu\text{g/mL}$ was observed (87). A single oral dose of curcumin (10 or 12 g, p.o) in human, the level of curcumin showed less than 50 ng/mL in human plasma (88). Later several studies conducted on the bioavailability of curcumin in patient. Oral dosing of 4-8 g of curcumin in patient presented plasma levels of 0.51-1.77 μM after 1.5 h of dosing (89). Similarly, in patient with colorectal cancer, 3.6 g of curcumin via oral administration was found a plasma level of 11.1 nmol/L after one hour of dosing (90). A Phase IIA clinical trial indicated that after oral administration of 4 g/kg curcumin for 30 days, the post intervention plasma concentration of curcumin was 3.8 ng/mL (91). Similarly, patient with colorectal cancer intake 3.6 g of curcumin for 7 days, trace concentration of curcumin was found in blood circulation (92). The distribution of curcumin in body tissue is crucial for biological activity, several studies have addressed this study. After intraperitoneal administration of curcumin (0.1 g/kg) to mice, the concentration of curcumin in the intestine, liver, spleen, kidneys and brain were 177.04, 26.90, 26.06, 7.51, and 0.41 $\mu\text{g/mg}$, respectively (93). Similarly, After oral administration of curcumin (340 mg/kg) in rats, curcumin levels found in intestine, liver, kidney, heart, plasma and urine were 1.4 mg/g, 3,671.8 ng/g, 206.8 ng/g, 206.8 ng/g, 16.1 ng/g, 2.0 ng/g, respectively, after two hours (94). In human, the level of curcumin in normal and malignant colorectal tissue of patients giving 3.6 mg of curcumin were 12.7 and 7.7 nmol/g, respectively (92).

Several studies of curcumin metabolism have been published (60-62, 95). Curcumin undergoes extensive metabolic reduction to dihydrocurcumin, tetrahydrocurcumin, hexahydrocurcumin and octahydrocurcumin, and conjugation form with glucuronide in intestinal and hepatic cytosol and microsome from human and rat, respectively (**Figure 4**). An *in vitro* metabolism found that hexahydrocurcumin is the major reductive metabolites in hepatic human and rat microsome and rat liver slice (60, 62). The enzymes responsible for the metabolic

reduction was alcohol dehydrogenases. Curcumin and its reductive metabolites were predominantly present as glucuronides, but a lower level of sulfate conjugates was also observed. The extent of curcumin glucuronide was more significant in intestinal microsome than those in hepatic microsome (61). The lack of oxidative metabolites of curcumin was observed using rat liver microsomes (60). Curcumin is conjugated with glutathione giving the formation of monogluthionyl curcumin conjugates (**Figure 4**) in human intestinal and hepatic cytosol. In caco-2 cells, curcumin and GSH conjugates present in the apical compartment more than in the basolateral compartment. Curcumin monogluthionyl conjugates can already exist during intestinal transport and are excreted to the intestinal lumen (95).

In vivo metabolism studies revealed that after i.p. administration of curcumin (0.1 g/kg) to mice, curcumin-glucuronide and THC-glucuronide were observed in plasma, and THC is a major metabolite of curcumin (93). In rats, after p.o. administration of curcumin (500 mg/kg), curcumin rapidly disappeared from the plasma and present at low levels near the limit of detection. The major metabolite in plasma were curcumin glucuronide and curcumin sulfate, while hexahydrocurcumin, hexahydrocurcuminol and hexahydrocurcumin glucuronide were found in small amount (61). In clinical study, after administered of curcumin at dose 10 g and 12 g to healthy human subjects, curcumin glucuronide and curcumin sulfates were recovered in all healthy subjects. The ratio of glucuronide: sulfate was 1.92:1 with not mixed conjugates (88). Phase I clinical trial, the study was set to monitor curcumin and its glucuronide and metabolites concentration in plasma, urine, and feces after patient with metastatic colorectal cancer refractory to standard chemotherapies consumed capsules with curcumin at dose 0.45-3.6 g daily. Curcumin, curcumin glucuronide and curcumin sulfate were found in plasma and urine. Abundant amounts of curcumin were detected from the feces at all consumed dose, whereas trace amounts of curcumin sulfate were observed (90). Phase II clinical trial, the study also investigated curcumin and its conjugated metabolite in patient

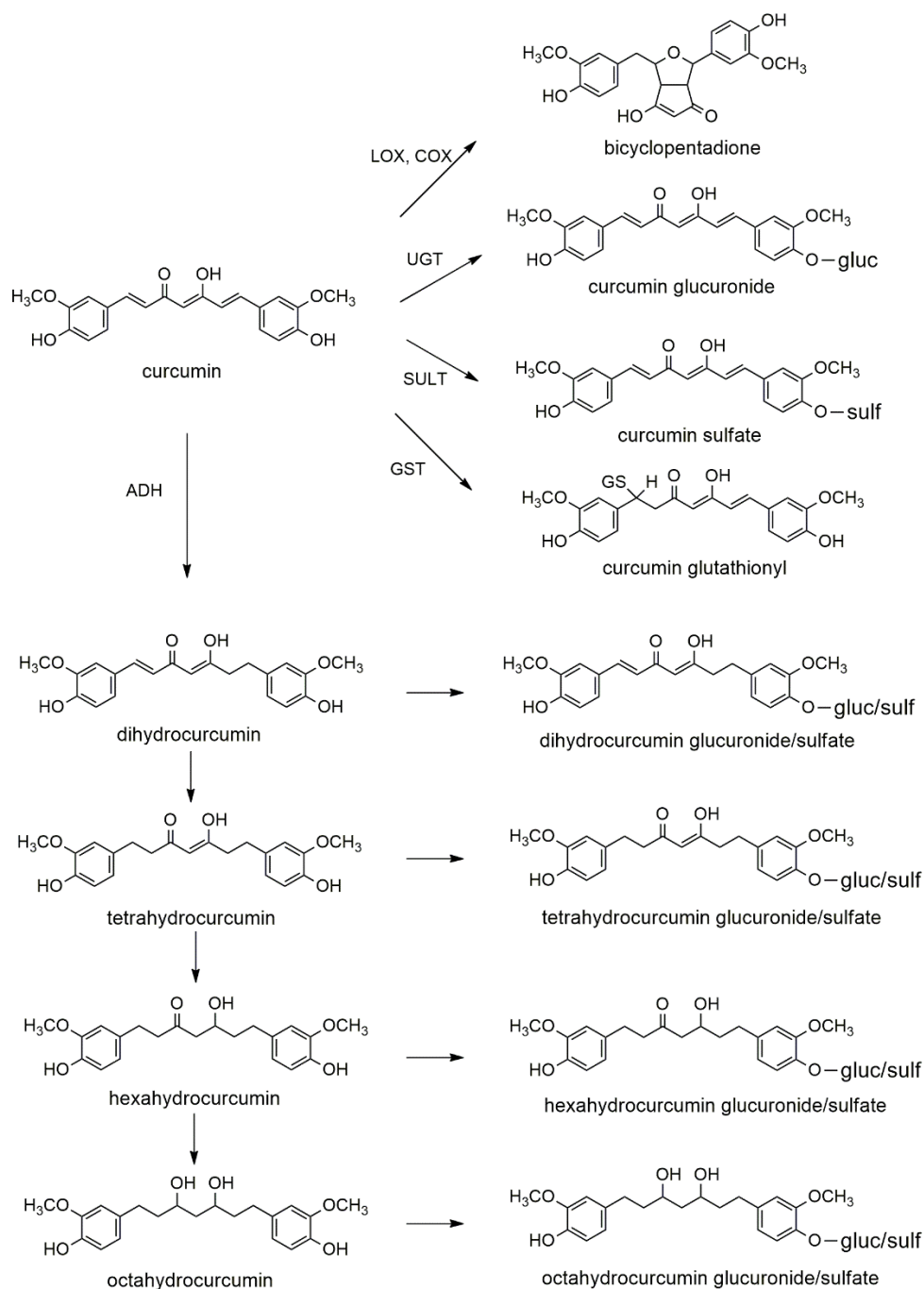


Figure 4. Metabolism of curcumin by reduction, conjugation, and autoxidation. ADH, alcohol dehydrogenase; UGT, UDP-glucuronosyltransferase; SULT, sulfotransferase; GST, glutathione S-transferase; LOX, lipoxygenase; COX, cyclooxygenase; gluc, glucuronide; sulf, sulfate; GS; glutathionyl (60, 70).

with early-stage chronic lymphocytic leukemia (CLL) or small lymphocytic lymphoma (SLL). The data demonstrated that the orally ingest curcumin was rapidly converted

to curcumin conjugate metabolites, and curcumin glucuronide was predominated conjugates (96).

In the microbiota involved metabolism, several studies reported that curcumin can be metabolized in the gastrointestinal tract of human by a specific microorganism. *Escherichia coli* is one of the curcumin-converting microorganisms that isolated from human feces. The purified NADPH-dependent curcumin/dihydrocurcumin reductase (CurA) from *E. coli* can convert curcumin to dihydrocurcumin and tetrahydrocurcumin (**Figure 5**) (97). *Blautia* sp. MRG-PMF1., the other isolated microorganism together with curcumin can produce two metabolites, demethylcurcumin and bisdemethylcurcumin by the methyl aryl ether cleavage reaction by methyltransferase (98, 99). In the perspective of the metabolic profile of metabolized curcumin, the number of novel curcumin metabolites such as reduced, demethylated, bisdemethylated, hydrogenated, dehydrogenated, hydroxylated and acetylated metabolites were detected and identified from supernatant of fresh human fecal samples by a method using UPLC-QTOF (100).

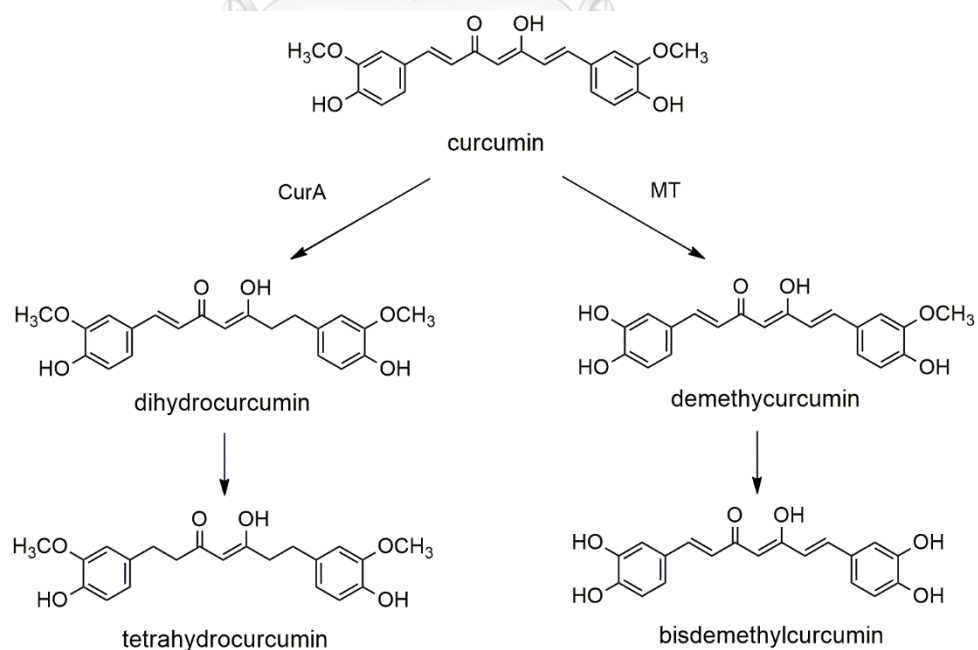


Figure 5. Microbiota metabolism. CurA, NADPH-dependent curcumin/dihydrocurcumin reductase; MT, methyltransferase (101).

As various curcumin metabolites generated by human intestine, hepatic and intestinal microorganism, the numerous *in vitro* and *in vivo* studies demonstrated that curcumin metabolites contributed the therapeutic efficacy of curcumin. Several studies report that the poly-pharmacology of curcumin can be attributed to its metabolites, which are recognized as antioxidant, anti-inflammatory, antitumor, cardioprotective, and anti-diabetic (79, 81, 101).

2.2. Prodrugs

The term “prodrug” was first introduced by Acrien Albert in 1958. The prodrug concept has been increasing used over recent years; around 10% of the world marketed medicines are prodrugs. In 2008, 33% of approved small molecular-weight drugs were prodrugs (102). Recently, considerable attention has been focused on the development of prodrugs, which provides an effective strategy for enhancing the water-solubility, absorption and membrane permeability, targeted release, intestinal stability, reducing metabolism and side effects of therapeutic drugs (103, 104). Most prodrugs are inactive compounds with carboxyl-ester, thio-ester, amide or carbamate, which are subsequently hydrolyzed to an active drug. Therefore, hydrolase enzymes and extent of hydrolysis affects the pharmacological activity and toxicity of prodrugs. Ester prodrugs have been found in antivirals, angiotensin-converting enzyme inhibitors and immunosuppressants (55). The formation of the ester prodrug is intended to increase the overall lipophilicity of the molecule and promote membrane permeability and oral absorption, which mostly leads to significant improvement in oral bioavailability (42, 44, 45).

2.3. Curcumin diethyl disuccinate

Curcumin is the attractive compound that shows numerous biological properties with lack of toxicity. Therefore, many prodrugs of curcumin have been developed to overcome the instability and poor bioavailability of curcumin. Curcumin prodrugs were generated in various approaches by conjugating curcumin with small molecules, oligo (ethylene glycol), polysaccharide, poly (ethylene glycol), polymer or

block of co-polymer (15). Among these derivatives, most curcumin prodrugs were conjugated via an ester bond such as curcumin-diglutaric acid (26), mono-PEGylated curcumin conjugates (24) and curcumin diethyl disuccinate (25).

The succinate ester prodrugs of curcumin to protect curcumin degradation through oxidative and hydrolyzed pathways was developed (25). Curcumin diethyl disuccinate (CDD), an ethyl succinate ester prodrug of curcumin was obtained (**Figure 6**). This prodrug was synthesized by esterifying both phenolic hydroxyl group with ethyl succinyl chloride. Recently, the synthesis of CDD were scaled up to supply for preclinical studies. Physical and chemical properties of CDD including crystallinity, solubility and partition coefficient were investigated. The previous study showed that CDD powders were in a crystal structure with a wide range of particle size- 0.5 μm to 300 μm . The solubility of CDD in water was found at 0.059 $\mu\text{g/mL}$, which nearly to curcumin at 0.068 $\mu\text{g/mL}$. Melting points of the synthesized CDD was in the range of 185-186 $^{\circ}\text{C}$, while curcumin was 95-96 $^{\circ}\text{C}$ (9). CDD was stable in 0.1 M phosphate buffer (pH 7.4) and its half-lives ($t_{1/2}$) was higher than that of curcumin. Degradation rate constant of CDD in phosphate buffer (pH 7.4) was $1.43 \pm 0.30 (\times 10^{-3}) \text{ min}^{-1}$ (27). In human plasma, CDD was hydrolyzed to its active metabolite curcumin within 2 h by plasma esterase (25). CDD showed the higher level of curcumin than free curcumin during the transport across Caco-2 monolayers at 60 to 240 min (105).

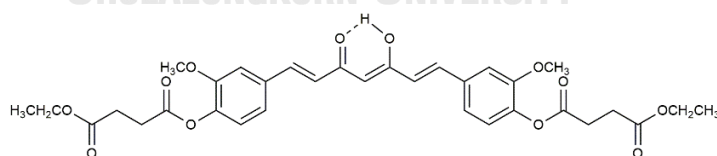


Figure 6. Structure of CDD

CDD exhibited an anticancer activity against colon cancer cells (Caco-2) (25) and human breast cancer cells (MDA-MB-231) (32). CDD can overcome the limitations of curcumin in terms of cellular transport and has a potential for extensive *in vitro* and *in vivo* anti-hepatocellular carcinoma effects. CDD can inhibit the growth of HepG2 and promoted the cell fate to early and late-stage apoptosis, which is higher

extent than that of curcumin. The results indicated that CDD increase Bax protein and LC3-II protein, while downregulated Bcl-2 protein, and activated caspase-3 and 9 in HepG2 (8). CDD show decreased the tumor size in HepG2-xenograft mice more than curcumin. The reduction of tumor growth can propose by enhancing the expression of Bax protein, the inhibition on VEGF secretion and the down regulation of COX-2 and Bcl-2 (9). Moreover, CDD showed an antinociceptive property in both central and peripheral pain model in mice. After orally administration of CDD, the lowest dose of CDD (25 mg/kg) gave a significant analgesic response in hot plate and the tail-flick test, a central analgesic activity. CDD 200 mg/kg also decreased the mean writhing response in visceral inflammation pain model compared to vehicle controls (30).

The pharmacokinetic profile of CDD was first investigated in comparison with that of curcumin in male wistar rats. The dose of intravenous and oral administrations of both compounds were 20 mg/kg and 40 mg/kg, respectively. The results demonstrated that CDD has better tissue distribution than the parent curcumin. After intravenous dosing of curcumin at 1 and 4 h, the results showed clearly that CDD has high tissue to plasma ratio of curcumin and curcumin glucuronide. However, the absolute oral bioavailability of curcumin from CDD and curcumin was not significant different (19). Another research found that the AUCs of curcumin in wistar rat after taking 40 mg/kg (i.v.) from CDD and curcumin was not different. The author noted that due to the administered dose of CDD was not molar equivalent to curcumin, this implied that CDD might have slightly higher curcumin plasma concentration (28).

The *in vitro* plasma metabolism in rat, dog, and human indicated that CDD rapidly hydrolyzed to monoethylsuccinyl curcumin and further catalyzed to curcumin by esterase. The hydrolytic rate was presented in the rank as: rat >> human > dog. The carboxylesterase played the major enzyme responded to the CDD hydrolysis in rats, while PON, AChE and serum albumin showed the hydrolytic role of CDD in dog and human. The BChE involved CDD hydrolysis in dog (27).

2.4. Enzymes involved in prodrug metabolism

Normally, the major reason for developing ester prodrugs is to increase oral bioavailability. The conversion of an alcohol or a carboxylic acid to ester promotes hydrophobicity which make more efficient in passive transport through cell membranes. After non-active ester prodrugs pass through systemic circulation, the ester bond of prodrugs was hydrolyzed and released the active parent drugs in plasma or tissues with located esterase. The most considerable esterases that hydrolyzed prodrugs are carboxylesterase, paraoxonase, acetylcholinesterase and butyrylcholinesterase. Oxidation cleavage of ester-based prodrugs is catalyzed by cytochrome P450s (46). A recent study has found that carboxymethylenebutenolidase was demonstrated to be the predominate activating enzyme for olmesartan medoxomil, ester-based prodrug (47). Esterase devised by the putative substrate-binding region containing serine, cysteine or histidine residues. Carboxylesterase, acetylcholinesterase, butyrylcholineaterase are serine hydrolase, while carboxymethylenebutenolidase and paraoxonase are cysteine and histidine hydrolase, respectively.

2.4.1. Carboxylesterases

Carboxylesterases (EC 3.1.1.1) are the key enzyme in hydrolysis metabolism of ester prodrugs (**Figure 7**). The role of carboxylesterases in drug metabolism including tissue distribution, substrate specificity, drug-drug interaction and factors affecting the regulation and activity of these enzymes are considerable. Carboxylesterase are members of an α/β -hydrolase-fold family. Carboxylesterases observed in mammals have been classified into five families, which are CES1, CES2, CES3, CES4 and CES5, depending on amino acid homology, but the major enzymes were CES1 and CES2. Similarly, both CES1 and CES2 are two major enzymes in human (Laizuer et al., 2013; Liederer and Borchardt, 2005; Fukami and Yokoi, 2012). Because CES1 and CES2 lack of specification, substrates can be hydrolyzed by either enzyme, which generally one CES serves as a major pathway of hydrolysis. The CES1

enzyme prefers an ester substrate with a large, bulky acyl group and a small alcohol group, while CES2 prefers an ester substrate with a small acyl group and a large alcohol group (Sato et al., 2002).

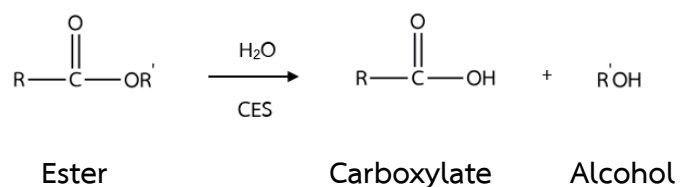


Figure 7. Hydrolysis by carboxylesterases (55)

In the recent years, the structure-activity relationship of 31 derivatives of atorvastatin esters, amides, thioesters and lactone have been investigated for metabolic activation by microsomes and hydrolyses. The result demonstrated that human CES1 was influent not only by the size of the acyl group and alkoxy group, and also by the degree of steric crowding around the alkoxy group. In contrast, human CES2 activity increased caused by a decrease of in the electron density environing the alkoxy group of the substrate (106).

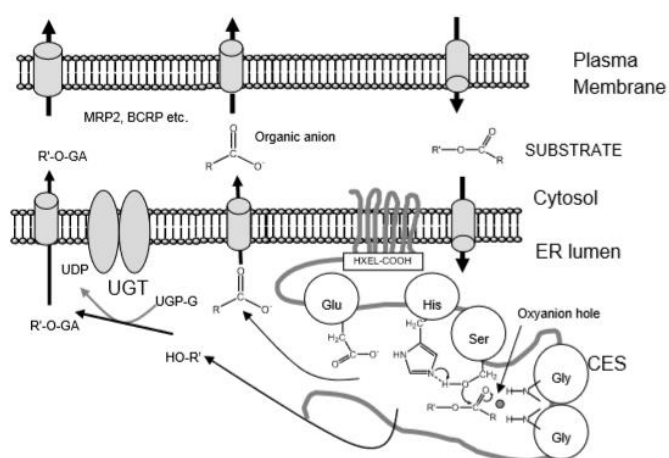
Molecular properties and localization

The molecular properties of CES1 and CES2 are present in **Table 1**. CES1 contains 567 amino acids with a molecular weight (MW) of 62521 Da, while CES2 compose of 559 amino acids with a MW of 61807 Da. CESs contain an N-terminal signaling peptide, which is responsible for the ER localization of these enzyme. The C-terminal sequence (HXEL) not only binds to the KDEL retention sequence of the ER receptor but prevents the secretion of CES from the cells (50, 107).

Table 1. Molecular properties of CES1 and CES2.

Property	CES1	CES2
Molecular weight	62521 D (monomer) 180 kD (trimer)	61807 D (monomer)
Isoelectric point	5.6 -5.8	4.8-5.0
Optimal pH	6.5	7.5-8.0
C-terminal signal peptide	HIEL	HTEL
Catalytic triad	Ser ²²¹ , GLU ³⁵⁴ and His ⁴⁶⁸	Ser ²²⁸ , GLU ³⁴⁵ and His ⁴⁵⁷
Glycosylation site	Asn-X-Thr and Asn ⁷⁹	Asn-X-Ser/Thr, Asn ¹⁰³ and Asn ²⁶⁷

The catalytic domain catalytic triad of human carboxylesterase (Ser-Glu-His) is crucial for the enzyme catalysis. CESs are mostly membrane-bound and local on the lumen of endoplasmic reticulum (ER) (**Figure 8**), but they are also present in the cytosol with lower amount (50).

**Figure 8.** Cellular location of CES and UGT in hepatocytes (51)

Mechanism of action

The CES hydrolyze substrates using the essential catalytic triad which composed by three residues (Ser-His-Glu) within the active site. Hydrolysis by CESs is catalyzed by acid-base mechanism via a charge-relay complex. The three amino acid serine, histidine and glutamine act as a nucleophile, an acid and a base, respectively. The base-catalysed mechanism via a two-step process which is conserved in the serine hydrolases, including proteases, peptidases and lipases (**Figure 9**).

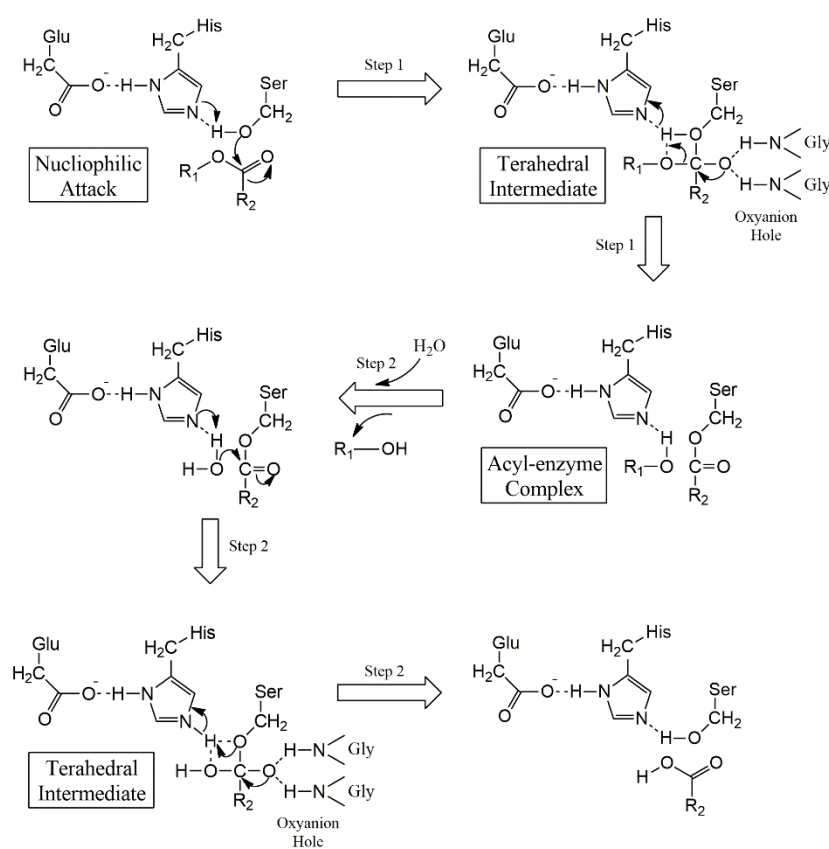


Figure 9. Proposed catalytic mechanism of carboxylesterases (50, 51, 107)

First, the oxygen from the hydroxyl group of the serine attacks the carbonyl carbon of the substrate leads to form a tetrahedral intermediate. The transition state negative charge on a deprotonated oxygen is stabilized through hydrogen bonding of the two glycine on an oxyanion hole in the active site of an enzyme (50). The reaction leads to produce an acyl-enzyme intermediate and

release an alcohol, thiol, or amine product. Second, the histidine activated water as the nucleophile attacked the carbonyl group of the acyl-enzyme intermediate, leading to release of carboxylic acid metabolite, and recover the enzyme to its original state with unbound serine residue. The environment around the catalytic triad is essential for these hydrolytic steps (50, 51, 107, 108).

Tissue distribution of CES1 and CES2

Carboxylesterases are mainly located in endoplasmic reticulum of various tissues such as the liver, small intestine, kidney, and lungs (51). The most amounts are investigated in liver and small intestine where they are function as first-pass metabolic hydrolysis of substrates. The liver greatly contains CES1 with less amounts of CES2, while the small intestine contains CES2 with no CES1 (55, 109). CES2 also expresses in kidney. Both CES1 and CES2 are localized in the lumen side of the endoplasmic reticulum, also present at comparable level in human liver cytosol (48). CES in liver has highest activity (46). After oral administration in human, it is possible that ester prodrugs could be hydrolyzed when they access to intestinal CES2 and liver CES1 with little of CES2 through enterohepatic circulation and reach systemic circulation (55).

Species differences

In species differences, different isoforms of carboxylesterases are distributed in liver as shown in **Table 2** (51). Their respective specificities and specific activities are different (46).

Table 2. Interspecies differences in tissue expression of carboxylesterases.

Species	Isozyme	Liver	Small intestine	Kidney	Lung
Rat	CES1	+++	-	+++	+++
	CES2	-	+++	-	-
Beagle Dog	CES1	+++	-	NT	+++
	CES2	++	-	NT	+
Monkey	CES1	+++	++	-	NT
	CES2	+	+++	+	NT
Human	CES1	+++	-	+	+++
	CES2	+	+++	+++	-

+++ high expression, ++ moderate expression, + low expression, - undetectable

The tissue distribution and multi-isoform of CES1 and CES2 in animal species are shown in **Table 3**. Human is devoid of CES1 in the intestine, while dog lacks of CES activity in the small intestine. CES expression in monkey liver is similar to human, suggesting a monkey could be an animal model of CES substrate for human, although only CES1 express in the monkey intestine while not detect in human (50). CES2 genes such as mfCES2A, mfCES2B, and mfCES2C were identified in monkeys. the expression of mfCES2A in several organs, while mfCES2C is only expressed in the small intestine, kidney, and skin. The mfCES2C shows different hydrolytic properties to mfCES2A, depending on the substrate (110). Rats have multi-isoforms compared to human and monkeys, causing them highly efficient in hydrolyzing the substrates. The previous study reported that the CES2 isoform of rat including Ces2a, CES2e, Ces2c and Ces2g were found in liver (50, 111) Human, monkey and dog do not have CES in the plasma while rat have a high abundance of CES plasma (50) as shown in Table 3.

Table 3. Interspecies different CES isoform in tissue distribution and multi-isoform of CES1 and CES2 in Rat.

Species	Liver		Intestine		Kidney		Lung		Plasma
Human	CES1	CES2	-	CES2	-	CES2	CES1	-	None
Monkey	Ces1	Ces2	Ces1	Ces2	Ces1	Ces2	-	-	None
Dog	Ces1	Ces2	None		Ces1	Ces2	Ces1	Ces2	None
Rat	Ces1c	Ces1d	Ces1e	Ces1f	Ces1e	Ces1f	Ces1d	-	Ces1c
	Ces1e	Ces1f	Ces2a	Ces2c	Ces2g	-	-	-	-
	Ces2a	Ces2c	Ces2h	-	-	-	-	-	-
	Ces2e	Ces2g	-	-	-	-	-	-	-

Based on amino acid sequencing alignment of the encoding genes, the homology of enzyme including CES1 and CES2 in rat, dog, and monkey shared with human protein are shown in **Table 4**.

Table 4. The homology of carboxylesterase isozyme and CMBL in rat, dog and monkey with a human

Species	Isozyme	Homology
Rat	CES1 (Hydrolase A)	77.6% ^a
	CES2 (RL4)	42.8% ^a
	CMBL	84% ^b
Dog	CES1 (CES D1)	79.7% ^a
	CES2	NT
	CMBL	87% ^c
Monkey	CES1 (AB010633)	92.9% ^a
	CES2	NT
	CMBL	NT

NT, not tested. a = Data of the homology of carboxylesterase reported by Taketani, Shii (52) b, c = Data of the homology of CMBL reported by Ishizuka, Fujimori (47) and Ishizuka, Yoshigae (112), respectively.

Factor affecting the activity of carboxylesterase

There are several factors affecting carboxylesterase activity such as inter-individual variability, enzyme regulation through the pregnane x receptor (PXR) and CAR receptors, specific isozyme, drug-disease interaction, different gender, age and interspecies. Large inter-individual variability in the hydrolysis clearance of substrate drugs was related to genetic variations which were identified in the carboxylesterase genes. A nonsynonymous transition of G to A at cDNA position 428 of CES1 results in a change of protein translation from glycine to glutamic acid, with a complete loss of hydrolytic activity (55).

The regulation of CES1 and CES2 expression was influenced by the PXR and constitutive androstane receptor (CAR) proteins, which upon activation, move to the nucleus and bind to DNA response elements in promoters to induce the expression of many phase I and phase II metabolizing enzymes. The expression of CES is likely to be induced by the same ligands that induce cytochrome P450 enzymes through the PXR and CAR receptors. The proinflammatory cytokine interleukin-6 (IL-6) has been found to decrease hydrolysis of clopidogrel (CES1 substrate) and irinotecan (CES2 substrate) which implied in downregulating the expression of a number of CES1 and CES2 (55).

In general, isozymes can possess very different substrate specificities. This has been shown by significantly distinct enzyme-catalyzed bioconversion rates of various substrates. For hydrolyzed irinotecan as an ester prodrug, the report indicated that human CES2 has more activity than CES1A1 and CES3 (46).

There are several drug-disease, drug-food, and drug-drug interactions. Based on the location of CES in endoplasmic reticulum, the metabolism of substrates by CYP3A4 and its hydrolysis by carboxylesterases to metabolites is decreased in microsomes from subjects with liver dysfunction. As for different genders, there is evidence that carboxylesterase activity differs between men and

women, in which women have greater CES1 activity than men. Moreover, investigating the relationship between age and the esterase activity, both CES1 and CES2 expression and hydrolytic activity in microsomes are developmental changes from neonates to adult. These enzymes are lower in children and higher in adult (55). In addition, the difference in substrate specificity of CES enzymes between human and interspecies was reported (48).

Drug interaction

Patrick, Straughn (113) carried out the drug interaction study of methylphenidate (CES1 substrate) and ethanol in human, the result showed that C_{max} and AUC of methylphenidate were increased. Thus, ethanol could inhibit hydrolysis of methylphenidate catalyzed by CES1. The same effect was also observed in inhibiting cocaine's hydrolysis in human. Ethanol also inhibited CES2 hydrolysis of cocaine in liver microsomes. The most reports demonstrated that drug-drug interaction based on competitive inhibition occurred when two or more of CES1 and CES2 substrates were co-administered (55).

2.4.2. Acetylcholinesterase

In human cholinesterases, there are two enzymes, namely acetylcholinesterase (AChE) and butyrylcholinesterase (BChE). Acetylcholinesterase (AChE) (EC 3.1.1.7) in physiological function appears to hydrolyze the neurotransmitter acetylcholine at cholinergic synapses and neuromuscular junctions. It can be catalyzed hydrolysis of esters, amides, and anilides involved prodrugs. Unlike CES, AChE act more specific substrates. The cholinesterase of human present in liver and plasma are mainly G4 and light globular species (G2 and G1).

AChE is mainly observed in red blood cell and brain or at neuromuscular junctions, depending on its molecular form (46). In human, the major molecular form of AChE is G1 and G2 forms in liver, plasma and red blood cell while G4 form found in CSF and brain (114). In rat, The G2 and G4 form of AChE were

found in liver, while only G4 form was found plasma (115). Most of the AChE was membrane-bound, one-half of G4 form and G2 form was anchored to the membrane via phosphatidylinositol. The active site of AChE composed of catalytic triad Ser²⁰³, Glu³³⁴ and His⁴⁴⁷ and anionic subsite (Gly¹²¹, Gly¹²², Ala²⁰⁴) (116, 117). The mechanism of catalysis is serine hydrolysis (118) **(Figure 9)**

2.4.3. Butyrylcholinesterase

Butyrylcholinesterase (BChE) (EC 3.1.1.8) is one of the cholinesterase enzymes, mainly selective for butyrylcholine and propionylcholine. BChE has an acyl binding pocket at the active site and differences in amino acid residues and is also responsible for bioactivation of prodrugs. In human, the BChE in molecular form of G1, G2 and G4 were synthesized in liver. G4 molecular form of BChE is mainly found in plasma because it is synthesized in liver and secreted into plasma, approximately 160 time higher than AChE (119). BChE expressed in liver, lung, brain, and heart tissue (46, 48). In rat, the G2 and G1 form of BChE were found in liver and no G4 form was not detected (115). Both form of BChE were found soluble within the lumen of the Golgi vesicles, suggesting that liver secreted G 1 and G2 of BChE molecular forms and not the G4 form found in plasma. BChE of human contains a catalytic triad including Ser²²⁶, Glu³⁵³ and His⁴⁴⁶ (120). The mechanism of catalyst and the active site of BChE is similar to the other serine hydrolase (121) **(Figure 9)**

In human and rat species, the depletion of the G4 of BChE in human plasma or G4 of AChE in rat plasma, is related to chronic liver disease and reflects tissue damage (119).

2.4.4. Carboxymethylenebutenolidase

Carboxymethylenebutenolidase (CMBL) (EC 3.1.1.45) is a member of cysteine hydrolases belongs to the α/β hydrolase fold family, which contain a conserved nucleophile (serine/cysteine)-histidine acid catalytic triad. This enzyme is high expression in liver, followed by the and the kidney, small intestine and colon.

The protein of CMBL had an apparent molecular mass of 30 kD. Human CMBL has a catalytic triad composed of Cys¹³²- His²¹²-Asp¹⁷⁹. The Cys¹³² residue (nucleophile) is crucial for catalytically activity in CMBL (47).

CMBL is a cytosolic protein found in the intestine, liver and kidney and low in the lung of various species (**Figure 10**), exceptional dog CMBL was not detected in intestinal cytosols. Besides, weaker bands in the western plot analysis were observed in microsomal fractions, but not detected in plasma (112).

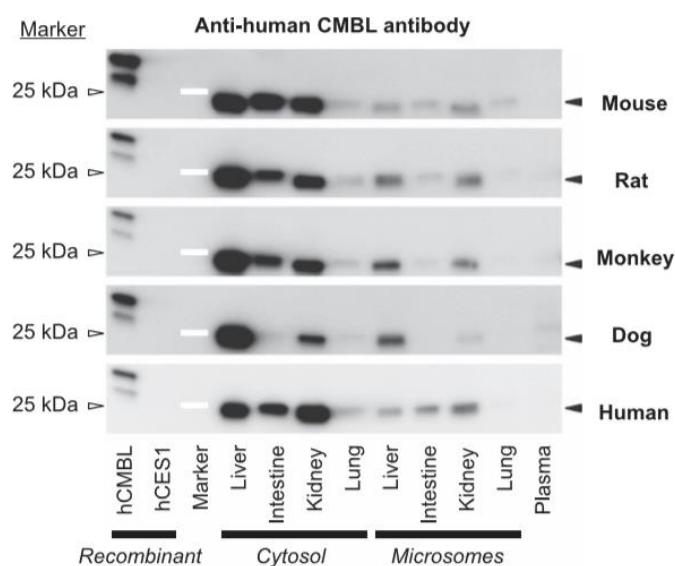


Figure 10. Western blot analysis of CMBL expressions in tissue of mouse, rat, monkey dog and human (112).

CMBL quite likely prefers cyclic esters as a substrate more than noncyclic esters, and it activates medoxomil-ester prodrugs in which the medoxomil moiety is linked to an oxygen atom such as olmesartan medoxomil. Inhibitor studies showed that CMBL was almost completely inhibited by a free thiol modifier (PCMB) and partially inhibited by a carboxylesterase inhibitor (BNPP), and indicating that CMBL is a cysteine hydrolase (47). However, this enzyme displayed the carboxylesterase activity toward p-nitrophenyl caprylate (C8) from *Sulfolobus solfataricus* P1 (122) and low activity on p-nitrophenyl acetate (C4) from *Pseudomonas* sp. B13 (123).

hCMBL's mechanism involves the formation of covalently bound acyl intermediate via a tetrahedral intermediate similar to serine hydrolase (47). The propose mechanism of CMBL was divide in diene lactone hydrolase (**Figure 11**) and carboxylic ester hydrolase (**Figure 12**). The homology of enzyme CMBL in rat and dog are present in **Table 4**.

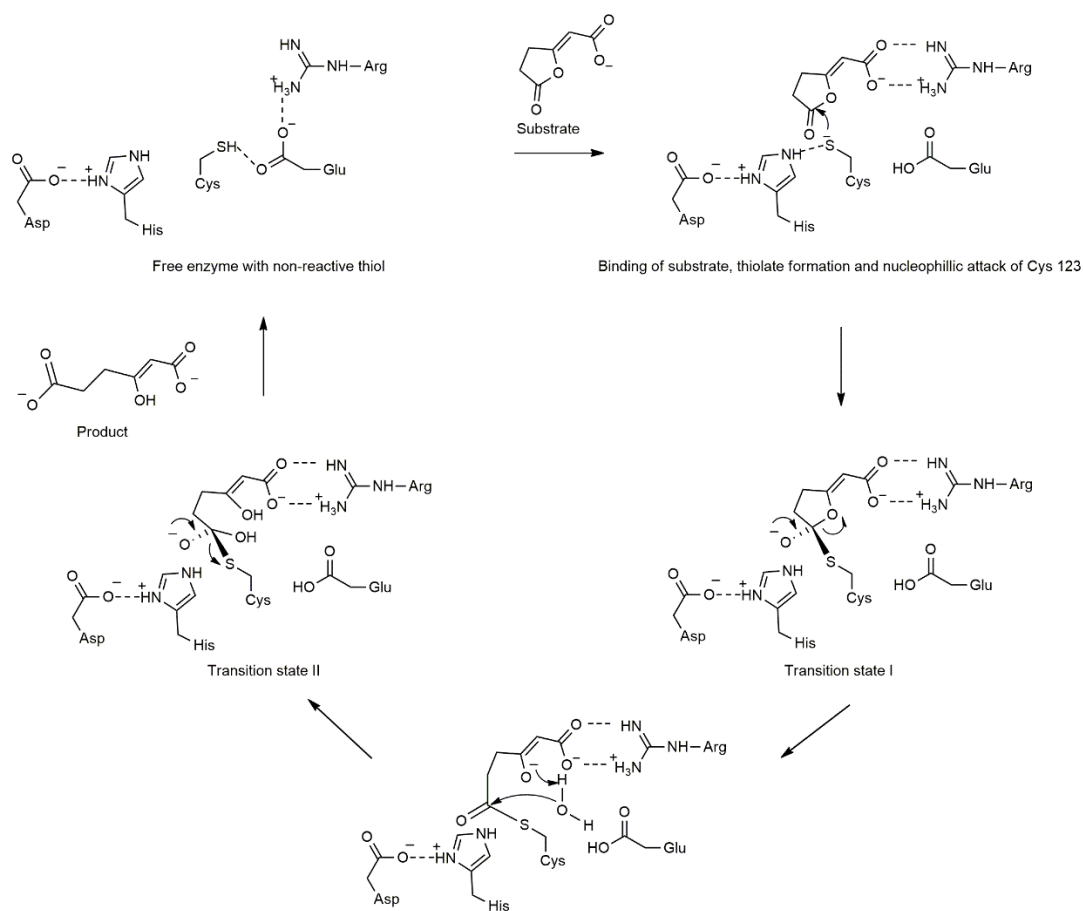


Figure 11. Proposed catalytic mechanism in diene lactone hydrolase of Carboxymethylenebutenolidase (124, 125)

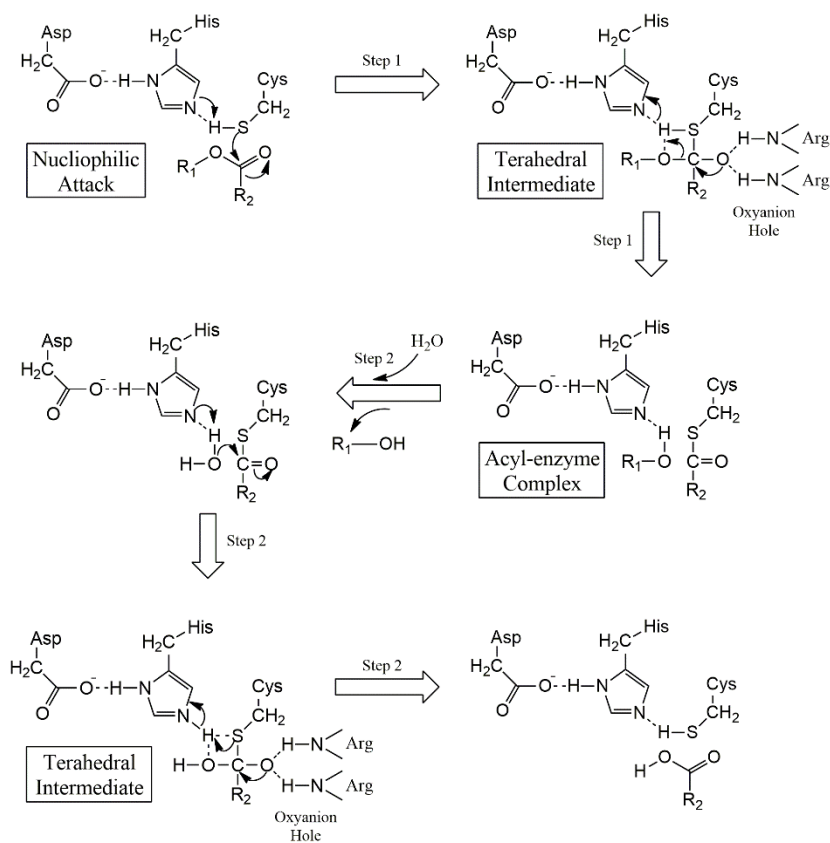


Figure 12. Proposed catalytic mechanism in carboxylic ester hydrolase of Carboxymethylenebutenolidase (124, 126).

2.4.5. Paraoxonase

Paraoxonase (PON) (EC 3.1.8.1) is one of the most important groups of esterases which has three members including Paraoxonase 1 (PON1), Paraoxonase 2 (PON2) and Paraoxonase 3 (PON3). Paraoxonase 1 (PON1) or arylesterase hydrolyzes compounds which are aromatic carboxylic acid esters, organophosphates, organophosphinates, lactones and cyclic carbonate. In fact, PON2 and PON3 have no hydrolytic activity. Both enzymes have an important role in antioxidant properties, providing protection against atherosclerosis and cardiovascular diseases. Human PON1 prominently located in blood where are bound to high density lipoprotein (HDL) and in the microsomal fraction of liver (46). Different from other esterases, paraoxonase requires calcium to exert their activities and stabilities. In human, the activity of PON in liver is lower compared to that in plasma because the calcium concentration in liver is lower (48). Clearly, the residue Cys284 in active PON is not

required for either arylesterase or paraoxonase activities (127), while His115-His134 dyad with two calcium atoms in active site is proposed element for action of PON1 on ester substrates such as phenyl and 2-naphthylacetate (128) (**Figure 13**). The first step is deprotonation of one water molecule by the His-His dyad to generate a hydroxide anion that attacks the carbonyl of ester, forming the oxyanionic tetrahedral intermediate. The second step is that this intermediate break down to an acetate ion and either phenol or 2-naphthol.

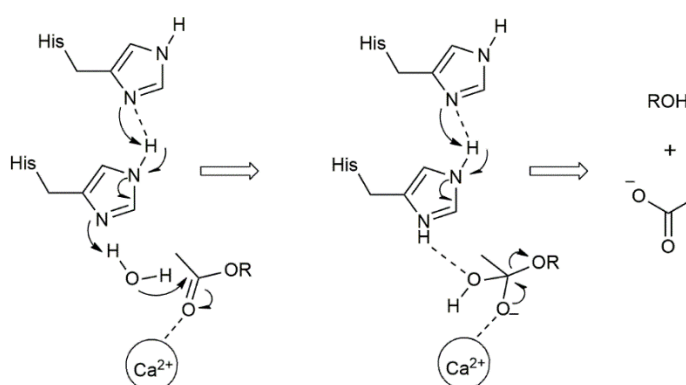


Figure 13. The proposed mechanism of PON1 (128).

Furthermore, in some cases, the hydrolysis of a drug is catalyzed by more than two esterases in various tissues and blood. Predicting the contribution of each esterase to the hydrolysis of drugs in the body is also important (48).

2.5. Enzymes inhibitors

The assignment of metabolizing enzyme is important study in *in vitro* metabolism and in potential clinical consequence. The indirect method using specific enzyme inhibitors is one of the identifications of the enzyme involved in the metabolite formation. Prodrug bioconverted to its pharmacologically active form by esterase enzyme. For identification of hydrolase, the method is preparation by adding hydrolase inhibitors into the incubation with the substrate and liver fractions, and the metabolite formation is quantitative. The several hydrolase inhibitors are categorized into three group including serine, cysteine/thio and histidine-containing esterase inhibitors as the list in **Table 5**.

Table 5. Hydrolase inhibitors to screen responsive enzyme for *in vitro* metabolism study

Enzymes	Inhibitors	Reference
Serine esterase	PMSF, Paraoxon, DFP	(46, 58, 129) (130)
Carboxylesterase	BNPP, Benzil	(131)
Carboxylesterase1	Digitonin	(130) (58)
Carboxylesterase2	Loperamide	(130)
Cholinesterase	Eserine (physostigmine)	(130)
Acetylcholinesterase	BW284c51	(130, 132)
Butyrylcholinesterase	Iso-OMPA	(47)
Cysteine/thio-containing esterase	DTNB	
Carboxymethylenebutenolidase	PCMB	(46)
Histidine esterase (a calcium dependent enzyme)		
Paraoxonase/arylesterase	EDTA	

2.6. *In vitro* metabolism

2.6.1. System of *in vitro* metabolism study

In 2002, a new chemical entity (NCE) developed in U.S. costed approximately one billion USD and only 17 NCEs were approved from US-FDA, which was the lowest approval in last ten years. The main reason for failure of NCEs was due to inadequate metabolic and pharmacokinetic parameters. The data was identified as lack of efficacy and safety. In 2005, pharmaceutical companies start the new strategies of *in vitro* technique to early investigate and predict metabolism of NCEs. The *in vitro* approach in drug metabolism studies has several advantages. Firstly, it allows for determination and development of preferably metabolic properties of NCEs in the early of drug discovery process. Secondly, it can use human cells, liver fraction and enzymes which led to the data that are more relevant to human. Thirdly, it might identify enzyme and its isoform involved in the metabolism

for better understanding of potential role of genetic polymorphism in drug clearance and for prediction of possible drug-drug interactions (133). Lastly, the *in vitro* metabolism is considered to be very simple, easy, fast and cost-effective to perform.

Generally, drug metabolism divided into phase I and II. Phase I involves oxidation, reduction, and hydrolysis. The reactions are catalyzed by various enzymes and the most important enzyme is cytochrome (CYP) P450. The phase II metabolic enzymes are UDP-gucuronyltransferase (UGTs) and sulfotransferase, catalyzing conjugation reactions of various endogenous substrates to lipophilic drugs that previously undergo phase I reaction. However, several drugs can also directly conjugate with endogenous substrates by phase II enzymes without previous involvement of phase I enzymes such as glucuronidation of morphine (133). For phase I hydrolysis, esterases are the most considerable enzymes involving in bioactivation of prodrugs to active drugs (46).

Biotransformation research of a new drug can start with a simple model while the model can become more complex at later stages. The best sequence is to start with microsome and cytosol, then S9 fraction, followed by transfected cell lines and primary hepatocytes, and finally liver slices. Considering drug-drug interactions, the influence of polymorphisms can be studied using different *in vitro* techniques (134). In addition, due to the ease of handling and reproducibility, subcellular fractions including microsome, cytosol and S9 are the beginning models of *in vitro* tools to assess drug metabolism. They are easy to prepare and can be stored for several years. However, the addition of cofactors was required for subcellular fraction activity (135).

Homogenization and differential centrifugation of a liver tissue enable the concentrated source of enzymes available in the S9 fraction, microsome and cytosol (**Figure 14**). Liver S9 fractions, the 9000g supernatant of a liver homogenate,

are obtained during the early step of liver microsomal preparation, and they contain both microsomal and cytosolic fractions (41).

Liver microsomes contain only endoplasmic reticulum subcellular fractions which include prominent cytochrome P450's or CYPs, Uridine 5'-diphosphoglucuronosyltransferase; UGTs), carboxylesterase (CES) (41), paraoxonase (PON) (136), acetylcholinesterase (AChE) and butyrylcholinesterase (BChE) (115, 137), while S9 fractions additional facilitate the cytosolic enzymes such as aldehyde oxidase, xanthine oxidase, sulfotransferases, methyltransferases, N-acetyl transferases, alcohol dehydrogenase, glutathione transferases and carboxymethylenebutenolidase (CMBL) (47, 112) (Table 6).

Table 6. Enzymes in liver subcellular fractions.

Subcellular fractions/ Enzymes	Reaction
Microsome	
Cytochrome P450	Oxidation
Cytochrome P reductase	Reduction
UDP-glucuronosyltransferase, UGT	Glucuronidation
Carboxylesterase, CES	Hydrolysis
Paraoxonase, PON	Hydrolysis
Acetylcholinesterase, AChE	Hydrolysis
Butyrylcholinesterase, BChE	Hydrolysis
Cytosol	
Aldehyde oxidase	Oxidation
Xanthine oxidase	Oxidation
Methyltransferases	Methylation
N-acetyl transferase	Acetylation
Alcohol dehydrogenase	Oxidation and reduction
Sulfotransferases, SULT	Sulfation
Glutathione S-transferases, GST	Glutathionylation
Carboxymethylenebutenolidase, CMBL	Hydrolysis

Therefore, the S9 data set provides researcher with an opportunity to investigate stability of compound in phase I and II. One disadvantage of S9 fractions to microsomal preparations is the dilution of enzymes (41).

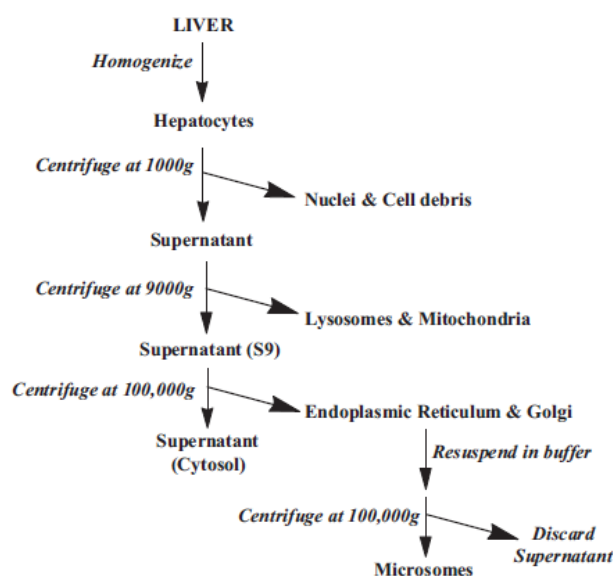


Figure 14. Preparation of liver subcellular fraction.

(obtained from Richardson, Bai (41))

Unlike hepatocytes, S9 fractions require external cofactors such as β -nicotinamide adenine dinucleotide phosphate-regenerating system (NADPH; Phase I oxidation), uridine 5'-diphospho- α -D-glucuronic acid (UDPGA; Phase II glucuronidation), glutathione (GSH; Phase II), and 3'-phosphoadenosine-5'-phosphosulphate (PAPS; Phase II sulfation) for enzyme activity. However, they have a significant cost benefit and are easy to store and use. Thus, they are much more amenable to high throughput screening. Furthermore, they do not have an additional layer of complexity which involves permeability across the hepatocyte cell membrane to gain access to the metabolizing enzymes and can also be easily used in mechanistic studies with inhibitors. The disadvantages, consistent with any cell-free system, include the potential inactivation or lack of some enzymes during preparations, like flavin-monooxygenases (FMO's), loss of cellular compartmentalization and the need for cofactors to be added during incubation (41).

Recently, there are several studies which demonstrate that liver S9 is a robust *in vitro* system. Richardson (2016) reported that liver S9 and hepatocyte performed equally well predicting stability clearance of drugs whereas liver S9 provides the combined benefit of comprehensive and high-quality data at a reasonable expense for *in vitro* metabolism. Nishimuta, Houston (45) observed that compared to hepatocytes, liver S9 reduced prediction bias in high clearance prodrugs. It emphasized that liver S9 applicable used *in vitro* system for investigation of prodrugs.

Different *in vitro* models is able to use at different stages in drug biotransformation research (134). However, there are five basics *in vitro* studies for the characterization of metabolism and metabolic Interactions of potential drugs including metabolic stability, major and minor metabolite identification, including potentially toxic metabolites, metabolite profile, identification of metabolizing enzymes, enzyme inhibition and enzyme induction (135). The first and prominent screening of an NCE is to investigate the metabolic stability (41).

2.6.2. *In vitro* subcellular hepatic metabolism of curcumin

There are several studies of *in vitro* subcellular hepatic metabolism of curcumin. Ireson, Jones (61) studied oxidation, reduction and glucuronidation in microsome and investigated reduction and sulfation in cytosol. The reaction of curcumin with various subcellular fractions of liver in the presence of cofactors is shown in **Table 7**. After curcumin was incubated with microsome or cytosol at 37°C for 90 minutes, the extracted metabolites including hexahydrocurcumin and octahydrocurcumin were found in microsome, but oxidative metabolites were not found.

Table 7. Cofactors used for enzymatic reaction in liver subcellular fractions.

Subcellular fractions	Enzymes	Cofactors	Reference
Microsome			
Oxidation	Cytochrome P450, CYP450	NADPH	(138)
Reduction	Cytochrome P reductase	NADPH	(61)
Glucuronidation	UDP-glucuronosyltransferase, UGT	UDPGA	(60)
Hydrolysis	Carboxylesterase, CES	N/R	(138)
	Butyrylcholinesterase, BChE		
	Acetylcholinesterase, AChE		
	Paraoxonase, PON		
Cytosol			
Reduction	Alcohol dehydrogenase	NADH	(60)
Sulfation	Sulfotransferases, SULT	PAPS	(61)
Glutathionylation	Glutathione S-transferases, GST	N/R	(95)
Hydrolysis	Carboxymethylenebutenolidase,	N/R	(112)
	CMBL		

Note: N/R is not required

For curcumin metabolites in cytosol, curcumin sulfate and reductive major metabolites such as tetrahydrocurcumin, hexahydrocurcumin and octahydrocurcumin were observed. According to enzymes responsible for curcumin metabolism, the reduction of hexahydrocurcumin to octahydrocurcumin has been proposed to be mediated by cytochrome P 450 reductase and alcohol dehydrogenase in microsome and in cytosol, respectively. The SULT1A1 and SULT1A3 enzymes involved in converting curcumin to curcumin sulfate. The SULT1A3 isozyme is more effective in catalyzing the sulfation of curcumin than the SULT1A1 isozyme. Interspecies in *in vitro* metabolism of curcumin demonstrated that hexahydrocurcumin and curcumin glucuronide in human liver microsome, and curcumin sulfate in human liver cytosol were found more than those in rat.

Hoehle, Pfeiffer (60) investigated oxidative and glucuronide metabolites of curcumin in microsome and reductive metabolites in cytosol. In microsome, no oxidative metabolite was found while reductive metabolites including

hexahydrocurcumin and octahydrocurcumin were found. In cytosol, metabolites of curcumin were found as follows: hexahydrocurcumin > tetrahydrocurcumin > octahydrocurcumin > dihydrocurcumin. When curcumin was incubated with cytosol and microsome in the presence of the respective cofactors, curcumin glucuronide together with hexahydrocurcumin, tetrahydrocurcumin and octahydrocurcumin were observed. Three metabolites including dihydrocurcumin, tetrahydrocurcumin and curcumin glucuronide was able to identify using LC-MS/MS when incubated ¹⁸O-labeled curcumin with NADPH and UDPGA in human liver microsome at 37°C for 90 min (139).

The previous *in vitro* study conducted on the glucuronidation of curcumin and hexahydrocurcumin as a major reductive metabolite. Curcumin and hexahydrocurcumin glucuronide were present in rat and human liver microsomes. All UGT isoforms generated the formation of the phenolic glucuronide of curcumin. The human UGT1A1, UGT1A8 and UGT1A10 are the isoform with highest activity for curcumin, whereas UGT1A9, 2B7 and 1A8 exhibited high activities for hexahydrocurcuminoids. The enzyme activity of the glucuronidation of curcumin was 3-fold higher in intestine microsome than in hepatic microsome from human, while no difference was investigated in the microsome from rat (62).

Curcumin is conjugated with glutathione giving the formation of two diastereoisomeric monogluthionyl curcumin conjugates. In the previous study demonstrated that two diastereoisomeric monogluthionyl curcumin conjugates were identified in the incubations with human intestinal and hepatic cytosol or purified human glutathione S-transferase and in human Caco-2 cells. Curcumin monogluthionyl was unstable and degraded with a half-life of about 4 h to curcumin and other unidentified degradation products. The rate of enzymatic conjugation in intestinal and hepatic cytosol was about 4.3 and 9.3 times higher than the chemical formation, respectively. The conjugated formation is involved GSTM1a-1a, GSTA1-1, and/or GSTP1-1 with depending on stereoselective preference.

Curcumin and its GSH conjugates present about 65% in the apical compartment and 35% in the basolateral compartment in Caco-2 cells. The author suggested that curcumin monogluthionyl conjugates can already exist during intestinal transport and are excreted to the intestinal lumen (95).

Curcumin is readily converted to several reductive metabolite and conjugate metabolite with sulfate and glucuronic acid in liver. In previous study, these metabolite formations rate have been investigated in hepatic subcellular fraction of rat and human. After curcumin (100 μM) was incubated for 1 h with hepatic at 37°C, the hexahydrocurcumin and curcumin sulfate formation in rat cytosol were 25 ± 12 and 182 ± 39 $\text{nmol h}^{-1}\text{mg}^{-1}$ protein, respectively, while that in human cytosol were 121 ± 116 and 39 ± 8 $\text{nmol h}^{-1}\text{mg}^{-1}$ protein, respectively. Curcumin glucuronide formation in microsome of rat and human were 980 ± 150 and 94 ± 30 $\text{nmol h}^{-1}\text{mg}^{-1}$ protein (61). Similarly, other study investigated curcuminoid (100 μM) in hepatic microsome for 1 h. the data of curcumin glucuronide formation in rat and human liver microsome were 4,589 and 4,641 $\text{pmol min}^{-1} \text{mg}^{-1}$ protein, respectively (62).

2.7. *In vitro* metabolism of prodrug

In the last decade, there are several studies try to elucidate CES catalytic pathways for ester prodrugs. However, there are some researches overlooked this pathway, leading to the loss of identifying important metabolites. Several studies implied that the enzymatic (carboxylesterase) hydrolysis of prodrug, is faster than CYP450-mediated reactions (52) and the primary metabolites of hydrolysis are generated prior to the formation of oxidative metabolites (59). To clarify *in vitro* metabolism of a new candidate prodrug, metabolic stability, metabolite identification and enzyme identification of hydrolysis pathway were required to perform. The bioanalytical method in this early stage of drug development should focus specificity, linearity, and precision.

2.7.1. Metabolic stability

The use of *in vitro* metabolic stability to predict *in vivo* clearance is a well-accepted procedure. Isolated hepatocytes hepatic microsome and hepatic S9 fraction have been provided as suitable sources for kinetic parameters. Kinetic parameters from either substrate depletion (clearance or half-life) and metabolite formation (V_{max} and K_m) can be used (140, 141). Clearance (CL) is crucial parameter as it provides insight into the rate of metabolism and elimination of the candidate drug from the body. It gives an information of the extent of oral first pass metabolism and the potential routes of elimination (142).

Microsome, S9 and hepatocyte stability assays are the key methods in high-throughput screening of candidate drug leading to the prediction of *in vivo* hepatic clearance. The *in vitro-in vivo* extrapolation approach (IVIVE) incorporated physiological-based scaling factors (PBSFs) to transform the units of *in vitro* clearance to the rate of metabolism per gram of liver (141, 142). Scaling factors of microsome, S9 and hepatocyte were 45 (39), 121 mg/g liver for human, monkey and rat, and 120×10^6 cells/g liver for human, monkey and rat and 240×10^6 cells/g liver for dog (45). The liver weight per kilogram of body weight of human, monkey, dog and rat were 25.7, 30, 32 and 40, respectively (143).

The drug metabolic stability could be interpreted during the drug discovery and development process. Candidate drug with CL_{int} above 45, between 15 and 45 and below 15 $\text{mL min}^{-1} \text{kg}^{-1}$ were classified as high, intermediate, and low clearance compounds, respectively. Compounds with $t_{1/2} > 30$, between 10 and 30 and below 10 min were distinguished as long, moderate, and short half-life compounds, respectively. High CL_{int} and low *in vitro* $t_{1/2}$ values indicated that the compound is trend to rapidly metabolized and low bioavailability *in vivo*. Moreover, the substrate depletion can be categories: very fast (>80%), fast (50-80%), moderate (20-49%), slow, (5-19%) and very slow (<5%) after 15 min (39).

Prodrugs are inactive compounds that commonly contain carboxyl-ester, thio-ester or amide groups, which are subsequently hydrolyzed to active drugs. Therefore, the rate of esterase-catalyzed bioconversion of prodrug affected the pharmacological activity and toxicity of drug. There are several researches on *in vitro* hydrolysis study. Nishimuta, Houston (45) studied hydrolysis clearance of prodrug substrates in human liver S9 (CES1, CES2 and CMBL), intestine (CES2 and CMBL) and kidney (CES2 and CMBL). The source of enzymes was appropriately selected to match prodrug substrates. Intrinsic clearance (CL_{int}) could be calculated from the slope of remaining prodrugs against an incubation time. The results showed that the different CL_{int} of prodrugs depending on their chemical structures, specific responsible enzymes located in tissues and species differences. To predict *in vivo* hepatic clearance, the scaling factor and were used to generate the data (45, 130, 144, 145).

Assessment of metabolic stability in animal species is one of the most important study of new drug. The different *in vitro* animal models in metabolic stability study is the direct interspecies comparison of metabolic rate and metabolic pathway (39, 45, 144, 145). These data aid the selection of a suitable animal model for *in vivo* studies and to identify the appropriate surrogate species to human. In general, the assessment of safety coverage is made based on total exposure metabolite in animals versus humans. While the FDA guidance implies that the similar exposure of the metabolite in human and animals is needed, the ICH M3(R2) Questions and Answers indicate that characterization of metabolite toxicity would be considered adequate when animal exposure is at least 50% of its human exposure (146). The most common strategy is the presence of the major human metabolite at adequate concentrations in one animal species. The toxicity studies with the parent drug should demonstrate adequate metabolite coverage in selected animal (42).

2.7.2. Metabolite identification

Thomsen et al. (2015) pointed out the weakness of a previous study by Takayama (59). Takayama et al. (2014) investigated the metabolites of amide, ester

and AB-PINACA in microsome in the presence or absence of NADPH (138) This made investigators to lose the finding of the major hydrolysis metabolite, namely AB-PINACA-COOH (M1). Therefore, Thomsen, Nielsen (59) set the experiment to observe the metabolite of prodrugs, AB-PINACA, with two incubated systems in human liver microsome (HLM). One system incubated drug with NADPH and the others without NADPH for investigating metabolites in phase I and hydrolysis metabolism, respectively. After incubation, ten metabolites were identified by liquid chromatography quadrupole time-of-flight mass spectrometry (LC-QToF-MS) and quantified by liquid chromatography-tandem mass spectrometry (LC-MS/MS). The report clarified that AB-PINACA-COOH was the major hydrolysis metabolite and it could be a substrate for CYP enzymes to produce mono- and di-hydroxylated metabolites.

2.7.3. Enzyme identification

There are two strategies to identify responsible enzymes for metabolism of drugs. Firstly, ester prodrugs were incubated with recombinant enzymes which are CES1, CES1-b, CES1-c, or CES2. Secondly, substrates were incubated in HLM or S9 with enzyme inhibitors. Many enzyme inhibitors such as benzil (CES inhibitor), BNPP (CES inhibitor), loperamide (CES2 inhibitor), 4-HMB (PON inhibitor) and physostigmine (AADAC, BChE, AChE and CES2 inhibitor) can be used. The data was presented as percentage of control which is the hydrolytic product formation compared to a control without inhibitors (42, 59, 130). Thomsen, Nielsen (59) demonstrated that CES1 was the major enzyme responsible for biotransformation AB-PINACA to its hydrolytic metabolite. Similarly, Fu, Pacyniak (42) identified the major enzyme using recombinant enzymes and enzyme inhibitors. The results provided that CES1-b was the major hydrolyzed enzyme for C2E5. However, Chanteux, Rosa (130) used only enzyme inhibition approach; BNPP (1 mM) as non-specific carboxylesterase inhibitor and loperamide (15 μ M) as a specific CES2 inhibitor were used. They reported that hCES1 was the dominate hydrolysis enzyme for CDP232.

The enzyme identification used chemical inhibitor for observing inhibition effect on specific enzyme with product formation. The strong inhibition effect mean that the enzymes have responsible on substrate catalysis. The condition for study should be optimized the parameters including pH, temperature, ionic strength, substrate and enzyme concentration for observing the rate only in the linear time-dependent formation of the product. The pH and temperature are chosen near the physiological condition of about 7.4 and 37 °C, respectively. Buffer about 0.1 M are suitable concentration for most enzyme assays. The substrate concentration should be saturating whereas the enzyme concentration should be as low as possible, but enough to detect the progressing reaction (147). In addition, the saturating sample could be 10-30% substrate depletion and the linear relationship between amount of enzyme and product formation should be considerate in *in vitro* evaluation of enzyme Inhibition (148).

2.7.4. Interspecies

The selected animal models are important for data submission of the preclinical study to FDA. In the different species, there are various enzyme isoforms with different enzyme distribution and activity. Therefore, the evaluation of interspecies differences in *in vitro* metabolism was required for better understanding the similarity or difference between animal models and human. In previous study, Nishimuta, Houston (45) carried out interspecies differences in the metabolism of ester prodrugs using liver, intestine and kidney S9 from monkey dog and rat compared to that of human. In case of human and dog intestinal S9, hydrolysis intrinsic clearance could not be found for CES1 substrates, but hydrolysis for CES2 substrate was detected in intestine S9 and kidney S9. Intrinsic clearance of liver S9 (CL_{int} , LS9) from monkey and rat are higher than in human, while an opposite trend appeared for dog CL_{int} , LS9.

Fu, Pacyniak (42) studied carboxylesterase-mediated metabolism of C2E5 and compared among intestine S9 and liver S9 metabolism in human, dog, and

rat. The percentages of prodrug remaining and metabolite forming over time in different species were observed and compared. The study found that, for intestinal hydrolysis, C2E4 was the only detected metabolite in human and rat. For hepatic hydrolysis, C2E4 was the major metabolite in human and dog, whereas C2E3 was prominent in rat. These data suggested that the reduction of C2E5 and formation of its metabolite in human was similar to those in dog. Therefore, dog might be the appropriate species for predicting human C2E5 metabolism.



CHAPTER III

MATERIALS AND METHODS

3.1. Materials

3.1.1. Equipment and instruments

- Analytical balance AG245 (Mettler Toledo, Switzerland)
- Barnstead MicroPure water purification system (Thermo Scientific, Germany)
- pH meter SevenCompact S220 (Mettler Toledo, USA)
- Ultra-high performance liquid chromatography Agilent 1290 Infinity II (Agilent Technologies, Germany)
- Liquid chromatography quadrupole time-of-flight mass spectrometry (LC-QTOF-MS): Ultimate 3000 UHPLC (Thermo Scientific, USA) - microTOF-Q II (Bruker, Germany)
- Stuart™ SBH130D Digital dry bath (Keison, UK)
- Microcentrifuge Mikro 22 R (Hettich, Germany)
- Vortex mixer VORTEX GENIE 2 (Scientific industries, USA)
- Transonic Ultrasonic Cleaning (Elma, Germany)
- Freezer Forma Upright Ultra-Low -86°C (Thermo Electron Corporation, USA)
- Refrigerator R-Z350R (Hitachi, Japan)
- Microplate reader CLARIOstar (BMG LABTECH, Germany)
- HPLC column HALO C8 (4.6 mm x 50 mm, 2.7 µM) (Advanced Materials Technology, USA)
- Acquity UPLC BEH C18 column (2.1 x 50 mm, 1.7 µm) (Waters, USA)
- Corning pipettes 0.5-10, 2-20, 20-200 and 100-1,000 µL (Corning, USA)
- Micropipette tips 20, 200, 1,000 and 5,000 µL (Corning, USA)
- Microcentrifuge tubes 1.7 mL (Corning, USA)
- Centrifuge tube 15 mL (Corning, USA)

- 96-well plates flat bottom (Corning, USA)

3.1.2. Chemicals and Reagents

- CDD powder (96.68% purity)
- Curcumin powder (99.49% purity)
- MSCUR (monoethylsuccinyl curcumin) powder (98.63% purity)
- DMC (dimethyl curcumin) powder (98.74% purity)
- Acetonitrile HPLC grade (Burdick & Jackson, Korea)
- Formic acid 98-100% (Merck, Germany)
- Absolute ethanol (Qchemical, Malasia)
- Potassium phosphate dibasic (K₂HPO₄) (Merck, Germany)
- Potassium dihydrogen phosphate (KH₂PO₄) (Merck, Germany)
- Ultrapure water (MicroPure water purification system, Germany)
- Human liver S9 fraction (Gibco, USA)
- Monkey (Cynomolgus) liver S9 fraction (Gibco, USA)
- Dog (Beagle) liver S9 fraction (Gibco, USA)
- Rat (Sprague-Dawley LS9 (Gibco, USA)
- 4-Nitrophenol (Sigma-Aldrich, USA)
- 4-Nitrophenyl acetate (Sigma-Aldrich, USA)
- 4-Nitrophenyl caprylate (Sigma-Aldrich, USA)
- Bis (4-nitrophenyl) phosphate (BNPP) (Sigma-Aldrich, USA)
- Digitonin (Sigma-Aldrich, USA)
- Phenylmethylsulfonyl fluoride (PMSF) (Sigma-Aldrich, USA)
- 1,5-bis (4-allyldimethylammoniumphenyl) pentan-3-one dibromide (BW284c51) (Sigma-Aldrich, USA)
- Tetra (monoisopropyl) pyrophosphortetramide (Iso-OMPA) (Sigma-Aldrich, USA)
- 4-(hydroxymercurio) benzoic acid sodium salt (PCMB) (Sigma-Aldrich, USA)

- 5,5' (dithiobis (2-nitrobenzoic acid) (DTNB) (Sigma-Aldrich, USA)
- Loperamide (Tokyo Chemical Industry, Japan)
- Ethylenediaminetetraacetic acid (EDTA) (Fishere scientific, UK)

CDD (**Figure 6**), curcumin (**Figure 1**), MSCUR and DMC (**Figure 15**) were synthesized and received from our lab (25, 27).

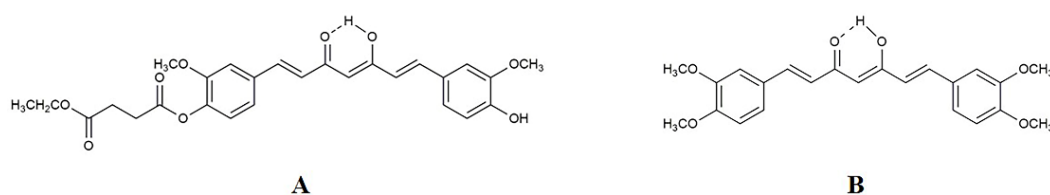


Figure 15. Structure of (A) MSCUR and (B) DMC

The chromatogram and purity of these standard, certification including 4-Nitrophenol, 4-Nitrophenyl acetate, 4-Nitrophenyl caprylate (4-Nitrophenyl caprylate), esterase inhibitors and LS9 of human, monkey, dog and rat were presented in Supporting document (**Appendix A**). Solution preparation for enzyme activity study of LS9 and *in vitro* metabolism study of CDD was described in **Appendix B and C**, respectively.

3.2. Methods

3.2.1. Esterase activity of LS9

The standard enzyme assay was carried out using *p*-nitrophenyl acetate (PNPA) and *p*-nitrophenyl caprylate (PNPC) as a substrate of carboxylesterase and arylesterase or paraoxonase and carboxymethylenebutenolidase (122, 149). Hydrolysis of both substrates to *p*-nitrophenol was determined using a 96 well plate method. The enzyme activity using PNPA and PNPC was determined spectrophotometrically by Microplate reader CLARIOstar because of the release of *p*-nitrophenolate (PNP) by continuously linear increase in absorbance of *p*-nitrophenolate at 405 nm with measurement every 10 sec and over 5 min. The enzyme reaction was started by the addition of 0.1 ml of freshly prepared and

prewarmed PNPA or PNPC (1000 μM in 50mM phosphate buffer pH7.4) to 0.1 mL LS9 (10 $\mu\text{g}/\text{mL}$ in 50mM phosphate buffer pH7.4) at 37°C after a 5-minute preincubation. The final concentration of substrate and LS9 of four test species was 500 μM and 5 $\mu\text{g}/\text{mL}$, respectively. The details of standard curve and sample preparation were described in **Appendix D**. Substrate concentration was greater than or equal to 500 μM was sufficient to achieve a maximum rate of reaction and linearity with time over the assay period (150). The experiment was performed in triplicate. The quantification of PNP was determined by comparing the absorbance with that of a standard curve (1.95-500 μM). The content of PNP in the control mixture incubated without the enzyme was determined. The rate of hydrolysis was determined by subtraction of the hydrolysis rate in control (slope) from that in LS9. Specific activities of enzyme for each substrate were expressed as $\mu\text{mol min}^{-1} \text{mg}^{-1}$ protein (mean \pm SD) and computed using the following equation:

$$\text{Specific activity} = (\text{Slope}_{\text{LS9}} - \text{Slope}_{\text{control}}) (\mu\text{M sec}^{-1}) \times 60 (\text{sec min}^{-1}) \times \frac{1}{1000} (\text{L ml}^{-1}) \times \frac{1}{0.005} (\text{mg mL}^{-1}) \text{ (Eq. 1)}$$

3.2.2. Metabolite identification of CDD in LS9

HLS9, MLS9, DLS9 and RLS9 diluted in 100 mM potassium phosphate buffer pH 7.4 (1 mg protein/mL) were incubated at 37°C in the absence of cofactors due to esterase was not require cofactors for hydrolysis (112, 138). The reaction was initiated by spiking the 49 μL pre-incubated LS9 with 1 μL CDD to a final concentration of 10 μM CDD. The amount of acetonitrile was less than 1%. After 0.5 min of incubation, a 50 μL of the reaction was transferred to 100 μL of ice-cold acetonitrile. The details of standard and sample preparation were described in **Appendix E**. Then, the mixture was vortexed and centrifuged at 14,000 rpm (14,488 g) at 4°C for 10 min. The supernatant was diluted to obtain a final concentration of acetonitrile in water at 50% before being transferred to an HPLC vial and analyzed using LC-QTOF-MS (Thermo Scientific Ultimate 3000 UHPLC-Bruker micrOTOF-Q III) for the identification of metabolites. Blank samples were performed without CDD.

The LC-QTOF-MS conditions were set as previously reported (27). Briefly, the chromatographic system was conducted by using a Dionex Ultimate 3000 UHPLC system (Thermo Scientific, USA). The separation of analytes was performed on an Acquity UPLC BEH C18 column (2.1 x 50 mm, 1.7 μm) at 35°C. An isocratic method consisted of acetonitrile-0.2% formic acid in water (70:30 v/v) at a flow rate of 120 $\mu\text{L min}^{-1}$. The injection volume was 15 μL . The sampling needle was washed with 50% methanol in water between each injection.

The mass spectrometric analysis was conducted in a micrO-TOF-Q II mass spectrometer (Bruker Daltonics, Germany) using positive ion electrospray mode. The ESI mass spectra were recorded over the range of m/z 50-1000 with a spectra rate at 1 Hz. The rolling average mode was activated and set at 2. Mass parameters were set as follows: end plate offset -500V; capillary voltage -4.5 kV; nebulizer pressure 2.5 bar; drying nitrogen gas flow rate 8.0 L min^{-1} , drying nitrogen gas temperature 220°C and $\Delta m/z$ 5 (151). The MS/MS acquisition was set a collision energy set at 20 eV and a mass range 50-1000 m/z .

The internal calibration was applied prior to each sample using the positive ions of the sodium formate cluster. System control, data acquisition and processing were performed using Bruker Compass DataAnalysis 4.0 software. Bruker Smart-Formula software was used to determine the molecular formulae of analytes. The accurate extracted-ion chromatography (the window was 0.005 Da) of CDD (m/z 625.2280). The five proposed metabolites from CDD hydrolysis at M1 (m/z 369.1333), M2 (m/z 497.1806), M3 (597.1966), M4 (569.1653) and M5 (469.1493) were processed (**Appendix F**). The retention time and MS/MS spectra with proposed fragmentation of CDD and metabolites were compared to CDD, curcumin and MSCUR standard.

3.2.3. *In vitro* metabolic stability of CDD in LS9

The metabolic stability of CDD was investigated in HLS9, MLS9, DLS9 and RLS9. The LS9 diluted in 100 mM potassium phosphate at pH 7.4 was pre-incubated at 37 °C for 5 min in the absence of cofactors. The protein concentration in the diluted LS9 was 1 mg/mL for all species. The reaction was initiated by spiking 15 µL CDD into the 735 µL pre-incubated LS9 to obtain a final concentration at 3 µM. The concentration of organic solvent was not greater than 1% for all assays to avoid metabolic effect by organic solvent (45, 55, 147, 148). The details of sample preparation were described in **Appendix E**. The samples were taken at 0.5, 1, 2, 3, 4, 5, 10, 15, 30, 45, 60, 90 and 120 min.

For sample processing, the reaction was terminated by transferring a 50 µL of the incubated samples to 100 µL of ice-cold acetonitrile containing 0.45 µM of DMC (internal standard). The mixture was then vortexed and centrifuged at 14,000 rpm (14,488 g) at 4°C for 10 min. The supernatant was diluted to obtain a final concentration of acetonitrile in water at 50% before being transferred to an HPLC vial for analysis. The sample was analyzed by UHPLC (Agilent series 1290, Agilent Technology, USA).

The UHPLC system consisted of an Agilent series 1290 quaternary pump with an online degasser, autosampler and diode array detector. A mobile phase consisted of 0.1% formic acid in acetonitrile (A) and 0.1% formic acid in water (B) and the mobile phase was filtered through a 0.22 µm Nylon filter (MS[®] Membrane Filters, Membrane solutions, USA) before use. The mobile phase was delivered at a flow rate of 1.2 mL/min in a gradient mode using an elution program as follows: 0-3 min, initial A-B (40:60, v/v); 4.5-7 min, isocratic elution A-B (50:50, v/v); 8.5-11 min, isocratic elution A-B (60:40, v/v) and 12-17 min, isocratic elution A-B (40:60, v/v). Analytes in the samples were separated from LS9 by using a HALO C8 column (4.6 mm x 50 mm, 2.7 µM). The detection was monitored at 400 nm due to

the maximum wavelength of CDD (400 nm), curcumin (427 nm), MSCUR (418 nm) and DMC (421 nm) was nearly 400 nm (**Appendix G**). The column was maintained at 35°C during the run. The injection volume was 20 µL.

Concentrations of CDD, curcumin and MSCUR in the samples were calculated against standard curves. The standard curves of CDD, curcumin and MSCUR were prepared by spiking individual working stock solutions of the compounds to heat-inactivated HLS9, MLS9, DLS9 and RLS9 (80 °C for 20min; 1 mg/mL protein) (1.52-1.54). Standard standards were prepared in microcentrifuge tubes with a total volume of 50 µL and were extracted with a 100 µL of ice-cold acetonitrile containing 0.45 µM of DMC and injected to UHPLC. Peak area ratios of CDD, curcumin and MSCUR to internal standard were computed against concentrations. The method was linear over the concentration ranges of 0.025-4.5 µM, 0.025-4.5 µM and 0.0125-0.75 µM for CDD, curcumin and MSCUR, respectively, with the coefficient of determination (r^2) values of greater than 0.99.

Peak area ratios of CDD, curcumin and MSCUR to the IS were used to calculate the concentrations of each compound in the LS9 samples. The percent content of CDD and its metabolites which is curcumin and MSCUR were plotted against incubation time. The kinetic order for *in vitro* metabolism study was described in **Appendix H**. The percent contents of the CDD versus incubation time plot was fitted to a two-step, consecutive, first-order irreversible reaction as a basic model for prodrug metabolism (155), as shown in Eq (2).



where A = CDD, B = MSCUR and C = curcumin

The following integrated equations for describing the change in amounts of CDD and MSCUR over time are shown below:

$$A = A_0 e^{-k_1 t} \quad (\text{Eq. 3})$$

$$B = \frac{k_1 A_0}{k_2 - k_1} (e^{-k_1 t} - e^{-k_2 t}) \quad (\text{Eq. 4})$$

where A_0 = CDD concentration at time 0, k_1 = degradation rate constant of CDD, and k_2 = degradation rate constant of MSCUR were determined by Eq. 3 and 4, respectively with nonlinear regression analysis using the SOLVER function of Microsoft Excel (156). The half-lives ($t_{1/2}$) were calculated using Eq.5.

$$t_{1/2} = \frac{0.693}{k} \quad (\text{Eq. 5})$$

Intrinsic clearance for *in vitro* ($CL_{\text{int, in vitro}}$) values of CDD in LS9 of the investigated species were calculated using Eq. 6:

$$CL_{\text{int, in vitro}} = k \times \frac{[V]_{\text{incubation}} (\text{ml})}{[P]_{\text{incubation}} (\text{mg protein})} \quad (\text{Eq. 6})$$

where $[V]$ is the incubation volume in ml and $[P]$ is the amount of LS9 used (133).

The intrinsic clearance for *in vivo* ($CL_{\text{int, in vivo}}$) was calculated from $CL_{\text{int, in vitro}}$ values using physiologically based scaling factors described by the following equation:

$$CL_{\text{int, in vivo}} = CL_{\text{int, in vitro}} \times S9 (\text{mg protein/g liver}) \times \frac{\text{Liver weight (g)}}{\text{Body weight (g)}} \quad (\text{Eq. 7})$$

The amount of S9 protein per gram of liver for preclinical species was assumed to be the same as the values reported for humans (121 mg/g) and applied to all species (45). The liver weight per kilogram of body weight for human, monkey, dog and rat were 25.7, 30, 32 and 40, respectively (143). The total intrinsic clearance *in vivo* ($CL_{\text{int, total in vivo}}$) was the sum of $CL_{\text{int, in vivo (CDD)}}$ and $CL_{\text{int, in vivo (MSCUR)}}$.

The predicted hepatic clearance was calculated using the well-stirred model (157) as described by Equation (8):

$$CL_H = \frac{Q_H \times CL_{\text{int, in vivo total}} \times fu_p}{Q_H + (CL_{\text{int, in vivo total}} \times fu_p)} \quad (8)$$

where Q_H = hepatic blood flow of 20, 44, 40 and 70 mL min⁻¹ kg⁻¹ in human, monkey, dog and rat, respectively (145, 157), and fu_p (fraction of unbound CDD in plasma), estimated at 0.0594, was derived from the Equation 9 (9, 158):

$$\log K = \log \left(\frac{1 - fu_p}{fu_p} \right) \quad (9)$$

where $\log K$ = the transformation of fu_p into a pseudo equilibrium constant; fu_p = the fraction unbound CDD in plasma. CDD is a neutral compound with $\log P$ of 2.55 (9). The $\log K$ value for a neutral compound with $\log P < 3$ is approximately 1.2 (158). The fraction unbound CDD in plasma (fu_p) was 0.0594. More than 90 % of CDD were bound to plasma proteins, indicating that CDD had a high protein binding property.

3.2.4. Enzyme identification of CDD hydrolysis in LS9

The identification of hepatic esterases involved in the hydrolytic cleavage of CDD at 3 μM in LS9 of the tested species was conducted by using chemical inhibitors. The condition of experiment was optimized before the observation of the esterase inhibitors effect on CDD hydrolysis in HLS9, MLS9, DLS9 and RLS9.

3.2.4.1. Optimization of condition for enzyme identification in LS9

The LS9 of each four tested species diluted in 100 mM potassium phosphate buffer pH 7.4 (0.01, 0.02, 0.05 and 0.1 mg/mL) were incubated at 37°C in

the absence of cofactors for 5 min. The reaction was initiated by adding CDD at 3 μ M into the incubated the LS9 of each tested species. The details of sample preparation were described in **Appendix E**. The samples were taken at 0.5, 1, 2, 3, 4, 5, 10, 15, 30, 45, 60 min. Each sample was processed as described in section 3.2.3 and analyzed by UHPLC. The peak area ratio of CDD and curcumin to IS was investigated and the percent remaining of CDD and percent formation of curcumin vs. time were plotted.

Then, the reaction condition for enzyme identification study was selected within a linear relationship between the percentage of curcumin formation and time. The experimental conditions were optimized to follow zero-order kinetics (**Appendix I**). CDD was present in an excess amount to ensure that the reaction was independent of substrate concentration and the formation of curcumin over the incubation time depended on the level of enzymes presented (147).

3.2.4.2. Effect of esterase inhibitors on CDD hydrolysis in LS9

Esterase inhibitors BNPP, digitonin, loperamide, PMSF, BW284c51, Iso-OMPA, PCMB, DTNB and EDTA were introduced into the incubation samples of LS9 with CDD to examine the responsible enzymes in CDD hydrolysis. The inhibitor structures are shown in **Appendix J**. The study focused on identification of carboxylesterase, cholinesterase, carboxymethylenebutenolidase and paraoxonase. PMSF was used as serine esterase inhibition (58) and subgroup inhibitors of serine esterase including BNPP, carboxylesterase inhibitor (130, 159); digitonin, carboxylesterase 1 inhibitor (131); loperamide, carboxylesterase 2 inhibitor; BW284c51, acetylcholinesterase inhibitor and Iso-OMPA, butyrylcholinesterase inhibitor (130). DTNB was used as inhibitor of cysteine esterase (130, 132) with PCMB, specific carboxymethylenebutenolidase inhibitor (47). EDTA was used as paraoxonase inhibitor (46).

Esterase Inhibitors were used as the final concentration of 100 μM , except for 1 mM for EDTA were pre-incubated individually with HLS9, MLS9, DLS9 and RLS9 diluted in 100 mM potassium phosphate buffer pH 7.4 for 30 min at 37°C in the absence of cofactors. The concentration of esterase inhibitor was consistent with the previous study point that chemical inhibitory effect on enzyme hydrolysis at 100 μM almost present in the report of enzyme identification (42, 58, 131, 159). The reaction was initiated by adding the CDD solution into the pre-incubated LS9 to obtain a final concentration of 3 μM . The total incubation volume was 50 μL . The details of sample preparation were described in **Appendix E**. After 0.5 or 1 min, the samples were extracted before UHPLC analysis for determining the appearance of curcumin concentration as described in section 3.2.3. The formation of curcumin was quantitated against a standard curve (0.025-4.5 μM). The experiment was performed in triplicate, including inhibitor-free control (incubation in the absence of inhibitor), enzyme-free control (incubation in the absence of enzymes) and the organic solvent-free control (incubation of CDD in the absence of organic solvent used in inhibitor solution preparation). The final concentration of organic solvent in all the incubation mixture was within 2% (130).

The curcumin formation rate and relative curcumin formation rate were calculated using Eq. 10 and Eq. 11 (59, 129, 130, 147).

$$\text{Curcumin formation rate (nmol min}^{-1} \text{ mg}^{-1}) = \frac{\text{Curcumin content } (\mu\text{M}) - \text{Enzyme-free control}}{\text{Incubation time} \times \text{LS9 protein content in mixture}} \quad (\text{Eq. 10})$$

$$\text{Relative curcumin formation rate (\%)} = \frac{\text{Curcumin formation rate}}{\text{Curcumin formation rate of inhibitor-free control}} \times 100 \quad (\text{Eq. 11})$$

The classification of enzymatic inhibition can be described as following (148):

- A strong inhibition: relative curcumin formation rate of < 20%

- A moderate inhibition: relative curcumin formation rate of 20-49%
- A weak inhibition: relative curcumin formation rate of 50-80%
- No inhibition: relative curcumin formation rate of > 80%

Statistical analyses were performed using one-way analysis of variance followed by Dunnett's test using IBM SPSS Statistics for Windows, Version 22.0 (IBM Corp., Armonk, NY) (130).



CHAPTER IV

RESULTS

4.1. Esterase activity in LS9

The mean activities of esterase from the PNPA and PNPC hydrolysis in HLS9, MLS9, DLS9 and RLS9 were shown in **Table 8**. The UV spectrum, standard curve of PNP and raw data were showed in **Appendix K**.

PNPA hydrolysis in LS9 fraction was higher than PNPC in all species due to PNPC has longer chain than PNPA. The rate of PNPA hydrolysis in LS9 fraction are in the following order: rat>dog>human>monkey. The rate of PNPA hydrolysis obtained from DLS9 and RLS9 are approximately 2.3 and 3.0-folds higher than that of HLS9, respectively, while the rate from monkey is 0.8-fold lower than the rate of PNPA hydrolysis from human. In contrast, the rate of PNPC hydrolysis in LS9 fraction are in the following order: dog>rat>monkey>human. The rate of PNPC hydrolysis in HLS9 is lower than in MLS9, RLS9 and DLS9 for 1.7-, 3.3-, and 3.3-fold, respectively. The results indicated the presence of the esterase activities in HLS9, MLS9, DLS9 and RLS9 and the suitability of all liver test species to conduct further *in vitro* metabolism studies.

Table 8. Specific activity of 0.5 mM p-nitrophenyl acetate and p-nitrophenyl caprylate hydrolysis in HLS9, MLS9, DLS9 and RLS9 ($\mu\text{mole min}^{-1} \text{mg}^{-1}$).

Substrate	Human	Monkey	Dog	Rat
PNPA	2.20 \pm 0.08	1.79 \pm 0.08	5.01 \pm 0.12	6.51 \pm 0.17
PNPC	0.56 \pm 0.02	0.93 \pm 0.02	1.83 \pm 0.03	1.81 \pm 0.03

4.2. Metabolite identification of CDD in LS9

Unknown metabolites generated after incubating CDD in HLS9, MLS9, DLS9 and RLS9 were identified using LC-QTOF-MS operated in a positive ion mode and confirmed by standard. The extraction in chromatogram shows peak of CDD at 3.6 min (**Figure 16**), while the other two unknown peaks, assigned as M1 and M2, had

the retention time at 1.7 and 2.3 min, respectively, compared with blank LS9 (Figure 17).

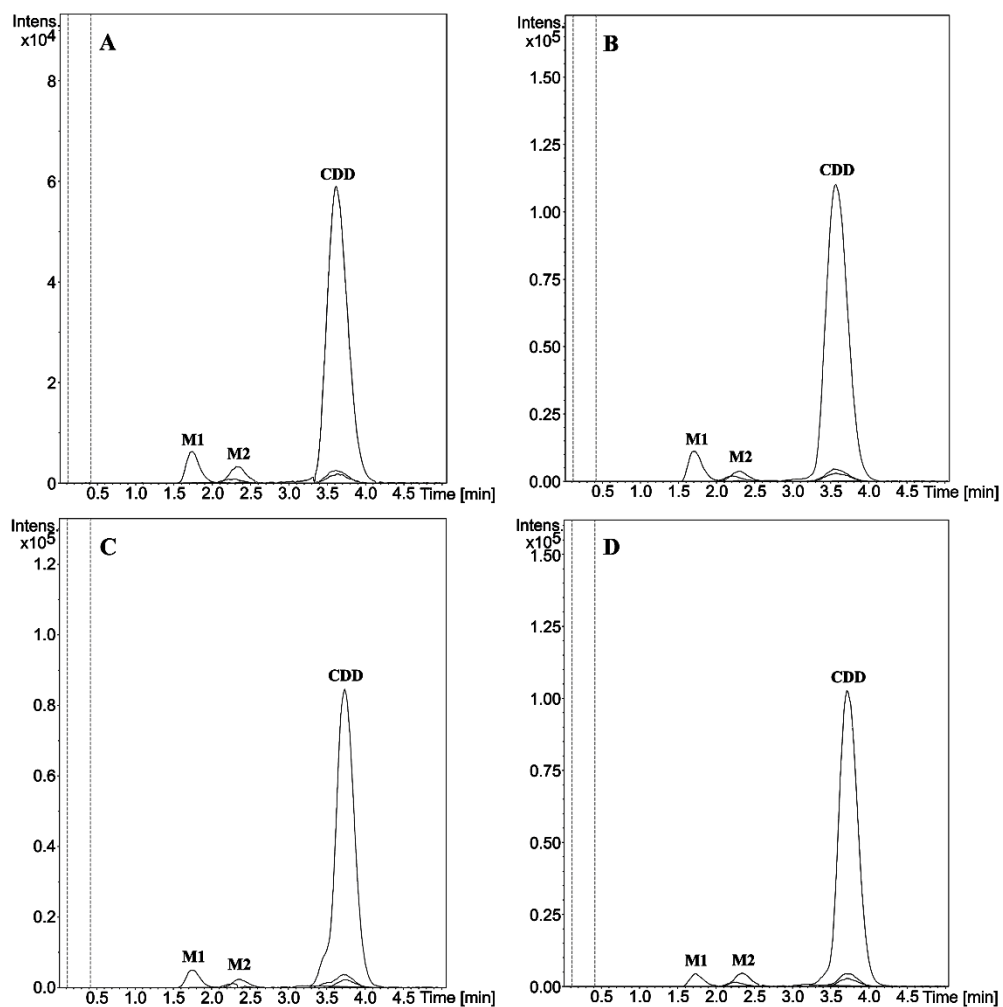


Figure 16. Extracted-ion chromatograms of CDD (625.2280), M1 (369.1333) and M2 (497.1806) after CDD at 10 μ M incubation in (A) HLS9, (B) MLS9, (C) DLS9 and (D) RLS9 for 0.5 min.

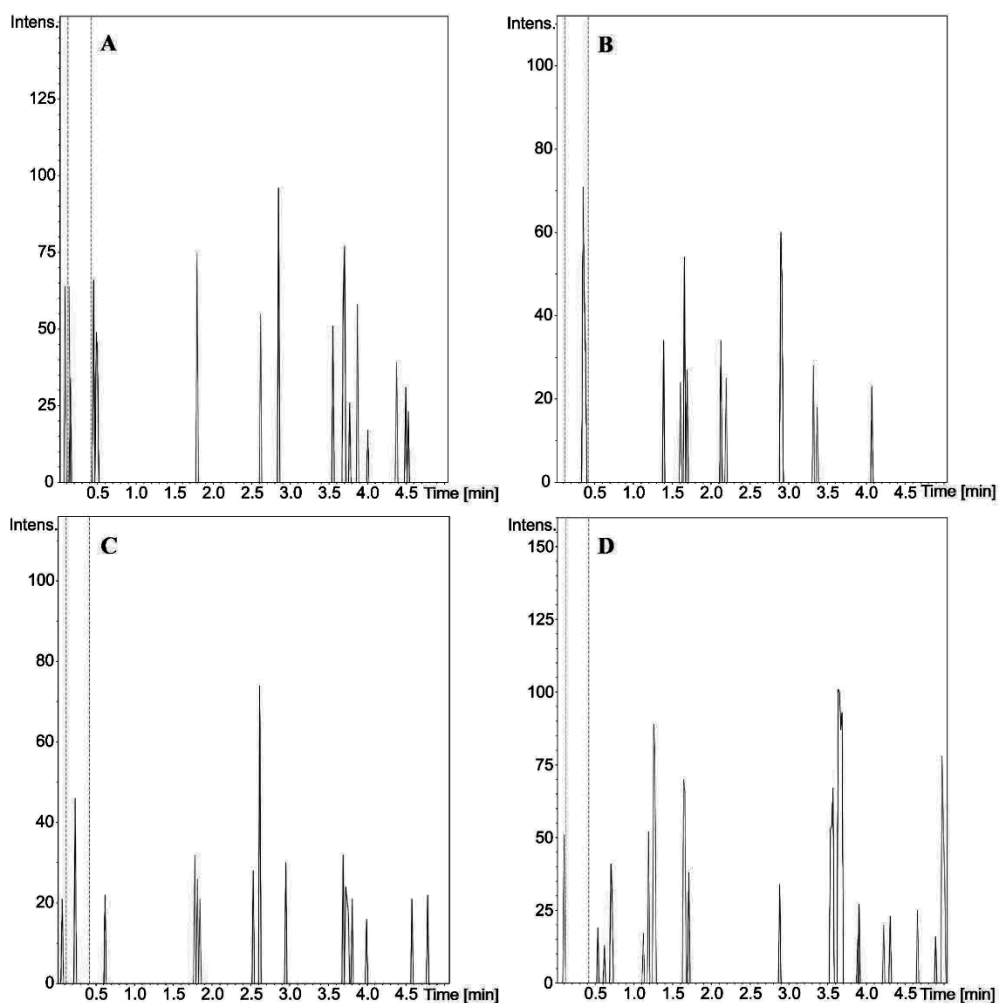


Figure 17. Extracted-ion chromatograms of CDD (625.2280), M1 (369.1333) and M2 (497.1806) after incubation without CDD in (A) HLS9, (B) MLS9, (C) DLS9 and (D) RLS9 for 0.5 min.

The molecular ion of M1, $[M1 + H]^+$, were observed at m/z 369.1327, 369.1331, 369.1336, and 369.1332 in HLS9, MLS9, DLS9 and RLS9, respectively (**Table 9**). The M2 had a different molecular ion $[M2 + H]^+$ from M1 which exhibited molecular ion at m/z 497.1809, 497.1811, 497.1797 and 497.1809 in HLS9, MLS9, DLS9 and RLS9, respectively. However, the mass of others proposed metabolites with m/z 597.1966, 569.1653 and 469.1493 were not found.

Table 9. LC-QTOF-MS/MS data of CDD, M1 and M2 after incubation in HLS9, MLS9, DLS9 and RLS9.

ID	Species	RT (min)	Elemental composition	Theoretical mass (m/z)	Measured mass (m/z)	Error (ppm)	Product ions (m/z)
CDD	Standard	3.60	C ₃₃ H ₃₇ O ₁₂	625.2280	625.2282	0.4	129.0533, 177.0543, 369.1292, 497.1820
Curcumin	Standard	1.70	C ₂₁ H ₂₁ O ₆	369.1333	369.1331	0.6	177.0547, 285.1136
MSCUR	Standard	2.32	C ₂₇ H ₂₉ O ₉	497.1806	497.1807	0.2	129.0532, 177.0543, 369.1338
M1	HLS9	1.74	C ₂₁ H ₂₁ O ₆	369.1333	369.1327	1.7	177.0550, 285.1140
	MLS9	1.71	C ₂₁ H ₂₁ O ₆	369.1333	369.1331	0.4	177.0563, 285.1145
	DLS9	1.74	C ₂₁ H ₂₁ O ₆	369.1333	369.1336	1.0	177.0574, 285.1147
	RLS9	1.73	C ₂₁ H ₂₁ O ₆	369.1333	369.1332	0.2	177.0569, 285.1122
M2	HLS9	2.32	C ₂₇ H ₂₉ O ₉	497.1806	497.1809	0.5	129.0542, 177.0538, 369.1324
	MLS9	2.30	C ₂₇ H ₂₉ O ₉	497.1806	497.1811	1.0	129.0543, 177.0572, 369.1344
	DLS9	2.35	C ₂₇ H ₂₉ O ₉	497.1806	497.1797	1.8	129.0537, 177.0539, 369.1313
	RLS9	2.34	C ₂₇ H ₂₉ O ₉	497.1806	497.1809	0.5	129.0546, 177.0540, 369.1364

A difference in m/z value between CDD, parent compound, and M1 and M2 were determined. The M1 metabolite m/z 369 corresponded to the loss from CDD of m/z 256 Da attributed to hydrolysis of di-ethylsuccinyl group adjacent to the phenolic functional group. The M2 metabolite m/z 497 corresponded to the loss of mono-ethylsuccinyl moiety at m/z 128 Da from the parent.

The MS/MS spectrum of M1 and M2 presented different fragmentation pattern (**Table 9**). The fragmentation pattern of M1 and M2 was the same in HLS9, MLS9, DLS9 and RLS9. The fragmentation of M1 generated product ions m/z 177 and 285 (**Figure 18**), while that of M2 was characterized product ion at m/z 129, 177 and 369 (**Figure 19**).

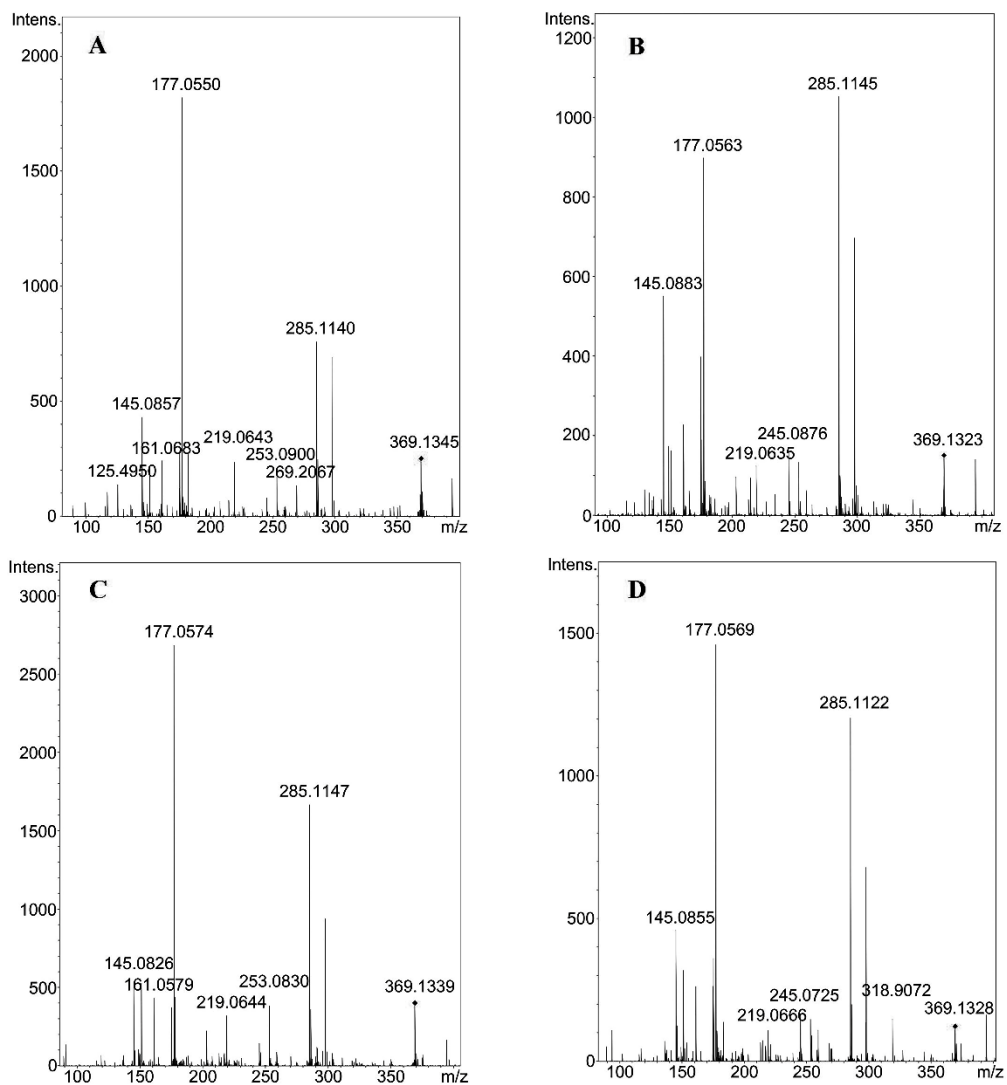


Figure 18. MS/MS spectrum of M1 in (A) HLS9, (B) MLS9, (C) DLS9 and (D) RLS9

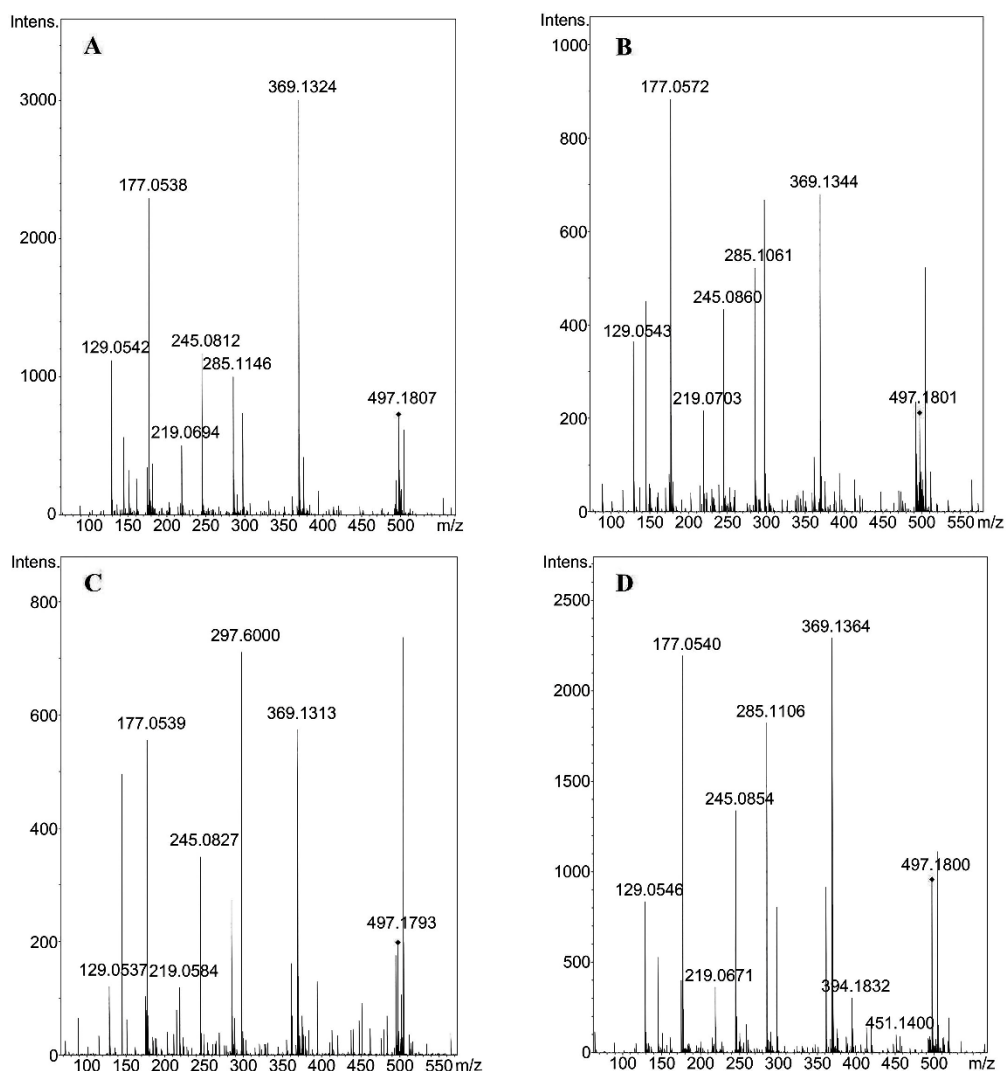


Figure 19. MS/MS spectrum of M2 in (A) HLS9, (B) MLS9, (C) DLS9 and (D) RLS9

CHULALONGKORN UNIVERSITY

The EIC and MS/MS spectra of CDD were showed in **Figure 20** and **Figure 21**, respectively. The curcumin and MSCUR standard were used to identify the M1 and M2 metabolite, respectively. The retention time of M1 and M2 was similar to that of curcumin and MSCUR, respectively, when running under the same LC condition (**Table 9**, **Figure 20**). The MS/MS spectrum of M1 and M2 produced the same fragmentation patterns as curcumin and MSCUR standard, respectively (**Figure 21**). The possible proposed fragmentation of curcumin and MSCUR was showed in **Figure 22**. Therefore, the M1 and M2 metabolite were elucidated as the structure of curcumin and MSCUR, respectively.

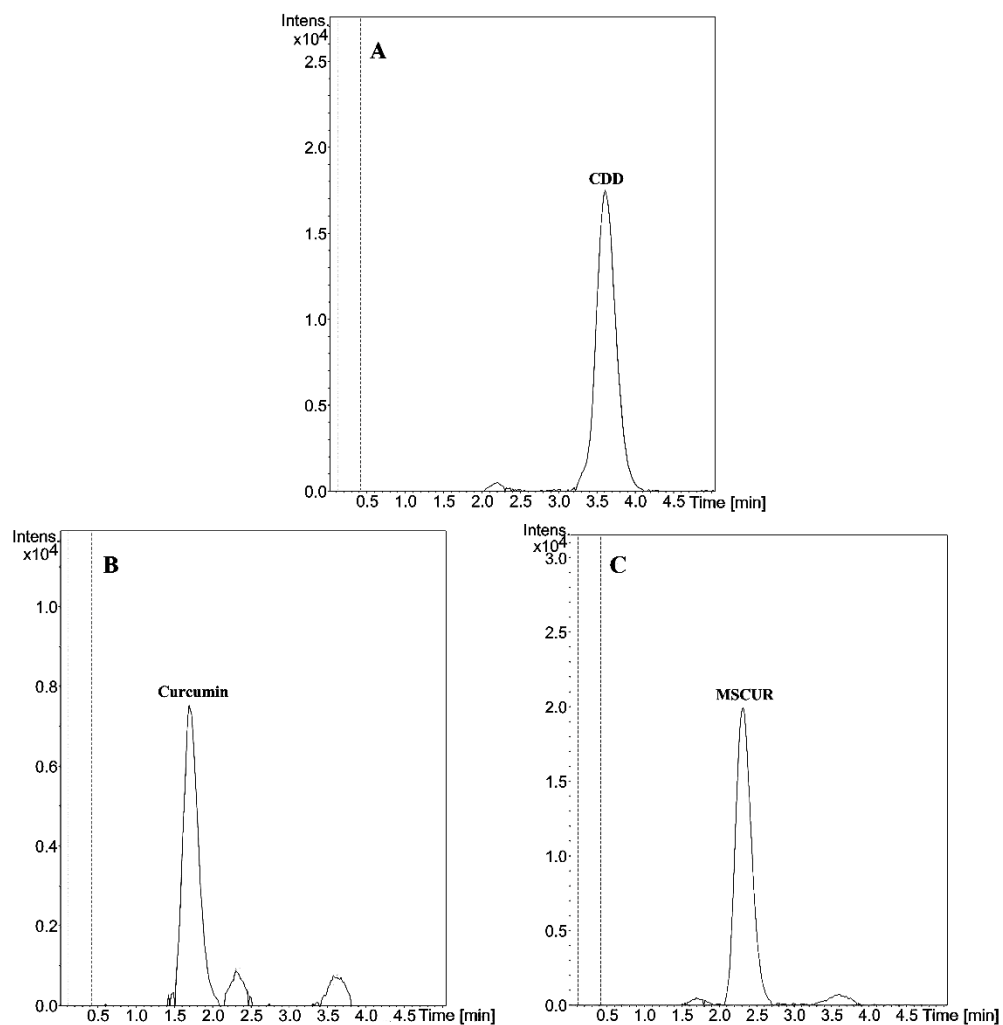


Figure 20. Extracted-ion chromatograms of (A) CDD (m/z 625.2280), (B) curcumin (m/z 369.1333) and (C) MSCUR (m/z 497.1806) standard.

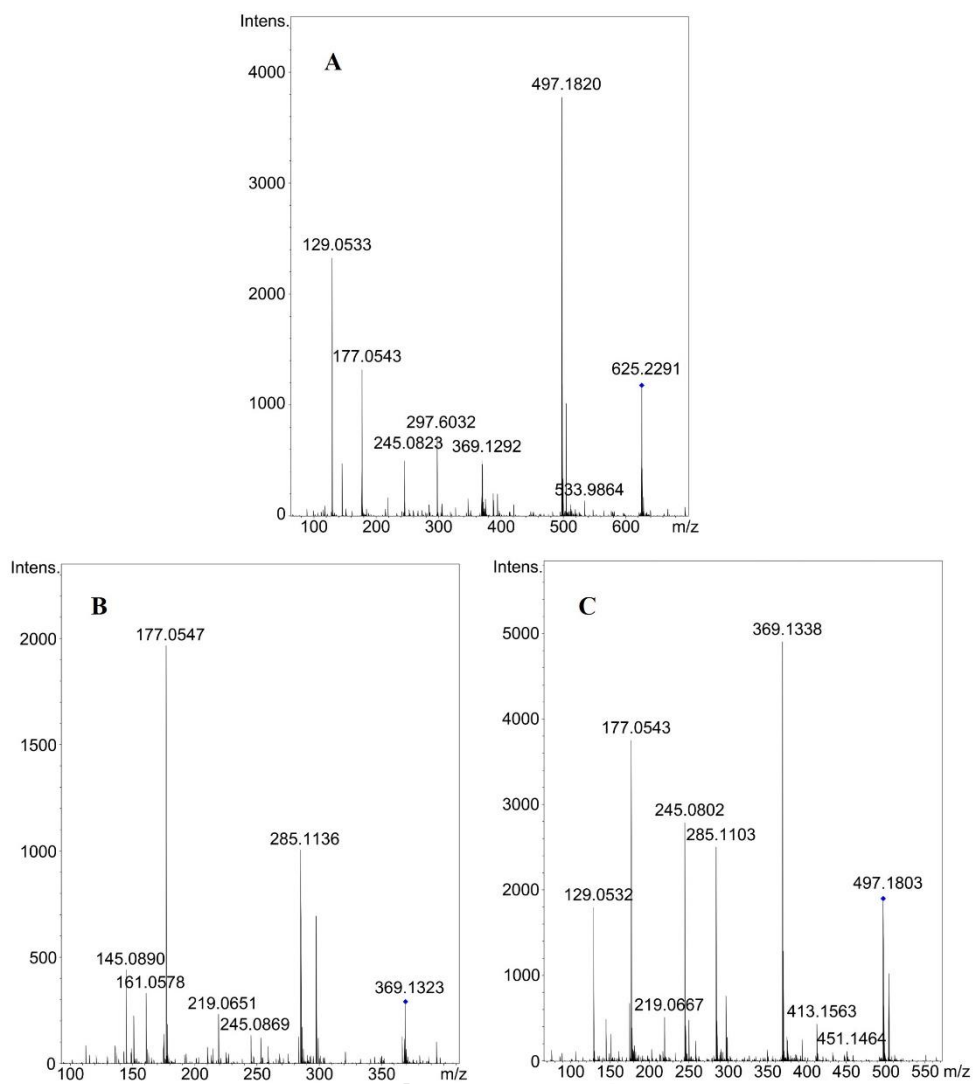


Figure 21. MS/MS spectrum of (A) CDD, (B) curcumin and (C) MSCUR standard.

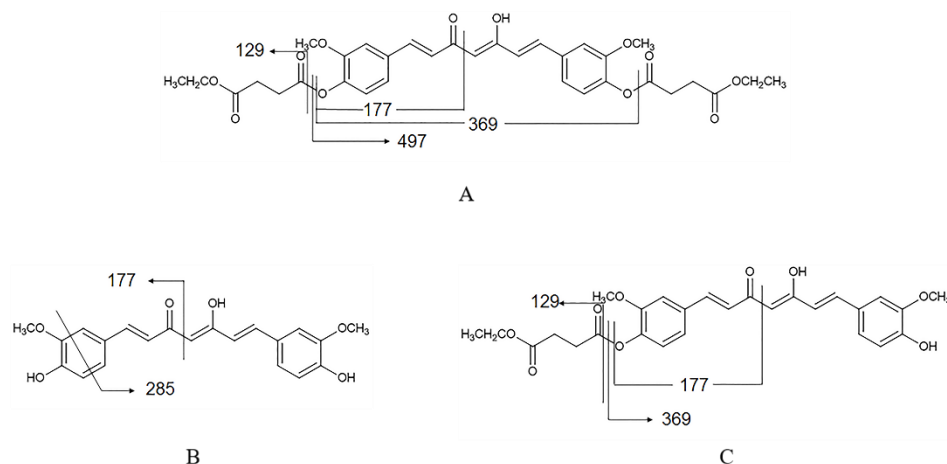


Figure 22. Proposed fragmentation of (A) CDD, (B) curcumin and (C) MSCUR.

4.3. *In vitro* metabolic stability of CDD in LS9

UHPLC/DAD chromatograms of CDD and its metabolites following incubation of CDD with HLS9, MLS9, DLS9 and RLS9 were depicted in **Figure 23**. CDD and DMC were showed at 9.8 min and 5.7 min, respectively. The peak with a retention time of 9.5 min (Figure 23) is a tautomer of CDD, keto form, as it exhibited the same mass-to-charge ratio as CDD (m/z 625.2279, mass error = 0.1 ppm) (27, 28, 75, 160).

M1 and M2 metabolites were formed and observed in LS9 samples of all tested species with the retention times at 2.5 and 6.3 min, respectively. These peaks were not found in blanks of HLS9, MLS9, DLS9 and RLS9 without CDD (**Figure 24**).

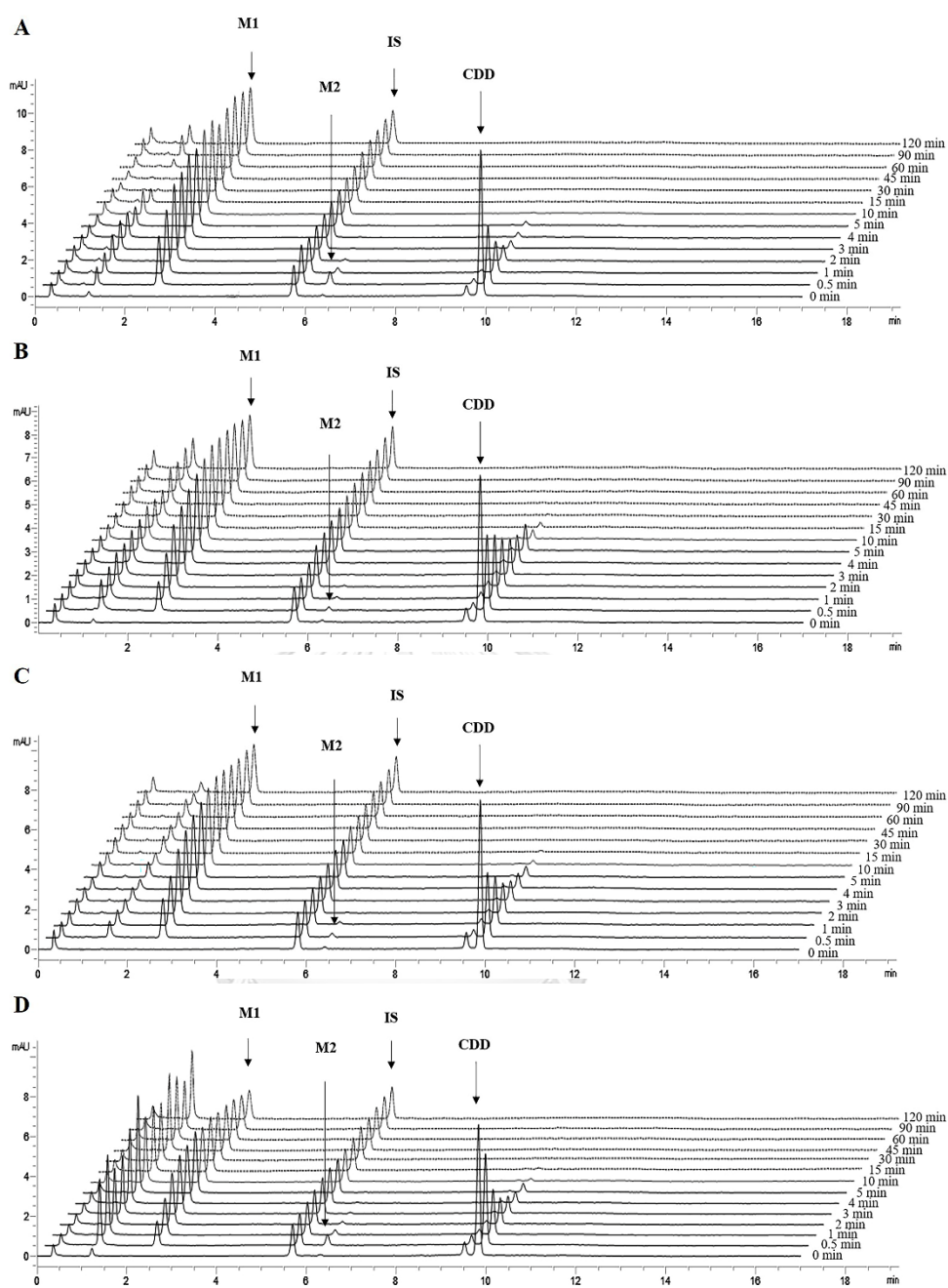


Figure 23. Representative chromatograms of CDD and metabolites in (A) HLS9, (B) MLS9, (C) DLS9, and (D) RLS9. After incubation CDD with HLS9, MLS9, DLS9 and RLS9 at 37°C, Aliquots were taken at 0.5, 1, 2, 3, 4, 5, 10, 15, 30, 45, 60, 90, 120 min and analyzed for concentration of CDD, M1 and M2. Peak: 1 = M1

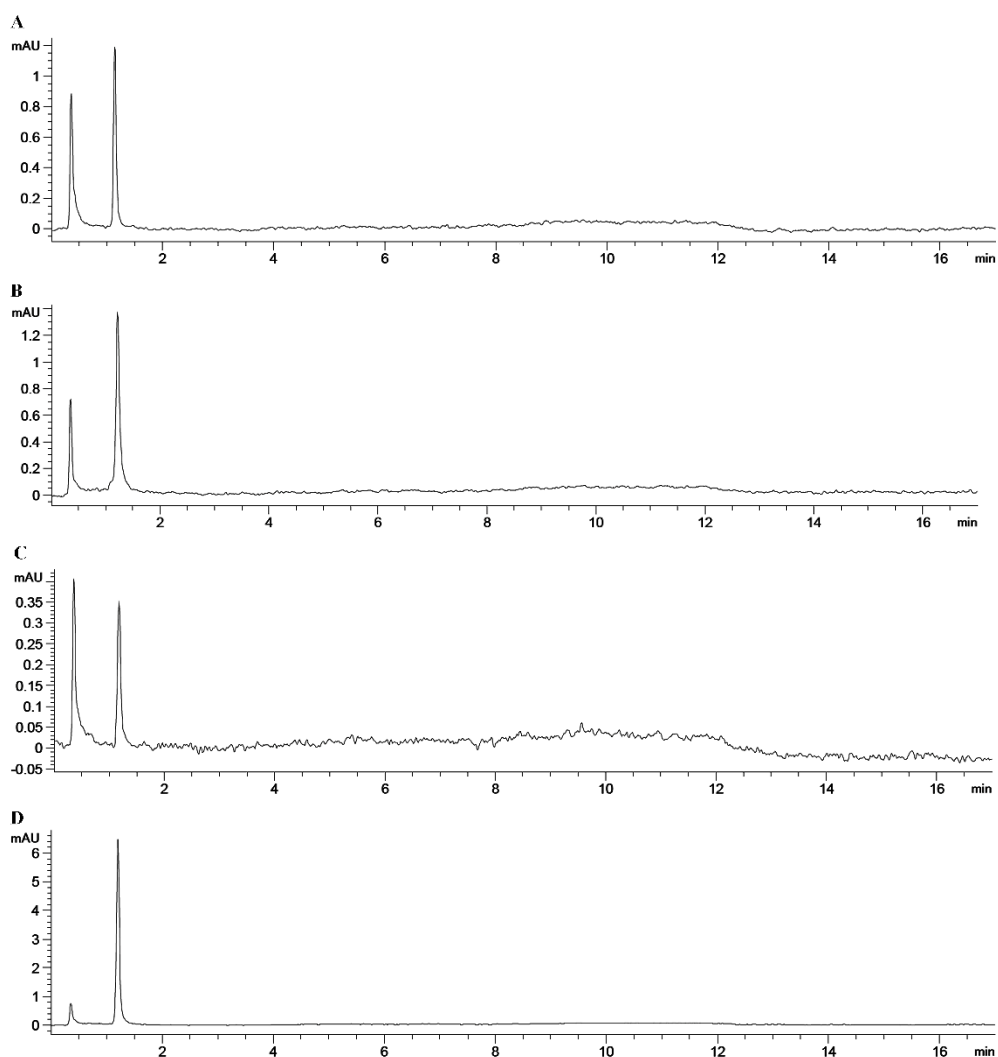


Figure 24. Representative chromatograms of blank: (A) HLS9, (B) MLS9, (C) DLS9 and (D) RLS9. After incubating HLS9, MLS9, DLS9 and RLS9 without CDD at 37°C for 120 min and analyzed by HPLC. The chromatogram of each blank LS9 appeared prior to 2 min and had no metabolites in blank.

The standard contained CDD, curcumin, MSCUR and DMC was analyzed to confirm M1 and M2 metabolites by UHPLC. The curcumin and MSCUR standard were used to characterized M1 and M2. The result indicated that curcumin and MSCUR standard was eluted at the same time as M1 and M2, respectively (**Figure 25**). Thus, M1 and M2 were determined as curcumin and MSCUR, respectively.

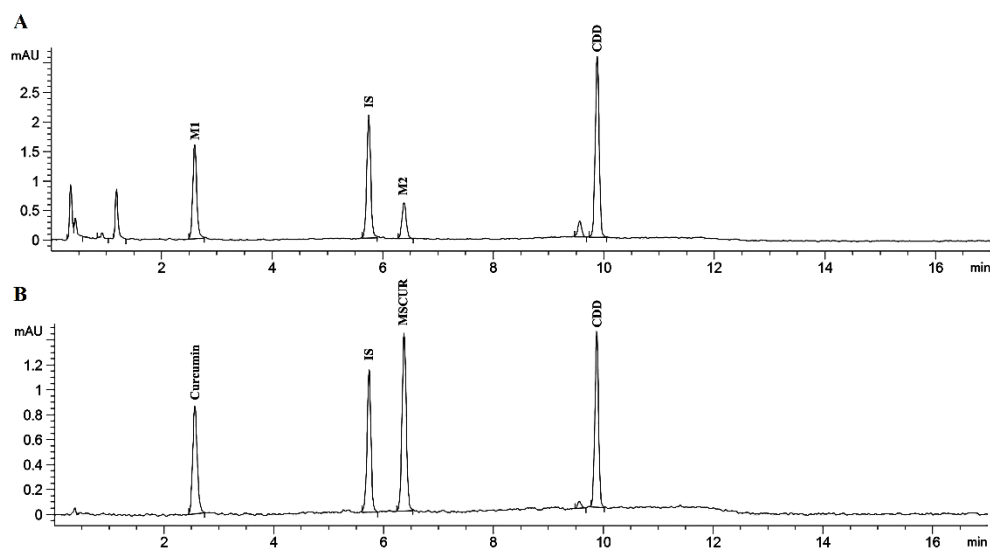


Figure 25. Representative (A) chromatogram of CDD after incubation with HLS9 at 37 °C for 0.5 min (B) chromatogram of standard CDD, curcumin, MSCUR and DMC (IS) with each concentration at 0.15 μM .

The metabolic stability-time profiles of CDD, and the percent content of CDD (%Total) -time profiles of M1 (curcumin) and M2 (MSCUR) showed similar pattern and content among the HLS9, MLS9, DLS9 and RLS9 (**Figure 26**). The metabolic profiles expressed the consecutive hydrolysis of CDD to M1 through M2 intermediate metabolites. The depletion of CDD in LS9 of all test species resulted in the formation of M1, major metabolite and M2, a small quantity metabolite. After addition of CDD in HLS9, MLS9, DLS9 and RLS9, CDD rapidly and completely hydrolyzed which more than 95% of CDD were hydrolyzed with in the first 15 min. Simultaneously, the M1 was produced maximum content with nearly 70% detected in each LS9 species after incubation for 15 min. The content of curcumin decreased by 20% and 30% over 15 to 120 min. The maximum level of M2 metabolite approximately 10% were formed at 0.5 min of incubation and decreased afterward.

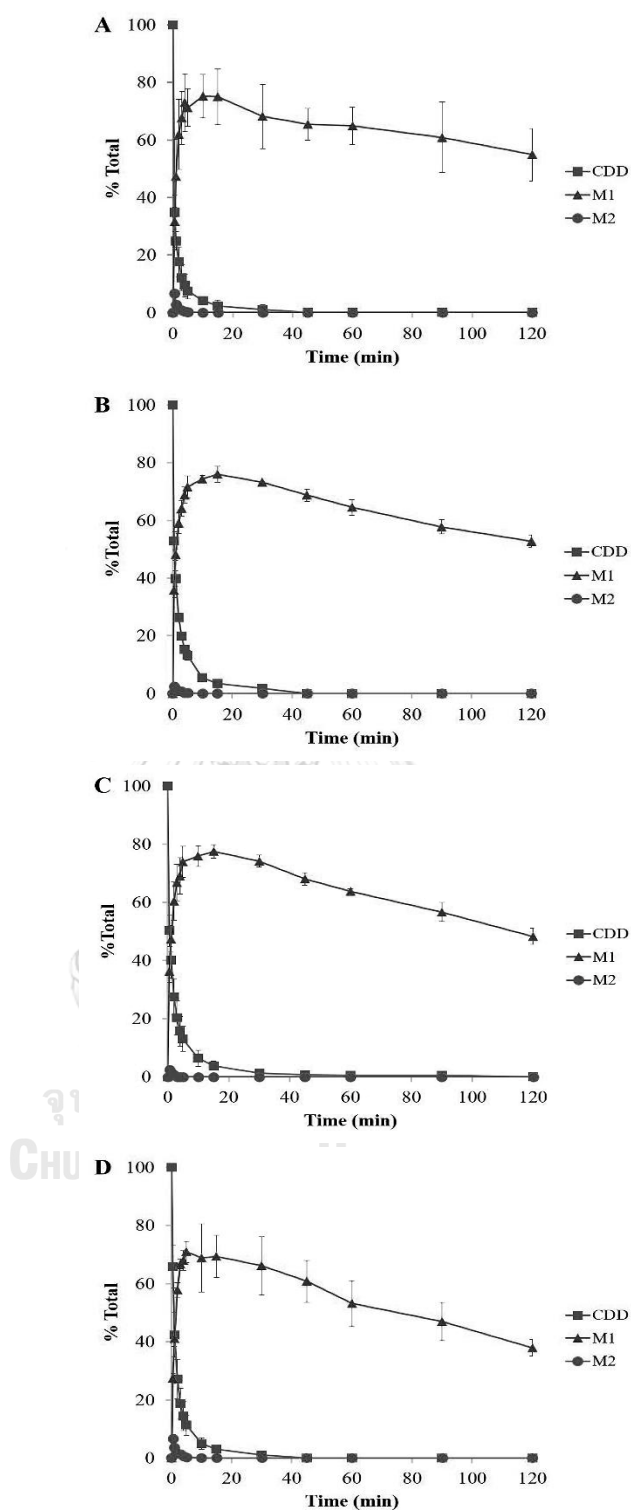


Figure 26. Percent CDD and its metabolites-time profiles in (A) HLS9, (B) MLS9, (C) DLS9 and (D) RLS9 as a function of incubation time. The incubation mixtures contained CDD and HLS9, MLS9, DLS9 and RLS9 at 37 °C

The metabolic stability data was processed statistical pseudo-first-order kinetic analysis based on best fit of linear least-squares regression or non-linear least squares regression. The statistical data indicated that linear least-square analysis was not good fit with R^2 less than 0.8539 (**Appendix H**). Nonlinear least-squares has been suggested for curve-fitting the kinetics of two-step consecutive pseudo-first order instead due to R^2 was around 0.9 and all observed value lie within the 95% confident level.

The kinetic parameters including the degradation rate constants of CDD (k_1), degradation rate constants of MSCUR (k_2), $t_{1/2}$ of CDD ($t_{1/2}$ (CDD)), $t_{1/2}$ of MSCUR ($t_{1/2}$ (MSCUR)), $CL_{int, in vitro}$ of CDD ($CL_{int, in vitro}$ (CDD)), $CL_{int, in vitro}$ of M2 ($CL_{int, in vitro}$ (MSCUR)), $CL_{int, in vivo}$ of CDD ($CL_{int, in vivo}$ (CDD)), $CL_{int, in vivo}$ of MSCUR ($CL_{int, in vivo}$ (MSCUR)) and $CL_{int, in vivo total}$ obtained from the metabolism of CDD in HLS9, MLS9, DLS9, and RLS9 were determined and summarized in **Table 10**.

Table 10. Kinetic parameters for hepatic metabolism of CDD and MSCUR in the LS9 of human, monkey, dog and rat.

Parameters	Human	Monkey	Dog	Rat
k_1 (CDD) (min^{-1})	1.51 ± 0.22	0.81 ± 0.13	0.85 ± 0.29	0.68 ± 0.13
k_2 (MSCUR) (min^{-1})	12.07 ± 0.86	20.79 ± 3.13	24.61 ± 2.55	9.66 ± 0.60
$t_{1/2}$ (CDD) (min)	0.46 ± 0.06	0.87 ± 0.13	0.87 ± 0.25	1.04 ± 0.18
$t_{1/2}$ (MSCUR) (min)	$5.76 \pm 0.42 \times 10^{-2}$	$3.39 \pm 0.54 \times 10^{-2}$	$2.84 \pm 0.30 \times 10^{-2}$	$7.19 \pm 0.44 \times 10^{-2}$
$CL_{int, in vitro}$ (CDD) ($\text{mL min}^{-1} \text{mg protein}^{-1}$)	1.51 ± 0.22	0.81 ± 0.13	0.85 ± 0.29	0.68 ± 0.13
$CL_{int, in vitro}$ (MSCUR) ($\text{mL min}^{-1} \text{mg protein}^{-1}$)	12.07 ± 0.86	20.79 ± 3.13	24.61 ± 2.55	9.66 ± 0.60
$CL_{int, in vivo}$ (CDD) ($\text{L h}^{-1} \text{kg}^{-1}$)	282.18 ± 41.74	176.96 ± 27.49	198.61 ± 66.73	197.51 ± 37.52
$CL_{int, in vivo}$ (MSCUR) ($\text{L h}^{-1} \text{kg}^{-1}$)	2251.20 ± 161.06	4527.30 ± 682.15	5716.98 ± 592.58	2805.37 ± 174.76
$CL_{int, in vivo total}$ ($\text{L h}^{-1} \text{kg}^{-1}$)	2533.38 ± 124.30	4704.26 ± 695.64	5915.59 ± 535.14	3002.88 ± 180.63
CL_H ($\text{L h}^{-1} \text{kg}^{-1}$)	$1.19 \pm 4.61 \times 10^{-4}$	$2.61 \pm 3.87 \times 10^{-3}$	$2.38 \pm 1.48 \times 10^{-3}$	$4.10 \pm 5.77 \times 10^{-3}$

The kinetic parameters of CDD metabolism in liver were difference among human, monkey, dog and rat. The k_2 values are 10 to 20-fold higher than k_1 values in all species. The $CL_{int, in vitro}$ (CDD) values in LS9 fractions are in the following order: human>dog>monkey>rat. The $CL_{int, in vitro}$ (CDD) in HLS9 is higher than in DLS9, MLS9 and RLS9 for 1.8-, 1.9-, and 2.2-fold, respectively. In contrast, the order of $CL_{int, in vitro}$ (MSCUR) values is dog>monkey>human>rat. The $CL_{int, in vitro}$ (MSCUR) values obtained from

DLS9 and MLS9 are approximately 2- and 1.7-fold higher than the that of HLS9 while the $CL_{\text{int, in vitro (MSCUR)}}$ from RLS9 is 0.8-fold lower than the $CL_{\text{int, in vitro (MSCUR)}}$ from HLS9. Both CDD and MSCUR are unstable in hepatic S9 fractions, which their $t_{1/2}$ values are lower than 1 min in all species and CDD was stable than MSCUR.

The predicted $CL_{\text{int, in vivo}}$ data of CDD in HLS9, MLS9, DLS9 and RLS9 based on scaling factor in different species present in **Table 10**. $CL_{\text{int, in vivo (CDD)}}$ and $CL_{\text{int, in vivo (MSCUR)}}$ corresponded to its *in vitro* clearances. Here, the process metabolism of CDD is hydrolysis and produces MSCUR, intermediate metabolite and curcumin, active compound, respectively. Therefore, the predicted hepatic elimination of this prodrug lead to evaluated by the sum of *in vivo* CDD clearance and *in vivo* MSCUR clearance, $CL_{\text{int, in vivo total}}$. The $CL_{\text{int, in vivo total}}$ value expressed in the following order: DLS9 > MLS9 > RLS9 > HLS9. Using Well-Stirred model, the order of CL_H value in HLS9, MLS9, DLS9 and RLS9 did not correspond to the $CL_{\text{int, in vivo total}}$ in any specific manner.

4.4. Enzyme identification of CDD hydrolysis in LS9

4.4.1. Optimization of condition for enzyme identification in LS9

The identification of hepatic esterases involved in the hydrolytic cleavage of CDD in LS9 of the tested species was investigated by using chemical inhibitors. The single reaction condition was conducted in this study. The hydrolytic reaction was evaluated within a linear relationship between the percent curcumin formation and incubation time. The experimental conditions were optimized to follow zero-order kinetics (**Appendix I**).

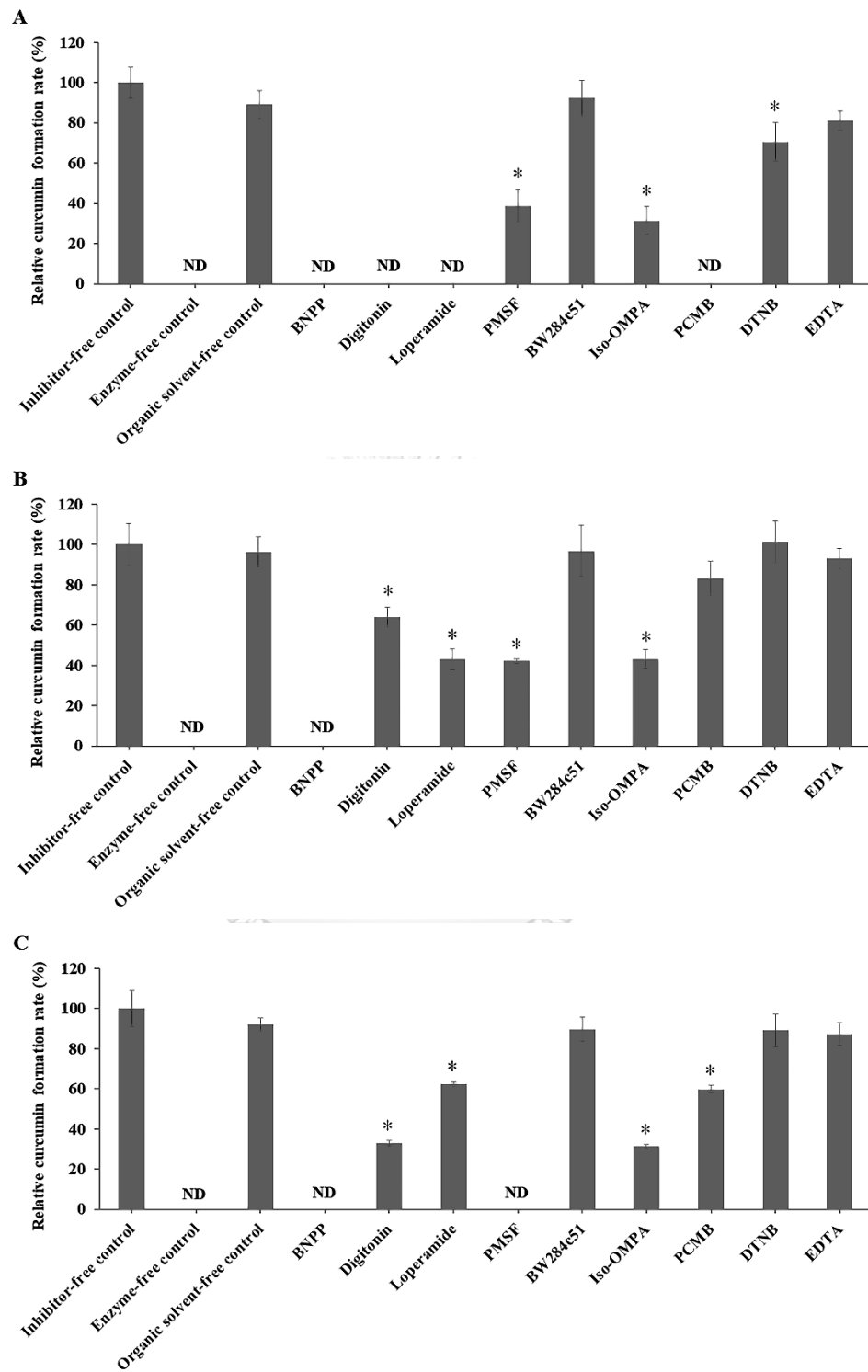
The condition demonstrated a zero-order reaction with less than 30% substrate depletion when the mixture contained CDD 3 μM and LS9 concentration 0.02 mg/mL and incubated time at 37°C at 0.5 min for HLS9 and RLS9 and 1 min for MLS9 and DLS9. The result indicated that formation of curcumin over the incubation time depended on the level of enzymes present. This optimized condition was appropriated to apply in further responsive enzyme of CDD-hydrolysis studies.

4.4.2. Effect of esterase inhibitors on CDD hydrolysis in LS9

Liver S9 esterases of human, monkey, dog and rat involved in the hydrolytic cleavage of CDD were investigated using different types of chemical inhibitors. Nine esterase inhibitors including BNPP, digitonin, loperamide, PMSF, BW284c51, Iso-OMPA, PCMB, DTNB and EDTA are known to inhibit carboxylesterases (CESs), CES1, CES2, serine hydrolase, acetylcholinesterase (AChE), butyrylcholinesterase (BChE), carboxymethylenebutenolidase (CMBL), cysteine hydrolase and paraoxonase (PON), respectively. The effects of these esterase inhibitors on CDD hydrolysis in LS9s were investigated, and the results were summarized in **Figure 27**. All raw data and % of control are present in **Appendix L**.

In the absence of inhibitors, the rates of curcumin formation in HLS9, MLS9, DLS9, and RLS9 were 10.77 ± 0.82 , 14.60 ± 1.51 , 26.79 ± 2.43 , and 12.71 ± 0.25 nmol min⁻¹ mg⁻¹ protein, respectively with a relative curcumin formation rate of 100%. The organic solvent did not exhibit any influence on the degradation profiles of CDD into curcumin. A relative curcumin formation rate of 100% was attained in tests of organic solvent-free control. These results indicated that CDD degraded via enzymatic hydrolysis in LS9 of all test species.

The hydrolysis of CDD in all tested species was completely inhibited by BNPP. PMSF could effectively prevent CDD hydrolysis in DLS9 and RLS9 but partially inhibited the conversion of CDD to curcumin in HLS9 and MLS9. DTNB slightly inhibited the hydrolytic cleavage of CDD in HLS9. Digitonin and loperamide showed strong inhibition in HLS9 but exhibited moderate prevention on the hydrolytic cleavage of CDD in MLS9, DLS9 and RLS9. Iso-OMPA moderately inhibited curcumin formation from CDD in the LS9 in all tested species. BW284c51 could exhibit moderate inhibitory effect in RLS9 but it did not prevent the formation of curcumin in HLS9, MLS9 and DLS9. PCMB showed suppression of the conversion of CDD to curcumin in HLS9, DLS9 and RLS9. Unlike other inhibitors, EDTA did not exhibit an inhibitory effect in the LS9 of all tested species.



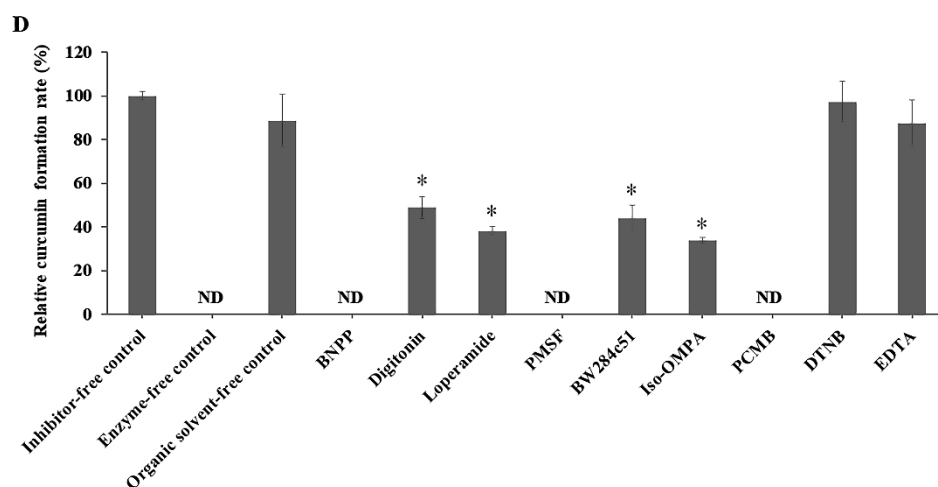


Figure 27. Percent curcumin formation rate of control (% of Control) in present of inhibitors. CDD (3 μ M) was incubated with (A) HLS9, (B) MLS9, (C) DLS9 and (D) RLS9 (0.02 mg/mL) in the presence of nine inhibitors. Control was prepared by using diluent with less than 2% organic solvent and without inhibitors. Data are expressed as the mean \pm SD (n = 3). One-way ANOVA analysis with Dunnett's post hoc test was used to indicate the statistical difference. ND = not detected since the curcumin concentration was below the limit of quantification; statistical significance, * p < 0.001 (vs. control).

CHAPTER V

DISCUSSION AND CONCLUSION

CDD hydrolysis by hepatic esterase of human, monkey, dog and rat were characterized in terms of its metabolites, kinetic parameters including degradation rate, half-life and *in vitro* intrinsic clearance and responsive enzymes. The study demonstrates that the *in vitro* metabolism of CDD in LS9 follows the consecutive CDD hydrolysis to curcumin through MSCUR intermediate using carboxylesterase, a member of serine hydrolase. As expected, the only two metabolites (curcumin and MSCUR) from five possible metabolites were generated in the LS9 by hydrolytic pathways (**Appendix F**). The results implied that the CDD catalyzed preferred to cleave by esterase enzyme in LS9 at the phenolate ester more than that at the ethyl ester consistent with previous study on the metabolism of CDD in plasma (27). The carbonyl carbon link to the phenolic group can be attacked by esterase easier than that of the ethoxy group due to its higher electrophilic properties (50, 107). CDD is a symmetrical molecule and it can undergo dynamic equilibrium between β -diketo and keto-enol forms with intramolecular hydrogen bond. Therefore, there is no difference between the two acyl groups of CDD and the order of hydrolytic cleavage of the two acyl groups. If one acyl group of CDD is removed, the MSCUR metabolite is formed as shown in Figure 15A. The tautomerization of MSCUR results in the same compound regardless of the remaining of ethyl succinate on either side of curcumin.

The *in vitro* metabolic profiling of CDD in human and animal species was performed to investigate the individual species metabolism. The metabolic profiling of CDD hydrolysis in LS9 of four animal species demonstrated similar pattern. The results suggest that CDD is rapidly metabolized in LS9 of all test species giving curcumin as the major product through the MSCUR intermediate. Thus, any metabolites of CDD potentially observed in human could be found in animals to a similar extent in the preclinical safety assessment study. The curcumin generated from CDD was further degraded in the phosphate buffer used in the present study,

resulting in a reduction of curcumin content over 15 to 120 min incubation. These results consist previous studies indicating that curcumin has been shown to rapidly degrade in a phosphate buffer (pH 7.4, 37 °C) (25, 77).

In this study, the metabolism kinetic parameters differ between the species. The lower of k_1 (CDD) may denote that the changing of CDD to MSCUR is rate limiting step. The k_1 (CDD) slower than k_2 (MSCUR) due to CDD had the number of acyl groups in their structure more than MSCUR, consisting with experiment of esterase activity in LS9. The hydrolytic activity of esterase in LS9 tended to decrease from PNPA to PNPC, as the carbon chain was extended from 4 to 8 carbons. The result suggesting that the degree of steric crowding around alkoxy group influenced the activity of CES1, major esterase in LS9, in four animal species (106). CDD and MSCUR were rapidly metabolized by all LS9s with $t_{1/2}$ of less than 1.04 and 7.19×10^{-2} min, respectively. The short half-lives of CDD and MSCUR investigated in this study is consisting with the hydrolysis of the ester compounds such as vicagrel ($t_{1/2}$ about 1.6 min) (144) and GS-6620 ($t_{1/2}$ about 1.6 min) (44). The low $t_{1/2}$ indicated that CDD and MSCUR bioavailability would probably low (39).

Interspecies variation of *in vitro* hepatic clearance ($CL_{in vitro}$) of both CDD and MSCUR might be due to the bioinformatic differences (51, 52, 161). The amino acid sequences and structural homology of metabolic enzymes are animal species dependent. This could be the reason of differences in the enzyme activities and substrate specificity of esterase of different species sources (52-54, 109, 162, 163). Apparently, the *in vitro* hepatic clearance of CDD and MSCUR in DLS9, MLS9 and RLS9 were parallel to predicted *in vivo* total clearance profiles. The HLS9, on the other hand, was correlated to a relatively small *in vivo* total clearance. Despite it exhibited a relatively high *in vitro* CDD clearance and had an *in vitro* MSCUR clearance higher than RLS9. This could be resulted from the fact that the ratio of liver mass-to-body mass of human is less than rat. A larger hepatic blood flow was translated to a higher level of CL_H . The enzyme, ratio of liver mass-to-body mass,

hepatic blood flow and protein binding might govern the *in vivo* hepatic metabolism of CDD (145, 157).

Enzyme identification assay used specific inhibitors of each enzyme to determine the esterase responsible for CDD metabolism. CESs are the significant enzyme in liver of human, monkey, dog and rat (50), while AChE, BChE and PON were low level in liver and highly expressed in plasma (46, 48, 164, 165). In this study, the esterase contribution in liver was determined. Most inhibitions are likely due to an carboxylesterase-specific inhibitor (BNPP) present in the liver subfraction (58, 130). The chemical inhibition assays demonstrated the differential effects of nine inhibitors on CDD hydrolysis in LS9 among various species, consistent with the previous study (53). In human, CDD hydrolysis in HLS9 was inhibited by BNPP, digitonin, loperamide and PCMB, and to a lesser extent by PMSF, Iso-OMPA and DTNB. The esterases of HLS9 responsible for CDD hydrolysis were primarily CESs (including CES1 and CES2) and CMBL, and partially BChE. AChE and PON did not play a critical role in CDD hydrolysis by HLS9. CESs and CMBL play an essential role in the hydrolysis of prodrugs in the liver because CESs are primal enzyme and expressed in the hepatic microsome, while CMBL is highly expressed in the hepatic cytosol of human, monkey, dog and rat (50, 112). The involvement of CESs and CMBL in the ester hydrolysis of CDD in HLS9 is consistent with the ester hydrolysis of other ester prodrugs such as oseltamivir, methylphenidate or olmesartan medoxomil (55, 112).

CDD hydrolysis in MLS9 was inhibited by BNPP, and to a lesser extent by digitonin, loperamide, PMSF and Iso-OMPA. BW284c51, PCMB, DTNB and EDTA had no enzyme inhibitory effects. The esterases of MLS9 responsible for hydrolysis of CDD were CESs (including CES1 and CES2) and BChE. In the case of DLS9, the relative contribution of esterases in the hydrolysis of CDD was as follows: CESs (CES1 and CES2) > BChE > CMBL. With reference to RLS9, the relative contribution of esterases in the hydrolysis of CDD progressed in the following order: CES1 and CES2, \approx CMBL > BChE > AChE.

In summary, CDD can be hydrolyzed by CESs (including CES1 and CES2), AChE, BChE and CMBL. These enzymes are expressed in the liver of human and preclinical species and belong to the $\alpha\beta$ hydrolase fold family that may have a broad and overlapping substrate specificities (46, 112, 125). CESs, AChE, BChE and CMBL are known to involve in bioactivation of various ester prodrugs. For example, irinotecan (CPT-11), an anticancer prodrug of SN-38, can be transformed into its active metabolite by both CESs and BChE (46). For bioactivation of CDD, an ester prodrug of curcumin, the common ester hydrolytic enzymes in LS9 of all tested species are CESs (including CES1 and CES2) and BChE, with CESs having a major contribution in the hepatic hydrolysis of CDD.

The data of *in vitro* metabolism provide the assessment for *in vivo* prediction of CDD metabolism in liver of human, monkey, dog and rat, and aid to select appropriate animal model for preclinical study. CDD could rapidly metabolize in liver of all test species, might has low bioavailability and high protein binding. The hepatic clearance may useful for dose calculation for preclinical pharmacology/toxicity study (166). Furthermore, the CDD remaining profiles and its major metabolite formation profiles from four animal species were similar to humans, indicating that rats, dogs and monkeys may be the appropriate species for predicting human CDD metabolism (42). The similarity of curcumin and MSCUR metabolite profiles, including type and content among different species suggested that rats, dogs and monkeys might be useful for clarifying the potential toxicity of CDD metabolites in human (146). The major metabolite (curcumin) and minor metabolite (MSCUR) could be the risk of *in vivo* toxicity in four animal species. CDD and MSCUR might interaction with drug mediated hydrolysis by CES (63).

Differ from liver, gut is another site that plays an important role in the hydrolysis of orally administered ester-based drugs (45, 50). CESs are the major enzymes responsible for CDD hydrolysis. However, the difference in expression profiles of CES1 and CES2 isoforms between the liver and gut results in different

extents of hydrolysis of CDD. Our results showed that CDD was metabolized primarily by CES1, which is a predominant isoform in the liver (50, 55). However, the involvement of CES1 and CES2 in the gut metabolism of CDD may be different from that of the hepatic metabolism because CES2 is the major isoform in small intestine instead (50, 55). In addition to hydrolysis, other metabolic pathways may also play a role in the overall metabolism of CDD and its metabolites. It has been previously shown that tetrahydrocurcumin, curcumin glucuronide, and tetrahydrocurcumin glucuronide are the significant metabolites of curcumin (60-62, 93). MSCUR and curcumin generated from CDD hydrolysis may undergo reduction and glucuronidation. The alternative metabolic pathways and gut metabolism promises future investigation.

In conclusion, this study provides the comparative data on the hepatic metabolism of CDD in the LS9 of rat, dog, monkey, and human. The *in vitro* hepatic metabolism using LS9, a nearly complete represent of all hepatic metabolizing enzymes, from four animal species. CDD was rapidly hydrolyzed into MSCUR and curcumin in HLS9, MLS9, DLS9 and RLS9 with similar metabolite profile mainly by CESs (CES1 and CES2) and BChE. The formation of curcumin in MLS9 and DLS9 are faster than that in HLS9 and RLS9. The *in vitro* intrinsic clearance of CDD progressed in the following order: human > dog > monkey > rat LS9. The *in vitro* intrinsic clearance of MSCUR followed the order of dog > monkey > human > rat LS9. The *in vitro* intrinsic clearance was not correlated to the *in vivo* clearance of CDD and MSCUR where dog > monkey > rat > human LS9. Human had a smaller liver to body mass than monkey, dog and rat. This factor controlled *in vivo* CDD and MSCUR intrinsic clearance. The *in vivo* LS9 metabolism data consider the physiological factor of the test subject using *in vitro* to *in vivo* extrapolation (IVIVE) model. *In vitro* drug metabolism data from LS9 of animals especially rat, monkey and dog could be inferred as preclinical data for clinical trials. Additional studies including gut metabolism, phase I and II metabolisms of CDD metabolites and the extent of

protein binding should be further investigated to represent the metabolism profiles of CDD.



REFERENCES

1. Calabrese V, Bates TE, Mancuso C, Cornelius C, Ventimiglia B, Cambria MT, et al. Curcumin and the cellular stress response in free radical-related diseases. *Mol Nutr Food Res*. 2008;52(9):1062-73.
2. Khan MS, Muhammad T, Ikram M, Kim MO. Dietary Supplementation of the Antioxidant Curcumin Halts Systemic LPS-Induced Neuroinflammation-Associated Neurodegeneration and Memory/Synaptic Impairment via the JNK/NF-kappaB/Akt Signaling Pathway in Adult Rats. *Oxid Med Cell Longev*. 2019;2019:7860650.
3. Buadonpri W, Wichitnithad W, Rojsitthisak P, Towiwat P. Synthetic curcumin inhibits carrageenan-induced paw edema in rats. *Journal of health research*. 2009;23(1):11-6.
4. Chaniad P, Morales NP, Rojsitthisak P, Luechapudiporn R. Effects of turmeric extract on hemin-induced low-density lipoprotein oxidation. *Journal of Food Biochemistry*. 2018;42(3):e12507.
5. Shimizu K, Funamoto M, Sunagawa Y, Shimizu S, Katanasaka Y, Miyazaki Y, et al. Anti-inflammatory Action of Curcumin and Its Use in the Treatment of Lifestyle-related Diseases. *Eur Cardiol*. 2019;14(2):117-22.
6. Praditya D, Kirchhoff L, Bruning J, Rachmawati H, Steinmann J, Steinmann E. Anti-infective Properties of the Golden Spice Curcumin. *Front Microbiol*. 2019;10:912.
7. Aggarwal BB, Kumar A, Bharti AC. Anticancer potential of curcumin: preclinical and clinical studies. *Anticancer Res*. 2003;23(1a):363-98.
8. Muangnoi C, Ratnatilaka Na Bhuket P, Jithavech P, Supasena W, Paraoan L, Patumraj S, et al. Curcumin diethyl disuccinate, a prodrug of curcumin, enhances anti-proliferative effect of curcumin against HepG2 cells via apoptosis induction. *Sci Rep*. 2019;9(1):11718.
9. Muangnoi C, Ratnatilaka Na Bhuket P, Jithavech P, Wichitnithad W, Srikun O, Nerungsi C, et al. Scale-Up Synthesis and In Vivo Anti-Tumor Activity of Curcumin Diethyl Disuccinate, an Ester Prodrug of Curcumin, in HepG2-Xenograft Mice. *Pharmaceutics*. 2019;11(8).

10. Gomez C, Muangnoi C, Sorasitthiyakarn FN, Wongpiyabovorn J, Rojsitthisak P, Rojsitthisak P. Synergistic Effects of Photo-Irradiation and Curcumin-Chitosan/Alginate Nanoparticles on Tumor Necrosis Factor-Alpha-Induced Psoriasis-Like Proliferation of Keratinocytes. *Molecules*. 2019;24(7).
11. Rafiee Z, Nejatian M, Daeihamed M, Jafari SM. Application of different nanocarriers for encapsulation of curcumin. *Crit Rev Food Sci Nutr*. 2019;59(21):3468-97.
12. Pagano E, Romano B, Izzo AA, Borrelli F. The clinical efficacy of curcumin-containing nutraceuticals: An overview of systematic reviews. *Pharmacol Res*. 2018;134:79-91.
13. Strimpakos AS, Sharma RA. Curcumin: preventive and therapeutic properties in laboratory studies and clinical trials. *Antioxid Redox Signal*. 2008;10(3):511-45.
14. Pouliquen DL. Curcumin: Synthesis, Emerging Role in Pain Management and Health Implications: Nova Science Publishers, Incorporated; 2014.
15. Ratnatilaka Na Bhuket P, El-Magboub A, Haworth IS, Rojsitthisak P. Enhancement of Curcumin Bioavailability Via the Prodrug Approach: Challenges and Prospects. *Eur J Drug Metab Pharmacokinet*. 2017;42(3):341-53.
16. Xu XY, Meng X, Li S, Gan RY, Li Y, Li HB. Bioactivity, Health Benefits, and Related Molecular Mechanisms of Curcumin: Current Progress, Challenges, and Perspectives. *Nutrients*. 2018;10(10).
17. Soleimani V, Sahebkar A, Hosseinzadeh H. Turmeric (*Curcuma longa*) and its major constituent (curcumin) as nontoxic and safe substances: Review. *Phytother Res*. 2018;32(6):985-95.
18. Anand P, Kunnumakkara AB, Newman RA, Aggarwal BB. Bioavailability of curcumin: problems and promises. *Mol Pharm*. 2007;4(6):807-18.
19. Bangphumi K, Kittiviriyakul C, Towiwat P, Rojsitthisak P, Khemawoot P. Pharmacokinetics of Curcumin Diethyl Disuccinate, a Prodrug of Curcumin, in Wistar Rats. *Eur J Drug Metab Pharmacokinet*. 2016;41(6):777-85.
20. Dei Cas M, Ghidoni R. Dietary Curcumin: Correlation between Bioavailability and Health Potential. *Nutrients*. 2019;11(9).
21. Toden S, Goel A. The Holy Grail of Curcumin and its Efficacy in Various Diseases: Is Bioavailability Truly a Big Concern? *J Restor Med*. 2017;6(1):27-36.

22. Boonyasirisri P, Nimmannit U, Rojsitthisak P, Bhunchu S, Rojsitthisak P, editors. Optimization of curcuminoid-loaded PLGA nanoparticles using Box-Behnken statistical design. *Journal of Nano Research*; 2015: Trans Tech Publ.
23. Luckanagul JA, Pitakchatwong C, Ratnatilaka Na Bhuket P, Muangnoi C, Rojsitthisak P, Chirachanchai S, et al. Chitosan-based polymer hybrids for thermo-responsive nanogel delivery of curcumin. *Carbohydr Polym*. 2018;181:1119-27.
24. Wichitnithad W, Nimmannit U, Callery PS, Rojsitthisak P. Effects of different carboxylic ester spacers on chemical stability, release characteristics, and anticancer activity of mono-PEGylated curcumin conjugates. *J Pharm Sci*. 2011;100(12):5206-18.
25. Wichitnithad W, Nimmannit U, Wacharasindhu S, Rojsitthisak P. Synthesis, characterization and biological evaluation of succinate prodrugs of curcuminoids for colon cancer treatment. *Molecules*. 2011;16(2):1888-900.
26. Muangnoi C, Jithavech P, Ratnatilaka Na Bhuket P, Supasena W, Wichitnithad W, Towiwat P, et al. A curcumin-diglutaric acid conjugated prodrug with improved water solubility and antinociceptive properties compared to curcumin. *Biosci Biotechnol Biochem*. 2018;82(8):1301-8.
27. Ratnatilaka Na Bhuket P, Jithavech P, Ongpipattanakul B, Rojsitthisak P. Interspecies differences in stability kinetics and plasma esterases involved in hydrolytic activation of curcumin diethyl disuccinate, a prodrug of curcumin. *RSC Adv*. 2019;9(8):4626-34.
28. Ratnatilaka Na Bhuket P, Niwattisaiwong N, Limpikirati P, Khemawoot P, Towiwat P, Ongpipattanakul B, et al. Simultaneous determination of curcumin diethyl disuccinate and its active metabolite curcumin in rat plasma by LC-MS/MS: Application of esterase inhibitors in the stabilization of an ester-containing prodrug. *J Chromatogr B Analyt Technol Biomed Life Sci*. 2016;1033-1034:301-10.
29. Muangnoi C, Sharif U, Ratnatilaka Na Bhuket P, Rojsitthisak P, Paraoan L. Protective Effects of Curcumin Ester Prodrug, Curcumin Diethyl Disuccinate against H₂O₂-Induced Oxidative Stress in Human Retinal Pigment Epithelial Cells: Potential Therapeutic Avenues for Age-Related Macular Degeneration. *Int J Mol Sci*. 2019;20(13).
30. Wongsrisakul J, Wichitnithad W, Rojsitthisak P, Towiwat P. Antinociceptive effects of curcumin diethyl disuccinate in animal models. *J Health Res*. 2010;24(4):175-80.

31. Bhunchu S, Rojsitthisak P, Rojsitthisak P. Effects of preparation parameters on the characteristics of chitosan–alginate nanoparticles containing curcumin diethyl disuccinate. *Journal of Drug Delivery Science and Technology*. 2015;28:64-72.
32. Bhunchu S, Muangnoi C, Rojsitthisak P, Rojsitthisak P. Curcumin diethyl disuccinate encapsulated in chitosan/alginate nanoparticles for improvement of its in vitro cytotoxicity against MDA-MB-231 human breast cancer cells. *Pharmazie*. 2016;71(12):691-700.
33. Sorasitthiyankarn FN, Rojsitthisak P, Rojsitthisak P. Kinetic Study of Chitosan-Alginate Biopolymeric Nanoparticles for the Controlled Release of Curcumin Diethyl Disuccinate. *J Met Mater Miner*. 2017;27(2):17-22.
34. Jang GR, Harris RZ, Lau DT. Pharmacokinetics and its role in small molecule drug discovery research. *Med Res Rev*. 2001;21(5):382-96.
35. Zhang D, Luo G, Ding X, Lu C. Preclinical experimental models of drug metabolism and disposition in drug discovery and development. *Acta Pharm Sin B*. 2012;2(6):549-61.
36. Almazroo OA, Miah MK, Venkataramanan R. Drug Metabolism in the Liver. *Clin Liver Dis*. 2017;21(1):1-20.
37. Costa A, Sarmiento B, Seabra V. An evaluation of the latest in vitro tools for drug metabolism studies. *Expert Opin Drug Metab Toxicol*. 2014;10(1):103-19.
38. Wilk-Zasadna I, Bernasconi C, Pelkonen O, Coecke S. Biotransformation in vitro: An essential consideration in the quantitative in vitro-to-in vivo extrapolation (QIVIVE) of toxicity data. *Toxicology*. 2015;332:8-19.
39. Sloczynska K, Gunia-Krzyzak A, Koczurkiewicz P, Wojcik-Pszczola K, Zelaszczyk D, Popiol J, et al. Metabolic stability and its role in the discovery of new chemical entities. *Acta Pharm*. 2019;69(3):345-61.
40. Dudda A, Kürzel GU. Metabolism Studies in vitro and in vivo. In: Vogel HG, Hock FJ, Maas J, Mayer D, editors. *Drug Discovery and Evaluation: Safety and Pharmacokinetic Assays*. Berlin, Heidelberg: Springer Berlin Heidelberg; 2013. p. 493-520.
41. Richardson SJ, Bai A, Kulkarni AA, Moghaddam MF. Efficiency in Drug Discovery: Liver S9 Fraction Assay As a Screen for Metabolic Stability. *Drug Metab Lett*. 2016;10(2):83-90.

42. Fu J, Pacyniak E, Leed MGD, Sadgrove MP, Marson L, Jay M. Interspecies Differences in the Metabolism of a Multiester Prodrug by Carboxylesterases. *J Pharm Sci.* 2016;105(2):989-95.
43. Laizure SC, Parker RB, Herring VL, Hu ZY. Identification of carboxylesterase-dependent dabigatran etexilate hydrolysis. *Drug Metab Dispos.* 2014;42(2):201-6.
44. Murakami E, Wang T, Babusis D, Lepist EI, Sauer D, Park Y, et al. Metabolism and pharmacokinetics of the anti-hepatitis C virus nucleotide prodrug GS-6620. *Antimicrob Agents Chemother.* 2014;58(4):1943-51.
45. Nishimuta H, Houston JB, Galetin A. Hepatic, intestinal, renal, and plasma hydrolysis of prodrugs in human, cynomolgus monkey, dog, and rat: implications for in vitro-in vivo extrapolation of clearance of prodrugs. *Drug Metab Dispos.* 2014;42(9):1522-31.
46. Liederer BM, Borchardt RT. Enzymes involved in the bioconversion of ester-based prodrugs. *J Pharm Sci.* 2006;95(6):1177-95.
47. Ishizuka T, Fujimori I, Kato M, Noji-Sakikawa C, Saito M, Yoshigae Y, et al. Human carboxymethylenebutenolidase as a bioactivating hydrolase of olmesartan medoxomil in liver and intestine. *J Biol Chem.* 2010;285(16):11892-902.
48. Fukami T, Yokoi T. The emerging role of human esterases. *Drug Metab Pharmacokinet.* 2012;27(5):466-77.
49. Najjar A, Karaman R. The prodrug approach in the era of drug design. *Expert Opin Drug Deliv.* 2019;16(1):1-5.
50. Di L. The Impact of Carboxylesterases in Drug Metabolism and Pharmacokinetics. *Curr Drug Metab.* 2019;20(2):91-102.
51. Hosokawa M. Structure and catalytic properties of carboxylesterase isozymes involved in metabolic activation of prodrugs. *Molecules.* 2008;13(2):412-31.
52. Taketani M, Shii M, Ohura K, Ninomiya S, Imai T. Carboxylesterase in the liver and small intestine of experimental animals and human. *Life Sci.* 2007;81(11):924-32.
53. Ma HY, Yang JD, Hou J, Zou LW, Jin Q, Hao DC, et al. Comparative metabolism of DDAO benzoate in liver microsomes from various species. *Toxicol In Vitro.* 2017;44:280-6.
54. Wang YQ, Shang XF, Wang L, Zhang P, Zou LW, Song YQ, et al. Interspecies

- variation of clopidogrel hydrolysis in liver microsomes from various mammals. *Chem Biol Interact.* 2020;315:108871.
55. Laizure SC, Herring V, Hu Z, Witbrodt K, Parker RB. The role of human carboxylesterases in drug metabolism: have we overlooked their importance? *Pharmacotherapy.* 2013;33(2):210-22.
56. Rautio J, Karkkainen J, Sloan KB. Prodrugs - Recent approvals and a glimpse of the pipeline. *Eur J Pharm Sci.* 2017;109:146-61.
57. Rautio J, Meanwell NA, Di L, Hageman MJ. The expanding role of prodrugs in contemporary drug design and development. *Nat Rev Drug Discov.* 2018;17(8):559-87.
58. Abe Y, Ota E, Harada H, Kanbe H, Kojima Y, Kanazawa T, et al. Species differences in the metabolism of ritobegron in vitro and assessment of potential interactions with transporters and cytochrome P450 enzymes. *Pharmazie.* 2015;70(1):38-46.
59. Thomsen R, Nielsen LM, Holm NB, Rasmussen HB, Linnet K. Synthetic cannabimimetic agents metabolized by carboxylesterases. *Drug Test Anal.* 2015;7(7):565-76.
60. Hoehle SI, Pfeiffer E, Solyom AM, Metzler M. Metabolism of curcuminoids in tissue slices and subcellular fractions from rat liver. *J Agric Food Chem.* 2006;54(3):756-64.
61. Ireson CR, Jones DJ, Orr S, Coughtrie MW, Boocock DJ, Williams ML, et al. Metabolism of the cancer chemopreventive agent curcumin in human and rat intestine. *Cancer Epidemiology and Prevention Biomarkers.* 2002;11(1):105-11.
62. Pfeiffer E, Hoehle SI, Walch SG, Riess A, Solyom AM, Metzler M. Curcuminoids form reactive glucuronides in vitro. *J Agric Food Chem.* 2007;55(2):538-44.
63. Shi D, Yang J, Yang D, LeCluyse EL, Black C, You L, et al. Anti-influenza prodrug oseltamivir is activated by carboxylesterase human carboxylesterase 1, and the activation is inhibited by antiplatelet agent clopidogrel. *J Pharmacol Exp Ther.* 2006;319(3):1477-84.
64. Amalraj A, Pius A, Gopi S, Gopi S. Biological activities of curcuminoids, other biomolecules from turmeric and their derivatives - A review. *J Tradit Complement Med.* 2017;7(2):205-33.

65. Kim K, Kim JJ, Jung Y, Noh JY, Syed AS, Kim CY, et al. Cyclocurcumin, an Antivasoconstrictive Constituent of *Curcuma longa* (Turmeric). *J Nat Prod*. 2017;80(1):196-200.
66. Gryniewicz G, Slifirski P. Curcumin and curcuminoids in quest for medicinal status. *Acta Biochim Pol*. 2012;59(2):201-12.
67. Ragunathan I, Panneerselvam N. Antimutagenic potential of curcumin on chromosomal aberrations in *Allium cepa*. *J Zhejiang Univ Sci B*. 2007;8(7):470-5.
68. Teow SY, Liew K, Ali SA, Khoo AS, Peh SC. Antibacterial Action of Curcumin against *Staphylococcus aureus*: A Brief Review. *J Trop Med*. 2016;2016:2853045.
69. Anjomshoa S, Namazian M, Noorbala MR. The effect of solvent on tautomerism, acidity and radical stability of curcumin and its derivatives based on thermodynamic quantities. *Journal of Solution Chemistry*. 2016;45(7):1021-30.
70. Metzler M, Pfeiffer E, Schulz SI, Dempe JS. Curcumin uptake and metabolism. *Biofactors*. 2013;39(1):14-20.
71. Nelson KM, Dahlin JL, Bisson J, Graham J, Pauli GF, Walters MA. The Essential Medicinal Chemistry of Curcumin. *J Med Chem*. 2017;60(5):1620-37.
72. Tsuda T. Curcumin as a functional food-derived factor: degradation products, metabolites, bioactivity, and future perspectives. *Food Funct*. 2018;9(2):705-14.
73. Payton F, Sandusky P, Alworth WL. NMR study of the solution structure of curcumin. *J Nat Prod*. 2007;70(2):143-6.
74. Kolev TM, Velcheva EA, Stamboliyska BA, Spiteller M. DFT and experimental studies of the structure and vibrational spectra of curcumin. *International Journal of Quantum Chemistry*. 2005;102(6):1069-79.
75. Kawano S-i, Inohana Y, Hashi Y, Lin J-M. Analysis of keto-enol tautomers of curcumin by liquid chromatography/mass spectrometry. *Chinese Chemical Letters*. 2013;24(8):685-7.
76. Lou Y, Zheng J, Hu H, Lee J, Zeng S. Application of ultra-performance liquid chromatography coupled with quadrupole time-of-flight mass spectrometry to identify curcumin metabolites produced by human intestinal bacteria. *J Chromatogr B Analyt Technol Biomed Life Sci*. 2015;985:38-47.
77. Wang YJ, Pan MH, Cheng AL, Lin LI, Ho YS, Hsieh CY, et al. Stability of curcumin

in buffer solutions and characterization of its degradation products. *J Pharm Biomed Anal.* 1997;15(12):1867-76.

78. Gordon ON, Luis PB, Sintim HO, Schneider C. Unraveling curcumin degradation autoxidation proceeds through spiroepoxide and vinyl ether intermediates en route to the main bicyclopentadione. *Journal of Biological Chemistry.* 2015;290(8):4817-28.

79. Jankun J, Wyganowska-Swiatkowska M, Dettlaff K, Jelinska A, Surdacka A, Watrobska-Swietlikowska D, et al. Determining whether curcumin degradation/condensation is actually bioactivation (Review). *Int J Mol Med.* 2016;37(5):1151-8.

80. Schneider C, Gordon ON, Edwards RL, Luis PB. Degradation of Curcumin: From Mechanism to Biological Implications. *J Agric Food Chem.* 2015;63(35):7606-14.

81. Zhu J, Sanidad KZ, Sukamtoh E, Zhang G. Potential roles of chemical degradation in the biological activities of curcumin. *Food Funct.* 2017;8(3):907-14.

82. Tóth G, Roth M, Weckerle B, Schreier P. Structural elucidation of two novel products from the soybean lipoxygenase-catalysed dioxygenation of curcumin. *Magnetic Resonance in Chemistry.* 2000;38(1):51-4.

83. Tonnesen HH, Karlsen J, van Henegouwen GB. Studies on curcumin and curcuminoids. VIII. Photochemical stability of curcumin. *Z Lebensm Unters Forsch.* 1986;183(2):116-22.

84. Anand P, Kunnumakkara AB, Newman RA, Aggarwal BB. Bioavailability of Curcumin: Problems and Promises. *Molecular Pharmaceutics.* 2007;4(6):807-18.

85. Yang KY, Lin LC, Tseng TY, Wang SC, Tsai TH. Oral bioavailability of curcumin in rat and the herbal analysis from *Curcuma longa* by LC-MS/MS. *J Chromatogr B Analyt Technol Biomed Life Sci.* 2007;853(1-2):183-9.

86. Chang MT, Tsai TR, Lee CY, Wei YS, Chen YJ, Chen CR, et al. Elevating bioavailability of curcumin via encapsulation with a novel formulation of artificial oil bodies. *J Agric Food Chem.* 2013;61(40):9666-71.

87. Shoba G, Joy D, Joseph T, Majeed M, Rajendran R, Srinivas PS. Influence of piperine on the pharmacokinetics of curcumin in animals and human volunteers. *Planta Med.* 1998;64(4):353-6.

88. Vareed SK, Kakarala M, Ruffin MT, Crowell JA, Normolle DP, Djuric Z, et al. Pharmacokinetics of curcumin conjugate metabolites in healthy human subjects. *Cancer Epidemiol Biomarkers Prev.* 2008;17(6):1411-7.
89. Cheng AL, Hsu CH, Lin JK, Hsu MM, Ho YF, Shen TS, et al. Phase I clinical trial of curcumin, a chemopreventive agent, in patients with high-risk or pre-malignant lesions. *Anticancer Res.* 2001;21(4b):2895-900.
90. Sharma RA, Euden SA, Platton SL, Cooke DN, Shafayat A, Hewitt HR, et al. Phase I clinical trial of oral curcumin: biomarkers of systemic activity and compliance. *Clin Cancer Res.* 2004;10(20):6847-54.
91. Carroll RE, Benya RV, Turgeon DK, Vareed S, Neuman M, Rodriguez L, et al. Phase IIa clinical trial of curcumin for the prevention of colorectal neoplasia. *Cancer Prev Res (Phila).* 2011;4(3):354-64.
92. Garcea G, Berry DP, Jones DJ, Singh R, Dennison AR, Farmer PB, et al. Consumption of the putative chemopreventive agent curcumin by cancer patients: assessment of curcumin levels in the colorectum and their pharmacodynamic consequences. *Cancer Epidemiol Biomarkers Prev.* 2005;14(1):120-5.
93. Pan MH, Huang TM, Lin JK. Biotransformation of curcumin through reduction and glucuronidation in mice. *Drug Metab Dispos.* 1999;27(4):486-94.
94. Marczylo TH, Steward WP, Gescher AJ. Rapid analysis of curcumin and curcumin metabolites in rat biomatrices using a novel ultraperformance liquid chromatography (UPLC) method. *J Agric Food Chem.* 2009;57(3):797-803.
95. Usta M, Wortelboer HM, Vervoort J, Boersma MG, Rietjens IM, van Bladeren PJ, et al. Human glutathione S-transferase-mediated glutathione conjugation of curcumin and efflux of these conjugates in Caco-2 cells. *Chem Res Toxicol.* 2007;20(12):1895-902.
96. Kunati SR, Yang S, William BM, Xu Y. An LC-MS/MS method for simultaneous determination of curcumin, curcumin glucuronide and curcumin sulfate in a phase II clinical trial. *Journal of pharmaceutical and biomedical analysis.* 2018;156:189-98.
97. Hassaninasab A, Hashimoto Y, Tomita-Yokotani K, Kobayashi M. Discovery of the curcumin metabolic pathway involving a unique enzyme in an intestinal microorganism. *Proc Natl Acad Sci U S A.* 2011;108(16):6615-20.
98. Burapan S, Kim M, Han J. Curcuminoid demethylation as an alternative

metabolism by human intestinal microbiota. *Journal of agricultural and food chemistry*. 2017;65(16):3305-10.

99. Burapan S, Kim M, Han J. Demethylation of polymethoxyflavones by human gut bacterium, *Blautia* sp. MRG-PMF1. *Journal of agricultural and food chemistry*. 2017;65(8):1620-9.

100. Lou Y, Zheng J, Hu H, Lee J, Zeng S. Application of ultra-performance liquid chromatography coupled with quadrupole time-of-flight mass spectrometry to identify curcumin metabolites produced by human intestinal bacteria. *Journal of Chromatography B*. 2015;985:38-47.

101. Luca SV, Macovei I, Bujor A, Miron A, Skalicka-Wozniak K, Aprotosoie AC, et al. Bioactivity of dietary polyphenols: The role of metabolites. *Crit Rev Food Sci Nutr*. 2020;60(4):626-59.

102. Huttunen KM, Raunio H, Rautio J. Prodrugs--from serendipity to rational design. *Pharmacol Rev*. 2011;63(3):750-71.

103. Abet V, Filace F, Recio J, Alvarez-Builla J, Burgos C. Prodrug approach: An overview of recent cases. *Eur J Med Chem*. 2017;127:810-27.

104. Ettmayer P, Amidon GL, Clement B, Testa B. Lessons Learned from Marketed and Investigational Prodrugs. *Journal of Medicinal Chemistry*. 2004;47(10):2393-404.

105. Muangnoi C, Bhuket PRN, Jithavech P, Supasena W, Paraoan L, Patumraj S, et al. Curcumin diethyl disuccinate, a prodrug of curcumin, enhances anti-proliferative effect of curcumin against HepG2 cells via apoptosis induction. *Scientific reports*. 2019;9(1):1-9.

106. Mizoi K, Takahashi M, Sakai S, Ogihara T, Haba M, Hosokawa M. Structure-activity relationship of atorvastatin derivatives for metabolic activation by hydrolases. *Xenobiotica*. 2020;50(3):261-9.

107. Wang D, Zou L, Jin Q, Hou J, Ge G, Yang L. Human carboxylesterases: a comprehensive review. *Acta Pharm Sin B*. 2018;8(5):699-712.

108. Imai T. Human carboxylesterase isozymes: catalytic properties and rational drug design. *Drug Metab Pharmacokinet*. 2006;21(3):173-85.

109. Satoh T, Taylor P, Bosron WF, Sanghani SP, Hosokawa M, La Du BN. Current progress on esterases: from molecular structure to function. *Drug Metab Dispos*. 2002;30(5):488-93.

110. Ohura K, Igawa Y, Tanaka M, Matsumoto K, Kasahara A, Wada N, et al. Identification and Characterization of a New Carboxylesterase 2 Isozyme, mfCES2C, in the Small Intestine of Cynomolgus Monkeys. *Drug Metab Dispos.* 2020;48(3):146-52.
111. Kurokawa T, Fukami T, Nakajima M. Characterization of Species Differences in Tissue Diltiazem Deacetylation Identifies Ces2a as a Rat-Specific Diltiazem Deacetylase. *Drug Metab Dispos.* 2015;43(8):1218-25.
112. Ishizuka T, Yoshigae Y, Murayama N, Izumi T. Different hydrolases involved in bioactivation of prodrug-type angiotensin receptor blockers: carboxymethylenebutenolidase and carboxylesterase 1. *Drug Metab Dispos.* 2013;41(11):1888-95.
113. Patrick KS, Straughn AB, Minhinnett RR, Yeatts SD, Herrin AE, DeVane CL, et al. Influence of ethanol and gender on methylphenidate pharmacokinetics and pharmacodynamics. *Clin Pharmacol Ther.* 2007;81(3):346-53.
114. García-Ayllón M-S, Riba-Llena I, Serra-Basante C, Alom J, Boopathy R, Sáez-Valero J. Altered levels of acetylcholinesterase in Alzheimer plasma. *PLoS One.* 2010;5(1).
115. Perelman A, Abeijon C, Hirschberg CB, Inestrosa NC, Brandan E. Differential association and distribution of acetyl- and butyrylcholinesterases within rat liver subcellular organelles. *J Biol Chem.* 1990;265(1):214-20.
116. Cheung J, Gary EN, Shiomi K, Rosenberry TL. Structures of human acetylcholinesterase bound to dihydrotanshinone I and territrem B show peripheral site flexibility. *ACS Med Chem Lett.* 2013;4(11):1091-6.
117. Wiesner J, Kriz Z, Kuca K, Jun D, Koca J. Acetylcholinesterases--the structural similarities and differences. *J Enzyme Inhib Med Chem.* 2007;22(4):417-24.
118. Chen X, Fang L, Liu J, Zhan C-G. Reaction Pathway and Free Energy Profiles for Butyrylcholinesterase-Catalyzed Hydrolysis of Acetylthiocholine. *Biochemistry.* 2012;51(6):1297-305.
119. García-Ayllón MS, Millán C, Serra-Basante C, Bataller R, Sáez-Valero J. Readthrough acetylcholinesterase is increased in human liver cirrhosis. *PLoS One.* 2012;7(9):e44598.
120. Darvesh S, Hopkins DA, Geula C. Neurobiology of butyrylcholinesterase. *Nat Rev*

Neurosci. 2003;4(2):131-8.

121. Colovic MB, Krstic DZ, Lazarevic-Pasti TD, Bondzic AM, Vasic VM.

Acetylcholinesterase inhibitors: pharmacology and toxicology. *Curr Neuropharmacol.* 2013;11(3):315-35.

122. Park YJ, Yoon SJ, Lee HB. A novel diene lactone hydrolase from the thermoacidophilic archaeon *Sulfolobus solfataricus* P1: purification, characterization, and expression. *Biochim Biophys Acta.* 2010;1800(11):1164-72.

123. Pathak D, Ashley G, Ollis D. Thiol protease-like active site found in the enzyme diene lactone hydrolase: localization using biochemical, genetic, and structural tools. *Proteins.* 1991;9(4):267-79.

124. Cheah E, Ashley GW, Gary J, Ollis D. Catalysis by diene lactone hydrolase: a variation on the protease mechanism. *Proteins.* 1993;16(1):64-78.

125. Holmquist M. Alpha/Beta-hydrolase fold enzymes: structures, functions and mechanisms. *Curr Protein Pept Sci.* 2000;1(2):209-35.

126. Sfakianos MK, Wilson L, Sakalian M, Falany CN, Barnes S. Conserved residues in the putative catalytic triad of human bile acid Coenzyme A:amino acid N-acetyltransferase. *J Biol Chem.* 2002;277(49):47270-5.

127. Sorenson RC, Primo-Parmo SL, Kuo CL, Adkins S, Lockridge O, La Du BN. Reconsideration of the catalytic center and mechanism of mammalian paraoxonase/arylesterase. *Proc Natl Acad Sci U S A.* 1995;92(16):7187-91.

128. Harel M, Aharoni A, Gaidukov L, Brumshtein B, Khersonsky O, Meged R, et al. Structure and evolution of the serum paraoxonase family of detoxifying and anti-atherosclerotic enzymes. *Nat Struct Mol Biol.* 2004;11(5):412-9.

129. Koyama K, Ogura Y, Nakai D, Watanabe M, Munemasa T, Oofune Y, et al. Identification of bioactivating enzymes involved in the hydrolysis of laninamivir octanoate, a long-acting neuraminidase inhibitor, in human pulmonary tissue. *Drug Metab Dispos.* 2014;42(6):1031-8.

130. Chanteux H, Rosa M, Delatour C, Prakash C, Smith S, Nicolas JM. In vitro hydrolysis and transesterification of CDP323, an alpha4beta1/alpha4beta7 integrin antagonist ester prodrug. *Drug Metab Dispos.* 2014;42(1):153-61.

131. Shimizu M, Fukami T, Nakajima M, Yokoi T. Screening of specific inhibitors for

- human carboxylesterases or arylacetamide deacetylase. *Drug Metab Dispos.* 2014;42(7):1103-9.
132. Bull P, Wyneken U, Valenzuela P. The reactivity of sulfhydryl groups of yeast DNA dependent RNA polymerase I. *Nucleic Acids Res.* 1982;10(17):5149-60.
133. Baranczewski P, Stańczak A, Sundberg K, Svensson R, Wallin A, Jansson J, et al. Introduction to in vitro estimation of metabolic stability and drug interactions of new chemical entities in drug discovery and development. *Pharmacol Rep.* 2006;58(4):453-72.
134. Brandon EFA, Raap CD, Meijerman I, Beijnen JH, Schellens JHM. An update on in vitro test methods in human hepatic drug biotransformation research: pros and cons. *Toxicology and Applied Pharmacology.* 2003;189(3):233-46.
135. Pelknen O, Turpeinen M, and Uusitalo J. *In vitro* metabolism in preclinical drug development. In: C. G, editor. *Pharmaceutical Sciences Encyclopedia: Drug Discovery, Development, and Manufacturing.* New York: John Wiley & Sons, Inc.; 2010.
136. Riedmaier S, Klein K, Winter S, Hofmann U, Schwab M, Zanger UM. Paraoxonase (PON1 and PON3) Polymorphisms: Impact on Liver Expression and Atorvastatin-Lactone Hydrolysis. *Front Pharmacol.* 2011;2:41.
137. Jbilo O, Bartels CF, Chatonnet A, Toutant JP, Lockridge O. Tissue distribution of human acetylcholinesterase and butyrylcholinesterase messenger RNA. *Toxicol.* 1994;32(11):1445-57.
138. Takayama T, Suzuki M, Todoroki K, Inoue K, Min JZ, Kikura-Hanajiri R, et al. UPLC/ESI-MS/MS-based determination of metabolism of several new illicit drugs, ADB-FUBINACA, AB-FUBINACA, AB-PINACA, QUPIC, 5F-QUPIC and alpha-PVT, by human liver microsome. *Biomed Chromatogr.* 2014;28(6):831-8.
139. Gao D, Chen X, Yang X, Wu Q, Jin F, Wen H, et al. Stable isotope labeling strategy for curcumin metabolite study in human liver microsomes by liquid chromatography-tandem mass spectrometry. *J Am Soc Mass Spectrom.* 2015;26(4):686-94.
140. Choi GW, Lee YB, Cho HY. Interpretation of Non-Clinical Data for Prediction of Human Pharmacokinetic Parameters: In Vitro-In Vivo Extrapolation and Allometric

Scaling. *Pharmaceutics*. 2019;11(4).

141. Ito K, Houston JB. Comparison of the use of liver models for predicting drug clearance using in vitro kinetic data from hepatic microsomes and isolated hepatocytes. *Pharm Res*. 2004;21(5):785-92.

142. Ring BJ, Chien JY, Adkison KK, Jones HM, Rowland M, Jones RD, et al. PhRMA CPCDC initiative on predictive models of human pharmacokinetics, part 3: comparative assessment of prediction methods of human clearance. *J Pharm Sci*. 2011;100(10):4090-110.

143. Davies B, Morris T. Physiological parameters in laboratory animals and humans. *Pharm Res*. 1993;10(7):1093-5.

144. Qiu ZX, Gao WC, Dai Y, Zhou SF, Zhao J, Lu Y, et al. Species Comparison of Pre-systemic Bioactivation of Vicagrel, a New Acetate Derivative of Clopidogrel. *Front Pharmacol*. 2016;7:366.

145. Zhang C, Zhang X, Wang G, Peng Y, Zhang X, Wu H, et al. Preclinical Pharmacokinetics of C118P, a Novel Prodrug of Microtubules Inhibitor and Its Metabolite C118 in Mice, Rats, and Dogs. *Molecules*. 2018;23(11).

146. Luffer-Atlas D, Atrakchi A. A decade of drug metabolite safety testing: industry and regulatory shared learning. *Expert Opin Drug Metab Toxicol*. 2017;13(9):897-900.

147. Bisswanger H. Enzyme assays. *Perspectives in Science*. 2014;1(1-6):41-55.

148. Food Drug Administration Center for Drug Evaluation Research. Guidance for industry: drug interaction studies—study design, data analysis, implications for dosing, and labeling recommendations (draft guidance). US FDA, Maryland; 2012.

149. Jewell C, Ackermann C, Payne NA, Fate G, Voorman R, Williams FM. Specificity of procaine and ester hydrolysis by human, minipig, and rat skin and liver. *Drug Metab Dispos*. 2007;35(11):2015-22.

150. Ross MK, Borazjani A. Enzymatic activity of human carboxylesterases. *Curr Protoc Toxicol*. 2007;Chapter 4:Unit 4.24.

151. Tolonen A, Turpeinen M, Pelkonen O. Liquid chromatography–mass spectrometry in in vitro drug metabolite screening. *Drug Discovery Today*. 2009;14(3):120-33.

152. Alcorn J, Elbarbry FA, Allouh MZ, McNamara PJ. Evaluation of the assumptions

of an ontogeny model of rat hepatic cytochrome P450 activity. *Drug Metab Dispos.* 2007;35(12):2225-31.

153. Montoro-Garcia S, Martinez-Martinez I, Navarro-Fernandez J, Takami H, Garcia-Carmona F, Sanchez-Ferrer A. Characterization of a novel thermostable carboxylesterase from *Geobacillus kaustophilus* HTA426 shows the existence of a new carboxylesterase family. *J Bacteriol.* 2009;191(9):3076-85.

154. Singh RS, Das U, Dimmock JR, Alcorn J. A general HPLC-UV method for the quantitative determination of curcumin analogues containing the 1,5-diaryl-3-oxo-1,4-pentadienyl pharmacophore in rat biomatrices. *J Chromatogr B Analyt Technol Biomed Life Sci.* 2010;878(28):2796-802.

155. Cho S, Yoon Y-R. Understanding the pharmacokinetics of prodrug and metabolite. *Transl Clin Pharmacol.* 2018;26(1):1-5.

156. Brown AM. A step-by-step guide to non-linear regression analysis of experimental data using a Microsoft Excel spreadsheet. *Comput Methods Programs Biomed.* 2001;65(3):191-200.

157. Hosea NA, Collard WT, Cole S, Maurer TS, Fang RX, Jones H, et al. Prediction of human pharmacokinetics from preclinical information: comparative accuracy of quantitative prediction approaches. *J Clin Pharmacol.* 2009;49(5):513-33.

158. Gleeson MP. Plasma protein binding affinity and its relationship to molecular structure: an in-silico analysis. *J Med Chem.* 2007;50(1):101-12.

159. Blech S, Ebner T, Ludwig-Schwellinger E, Stangier J, Roth W. The metabolism and disposition of the oral direct thrombin inhibitor, dabigatran, in humans. *Drug Metab Dispos.* 2008;36(2):386-99.

160. Jia S, Du Z, Song C, Jin S, Zhang Y, Feng Y, et al. Identification and characterization of curcuminoids in turmeric using ultra-high performance liquid chromatography-quadrupole time of flight tandem mass spectrometry. *J Chromatogr A.* 2017;1521:110-22.

161. Satoh T, Hosokawa M. The mammalian carboxylesterases: from molecules to functions. *Annu Rev Pharmacol Toxicol.* 1998;38:257-88.

162. Satoh T, Hosokawa M. Carboxylesterases: structure, function and polymorphism. *The Korean Society of Applied Pharmacology.* 2009;17(4):335-47.

163. Williams ET, Bacon JA, Bender DM, Lowinger JJ, Guo WK, Ehsani ME, et al. Characterization of the expression and activity of carboxylesterases 1 and 2 from the beagle dog, cynomolgus monkey, and human. *Drug Metab Dispos.* 2011;39(12):2305-13.
164. Bahar FG, Ohura K, Ogihara T, Imai T. Species difference of esterase expression and hydrolase activity in plasma. *J Pharm Sci.* 2012;101(10):3979-88.
165. Yang Y-h, Aloysius H, Inoyama D, Chen Y, Hu L-q. Enzyme-mediated hydrolytic activation of prodrugs. *Acta Pharmaceutica Sinica B.* 2011;1(3):143-59.
166. Smith DA, Beaumont K, Maurer TS, Di L. Clearance in Drug Design. *J Med Chem.* 2019;62(5):2245-55.
167. Perrin CL. Linear or nonlinear least-squares analysis of kinetic data? *Journal of Chemical Education.* 2017;94(6):669-72.
168. Bose A. HPLC calibration process parameters in terms of system suitability test. *Austin Chromatography.* 2014;1(2):1-4.
169. Chapter UG, editor 621>. *Chromatography, USP37-NF32, The United States Pharmacopeia Convention, official August; 2014.*
170. White S, Adcock N, Elbast W, Hiller J, Knutsson M, Lausecker B, et al. European Bioanalysis Forum: recommendation for dealing with internal standard variability. *Bioanalysis.* 2014;6(20):2767-74.

APPENDIX A

Supporting document for materials

1. Chromatogram and purity of standard

The standards of CDD, curcumin, MSCUR and DMC were analyzed for purity determination by HPLC. Each compound was dissolved in acetonitrile to prepare the final concentration at 10 μM . The chromatographic condition was set following.

Parameters	Conditions
Moblie phase:	A gradient mode using an elution program:
A: 0.1% Formic acid in acetonitrile	0-3 min, initial A-B (40:60, v/v); 4.5-7 min, isocratic elution A-B (50:50, v/v); 8.5-11 min, isocratic elution A-B (60:40, v/v) and 12-17 min, isocratic elution A-B (40:60, v/v)
B: 0.1% Formic acid in water	
Column	HALO C8 column (4.6 mm x 50 mm, 2.7 μM)
Flow rate	1.2 mL/min
Autosampler temperature	25°C
Column oven temperature	35°C
Injection volume	20 μL
Detection wavelength	400 nm

The chromatograms of CDD, curcumin, MSCUR and DMC standard are showed in **Figure 28-31**.

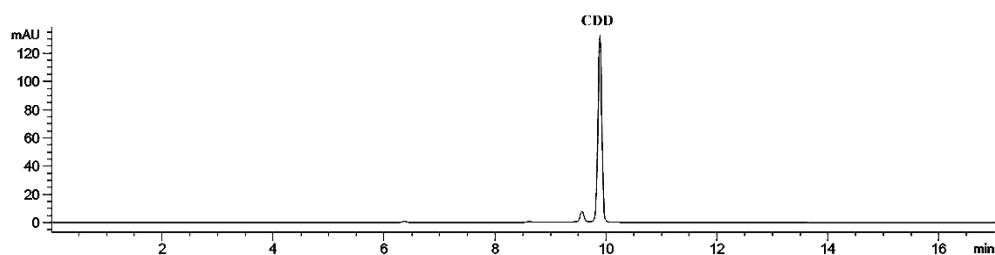


Figure 28. The chromatogram of CDD standard at 10 μM .

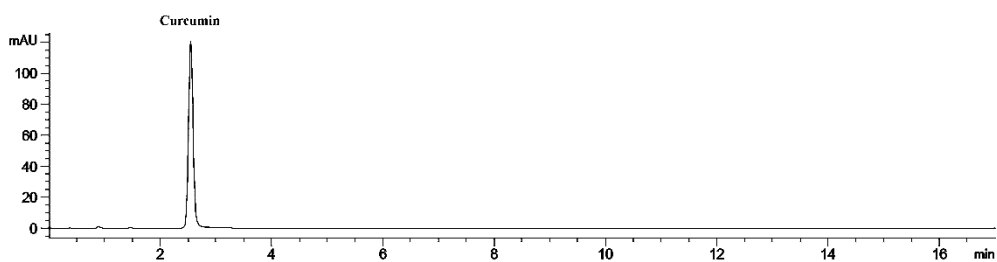


Figure 29. The chromatogram of curcumin standard at 10 μ M.

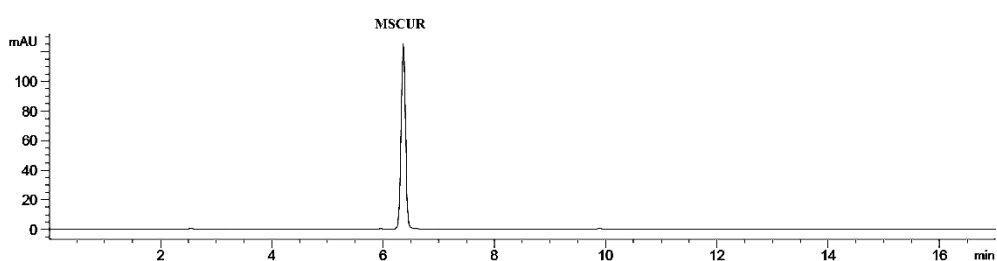


Figure 30. The chromatogram of MSCUR standard at 10 μ M.

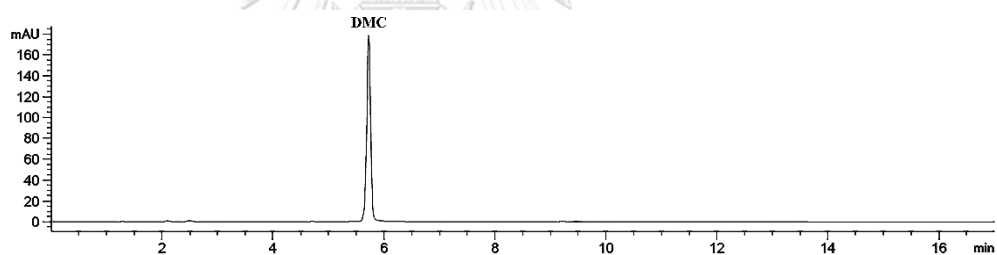


Figure 31. The chromatogram of DMC standard at 10 μ M.

The purity of CDD, curcumin, MSCUR and DMC standard was shown in Table

11.

Table 11. Purity of CDD, curcumin, MSCUR and DMC standard

Standard	% Impurity	% Purity
CDD	1.20 2.12 (keto form)	96.68 (enol form)
Curcumin	0.51	99.49
MSCUR	1.37	98.63
DMC	1.26	98.74

Certificate of analysis

Certification of 4-nitrophenol

SIGMA-ALDRICH®

sigma-aldrich.com

3050 Spruce Street, Saint Louis, MO 63103, USA

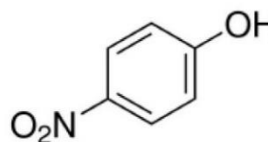
Website: www.sigmaaldrich.com

Email USA: techserv@sial.com

Outside USA: eurtechserv@sial.com

Certificate of AnalysisProduct Name:
4-Nitrophenol - ReagentPlus®, ≥99%

Product Number: 241326
 Batch Number: MKBP6945V
 Brand: ALDRICH
 CAS Number: 100-02-7
 MDL Number: MFCD00007331
 Formula: C6H5NO3
 Formula Weight: 139.11 g/mol
 Quality Release Date: 01 JUL 2013



Test	Specification	Result
Appearance (Color)	Yellow to Tan	Light Yellow
Appearance (Form)	Conforms to Requirements	Crystals
Powder, Crystalline Powder, Crystals, Granular Powder and/or Chunks		
Infrared spectrum	Conforms to Structure	Conforms
Purity (GC)	≥ 99.0 %	99.9 %

Jamie Gleason, Manager
 Quality Control
 Milwaukee, Wisconsin US

Sigma-Aldrich warrants, that at the time of the quality release or subsequent retest date this product conformed to the information contained in this publication. The current Specification sheet may be available at Sigma-Aldrich.com. For further inquiries, please contact Technical Service. Purchaser must determine the suitability of the product for its particular use. See reverse side of invoice or packing slip for additional terms and conditions of sale.

Certification of 4-nitrophenyl acetate

25/6/2562

Certificate Of Analysis

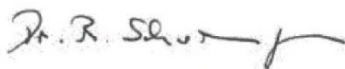
Certificate of Analysis

SIGMA-ALDRICH®

Product Name	4-Nitrophenyl acetate, esterase substrate
Product Number	N8130
Product Brand	SIGMA
CAS Number	830-03-5
Molecular Formula	CH ₃ CO ₂ C ₆ H ₄ NO ₂
Molecular Weight	181.15

TEST**SPECIFICATION****LOT BCBK4587V RESULTS****PDF**

[Click here](#). Certificate of Analysis and Specifications only available in PDF format



Dr. Reinhold Schwenninger
Quality Assurance
Buchs, Switzerland

Certification of 4-nitrophenol caprylate

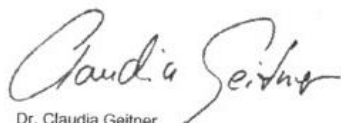
SIGMA-ALDRICH

 3050 Spruce Street, Saint Louis, MO 63103 USA
 Email USA: techserv@sigma.com Outside USA: eurtechserv@sigma.com

Certificate of Analysis

Product Name: 4-NITROPHENYL OCTANOATE
 >= 90.0 % GC
Product Number: 21742
Batch Number: BCBV4615
Brand: Sigma
CAS Number: 1956-10-1
Formula: C₁₄H₁₉NO₄
Formula Weight: 265.30
Storage Temperature: 2-8 C
Quality Release Date: 04 JUL 2017
Recommended Retest Date: JUN 2020

TEST	SPECIFICATION	RESULT
APPEARANCE (COLOR)	YELLOW TO VERY DEEP BROWNISH-YELLOW OR GREENISH-YELLOW	GREENISH-YELLOW
APPEARANCE (FORM)	LIQUID	LIQUID
PURITY (GC AREA %)	≥ 90.0 %	98.4 %
REFRACTIVE INDEX N20/D	1.504 - 1.512	1.508
PROTON NMR SPECTRUM	CONFORMS TO STRUCTURE	CONFORMS



Dr. Claudia Geitner
 Manager Quality Control
 Buchs, Switzerland

Sigma-Aldrich warrants that at the time of the quality release or subsequent retest date this product conformed to the information contained in this publication. The current specification sheet may be available at Sigma-Aldrich.com. For further inquiries, please contact Technical Service. Purchaser must determine the suitability of the product for its particular use. See reverse side of invoice or packing slip for additional terms and conditions of sale.

Certification of BNPP



Certificate of Analysis

Jun 25, 2019 (JST)

TOKYO CHEMICAL INDUSTRY CO., LTD.
4-10-1 Nihonbashi-Honcho, Chuo-ku, Tokyo 103-0023 Japan

Chemical Name: Bis(4-nitrophenyl) Phosphate [for Phosphodiesterase Substrate]		
Product Number: B1098 CAS RN: 645-15-8	Lot: LPTYN	
Tests	Results	Specifications
Purity(Neutralization titration)	99.1 %	min. 98.0 %
Melting point	175.8 deg-C	175.0 to 179.0 deg-C
Solubility in Water	almost transparency	almost transparency

TCI Lot numbers are 4-5 characters in length. Characters listed after the first 4-5 characters are control numbers for internal purpose only. The contents of the specifications are subject to change without advance notice. The specification values displayed here are the most up to date values. There may be cases where the product labels display a different specification, however, the product quality still meets the latest specification.

Customer service:

TCI EUROPE N.V.
Tel: +32-3-735-0700
Fax: +32-3-735-0701
E-mail: Sales-EU@TCIchemicals.com

TCI Deutschland GmbH
Tel: +49 6196 64053-00
Fax: +49 6196 64053-01
E-mail: Sales-DE@TCIchemicals.com

Tokyo Chemical Industry UK Ltd
Tel: +44 1865 78 45 60
Fax: +44 1865 78 45 61
E-mail: Sales-UK@TCIchemicals.com

Ryo Ogawa
Quality Assurance Dep. Manager



จุฬาลงกรณ์มหาวิทยาลัย
CHULALONGKORN UNIVERSITY

Certification of digitonin

SIGMA-ALDRICH3050 Spruce Street, Saint Louis, MO 63103 USA
Email USA: techserv@sial.com Outside USA: eurtechserv@sial.com

Certificate of Analysis

Product Name: DIGITONIN
Used as non-ionic detergent

Product Number: D141

Batch Number: BCBW7972

Brand: Sigma

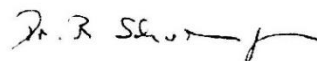
CAS Number: 11024-24-1

Formula: $C_{56}H_{92}O_{29}$

Formula Weight: 1229.31

Quality Release Date: 06 APR 2018

TEST	SPECIFICATION	RESULT
APPEARANCE (COLOR)	WHITE TO OFF WHITE	OFF-WHITE
APPEARANCE (FORM)	POWDER	POWDER
PURITY (TLC AREA %)	APPROX. 50 %	77.4 %
SPECIFIC ROTATION (20/D)	-53 ± 4 DEGREES	-53.2 %
CONCENTRATION	C=1 IN ETHANOL	--
SOLUBILITY (TURBIDITY)	1 G CAN BE DISSOLVED IN 20 ML OF WATER BY HEATING TO 95 - 98 DEG C	CLEAR
WATER	≤ 6.0 %	1.3 %
INFRARED SPECTRUM	CONFORMS TO STRUCTURE	CONFORMS



Dr. Reinhold Schwenninger
Quality Assurance
Buchs, Switzerland

Sigma-Aldrich warrants that at the time of the quality release or subsequent retest date this product conformed to the information contained in this publication. The current specification sheet may be available at Sigma-Aldrich.com. For further inquiries, please contact Technical Service. Purchaser must determine the suitability of the product for its particular use. See reverse side of invoice or packing slip for additional terms and conditions of sale.

Certification of loperamide



Certificate of Analysis

Jun 25, 2019 (JST)

TOKYO CHEMICAL INDUSTRY CO., LTD.
4-10-1 Nihonbashi-Honcho, Chuo-ku, Tokyo 103-0023 Japan

Chemical Name: Loperamide Hydrochloride		
Product Number: L0154 CAS RN: 34552-83-5	Lot: 4DIIB	
Tests	Results	Specifications
Purity(HPLC)	99.8 area%	min. 98.0 area%
Purity(Nonaqueous Titration)	98.5 %	min. 98.0 %
Solubility in Methanol	transparency	almost transparency

TCI Lot numbers are 4-5 characters in length. Characters listed after the first 4-5 characters are control numbers for internal purpose only. The contents of the specifications are subject to change without advance notice. The specification values displayed here are the most up to date values. There may be cases where the product labels display a different specification, however, the product quality still meets the latest specification.

Customer service:
TOKYO CHEMICAL INDUSTRY CO., LTD.
Tel: +81-3-5640-8878
Fax: +81-3-5640-8902
E-mail: globalbusiness@TCIchemicals.com

Ryo Ogawa
Ryo Ogawa
Quality Assurance Dep. Manager



Certification of PMSF

25/6/2562

Certificate Of Analysis

Certificate of Analysis

SIGMA-ALDRICH®

Product Name	Phenylmethanesulfonyl fluoride, ≥98.5% (GC)
Product Number	P7626
Product Brand	SIGMA
CAS Number	329-98-6
Molecular Formula	C ₇ H ₇ FO ₂ S
Molecular Weight	174.19

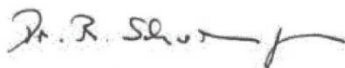
TEST**SPECIFICATION****LOT BCBP5502V RESULTS**

PDF

[Click here](#): Certificate of Analysis and Specifications only available in PDF format

COO

[Click here](#): Certificate of Origin available in PDF format



Dr. Reinhold Schwenninger
Quality Assurance
Buchs, Switzerland

Certification of BW284c51

SIGMA-ALDRICH

sigma-aldrich.com

3050 Spruce Street, Saint Louis, MO 63103, USA

Website: www.sigmaaldrich.com

Email USA: techserv@sial.com

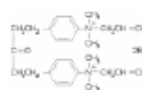
Outside USA: eurtechserv@sial.com

Certificate of Analysis

Product Name:

1,5-Bis(4-allyldimethylammoniumphenyl)pentan-3-one dibromide

Product Number: A9013
 Batch Number: 075M4086V
 Brand: SIGMA
 CAS Number: 402-40-4
 Formula: C₂₇H₃₈Br₂N₂O
 Formula Weight: 566.41 g/mol
 Quality Release Date: 29 JUN 2015
 Recommended Retest Date: JUN 2018



Test	Specification	Result
Appearance (Form)	Powder	Powder
Appearance (Colour)	White	White
Solubility (Solvent)	Water	Water
Solubility (Conc)	19.60 - 20.40 mg/ml	20.00 mg/ml
Solubility (Turbidity)	Clear	Clear
Solubility (Color)	Colorless	Colorless
Water (by Karl Fischer)	> 0.00 %	0.37 %
Elemental Anal. (%C anhydrous)	56.70 - 57.70 %	57.45 %
Purity (HPLC)	> 97.00 %	100.00 %
NMR (Solvent)	D ₂ O	D ₂ O
Identity by NMR	Consistent	Consistent with Structure

Theo Ackermann PhD MScEng CQM
 Manager, Quality and Regulatory Affairs
 Jerusalem, Israel IL

Sigma-Aldrich warrants, that at the time of the quality release or subsequent retest date this product conformed to the information contained in this publication. The current Specification sheet may be available at Sigma-Aldrich.com. For further inquiries, please contact Technical Service. Purchaser must determine the suitability of the product for its particular use. See reverse side of invoice or packing slip for additional terms and conditions of sale.

Certification of Iso-OMPA

25/6/2562

Certificate Of Analysis

Certificate of Analysis

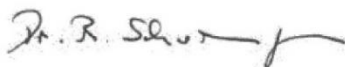
SIGMA-ALDRICH®

Product Name	Tetraisopropyl pyrophosphoramidate, butyrylcholinesterase inhibitor
Product Number	T1505
Product Brand	SIGMA
CAS Number	513-00-8
Molecular Formula	$C_{12}H_{32}N_4O_3P_2$
Molecular Weight	342.36

TEST**SPECIFICATION****LOT BCBN5735V RESULTS**

PDF

[Click here](#). Certificate of Analysis and Specifications only available in PDF format



Dr. Reinhold Schwenninger
Quality Assurance
Buchs, Switzerland

Certification of PCMB



Certificate of Analysis

8.20308.0005 4-(Hydroxymercuri)benzoic acid sodium salt for synthesis
Batch S4654608

Batch Values		
Assay (ex Hg)	97.3	%
Identity (IR)	passes test	

Date of examination (DD.MM.YYYY) 06.08.2015

Minimum shelf life (DD.MM.YYYY) 31.08.2020

Dr. Oliver Schramel
Responsible laboratory manager quality control

This document has been produced electronically and is valid without a signature.

Certification of DTNB

SIGMA-ALDRICH®3050 Spruce Street, Saint Louis, MO 63103 USA
Email USA: techserv@sial.com Outside USA: eurtechserv@sial.com

Certificate of Analysis

Product Name: 5,5'-DITHIOBIS(2-NITROBENZOIC ACID)
ReagentPlus™, 99 %

Product Number: D218200

Batch Number: STBD3094V

Brand: Aldrich

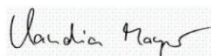
CAS Number: 69-78-3

Formula: $[-\text{SC}_6\text{H}_3(\text{NO}_2)\text{CO}_2\text{H}]_2$

Formula Weight: 396.35

Quality Release Date: 15 AUG 2013

TEST	SPECIFICATION	RESULT
APPEARANCE (COLOR)	YELLOW	LIGHT YELLOW
APPEARANCE (FORM)	POWDER OR CHUNKS	POWDER
TITRATION (T) NAOH 0.1M	98.5 - 101.5 %	98.7 %
PURITY (HPLC AREA %)	≥ 98.5 %	98.6 %
SOLUBILITY (COLOR)	COLORLESS TO LIGHT YELLOW	FAINT YELLOW
SOLUBILITY (TURBIDITY)	CLEAR TO SLIGHTLY HAZY	CLEAR
SOLUBILITY (METHOD)	10MG/ML, ETOH	10 MG/ML ETHANOL
INFRARED SPECTRUM	CONFORMS TO STRUCTURE	CONFORMS



Claudia Mayer, Manager
Quality Control
Steinheim, Germany

Sigma-Aldrich warrants that at the time of the quality release or subsequent retest date this product conformed to the information contained in this publication. The current specification sheet may be available at Sigma-Aldrich.com. For further inquiries, please contact Technical Service. Purchaser must determine the suitability of the product for its particular use. See reverse side of invoice or packing slip for additional terms and conditions of sale.

Certification of EDTA

ThermoFisher
SCIENTIFIC

Fisher Scientific UK Ltd.
part of Thermo Fisher Scientific
Bishop Meadow Road,
Loughborough,
Leicestershire,
LE11 5RG

Certificate of Analysis

Fisher Scientific's Quality System has been found to conform to Quality Management System Standard ISO9001:2015 by SAI Global Certificate Number QMS42099

This is to certify that units of the lot number below were tested and found to comply with the specifications of the grade listed. Certain data have been supplied by third parties. Thermo Fisher Scientific expressly disclaims all warranties, expressed or implied, including the implied warranties of merchantability and fitness for a particular purpose. Products are for research use or further manufacturing. Not for direct administration to humans or animals. It is the responsibility of the purchaser, formulator or those performing further manufacturing to determine suitability based upon the intended use of the end product. Products are tested to meet the analytical requirements of the noted grade. The following information is the actual analytical results obtained.

Catalogue Number:	D/0700/53	Quality Test / Release Date:	05-DEC-11
Lot Number:	1161444	Expiry Phrase:	Use within 5 yrs of opening

Description:	Diaminoethanetetra-acetic acid disodium salt		
Grade:	AR	Application:	For analysis

Appearance:	White Fine crystals (<2 mm)
--------------------	-----------------------------

Result Name	Test Value	Units	Specification
Assay	99.91	%	>= 99
Calcium (Ca)	0.12	ppm	<= 20
Copper (Cu)	<0.2	ppm	<= 2
Iron (Fe)	<0.2	ppm	<= 5
Lead (Pb)	<0.2	ppm	<= 2
Magnesium (Mg)	<0.05	ppm	<= 10
Potassium (K)	3.95	ppm	<= 30
Total chloride (Cl)	<0.005	%	<= 0.005
Total phosphorus (P)	<0.4	ppm	<= 50
Total silicon (Si)	0.3	ppm	<= 50
Total sulfur (S)	46.05	ppm	<= 200
Zinc (Zn)	<0.05	ppm	<= 20
pH (5% aq. solution)	4.45		>= 4 and <= 5

Additional Information:	
--------------------------------	--



Paula Faulkes

Mrs Paula Faulkes
Quality Assurance Manager.

Friday 10th of January 2020

Note: The data listed is valid for all package sizes of this lot of this product, expressed as an extension of the catalogue number listed above. If there are any questions with this certificate, please call Customer Services on +44(0)1509 555500

APPENDIX B

Preparation of solutions for enzyme activity study of LS9

1. Stock and working standard solutions

1.1. 100 mM 4-Nitrophenol stock standard solution

Approximately 13.91 mg of 4-Nitrophenol powder was weight and transferred to a 1-mL volumetric flask then dissolved and adjusted with ethanol.

1.2. 100 mM 4-Nitrophenyl acetate stock standard solution

Approximately 18.36 mg of 4-Nitrophenyl acetate powder was weight and transferred to a 1-mL volumetric flask then dissolved and adjusted with ethanol.

1.3. 100 mM 4-Nitrophenyl caprylate stock standard solution

Approximately 24 μL of 4-Nitrophenyl caprylate ($D= 1.095 \text{ g/mL}$) was pipetted and transferred to a 1-mL volumetric flask then dissolved and adjusted with ethanol.

2. Working standard solutions

2.1. 1000 μM 4-Nitrophenol working standard solution

A 10 μL of 100 mM 4-Nitrophenol stock standard solution was added to 990 μL of 50mM phosphate buffer pH7.4 in microcentrifuge tube and mixed

2.2. 1000 μM 4-Nitrophenyl acetate working standard solution

A 10 μL of 100 mM 4-Nitrophenyl acetate stock standard solution was added to 990 μL of 50mM phosphate buffer pH7.4 in microcentrifuge tube and mixed.

2.3. 1000 μM 4-Nitrophenyl caprylate working standard solution

A 10 μL of 1 mM 4-Nitrophenyl caprylate stock standard solution was added to 990 μL of 50mM phosphate buffer pH7.4 in microcentrifuge tube and mixed

3. Buffer solutions

3.1. 1 M Potassium phosphate dibasic (K_2HPO_4) solution

Potassium phosphate dibasic anhydrous was weighed about 87.09 g, dissolved in ultrapure water and adjusted in volumetric flask 500 mL.

3.2. Potassium dihydrogen phosphate (KH_2PO_4) solution

Potassium dihydrogen phosphate was weighed about 68.05 g, dissolved in ultrapure water and adjusted in volumetric flask 500 mL.

3.3. 100 mM Potassium phosphate buffer (pH 7.4)

A 80.2 mL of 1 M K_2HPO_4 and 19.8 mL of 1 M KH_2PO_4 were transfer to 1000 volumetric flask, then adjusted to the volume with ultrapure water.

3.4. 50 mM Potassium phosphate buffer (pH 7.4)

A 20 mL of 100 mM Potassium phosphate buffer (pH 7.4) was mixed with a 20 mL of ultrapure water in test tube.

APPENDIX C

Preparation solutions for *in vitro* metabolism study

1. Stock and working standard solutions

1.1. 1 mM CDD stock standard solution

Approximately 6.24 mg of CDD powder (96.68% purity) was weight and transferred to a 10-mL volumetric flask then dissolved and adjusted with acetonitrile.

1.2. 1 mM curcumin stock standard solution

Approximately 3.68 mg of curcumin powder (99.49% purity) was weight and transferred to a 10-mL volumetric flask then dissolved and adjusted with acetonitrile.

1.3. 1 mM MSCUR stock standard solution

Approximately 4.97 mg of CDD powder (98.63% purity) was weight and transferred to a 10-mL volumetric flask then dissolved and adjusted with acetonitrile.

1.4. 1 mM DMC stock standard solution

Approximately 3.96 mg of CDD powder (98.74% purity) was weight and transferred to a 10-mL volumetric flask then dissolved and adjusted with acetonitrile.

2. Working standard solutions

2.1. 100 μ M CDD working standard solution

A 500 μ L of 1 mM CDD stock standard solution was added to 500 μ L of acetonitrile in microcentrifuge tube and mixed.

2.2. 150 μ M CDD working standard solution

A 60 μ L of 1 mM CDD stock standard solution was added to 340 μ L of 40% acetonitrile in microcentrifuge tube and mixed.

2.3. 100 μ M Curcumin working standard solution

A 40 μL of 1 mM curcumin stock standard solution was added to 360 μL of 40% acetonitrile in microcentrifuge tube and mixed.

2.4. 100 μM MSCUR working standard solution

A 40 μL of 1 mM MSCUR stock standard solution was added to 360 μL of 40% acetonitrile in microcentrifuge tube and mixed.

2.5. 225 μM DMC working standard solution

A 90 μL of 1 mM DMC stock standard solution was added to 310 μL of 40% acetonitrile in microcentrifuge tube and mixed.

2.6. CDD working standards for standard curve

Final concentration (μM)	CDD standard solution		Volume of 40% acetonitrile (μL)	Final volume (μL)
	Added volume (μL)	Concentration (μM)		
1.25	5	100	395	400
12.5	50	100	350	400
25	100	100	300	400
75	30	1000	370	400
125	50	1000	350	400
175	70	1000	330	400
225	90	1000	310	400

CHULALONGKORN UNIVERSITY

2.7. Curcumin working standards for standard curve

Final concentration (μM)	Curcumin standard solution		Volume of 40% acetonitrile (μL)	Final volume (μL)
	Added volume (μL)	Concentration (μM)		
1.25	5	100	395	400
12.5	50	100	350	400
25	100	100	300	400
75	30	1000	370	400
125	50	1000	350	400
175	70	1000	330	400
225	90	1000	310	400

2.8. MSCUR working standards for standard curve

Final concentration (μM)	MSCUR standard solution Added volume (μL)	Concentration (μM)	Volume of 40% acetonitrile (μL)	Final volume (μL)
0.625	5	100	795	800
1.25	5	100	395	400
2.5	10	100	390	400
5	20	100	380	400
12.5	50	100	350	400
25	100	100	300	400
37.5	150	100	250	400

3. Acetonitrile with internal standard solution for protein precipitation

A 20 μL of 225 μM DMC working standard was added to 9.98 mL of acetonitrile in tube and mixed to obtain a concentration at 0.45 μM .

4. System suitability solutions

A 10 μL of 1 mM each stock standard solution including CDD, curcumin, MSCUR and DMC were added to 960 μL of acetonitrile. The 15 μL of mixture was transferred to 985 μL of 50% acetonitrile and mixed to obtain each standard concentration at 0.15 μM .

5. Buffer solutions

5.1. 1 M Potassium phosphate dibasic (K_2HPO_4) solution

Potassium phosphate dibasic anhydrous was weighed about 87.09 g, dissolved in ultrapure water and adjusted in volumetric flask 500 mL.

5.2. 1 M Potassium dihydrogen phosphate (KH_2PO_4) solution

Potassium dihydrogen phosphate was weighed about 68.05 g, dissolved in ultrapure water and adjusted in volumetric flask 500 mL.

5.3. 100 mM Potassium phosphate buffer (pH 7.4)

A 80.2 mL of 1 M K_2HPO_4 and 19.8 mL of 1 M KH_2PO_4 were transfer to 1000 volumetric flask, then adjusted to the volume with ultrapure water.

6. Esterase inhibitor solutions

6.1. 10 mM BNPP solution

BNPP was weighed about 3.40 mg, and dissolved in a 1000 μL of ultrapure water in a microcentrifuge tube.

6.2. 10 mM Digitonin solution

Digitonin was weighed about 12.29 mg, and dissolved in a 1000 μL of Ethanol in a microcentrifuge tube.

6.3. 10 mM Loperamide solution

Loperamide was weighed about 5.14 mg, and dissolved in a 1000 μL of Ethanol in a microcentrifuge tube.

6.4. 10 mM PMSF solution

PMSF was weighed about 1.74 mg, and dissolved in a 1000 μL of Ethanol in a microcentrifuge tube.

6.5. 10 mM BW284c51 solution

BW284c51 was weighed about 5.66 mg, and dissolved in a 1000 μL of ultrapure water in a microcentrifuge tube.

6.6. 10 mM Iso-OMPA solution

Iso-OMPA was weighed about 3.42 mg, and dissolved in a 1000 μL of ultrapure water in a microcentrifuge tube.

6.7. 10 mM PCMB solution

PCMB was weighed about 3.61 mg, and dissolved in a 1000 μL of 50% Ethanol in a microcentrifuge tube.

6.8. 10 mM DTNB solution

DTNB was weighed about 3.96 mg, and dissolved in a 1000 μL of Ethanol in a microcentrifuge tube.

6.9. 100 mM Na_2EDTA solution

Na_2EDTA was weighed about 37.2 mg, and dissolved in a 1000 μL of ultrapure water in a microcentrifuge tube.

6.10. 1 mM BNPP solution

A 100 μL of 10 mM BNPP solution was mixed with 900 μL of ethanol/phosphate buffer at pH 7.4 (10:80, V/V) in a microcentrifuge tube.

6.11. 1 mM Digitonin solution

A 100 μL of 10 mM digitonin solution was mixed with 900 μL of water/phosphate buffer at pH 7.4 (10:80, V/V) in a microcentrifuge tube.

6.12. 1 mM Loperamide solution

A 100 μL of 10 mM loperamide solution was mixed with 900 μL of water/phosphate buffer at pH 7.4 (10:80, V/V) in a microcentrifuge tube.

6.13. 1 mM PMSF solution

A 100 μL of 10 mM PMSF solution was mixed with 900 μL of water/phosphate buffer at pH 7.4 (10:80, V/V) in a microcentrifuge tube.

6.14. 1 mM BW284c51 solution

A 100 μL of 10 mM BW284c51 solution was mixed with 900 μL of ethanol/phosphate buffer at pH 7.4 (10:80, V/V) in a microcentrifuge tube.

6.15. 1 mM Iso-OMPA solution

A 100 μL of 10 mM Iso-OMPA solution was mixed with 900 μL of ethanol/phosphate buffer at pH 7.4 (10:80, V/V) in a microcentrifuge tube.

6.16. 1 mM PCMB solution

A 100 μL of 10 mM PCMB solution was mixed with 900 μL of 50% ethanol/phosphate buffer at pH 7.4 (10:80, V/V) in a microcentrifuge tube.

6.17. 1 mM DTNB solution

A 100 μL of 10 mM DTNB solution was mixed with 900 μL of water/phosphate buffer at pH 7.4 (10:80, V/V) in a microcentrifuge tube.

6.18. 10 mM Na_2EDTA solution

A 100 μL of 100 mM Na_2EDTA solution was mixed with 900 μL of ethanol/phosphate buffer at pH 7.4 (10:80, V/V) in a microcentrifuge tube.

7. Other solutions

7.1. 0.1% Formic acid in ultrapure water

A 1 mL of formic acid was added to 900 mL of ultrapure water in a beaker and adjusted to 1000 mL in 1000 mL-cylinder.

7.2. 0.2% Formic acid in ultrapure water

A 2 mL of formic acid was added to 900 mL of ultrapure water in a beaker and adjusted to 1000 mL in 1000 mL-cylinder.

7.3. 0.1% Formic acid in acetonitrile

A 1 mL of formic acid was added to 900 mL of acetonitrile in a beaker and adjusted to 1000 mL in 1000 mL-cylinder.

APPENDIX D

Standard curve and sample preparation for enzyme activity study

The standard curve, blank sample, and the reaction system were prepared to study esterase activity in LS9. The 4-nitrophenol was monitored using UV spectrophotometry method after incubation 4-nitrophenyl acetate and 4-nitrophenyl caprylate with LS9 from human, monkey, dog, and rat.

1. Diluted LS9

LS9 1 mg/mL

Solution	n = 1
20 mg/mL LS9 (μL)	2
50 mM PBS pH 7.4 (μL)	38
Total	40

LS9 10 $\mu\text{g}/\text{mL}$

Solution	n = 1
1 mg/mL LS9 (μL)	10
50 mM PBS pH 7.4 (μL)	990
Total	1000

Note: The LS9 at 10 $\mu\text{g}/\text{mL}$ was use for blank and sample preparation for enzyme activity test, and heated LS9 at 10 $\mu\text{g}/\text{mL}$ was used for standard curve.

2. Standard curve

4-Nitrophenol working standards for standard curve in 50 mM PBS (pH7.4)

Final concentration (μM)	4-Nitrophenol standard solution		Volume of 50 mM PBS pH 7.4 (μL)	Final volume (μL)
	Added volume (μL)	Concentration (μM)		
1.95	200	3.91	200	400
3.91	200	7.81	200	400
7.81	200	15.63	200	400
15.63	200	62.5	200	400
62.5	200	125	200	400
125	200	250	200	400
250	200	500	200	400
500	200	1000	200	400

4-Nitrophenol working standards for standard curve in LS9

Final concentration (μM)	4-Nitrophenol standard solution		Volume of LS9 (μL) ^a	Final volume (μL)
	Added volume (μL)	Concentration (μM)		
1.95	200	3.91	200	400
3.91	200	7.81	200	400
7.81	200	15.63	200	400
15.63	200	62.5	200	400
62.5	200	125	200	400
125	200	250	200	400
250	200	500	200	400
500	200	1000	200	400

Note: ^aThe standard curve of 4-nitrophenol was prepared in heated HLS9, MLS9, DLS9 and RLS9

3. Sample preparation in 96 well plate

3.1 Blank

3.1.1 Blank in 50 mM PBS pH 7.4

Solution	n = 1
50 mM PBS pH 7.4 (μL)	100
50 mM PBS pH 7.4 (μL)	100
Total	200

3.1.2 Blank in LS9

Solution	n = 1
50 mM PBS pH 7.4 (μL)	100
10 $\mu\text{g}/\text{mL}$ LS9 (μL)	100
Total	200

Note: The Blank was prepared in heated HLS9, MLS9, DLS9 and RLS9

3.2 Reaction mixture

3.2.1 Substrate: 4-Nitrophenyl acetate

Reaction mixture of 4-Nitrophenyl acetate in 50 mM PBS

pH 7.4

Solution	n = 1
1000 μM 4-Nitrophenyl acetate (μL)	100
50 mM PBS pH 7.4 (μL)	100
Total	200

Reaction mixture of 4-Nitrophenyl acetate in LS9

Solution	n = 1
1000 μ M 4-Nitrophenyl acetate (μ L)	100
10 μ g/mL LS9 (μ L)	100
Total	200

Note: The Reaction mixture of 4-nitrophenyl acetate was prepared in HLS9, MLS9, DLS9 and RLS9

3.2.2 Substrate: 4-Nitrophenyl caprylate

Reaction mixture of 4-Nitrophenyl caprylate in 50 mM PBS pH 7.4

Solution	n = 1
1000 μ M 4-Nitrophenyl caprylate (μ L)	100
50 mM PBS pH 7.4 (μ L)	100
Total	200

Reaction mixture of 4-Nitrophenyl caprylate in LS9

Solution	n = 1
1000 μ M 4-Nitrophenyl caprylate (μ L)	100
10 μ g/mL LS9 (μ L)	100
Total	200

Note: The Reaction mixture of 4-nitrophenyl acetate was prepared in HLS9, MLS9, DLS9 and RLS9

4. Reaction system

Description	4-Nitrophenol (μM)	LS9 ($\mu\text{g/mL}$)	Substrate (μM)	Reaction time (min)
Standard curve in 50mM PBS pH7.4	1.95-500	5	-	-
Standard curve in HLS9	1.95-500	5 ^a	-	-
Standard curve in MLS9	1.95-500	5 ^a	-	-
Standard curve in DLS9	1.95-500	5 ^a	-	-
Standard curve in RLS9	1.95-500	5 ^a	-	-
Blank 50mM PBS pH7.4	-	-	-	-
Blank HLS9	-	5	-	-
Blank MLS9	-	5	-	-
Blank DLS9	-	5	-	-
Blank RLS9	-	5	-	-
Reaction mixture in 50 mM PBS pH7.4	-	5	500	5
Reaction mixture in HLS9	-	5	500	5
Reaction mixture in MLS9	-	5	500	5
Reaction mixture in DLS9	-	5	500	5
Reaction mixture in RLS9	-	5	500	5

Note: Substrate: 4-nitrophenyl acetate or 4-nitrophenyl caprylate. Monitor the release of p-nitrophenol from reaction mixture using a UV spectrophotometer at 405 nm every 10 sec for 5 min. The reaction mixtures were incubated in triplicate with LS9. (a) Heated LS9 for standard curve preparation.

The graph was plotted the 4-nitrophenol formation against the reaction time in 50mM PBS pH 7.4, HLS9, MLS9, DLS9 and RLS9. The slope of graph from each reaction mixture in 50mM PBS pH 7.4 and in LS9 represent as a control and hydrolysis rate, respectively. The specific activity was determined by subtraction of the hydrolysis rate in 50mM PBS pH 7.4 from that in LS9 as described in Eq 1.

APPENDIX E

Standard and sample preparation for *in vitro* metabolism study

The Standard curve, blank and sample preparation of the experiment were prepared as described in this protocol, and the reaction systems were setup to study in hydrolysis of CDD for *in vitro* metabolism study including metabolite identification, metabolic stability, optimization of enzyme assay condition for linear range of product formation and enzyme identification.

1. Metabolite identification

1.1 Diluted LS9 1 mg/mL

Solution	n = 1
20 mg/mL LS9 (μ L)	2.5
100 mM PBS pH 7.4 (μ L)	46.5
Total	49

1.2 Blank preparation

Solution	n = 1
40%ACN	1
1 mg/mL LS9 (μ L)	49
Total	50

1.3 Sample preparation

Solution	n = 1
500 μ M CDD (μ L)	1
1 mg/mL LS9 (μ L)	49
Total	50

1.4 Reaction system

Reaction systems for the determination of metabolite identification.

Description	CDD (μM)	Curcumin (μM)	MSCUR (μM)	LS9 (mg/mL)	Substrate (μM)	Reaction time (min)
Standard solution	0.15	0.15	0.15	–	–	–
Blank LS9	–	–	–	1	–	0.5
Reaction mixture	–	–	–	1	10	0.5

Note. The blank LS9 and reaction mixtures were incubated with HLS9, MLS9, DLS9 and RLS9.



2. Metabolic stability

2.1 Diluted LS9 1 mg/mL

Solution	n = 1	n = 15
20 mg/mL LS9 (μL)	2.5	37.5
100 mM PBS pH 7.4 (μL)	46.5	697.5
Total	49	735

Note: Heat diluted LS9 at 1 mg/mL was used for standard curve and sample preparation at time0.

2.2 Standard curve

CDD standard curve

Final CDD in Heated LS9 concentration (μM)	CDD working standard solution		Added Heated LS9 Volume (μL)	Final volume (μL)
	Added volume (μL)	Concentration (μM)		
0.025	1	1.25	49	50
0.25	1	12.5	49	50
0.5	1	25	49	50
1.5	1	75	49	50
2.5	1	125	49	50
3.5	1	175	49	50
4.5	1	225	49	50

Curcumin standard curve

Final curcumin in Heated LS9 concentration (μM)	Curcumin working standard solution		Added Heated LS9 Volume (μL)	Final volume (μL)
	Added volume (μL)	Concentration (μM)		
0.025	1	1.25	49	50
0.25	1	12.5	49	50
0.5	1	25	49	50
1.5	1	75	49	50
2.5	1	125	49	50
3.5	1	175	49	50
4.5	1	225	49	50

MSCUR standard curve

Final MSCUR in Heated LS9 concentration (μM)	MSCUR working standard solution		Added Heated LS9 Volume (μL)	Final volume (μL)
	Added volume (μL)	Concentration (μM)		
0.0125	1	0.625	49	50
0.025	1	1.25	49	50
0.05	1	2.5	49	50
0.1	1	5	49	50
0.25	1	12.5	49	50
0.5	1	25	49	50
0.75	1	37.5	49	50

Note: The standard curve of CDD, curcumin and MSCUR were prepared in HLS9, MLS9, DLS9 and RLS9

2.3 Blank preparation

Solution	n = 1
40%ACN (μL)	1
1 mg/mL LS9 (μL)	49
Total	50

2.4 Sample preparation

Solution	n = 1	n = 15
150 μM CDD (μL)	1	15
1 mg/mL LS9 (μL)	49	735
Total	50	750

2.5 Reaction system

Reaction systems for the determination of metabolic stability.

Description	CDD (μM)	Curcumin (μM)	MSCUR (μM)	LS9 (mg/mL)	Substrate (μM)	Reaction time (min)
Standard curve	0.025-4.5	-	-	1 ^a	-	-
Standard curve	-	0.025-4.5	-	1 ^a	-	-
Standard curve	-	-	0.0125-0.75	1 ^a	-	-
Blank LS9	-	-	-	1	-	120
Reaction mixture	-	-	-	1	3	0-120

Note: The reaction mixtures were incubated in triplicate with HLS9, MLS9, DLS9 and RLS9. (a) Heated LS9 for standard curve preparation.



3. Optimization for enzyme assay condition in LS9

3.1 Diluted LS9

Diluted LS9 10 µg/mL

Solution	n = 1	n = 20
20 mg/mL LS9 (µL)	0.025	0.5
100 mM PBS pH 7.4 (µL)	48.975	979.5
Total	49	980

Diluted LS9 20 µg/mL

Solution	n = 1	n = 12
20 mg/mL LS9 (µL)	0.05	0.6
100 mM PBS pH 7.4 (µL)	48.95	587.4
Total	49	588

Diluted LS9 50 µg/mL

Solution	n = 1	n = 12
20 mg/mL LS9 (µL)	0.125	1.5
100 mM PBS pH 7.4 (µL)	48.875	586.5
Total	49	588

Diluted LS9 100 µg/mL

Solution	n = 1	n = 12
20 mg/mL LS9 (µL)	0.25	3
100 mM PBS pH 7.4 (µL)	48.75	586.5
Total	49	588

Note: Heat diluted LS9 at 10, 20, 50 and 100 µg/mL was used in sample preparation at time 0.

3.2 Sample preparation

Solution	n = 1	n = 12	n = 20
150 μ M CDD (μ L)	1	12	20
10, 20, 50, or 100 μ g/mL LS9 (μ L)	49	588	980
Total	50	600	1000

3.3 Reaction system

Reaction systems for the determination of linear range of curcumin formation.

Description	LS9 (μ g/mL)	Substrate (μ M)	Reaction time (min)
Reaction mixture No. 1	10	3	0-60
Reaction mixture No. 2	20	3	0-60
Reaction mixture No. 3	50	3	0-60
Reaction mixture No. 4	100	3	0-60

Note: The reaction mixtures No.1-4 were incubated in duplicate with HLS9, MLS9, DLS9 and RLS9.

4. Enzyme identification

4.1 Diluted LS9 20 $\mu\text{g}/\text{mL}$

Solution	n = 1	n = 10
20 mg/mL LS9 (μL)	0.05	0.5
100 mM PBS pH 7.4 (μL)	43.95	439.5
Total	44	440

4.2 Diluted LS9 20 $\mu\text{g}/\text{mL}$ for standard curve

Solution	n = 1	n = 10
20 mg/mL LS9 (μL)	0.5	0.5
100 mM PBS pH 7.4 (μL)	48.95	489.5
Total	49	490

Note: Heat diluted LS9 at 20 $\mu\text{g}/\text{mL}$ was used for standard curve.

4.3 Standard curve

Final curcumin in Heated LS9 concentration (μM)	Curcumin working standard solution		Added Heated LS9 Volume (μL)	Final volume (μL)
	Added volume (μL)	Concentration (μM)		
0.025	1	1.25	49	50
0.25	1	12.5	49	50
0.5	1	25	49	50
1.5	1	75	49	50
2.5	1	125	49	50
3.5	1	175	49	50
4.5	1	225	49	50

Note: The s curve of standard curcumin was prepared in HLS9, MLS9, DLS9 and RLS9

4.4 Inhibitor-free control, Enzyme-free control, Solvent-free control and Sample preparation

	Inhibitor-free control	Enzyme-free control	Solvent-free control	Sample control
150 μ M CDD (μ L)	1	1	1	1
Diluted LS9 (μ L)	44	-	44	44
Enzyme inhibitor (1-9) (μ L)	-	-	-	5
100 mM PBS pH 7.4 (μ L)	-	44	-	-
Diluted solvent:				
Ethanol: 100 mM PBS pH 7.4 (10:90) (μ L)	5	5	-	-
No Diluted solvent				
Water: 100 mM PBS pH 7.4 (10:90) (μ L)	-	-	5	-

4.5 Reaction system

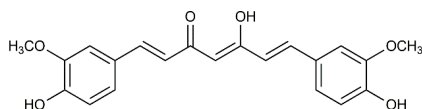
Reaction systems for the determination of enzyme identification.

Description	Curcumin (μ M)	LS9 (μ g/mL)	Substrate (μ M)	Solvent (%)	Enzyme inhibitor (μ M)	Reaction time (min)
Standard curve	0.025-4.5	20 ^a	-	-	-	-
Inhibitor-free control	-	20	3	2	-	b
Enzyme-free control	-	-	3	2	-	b
Solvent-free control	-	20	3	-	-	b
Reaction mixture with Enzyme inhibitors(1-8)	-	20	3	2	100	b
Reaction mixture with Enzyme inhibitors (9)	-	20	3	2	1000	b

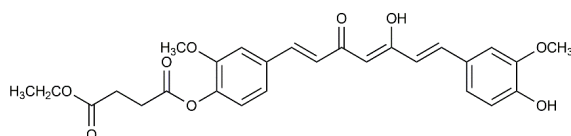
Note: The reaction mixtures were incubated in triplicate with HLS9, MLS9, DLS9 and RLS9. (a) Heated LS9 for standard curve preparation. (b) Selected time with 0.5 min for reaction in MLS9 and DLS9, and 1 min for reaction in HLS9 and RLS9. Enzyme inhibitor including (1) BNPP (2) Digitonin (3) Loperamide (4) PMSF (5) BW284c51 (6) Iso-OMPA (7) PCMB (8) DTNB (9) EDTA.

APPENDIX F

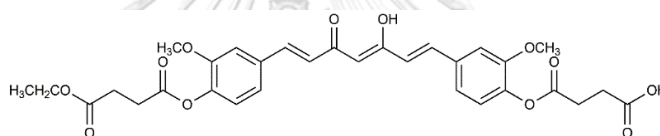
Proposed five metabolites structure



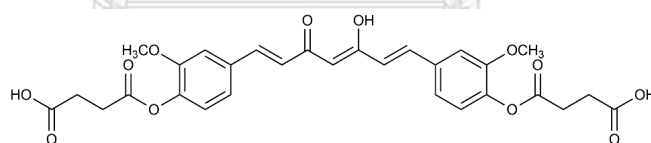
M1 m/z 369.1333 (curcumin)



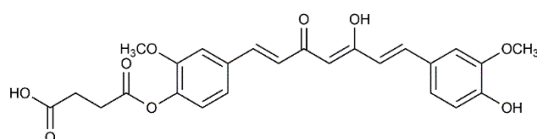
M2 m/z 497.1806 (MSCUR)



M3 m/z 597.1966



M4 m/z 569.1653



M5 m/z 469.1493

Figure 32. Proposed metabolite structure of CDD metabolism

APPENDIX G

UV spectrum

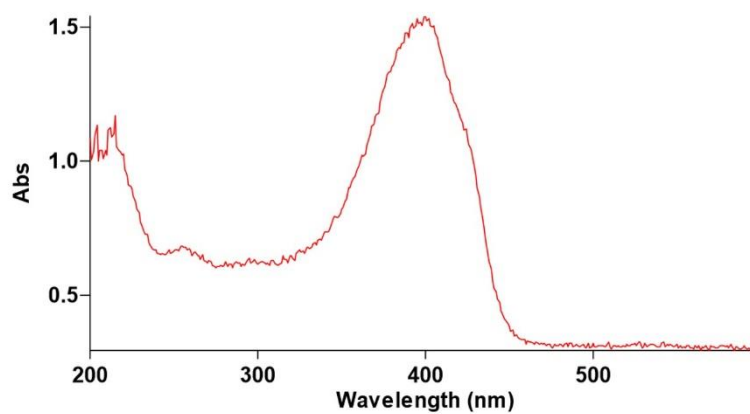


Figure 33. UV spectrum of CDD 10 $\mu\text{g/mL}$ in 0.1%formic acid in acetonitrile-0.1%formic acid in water (50:50, (v/v); $\lambda_{\text{max}} = 400 \text{ nm}$)

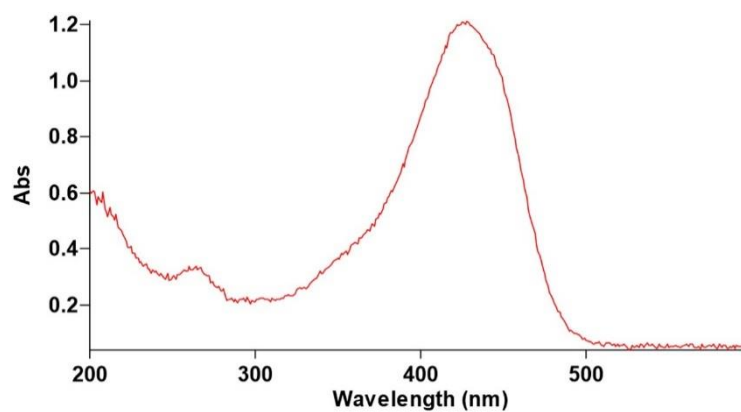


Figure 34. UV spectrum of curcumin 10 $\mu\text{g/mL}$ in 0.1%formic acid in acetonitrile-0.1%formic acid in water (50:50, (v/v); $\lambda_{\text{max}} = 427 \text{ nm}$)

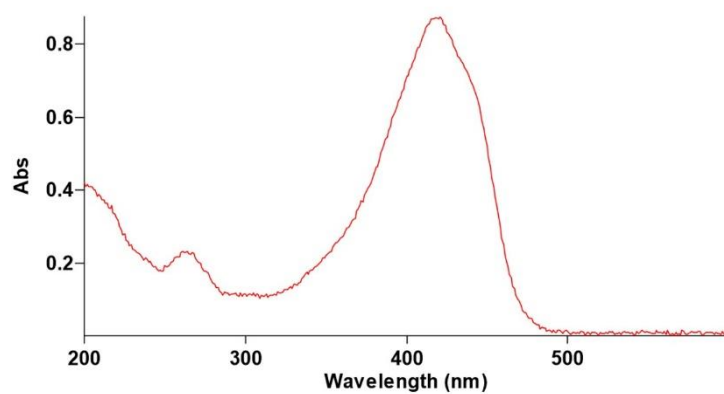


Figure 35. UV spectrum of MSCUR 10 $\mu\text{g/mL}$ in 0.1% formic acid in acetonitrile-0.1% formic acid in water (50:50, (v/v)); $\lambda_{\text{max}} = 418 \text{ nm}$

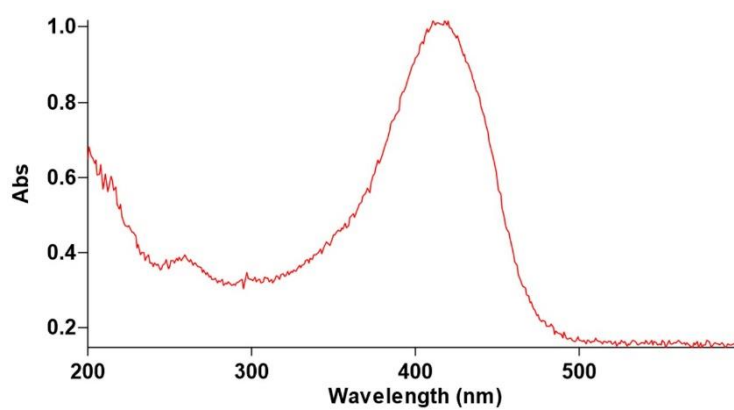


Figure 36. UV spectrum of DMC 10 $\mu\text{g/mL}$ in 0.1% formic acid in acetonitrile-0.1% formic acid in water (50:50, (v/v)); $\lambda_{\text{max}} = 421 \text{ nm}$

APPENDIX H

Kinetics reaction and raw data for metabolic stability

The metabolic stability study of CDD in HLS9, MLS9, DLS9 and RLS9 were set to pseudo-first-order reaction due to CDD substrate incubated with excess catalyst LS9 and consequence converted to curcumin, active metabolite (167). The degradation rate constant of CDD is proportional to the concentration of CDD, as in Eq. H1 and Eq. H2.

$$[A] = [A]_0 e^{-kt} \quad (\text{H1})$$

$$\ln[A] = \ln[A]_0 - kt \quad (\text{H2})$$

Where $[A]_0$ is the initial percentage of CDD at time 0, $[A]$ is the percentage of CDD at time t , k is degradation rate constant of CDD

Fist, the data was evaluated by linear least squares, the graphic plot of log-transform-percent remaining of CDD and time showed poor linearity. R^2 value estimated by Eq H3 (156).

$$r^2 = 1 - \frac{\sum(y - y_{\text{mean}})^2}{\sum(y^2) - \frac{\sum(y)^2}{n}} \quad (\text{H3})$$

The R^2 from metabolic stability study of CDD in HLS9, MLS9, DLS9 and RLS9 were not linear with ranged between 0.6807 and 0.8539 in four tested species. The data presented as following.

1. Pseudo-first-order kinetics by liner least squares

CDD degradation in HLS9

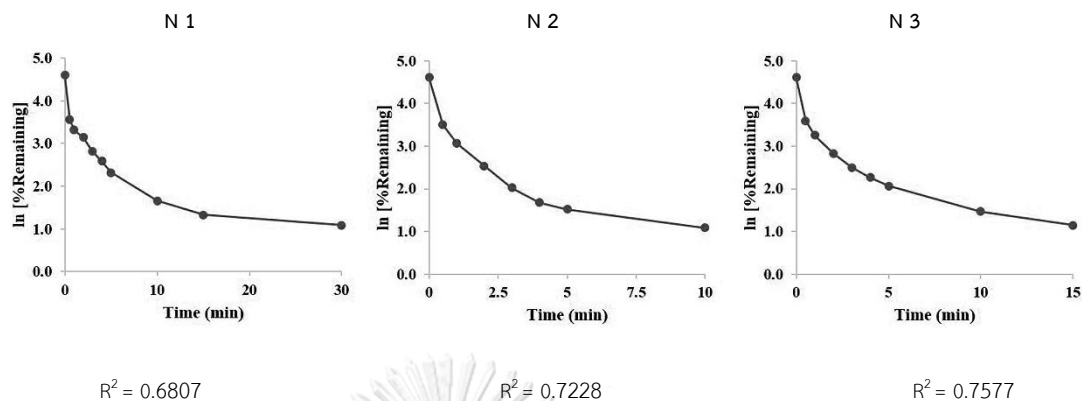


Figure 37. Ln [%Remaining] of CDD in HLS9 plotted against incubation time. CDD at $3 \mu\text{M}$ were incubated in triplicate with HLS9 1 mg/mL.

1.1 CDD degradation in MLS9

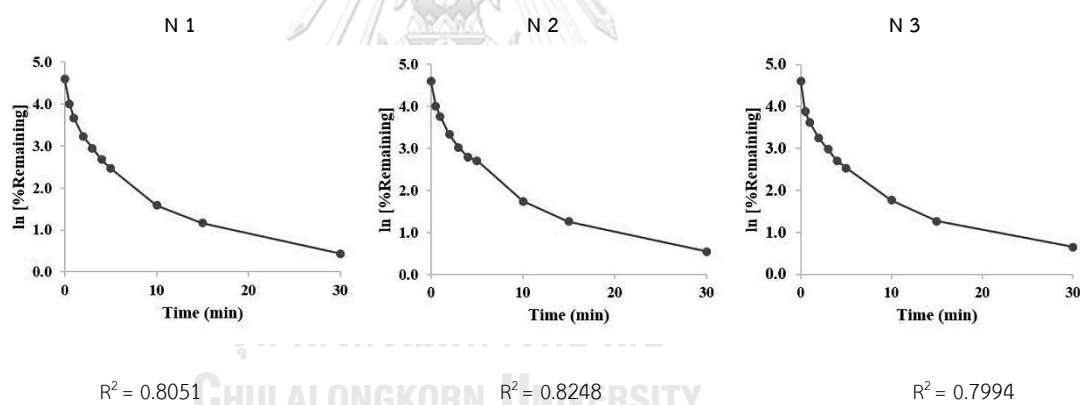


Figure 38. Ln [%Remaining] of CDD in MLS9 plotted against incubation time. CDD at $3 \mu\text{M}$ were incubated in triplicate with MLS9 1 mg/mL.

1.2 CDD degradation in DLS9

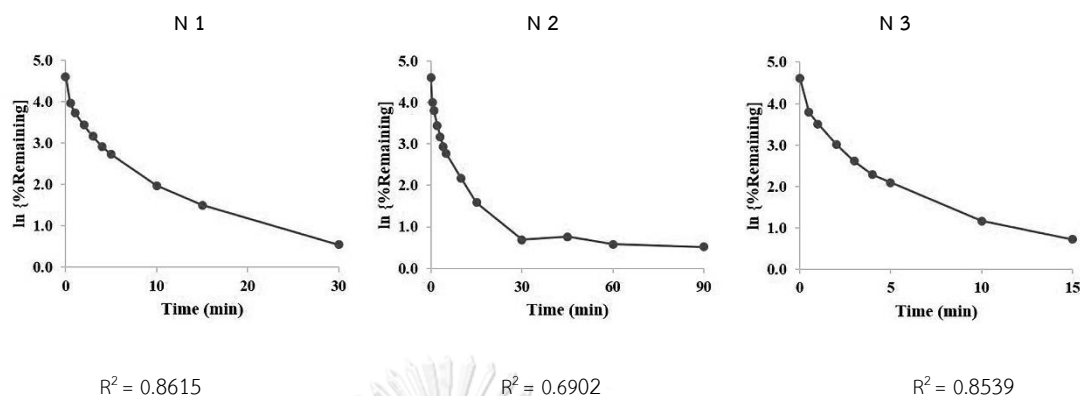


Figure 39. Ln [%Remaining] of CDD in DLS9 plotted against incubation time. CDD at 3 μM were incubated in triplicate with DLS9 1 mg/mL.

1.3 CDD degradation in RLS9

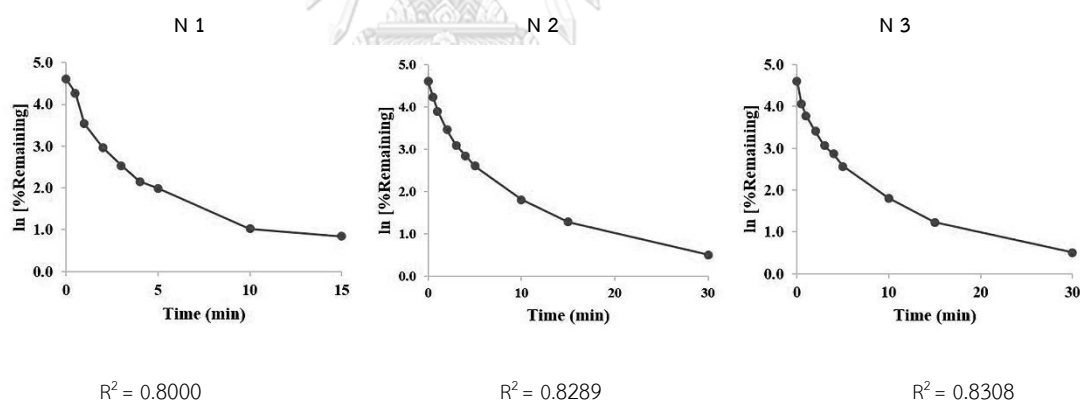


Figure 40. Ln [%Remaining] of CDD in RLS9 plotted against incubation time. CDD at 3 μM were incubated in triplicate with RLS9 1 mg/mL.

Thus, the nonlinear regression has recommended for curve-fitting was used instead of linear regression and could be evaluated by using Excel's Solver (155). In this study, CDD reacted with LS9 give active metabolite curcumin through intermediate metabolite MSCUR. A two-step consecutive irreversible pseudo-first-order reaction was assigned to the model for CDD hydrolysis.



H4)

$$A = A_0 e^{-k_1 t} \quad (\text{Eq. H5})$$

$$B = \frac{k_1 A_0}{k_2 - k_1} (e^{-k_1 t} - e^{-k_2 t}) \quad (\text{Eq. H6})$$

where A_0 = CDD concentration at time 0, B = MSCUR, C = curcumin, k_1 = degradation rate constant of CDD, and k_2 = degradation rate constant of MSCUR.

A goodness of fit on nonlinear regression (R^2) and confident interval (CI), were evaluated by Eq H7 and Eq H8 (156).

$$R^2 = 1 - \frac{\sum (y - y_{\text{fit}})^2}{\sum (y - y_{\text{mean}})^2} \quad (\text{Eq. H7})$$

$$95\% \text{ CI} = y_{\text{fit}} \pm t_c \text{ S.E.} \quad (\text{Eq. H8})$$

$$\text{S.E.} = \sqrt{\frac{\sum (y - y_{\text{fit}})^2}{df}} \quad (\text{Eq. H9})$$

The data of CDD and MSCUR depletion in HLS9, MLS9, DLS9 and RLS9 demonstrated good fit of nonlinear model. R^2 was nearly 0.9 which 90% of the variation of the independent variable can be explained by the variation of the dependent variable. The observed value of dependent variable line within the range of confident interval. The degradation rate constant of CDD (k_1) and MSCUR (k_2) in HLS9, MLS9, DLS9 and RLS9 were determined by Eq. H5 and Eq. H6, respectively. The data was showed as following.

2. Pseudo-first-order kinetics by nonlinear least squares

2.1 CDD degradation in HLS9

- N1

Time (min)	Y	\hat{Y}	$Y - \hat{Y}$	$(Y - \hat{Y})^2$	$(Y - \bar{Y})^2$	Lower CL	Upper CL	
0	3.2098	3.2098	0.0000	0.0000	7.0986	2.5850	3.8346	
0.5	1.1298	1.6046	-0.4748	0.2254	0.3415	0.9798	2.2294	
1	0.8834	0.8022	0.0812	0.0066	0.1142	0.1774	1.4270	
2	0.7425	0.2005	0.5421	0.2938	0.0388	-0.4243	0.8253	
3	0.5334	0.0501	0.4833	0.2336	0.0001	-0.5747	0.6749	
4	0.4270	0.0125	0.4145	0.1718	0.0140	-0.6123	0.6373	
5	0.3256	0.0031	0.3224	0.1040	0.0484	-0.6217	0.6280	
10	0.1686	0.0000	0.1686	0.0284	0.1420	-0.6248	0.6248	
15	0.1215	0.0000	0.1215	0.0148	0.1798	-0.6248	0.6248	
30	0.0951	0.0000	0.0951	0.0090	0.2028	-0.6248	0.6248	
45	0.0000	0.0000	0.0000	0.0000	0.2975	-0.6248	0.6248	
60	0.0000	0.0000	0.0000	0.0000	0.2975	-0.6248	0.6248	
90	0.0000	0.0000	0.0000	0.0000	0.2975	-0.6248	0.6248	
120	0.0000	0.0000	0.0000	0.0000	0.2975	-0.6248	0.6248	
\bar{Y}	$\Sigma (Y - \hat{Y})^2$	$\Sigma (Y - \bar{Y})^2$	df	S.E. of Y	Critical t	CI	R ²	k_1 (min ⁻¹)
0.5455	1.0874	9.3705	13	0.2892	2.1604	0.6248	0.8840	1.3866

- N2

Time (min)	Y	\hat{Y}	$Y - \hat{Y}$	$(Y - \hat{Y})^2$	$(Y - \bar{Y})^2$	Lower CL	Upper CL	
0	3.2890	3.2098	0.0792	0.0063	8.1149	2.8774	3.5422	
0.5	1.0856	1.3243	-0.2387	0.0570	0.4164	0.9919	1.6567	
1	0.7016	0.5464	0.1552	0.0241	0.0683	0.2140	0.8787	
2	0.4156	0.0930	0.3225	0.1040	0.0006	-0.2394	0.4254	
3	0.2489	0.0158	0.2331	0.0543	0.0366	-0.3165	0.3482	
4	0.1763	0.0027	0.1736	0.0301	0.0697	-0.3297	0.3351	
5	0.1501	0.0005	0.1496	0.0224	0.0842	-0.3319	0.3328	
10	0.0971	0.0000	0.0971	0.0094	0.1178	-0.3324	0.3324	
15	0.0000	0.0000	0.0000	0.0000	0.1939	-0.3324	0.3324	
30	0.0000	0.0000	0.0000	0.0000	0.1939	-0.3324	0.3324	
45	0.0000	0.0000	0.0000	0.0000	0.1939	-0.3324	0.3324	
60	0.0000	0.0000	0.0000	0.0000	0.1939	-0.3324	0.3324	
90	0.0000	0.0000	0.0000	0.0000	0.1939	-0.3324	0.3324	
120	0.0000	0.0000	0.0000	0.0000	0.1939	-0.3324	0.3324	
\bar{Y}	$\Sigma (Y - \hat{Y})^2$	$\Sigma (Y - \bar{Y})^2$	df	S.E. of Y	Critical t	CI	R ²	k_t (min ⁻¹)
0.4403	0.3077	10.0716	13	0.1538	2.1604	0.3324	0.9694	1.7706

- N3

Time (min)	Y	\hat{Y}	$Y - \hat{Y}$	$(Y - \hat{Y})^2$	$(Y - \bar{Y})^2$	Lower CL	Upper CL	
0	3.4152	3.2098	0.2054	0.0422	8.3329	2.7225	3.6971	
0.5	1.2463	1.6101	-0.3637	0.1323	0.5152	1.1228	2.0974	
1	0.8856	0.8076	0.0780	0.0061	0.1275	0.3203	1.2949	
2	0.5798	0.2032	0.3766	0.1418	0.0026	-0.2841	0.6905	
3	0.4176	0.0511	0.3664	0.1343	0.0123	-0.4362	0.5384	
4	0.3287	0.0129	0.3159	0.0998	0.0399	-0.4744	0.5001	
5	0.2705	0.0032	0.2672	0.0714	0.0666	-0.4840	0.4905	
10	0.1481	0.0000	0.1481	0.0219	0.1448	-0.4873	0.4873	
15	0.1077	0.0000	0.1077	0.0116	0.1771	-0.4873	0.4873	
30	0.0000	0.0000	0.0000	0.0000	0.2793	-0.4873	0.4873	
45	0.0000	0.0000	0.0000	0.0000	0.2793	-0.4873	0.4873	
60	0.0000	0.0000	0.0000	0.0000	0.2793	-0.4873	0.4873	
90	0.0000	0.0000	0.0000	0.0000	0.2793	-0.4873	0.4873	
120	0.0000	0.0000	0.0000	0.0000	0.2793	-0.4873	0.4873	
\bar{Y}	$\Sigma (Y - \hat{Y})^2$	$\Sigma (Y - \bar{Y})^2$	df	S.E. of Y	Critical t	CI	R ²	k_t (min ⁻¹)
0.5285	0.6614	10.8157	13	0.2256	2.1604	0.4873	0.9388	1.3799

2.2 CDD degradation in MLS9

- N1

Time (min)	Y	\hat{Y}	$Y - \hat{Y}$	$(Y - \hat{Y})^2$	$(Y - \bar{Y})^2$	Lower CL	Upper CL	
0	2.8328	2.8328	0.0000	0.0000	5.1934	2.4299	3.2357	
0.5	1.5418	1.9113	-0.3695	0.1366	0.9759	1.5084	2.3142	
1	1.1050	1.2896	-0.1846	0.0341	0.3037	0.8867	1.6925	
2	0.7183	0.5871	0.1312	0.0172	0.0270	0.1842	0.9900	
3	0.5385	0.2672	0.2713	0.0736	0.0002	-0.1357	0.6702	
4	0.4112	0.1217	0.2895	0.0838	0.0204	-0.2812	0.5246	
5	0.3343	0.0554	0.2790	0.0778	0.0482	-0.3475	0.4583	
10	0.1387	0.0011	0.1376	0.0189	0.1724	-0.4018	0.4040	
15	0.0908	0.0000	0.0908	0.0082	0.2145	-0.4029	0.4029	
30	0.0435	0.0000	0.0435	0.0019	0.2605	-0.4029	0.4029	
45	0.0000	0.0000	0.0000	0.0000	0.3068	-0.4029	0.4029	
60	0.0000	0.0000	0.0000	0.0000	0.3068	-0.4029	0.4029	
90	0.0000	0.0000	0.0000	0.0000	0.3068	-0.4029	0.4029	
120	0.0000	0.0000	0.0000	0.0000	0.3068	-0.4029	0.4029	
\bar{Y}	$\sum (Y - \hat{Y})^2$	$\sum (Y - \bar{Y})^2$	df	S.E. of Y	Critical t	CI	R ²	k_1 (min ⁻¹)
0.5539	0.4522	8.4436	13	0.1865	2.1604	0.4029	0.9464	0.7870

- N2

Time (min)	Y	\hat{Y}	$Y - \hat{Y}$	$(Y - \hat{Y})^2$	$(Y - \bar{Y})^2$	Lower CL	Upper CL	
0	2.8169	2.8328	-0.0159	0.0003	4.9980	2.3945	3.2711	
0.5	1.5496	1.9953	-0.4457	0.1986	0.9376	1.5570	2.4336	
1	1.2101	1.4054	-0.1952	0.0381	0.3954	0.9671	1.8437	
2	0.7905	0.6972	0.0933	0.0087	0.0438	0.2589	1.1355	
3	0.5792	0.3459	0.2334	0.0545	0.0000	-0.0924	0.7842	
4	0.4618	0.1716	0.2902	0.0842	0.0143	-0.2667	0.6099	
5	0.4220	0.0851	0.3369	0.1135	0.0254	-0.3532	0.5234	
10	0.1610	0.0026	0.1584	0.0251	0.1767	-0.4357	0.4409	
15	0.0987	0.0001	0.0986	0.0097	0.2329	-0.4382	0.4384	
30	0.0485	0.0000	0.0485	0.0024	0.2839	-0.4383	0.4383	
45	0.0000	0.0000	0.0000	0.0000	0.3379	-0.4383	0.4383	
60	0.0000	0.0000	0.0000	0.0000	0.3379	-0.4383	0.4383	
90	0.0000	0.0000	0.0000	0.0000	0.3379	-0.4383	0.4383	
120	0.0000	0.0000	0.0000	0.0000	0.3379	-0.4383	0.4383	
\bar{Y}	$\sum (Y - \hat{Y})^2$	$\sum (Y - \bar{Y})^2$	df	S.E. of Y	Critical t	CI	R ²	k_1 (min ⁻¹)
0.5813	0.5351	8.4596	13	0.2029	2.1604	0.4496	0.9367	0.7010

- N3

Time (min)	Y	\hat{Y}	$Y - \hat{Y}$	$(Y - \hat{Y})^2$	$(Y - \bar{Y})^2$	Lower CL	Upper CL	
0	2.6429	2.8328	-0.1900	0.0361	4.5387	2.3312	3.3345	
0.5	1.2979	1.7621	-0.4642	0.2155	0.6169	1.2604	2.2638	
1	0.9955	1.0961	-0.1005	0.0101	0.2334	0.5944	1.5977	
2	0.6821	0.4241	0.2580	0.0665	0.0288	-0.0776	0.9257	
3	0.5237	0.1641	0.3596	0.1293	0.0001	-0.3376	0.6657	
4	0.3981	0.0635	0.3347	0.1120	0.0131	-0.4382	0.5651	
5	0.3344	0.0246	0.3098	0.0960	0.0317	-0.4771	0.5262	
10	0.1554	0.0002	0.1552	0.0241	0.1275	-0.5014	0.5019	
15	0.0936	0.0000	0.0936	0.0088	0.1754	-0.5017	0.5017	
30	0.0504	0.0000	0.0504	0.0025	0.2134	-0.5017	0.5017	
45	0.0000	0.0000	0.0000	0.0000	0.2626	-0.5017	0.5017	
60	0.0000	0.0000	0.0000	0.0000	0.2626	-0.5017	0.5017	
90	0.0000	0.0000	0.0000	0.0000	0.2626	-0.5017	0.5017	
120	0.0000	0.0000	0.0000	0.0000	0.2626	-0.5017	0.5017	
\bar{Y}	$\sum (Y - \hat{Y})^2$	$\sum (Y - \bar{Y})^2$	df	S.E. of Y	Critical t	CI	R ²	k_t (min ⁻¹)
0.5124	0.7010	7.0293	13	0.2322	2.1604	0.5017	0.9003	0.9496

2.3 CDD degradation in DLS9

- N1

Time (min)	Y	\hat{Y}	$Y - \hat{Y}$	$(Y - \hat{Y})^2$	$(Y - \bar{Y})^2$	Lower CL	Upper CL	
0	2.8796	2.8796	0.0000	0.0000	5.1637	2.3541	3.4052	
0.5	1.5029	2.0609	-0.5580	0.3114	0.8022	1.5354	2.5864	
1	1.2032	1.4750	-0.2717	0.0738	0.3552	0.9494	2.0005	
2	0.8869	0.7555	0.1315	0.0173	0.0782	0.2299	1.2810	
3	0.6785	0.3870	0.2915	0.0850	0.0051	-0.1386	0.9125	
4	0.5253	0.1982	0.3271	0.1070	0.0067	-0.3273	0.7237	
5	0.4402	0.1015	0.3387	0.1147	0.0279	-0.4240	0.6270	
10	0.2061	0.0036	0.2025	0.0410	0.1609	-0.5220	0.5291	
15	0.1290	0.0001	0.1288	0.0166	0.2288	-0.5254	0.5257	
30	0.0499	0.0000	0.0499	0.0025	0.3106	-0.5255	0.5255	
45	0.0000	0.0000	0.0000	0.0000	0.3688	-0.5255	0.5255	
60	0.0000	0.0000	0.0000	0.0000	0.3688	-0.5255	0.5255	
90	0.0000	0.0000	0.0000	0.0000	0.3688	-0.5255	0.5255	
120	0.0000	0.0000	0.0000	0.0000	0.3688	-0.5255	0.5255	
\bar{Y}	$\sum (Y - \hat{Y})^2$	$\sum (Y - \bar{Y})^2$	df	S.E. of Y	Critical t	CI	R ²	k_t (min ⁻¹)
0.6073	0.7693	8.6144	13	0.2433	2.1604	0.5255	0.9107	0.6690

- N2

Time (min)	Y	\hat{Y}	$Y - \hat{Y}$	$(Y - \hat{Y})^2$	$(Y - \bar{Y})^2$	Lower CL	Upper CL	
0	2.6664	2.8796	-0.2132	0.0455	4.3029	2.3360	3.4233	
0.5	1.4530	2.0192	-0.5662	0.3206	0.7412	1.4756	2.5628	
1	1.2065	1.4159	-0.2094	0.0438	0.3775	0.8722	1.9595	
2	0.8381	0.6962	0.1419	0.0201	0.0605	0.1525	1.2398	
3	0.6322	0.3423	0.2899	0.0840	0.0016	-0.2014	0.8859	
4	0.5042	0.1683	0.3359	0.1128	0.0077	-0.3753	0.7119	
5	0.4235	0.0827	0.3407	0.1161	0.0284	-0.4609	0.6264	
10	0.2327	0.0024	0.2303	0.0530	0.1292	-0.5413	0.5460	
15	0.1298	0.0001	0.1297	0.0168	0.2137	-0.5436	0.5437	
30	0.0531	0.0000	0.0531	0.0028	0.2904	-0.5436	0.5436	
45	0.0571	0.0000	0.0571	0.0033	0.2862	-0.5436	0.5436	
60	0.0476	0.0000	0.0476	0.0023	0.2965	-0.5436	0.5436	
90	0.0448	0.0000	0.0448	0.0020	0.2996	-0.5436	0.5436	
120	0.0000	0.0000	0.0000	0.0000	0.3505	-0.5436	0.5436	
\bar{Y}	$\Sigma (Y - \hat{Y})^2$	$\Sigma (Y - \bar{Y})^2$	df	S.E. of Y	Critical t	CI	R ²	k_1 (min ⁻¹)
0.5921	0.8232	7.3861	13	0.2516	2.1604	0.5436	0.8880	0.7099

- N3

Time (min)	Y	\hat{Y}	$Y - \hat{Y}$	$(Y - \hat{Y})^2$	$(Y - \bar{Y})^2$	Lower CL	Upper CL	
0	2.8174	2.9428	-0.1254	0.0157	5.4559	2.5320	3.3536	
0.5	1.2453	1.6266	-0.3813	0.1454	0.5831	1.2158	2.0374	
1	0.9378	0.8991	0.0387	0.0015	0.2081	0.4883	1.3099	
2	0.5756	0.2747	0.3009	0.0906	0.0088	-0.1361	0.6855	
3	0.3843	0.0839	0.3003	0.0902	0.0095	-0.3269	0.4947	
4	0.2761	0.0256	0.2504	0.0627	0.0422	-0.3851	0.4364	
5	0.2291	0.0078	0.2213	0.0490	0.0637	-0.4029	0.4186	
10	0.0908	0.0000	0.0907	0.0082	0.1528	-0.4108	0.4108	
15	0.0583	0.0000	0.0583	0.0034	0.1792	-0.4108	0.4108	
30	0.0256	0.0000	0.0256	0.0007	0.2079	-0.4108	0.4108	
45	0.0256	0.0000	0.0256	0.0007	0.2079	-0.4108	0.4108	
60	0.0256	0.0000	0.0256	0.0007	0.2079	-0.4108	0.4108	
90	0.0256	0.0000	0.0256	0.0007	0.2079	-0.4108	0.4108	
120	0.0256	0.0000	0.0256	0.0007	0.2079	-0.4108	0.4108	
\bar{Y}	$\Sigma (Y - \hat{Y})^2$	$\Sigma (Y - \bar{Y})^2$	df	S.E. of Y	Critical t	CI	R ²	k_1 (min ⁻¹)
0.4816	0.4700	7.7431	13	0.1901	2.1604	0.4108	0.9393	1.1857

Time (min)	Y	\hat{Y}	Y - \hat{Y}	(Y - \hat{Y}) ²	(Y - \bar{Y}) ²	Lower CL	Upper CL	
0	2.7570	2.8796	-0.1227	0.0150	5.2654	2.4791	3.2802	
0.5	1.2185	1.5917	-0.3732	0.1392	0.5718	1.1911	1.9922	
1	0.9177	0.8798	0.0379	0.0014	0.2074	0.4792	1.2803	
2	0.5633	0.2688	0.2945	0.0867	0.0102	-0.1318	0.6693	
3	0.3760	0.0821	0.2939	0.0864	0.0075	-0.3184	0.4827	
4	0.2702	0.0251	0.2451	0.0601	0.0369	-0.3755	0.4256	
5	0.2242	0.0077	0.2166	0.0469	0.0567	-0.3929	0.4082	
10	0.0888	0.0000	0.0888	0.0079	0.1395	-0.4005	0.4006	
15	0.0570	0.0000	0.0570	0.0033	0.1643	-0.4006	0.4006	
30	0.0000	0.0000	0.0000	0.0000	0.2138	-0.4006	0.4006	
45	0.0000	0.0000	0.0000	0.0000	0.2138	-0.4006	0.4006	
60	0.0000	0.0000	0.0000	0.0000	0.2138	-0.4006	0.4006	
90	0.0000	0.0000	0.0000	0.0000	0.2138	-0.4006	0.4006	
120	0.0000	0.0000	0.0000	0.0000	0.2138	-0.4006	0.4006	
\bar{Y}	$\Sigma (Y - \hat{Y})^2$	$\Sigma (Y - \bar{Y})^2$	df	S.E. of Y	Critical t	CI	R ²	k_1 (min ⁻¹)
0.4623	0.4469	7.5284	13	0.1854	2.1604	0.4006	0.9406	1.1857

2.4 CDD degradation in RLS9

- N1

Time (min)	Y	\hat{Y}	Y - \hat{Y}	(Y - \hat{Y}) ²	(Y - \bar{Y}) ²	Lower CL	Upper CL	
0	2.7824	2.7824	0.0000	0.0000	5.1455	2.5441	3.0207	
0.5	1.9859	1.8392	0.1467	0.0215	2.1663	1.6009	2.0774	
1	0.9539	1.2157	-0.2618	0.0685	0.1935	0.9774	1.4539	
2	0.5406	0.5312	0.0095	0.0001	0.0007	0.2929	0.7694	
3	0.3494	0.2321	0.1173	0.0138	0.0271	-0.0062	0.4703	
4	0.2390	0.1014	0.1376	0.0189	0.0756	-0.1369	0.3397	
5	0.2030	0.0443	0.1587	0.0252	0.0968	-0.1940	0.2826	
10	0.0777	0.0007	0.0770	0.0059	0.1904	-0.2376	0.2390	
15	0.0646	0.0000	0.0646	0.0042	0.2020	-0.2382	0.2383	
30	0.0000	0.0000	0.0000	0.0000	0.2642	-0.2383	0.2383	
45	0.0000	0.0000	0.0000	0.0000	0.2642	-0.2383	0.2383	
60	0.0000	0.0000	0.0000	0.0000	0.2642	-0.2383	0.2383	
90	0.0000	0.0000	0.0000	0.0000	0.2642	-0.2383	0.2383	
120	0.0000	0.0000	0.0000	0.0000	0.2642	-0.2383	0.2383	
\bar{Y}	$\Sigma (Y - \hat{Y})^2$	$\Sigma (Y - \bar{Y})^2$	df	S.E. of Y	Critical t	CI	R ²	k_1 (min ⁻¹)
0.5140	0.1581	9.4191	13	0.1103	2.1604	0.2383	0.9832	0.8280

- N2

Time (min)	Y	\hat{Y}	$Y - \hat{Y}$	$(Y - \hat{Y})^2$	$(Y - \bar{Y})^2$	Lower CL	Upper CL
0	2.7530	2.8434	-0.0904	0.0082	4.5236	2.5399	3.1469
0.5	1.8870	2.1181	-0.2312	0.0534	1.5897	1.8146	2.4216
1	1.3616	1.5779	-0.2162	0.0468	0.5409	1.2744	1.8814
2	0.8788	0.8756	0.0032	0.0000	0.0639	0.5721	1.1791
3	0.6082	0.4859	0.1224	0.0150	0.0003	0.1824	0.7894
4	0.4748	0.2696	0.2052	0.0421	0.0229	-0.0339	0.5731
5	0.3733	0.1496	0.2237	0.0501	0.0639	-0.1539	0.4531
10	0.1688	0.0079	0.1609	0.0259	0.2092	-0.2956	0.3114
15	0.0991	0.0004	0.0987	0.0097	0.2778	-0.3031	0.3039
30	0.0457	0.0000	0.0457	0.0021	0.3369	-0.3035	0.3035
45	0.0289	0.0000	0.0289	0.0008	0.3567	-0.3035	0.3035
60	0.0289	0.0000	0.0289	0.0008	0.3567	-0.3035	0.3035
90	0.0289	0.0000	0.0289	0.0008	0.3567	-0.3035	0.3035
120	0.0289	0.0000	0.0289	0.0008	0.3567	-0.3035	0.3035

\bar{Y}	$\sum (Y - \hat{Y})^2$	$\sum (Y - \bar{Y})^2$	df	S.E. of Y	Critical t	CI	R ²	k_1 (min ⁻¹)
0.6261	0.2566	9.0559	13	0.1405	2.1604	0.3035	0.9717	0.5889

Time (min)	Y	\hat{Y}	$Y - \hat{Y}$	$(Y - \hat{Y})^2$	$(Y - \bar{Y})^2$	Lower CL	Upper CL
0	2.6939	2.7824	-0.0885	0.0078	4.3652	2.4873	3.0775
0.5	1.8465	2.0727	-0.2262	0.0512	1.5422	1.7776	2.3677
1	1.3324	1.5440	-0.2116	0.0448	0.5297	1.2489	1.8391
2	0.8600	0.8568	0.0032	0.0000	0.0652	0.5617	1.1518
3	0.5952	0.4754	0.1197	0.0143	0.0001	0.1804	0.7705
4	0.4646	0.2638	0.2008	0.0403	0.0196	-0.0312	0.5589
5	0.3653	0.1464	0.2189	0.0479	0.0573	-0.1486	0.4415
10	0.1651	0.0077	0.1574	0.0248	0.1931	-0.2874	0.3028
15	0.0970	0.0004	0.0966	0.0093	0.2577	-0.2946	0.2955
30	0.0448	0.0000	0.0448	0.0020	0.3135	-0.2951	0.2951
45	0.0000	0.0000	0.0000	0.0000	0.3656	-0.2951	0.2951
60	0.0000	0.0000	0.0000	0.0000	0.3656	-0.2951	0.2951
90	0.0000	0.0000	0.0000	0.0000	0.3656	-0.2951	0.2951
120	0.0000	0.0000	0.0000	0.0000	0.3656	-0.2951	0.2951

\bar{Y}	$\sum (Y - \hat{Y})^2$	$\sum (Y - \bar{Y})^2$	df	S.E. of Y	Critical t	CI	R ²	k_1 (min ⁻¹)
0.6046	0.2425	8.8058	13	0.1366	2.1604	0.2951	0.9717	0.5889

- N3

Time (min)	Y	\hat{Y}	$Y - \hat{Y}$	$(Y - \hat{Y})^2$	$(Y - \bar{Y})^2$	Lower CL	Upper CL	
0	2.8671	2.7824	0.0847	0.0072	5.1264	2.3884	3.1764	
0.5	1.6527	2.0372	-0.3845	0.1479	1.1019	1.6432	2.4312	
1	1.2456	1.4916	-0.2459	0.0605	0.4131	1.0976	1.8856	
2	0.8646	0.7996	0.0650	0.0042	0.0685	0.4056	1.1936	
3	0.6140	0.4286	0.1853	0.0343	0.0001	0.0347	0.8226	
4	0.5042	0.2298	0.2744	0.0753	0.0098	-0.1642	0.6238	
5	0.3741	0.1232	0.2509	0.0630	0.0524	-0.2708	0.5172	
10	0.1738	0.0055	0.1683	0.0283	0.1841	-0.3885	0.3994	
15	0.0975	0.0002	0.0973	0.0095	0.2554	-0.3937	0.3942	
30	0.0474	0.0000	0.0474	0.0022	0.3086	-0.3940	0.3940	
45	0.0000	0.0000	0.0000	0.0000	0.3635	-0.3940	0.3940	
60	0.0000	0.0000	0.0000	0.0000	0.3635	-0.3940	0.3940	
90	0.0000	0.0000	0.0000	0.0000	0.3635	-0.3940	0.3940	
120	0.0000	0.0000	0.0000	0.0000	0.3635	-0.3940	0.3940	
\bar{Y}	$\sum (Y - \hat{Y})^2$	$\sum (Y - \bar{Y})^2$	df	S.E. of Y	Critical t	CI	R ²	k_1 (min ⁻¹)
0.6029	0.4324	8.9744	13	0.1824	2.1604	0.3940	0.9518	0.6235

2.5 MSCUR degradation in HLS9

- N1

Time (min)	Y	\hat{Y}	$Y - \hat{Y}$	$(Y - \hat{Y})^2$	$(Y - \bar{Y})^2$	Lower CL	Upper CL	
0	0.0000	0.0000	0.0000	0.0000	0.0009	-0.0276	0.0276	
0.5	0.2190	0.2110	0.0080	0.0001	0.0360	0.1834	0.2386	
1	0.0844	0.1055	-0.0211	0.0004	0.0030	0.0779	0.1330	
2	0.0408	0.0261	0.0147	0.0002	0.0001	-0.0015	0.0537	
3	0.0329	0.0065	0.0264	0.0007	0.0000	-0.0211	0.0340	
4	0.0177	0.0016	0.0161	0.0003	0.0001	-0.0260	0.0292	
5	0.0159	0.0004	0.0155	0.0002	0.0002	-0.0272	0.0280	
10	0.0000	0.0000	0.0000	0.0000	0.0009	-0.0276	0.0276	
15	0.0000	0.0000	0.0000	0.0000	0.0009	-0.0276	0.0276	
30	0.0000	0.0000	0.0000	0.0000	0.0009	-0.0276	0.0276	
45	0.0000	0.0000	0.0000	0.0000	0.0009	-0.0276	0.0276	
60	0.0000	0.0000	0.0000	0.0000	0.0009	-0.0276	0.0276	
90	0.0000	0.0000	0.0000	0.0000	0.0009	-0.0276	0.0276	
120	0.0000	0.0000	0.0000	0.0000	0.0009	-0.0276	0.0276	
\bar{Y}	$\sum (Y - \hat{Y})^2$	$\sum (Y - \bar{Y})^2$	df	S.E. of Y	Critical t	CI	R ²	k_2 (min ⁻¹)
0.0293	0.0019	0.0463	12	0.0127	2.1788	0.0276	0.9585	12.1455

- N2

Time (min)	Y	\hat{Y}	$Y - \hat{Y}$	$(Y - \hat{Y})^2$	$(Y - \bar{Y})^2$	Lower CL	Upper CL	
0	0.0000	0.0000	0.0000	0.0000	0.0008	-0.0119	0.0119	
0.5	0.2422	0.2383	0.0040	0.0000	0.0455	0.2264	0.2502	
1	0.1074	0.1186	-0.0112	0.0001	0.0061	0.1067	0.1305	
2	0.0420	0.0289	0.0131	0.0002	0.0002	0.0170	0.0408	
3	0.0136	0.0071	0.0065	0.0000	0.0002	-0.0049	0.0190	
4	0.0000	0.0017	-0.0017	0.0000	0.0008	-0.0102	0.0136	
5	0.0000	0.0004	-0.0004	0.0000	0.0008	-0.0115	0.0123	
10	0.0000	0.0000	0.0000	0.0000	0.0008	-0.0119	0.0119	
15	0.0000	0.0000	0.0000	0.0000	0.0008	-0.0119	0.0119	
30	0.0000	0.0000	0.0000	0.0000	0.0008	-0.0119	0.0119	
45	0.0000	0.0000	0.0000	0.0000	0.0008	-0.0119	0.0119	
60	0.0000	0.0000	0.0000	0.0000	0.0008	-0.0119	0.0119	
90	0.0000	0.0000	0.0000	0.0000	0.0008	-0.0119	0.0119	
120	0.0000	0.0000	0.0000	0.0000	0.0008	-0.0119	0.0119	
\bar{Y}	$\sum (Y - \hat{Y})^2$	$\sum (Y - \bar{Y})^2$	df	S.E. of Y	Critical t	CI	R ²	k_2 (min ⁻¹)
0.0289	0.0004	0.0604	12	0.0055	2.1788	0.0119	0.9941	11.1650

- N3

Time (min)	Y	\hat{Y}	$Y - \hat{Y}$	$(Y - \hat{Y})^2$	$(Y - \bar{Y})^2$	Lower CL	Upper CL	
0	0.0000	0.0000	0.0000	0.0000	0.0007	-0.0171	0.0171	
0.5	0.2015	0.1945	0.0070	0.0000	0.0306	0.1774	0.2116	
1	0.0911	0.1081	-0.0170	0.0003	0.0042	0.0910	0.1252	
2	0.0435	0.0332	0.0103	0.0001	0.0003	0.0161	0.0503	
3	0.0205	0.0102	0.0103	0.0001	0.0000	-0.0069	0.0273	
4	0.0169	0.0031	0.0137	0.0002	0.0001	-0.0140	0.0202	
5	0.0000	0.0010	-0.0010	0.0000	0.0007	-0.0161	0.0181	
10	0.0000	0.0000	0.0000	0.0000	0.0007	-0.0171	0.0171	
15	0.0000	0.0000	0.0000	0.0000	0.0007	-0.0171	0.0171	
30	0.0000	0.0000	0.0000	0.0000	0.0007	-0.0171	0.0171	
45	0.0000	0.0000	0.0000	0.0000	0.0007	-0.0171	0.0171	
60	0.0000	0.0000	0.0000	0.0000	0.0007	-0.0171	0.0171	
90	0.0000	0.0000	0.0000	0.0000	0.0007	-0.0171	0.0171	
120	0.0000	0.0000	0.0000	0.0000	0.0007	-0.0171	0.0171	
\bar{Y}	$\sum (Y - \hat{Y})^2$	$\sum (Y - \bar{Y})^2$	df	S.E. of Y	Critical t	CI	R ²	k_2 (min ⁻¹)
0.0267	0.0007	0.0415	12	0.0079	2.1788	0.0171	0.9822	12.8859

2.6 MSCUR degradation in MLS9

- N1

Time (min)	Y	\hat{Y}	$Y - \hat{Y}$	$(Y - \hat{Y})^2$	$(Y - \bar{Y})^2$	Lower CL	Upper CL	
0	0.0000	0.0000	0.0000	0.0000	0.0001	-0.0050	0.0050	
0.5	0.0672	0.0662	0.0010	0.0000	0.0032	0.0612	0.0712	
1	0.0431	0.0451	-0.0021	0.0000	0.0011	0.0402	0.0501	
2	0.0209	0.0210	0.0000	0.0000	0.0001	0.0160	0.0259	
3	0.0154	0.0097	0.0057	0.0000	0.0000	0.0048	0.0147	
4	0.0000	0.0045	-0.0045	0.0000	0.0001	-0.0004	0.0095	
5	0.0000	0.0021	-0.0021	0.0000	0.0001	-0.0029	0.0071	
10	0.0000	0.0000	0.0000	0.0000	0.0001	-0.0049	0.0050	
15	0.0000	0.0000	0.0000	0.0000	0.0001	-0.0050	0.0050	
30	0.0000	0.0000	0.0000	0.0000	0.0001	-0.0050	0.0050	
45	0.0000	0.0000	0.0000	0.0000	0.0001	-0.0050	0.0050	
60	0.0000	0.0000	0.0000	0.0000	0.0001	-0.0050	0.0050	
90	0.0000	0.0000	0.0000	0.0000	0.0001	-0.0050	0.0050	
120	0.0000	0.0000	0.0000	0.0000	0.0001	-0.0050	0.0050	
\bar{Y}	$\sum (Y - \hat{Y})^2$	$\sum (Y - \bar{Y})^2$	df	S.E. of Y	Critical t	CI	R ²	k ₂ (min ⁻¹)
0.0105	0.0001	0.0055	12	0.0023	2.1788	0.0050	0.9887	23.6177

- N2

Time (min)	Y	\hat{Y}	$Y - \hat{Y}$	$(Y - \hat{Y})^2$	$(Y - \bar{Y})^2$	Lower CL	Upper CL	
0	0.0000	0.0000	0.0000	0.0000	0.0002	-0.0099	0.0099	
0.5	0.0658	0.0590	0.0069	0.0000	0.0028	0.0491	0.0689	
1	0.0414	0.0475	-0.0061	0.0000	0.0008	0.0376	0.0574	
2	0.0231	0.0308	-0.0077	0.0001	0.0001	0.0210	0.0407	
3	0.0205	0.0200	0.0005	0.0000	0.0001	0.0101	0.0299	
4	0.0156	0.0130	0.0026	0.0000	0.0000	0.0031	0.0229	
5	0.0182	0.0084	0.0098	0.0001	0.0000	-0.0015	0.0183	
10	0.0000	0.0010	-0.0010	0.0000	0.0002	-0.0089	0.0109	
15	0.0000	0.0001	-0.0001	0.0000	0.0002	-0.0098	0.0100	
30	0.0000	0.0000	0.0000	0.0000	0.0002	-0.0099	0.0099	
45	0.0000	0.0000	0.0000	0.0000	0.0002	-0.0099	0.0099	
60	0.0000	0.0000	0.0000	0.0000	0.0002	-0.0099	0.0099	
90	0.0000	0.0000	0.0000	0.0000	0.0002	-0.0099	0.0099	
120	0.0000	0.0000	0.0000	0.0000	0.0002	-0.0099	0.0099	
\bar{Y}	$\sum (Y - \hat{Y})^2$	$\sum (Y - \bar{Y})^2$	df	S.E. of Y	Critical t	CI	R ²	k ₂ (min ⁻¹)
0.0132	0.0002	0.0051	12	0.0045	2.1788	0.0099	0.9519	17.4221

- N3

Time (min)	Y	\hat{Y}	$Y - \hat{Y}$	$(Y - \hat{Y})^2$	$(Y - \bar{Y})^2$	Lower CL	Upper CL	
0	0.0000	0.0000	0.0000	0.0000	0.0001	-0.0075	0.0075	
0.5	0.0624	0.0604	0.0020	0.0000	0.0027	0.0529	0.0679	
1	0.0393	0.0440	-0.0047	0.0000	0.0008	0.0365	0.0514	
2	0.0254	0.0233	0.0021	0.0000	0.0002	0.0158	0.0308	
3	0.0198	0.0123	0.0075	0.0001	0.0001	0.0049	0.0198	
4	0.0000	0.0065	-0.0065	0.0000	0.0001	-0.0009	0.0140	
5	0.0000	0.0035	-0.0035	0.0000	0.0001	-0.0040	0.0109	
10	0.0000	0.0001	-0.0001	0.0000	0.0001	-0.0073	0.0076	
15	0.0000	0.0000	0.0000	0.0000	0.0001	-0.0075	0.0075	
30	0.0000	0.0000	0.0000	0.0000	0.0001	-0.0075	0.0075	
45	0.0000	0.0000	0.0000	0.0000	0.0001	-0.0075	0.0075	
60	0.0000	0.0000	0.0000	0.0000	0.0001	-0.0075	0.0075	
90	0.0000	0.0000	0.0000	0.0000	0.0001	-0.0075	0.0075	
120	0.0000	0.0000	0.0000	0.0000	0.0001	-0.0075	0.0075	
\bar{Y}	$\sum (Y - \hat{Y})^2$	$\sum (Y - \bar{Y})^2$	df	S.E. of Y	Critical t	CI	R ²	k_2 (min ⁻¹)
0.0105	0.0001	0.0049	12	0.0034	2.1788	0.0075	0.9714	21.3197

2.7 MSCUR degradation in DLS9

- N1

Time (min)	Y	\hat{Y}	$Y - \hat{Y}$	$(Y - \hat{Y})^2$	$(Y - \bar{Y})^2$	Lower CL	Upper CL	
0	0.0000	0.0000	0.0000	0.0000	0.0001	-0.0078	0.0078	
0.5	0.0762	0.0746	0.0016	0.0000	0.0044	0.0668	0.0825	
1	0.0403	0.0453	-0.0050	0.0000	0.0009	0.0375	0.0532	
2	0.0259	0.0167	0.0092	0.0001	0.0002	0.0089	0.0246	
3	0.0000	0.0062	-0.0062	0.0000	0.0001	-0.0017	0.0140	
4	0.0000	0.0023	-0.0023	0.0000	0.0001	-0.0056	0.0101	
5	0.0000	0.0008	-0.0008	0.0000	0.0001	-0.0070	0.0087	
10	0.0000	0.0000	0.0000	0.0000	0.0001	-0.0078	0.0079	
15	0.0000	0.0000	0.0000	0.0000	0.0001	-0.0078	0.0078	
30	0.0000	0.0000	0.0000	0.0000	0.0001	-0.0078	0.0078	
45	0.0000	0.0000	0.0000	0.0000	0.0001	-0.0078	0.0078	
60	0.0000	0.0000	0.0000	0.0000	0.0001	-0.0078	0.0078	
90	0.0000	0.0000	0.0000	0.0000	0.0001	-0.0078	0.0078	
120	0.0000	0.0000	0.0000	0.0000	0.0001	-0.0078	0.0078	
\bar{Y}	$\sum (Y - \hat{Y})^2$	$\sum (Y - \bar{Y})^2$	df	S.E. of Y	Critical t	CI	R ²	k_2 (min ⁻¹)
0.0102	0.0002	0.0067	12	0.0036	2.1788	0.0078	0.9766	24.8739

- N2

Time (min)	Y	\hat{Y}	$Y - \hat{Y}$	$(Y - \hat{Y})^2$	$(Y - \bar{Y})^2$	Lower CL	Upper CL	
0	0.0000	0.0000	0.0000	0.0000	0.0001	-0.0059	0.0059	
0.5	0.0580	0.0588	-0.0008	0.0000	0.0025	0.0530	0.0647	
1	0.0383	0.0380	0.0003	0.0000	0.0009	0.0322	0.0439	
2	0.0216	0.0159	0.0058	0.0000	0.0002	0.0100	0.0217	
3	0.0000	0.0066	-0.0066	0.0000	0.0001	0.0008	0.0125	
4	0.0000	0.0028	-0.0028	0.0000	0.0001	-0.0031	0.0086	
5	0.0000	0.0012	-0.0012	0.0000	0.0001	-0.0047	0.0070	
10	0.0000	0.0000	0.0000	0.0000	0.0001	-0.0058	0.0059	
15	0.0000	0.0000	0.0000	0.0000	0.0001	-0.0059	0.0059	
30	0.0000	0.0000	0.0000	0.0000	0.0001	-0.0059	0.0059	
45	0.0000	0.0000	0.0000	0.0000	0.0001	-0.0059	0.0059	
60	0.0000	0.0000	0.0000	0.0000	0.0001	-0.0059	0.0059	
90	0.0000	0.0000	0.0000	0.0000	0.0001	-0.0059	0.0059	
120	0.0000	0.0000	0.0000	0.0000	0.0001	-0.0059	0.0059	
\bar{Y}	$\sum (Y - \hat{Y})^2$	$\sum (Y - \bar{Y})^2$	df	S.E. of Y	Critical t	CI	R ²	k_2 (min ⁻¹)
0.0084	0.0001	0.0043	12	0.0027	2.1788	0.0059	0.9798	27.0157

- N3

Time (min)	Y	\hat{Y}	$Y - \hat{Y}$	$(Y - \hat{Y})^2$	$(Y - \bar{Y})^2$	Lower CL	Upper CL	
0	0.0000	0.0000	0.0000	0.0000	0.0001	-0.0080	0.0080	
0.5	0.0719	0.0761	-0.0042	0.0000	0.0037	0.0681	0.0842	
1	0.0567	0.0489	0.0078	0.0001	0.0021	0.0408	0.0569	
2	0.0212	0.0202	0.0011	0.0000	0.0001	0.0121	0.0282	
3	0.0000	0.0083	-0.0083	0.0001	0.0001	0.0003	0.0164	
4	0.0000	0.0034	-0.0034	0.0000	0.0001	-0.0046	0.0115	
5	0.0000	0.0014	-0.0014	0.0000	0.0001	-0.0066	0.0095	
10	0.0000	0.0000	0.0000	0.0000	0.0001	-0.0080	0.0081	
15	0.0000	0.0000	0.0000	0.0000	0.0001	-0.0080	0.0080	
30	0.0000	0.0000	0.0000	0.0000	0.0001	-0.0080	0.0080	
45	0.0000	0.0000	0.0000	0.0000	0.0001	-0.0080	0.0080	
60	0.0000	0.0000	0.0000	0.0000	0.0001	-0.0080	0.0080	
90	0.0000	0.0000	0.0000	0.0000	0.0001	-0.0080	0.0080	
120	0.0000	0.0000	0.0000	0.0000	0.0001	-0.0080	0.0080	
\bar{Y}	$\sum (Y - \hat{Y})^2$	$\sum (Y - \bar{Y})^2$	df	S.E. of Y	Critical t	CI	R ²	k_2 (min ⁻¹)
0.0107	0.0002	0.0072	12	0.0037	2.1788	0.0080	0.9774	21.9351

2.8 MSCUR degradation in RLS9

- N1

Time (min)	Y	\hat{Y}	$Y - \hat{Y}$	$(Y - \hat{Y})^2$	$(Y - \bar{Y})^2$	Lower CL	Upper CL	
0	0.0000	0.0000	0.0000	0.0000	0.0009	-0.0168	0.0168	
0.5	0.2342	0.2277	0.0065	0.0000	0.0417	0.2109	0.2446	
1	0.1057	0.1214	-0.0158	0.0002	0.0057	0.1046	0.1382	
2	0.0451	0.0335	0.0116	0.0001	0.0002	0.0167	0.0503	
3	0.0227	0.0092	0.0135	0.0002	0.0001	-0.0076	0.0260	
4	0.0129	0.0025	0.0103	0.0001	0.0003	-0.0143	0.0193	
5	0.0000	0.0007	-0.0007	0.0000	0.0009	-0.0161	0.0175	
10	0.0000	0.0000	0.0000	0.0000	0.0009	-0.0168	0.0168	
15	0.0000	0.0000	0.0000	0.0000	0.0009	-0.0168	0.0168	
30	0.0000	0.0000	0.0000	0.0000	0.0009	-0.0168	0.0168	
45	0.0000	0.0000	0.0000	0.0000	0.0009	-0.0168	0.0168	
60	0.0000	0.0000	0.0000	0.0000	0.0009	-0.0168	0.0168	
90	0.0000	0.0000	0.0000	0.0000	0.0009	-0.0168	0.0168	
120	0.0000	0.0000	0.0000	0.0000	0.0009	-0.0168	0.0168	
\bar{Y}	$\sum (Y - \hat{Y})^2$	$\sum (Y - \bar{Y})^2$	df	S.E. of Y	Critical t	CI	R ²	k ₂ (min ⁻¹)
0.0300	0.0007	0.0561	12	0.0077	2.1788	0.0168	0.9873	9.6032

- N2

Time (min)	Y	\hat{Y}	$Y - \hat{Y}$	$(Y - \hat{Y})^2$	$(Y - \bar{Y})^2$	Lower CL	Upper CL	
0	0.0000	0.0000	0.0000	0.0000	0.0007	-0.0162	0.0162	
0.5	0.1566	0.1504	0.0062	0.0000	0.0168	0.1342	0.1666	
1	0.1028	0.1104	-0.0076	0.0001	0.0058	0.0942	0.1266	
2	0.0470	0.0579	-0.0108	0.0001	0.0004	0.0417	0.0741	
3	0.0490	0.0303	0.0187	0.0003	0.0005	0.0141	0.0465	
4	0.0216	0.0159	0.0057	0.0000	0.0000	-0.0003	0.0321	
5	0.0000	0.0083	-0.0083	0.0001	0.0007	-0.0079	0.0245	
10	0.0000	0.0003	-0.0003	0.0000	0.0007	-0.0159	0.0165	
15	0.0000	0.0000	0.0000	0.0000	0.0007	-0.0162	0.0162	
30	0.0000	0.0000	0.0000	0.0000	0.0007	-0.0162	0.0162	
45	0.0000	0.0000	0.0000	0.0000	0.0007	-0.0162	0.0162	
60	0.0000	0.0000	0.0000	0.0000	0.0007	-0.0162	0.0162	
90	0.0000	0.0000	0.0000	0.0000	0.0007	-0.0162	0.0162	
120	0.0000	0.0000	0.0000	0.0000	0.0007	-0.0162	0.0162	
\bar{Y}	$\sum (Y - \hat{Y})^2$	$\sum (Y - \bar{Y})^2$	df	S.E. of Y	Critical t	CI	R ²	k ₂ (min ⁻¹)
0.9779	0.0007	0.0300	12	0.0074	2.1788	0.0162	0.9779	9.0892

- N3

Time (min)	Y	\hat{Y}	$Y - \hat{Y}$	$(Y - \hat{Y})^2$	$(Y - \bar{Y})^2$	Lower CL	Upper CL	
0	0.0000	0.0000	0.0000	0.0000	0.0007	-0.0215	0.0215	
0.5	0.1595	0.1472	0.0123	0.0002	0.0176	0.1256	0.1687	
1	0.0878	0.1053	-0.0175	0.0003	0.0037	0.0838	0.1269	
2	0.0442	0.0531	-0.0089	0.0001	0.0003	0.0316	0.0746	
3	0.0432	0.0268	0.0164	0.0003	0.0003	0.0052	0.0483	
4	0.0139	0.0135	0.0004	0.0000	0.0002	-0.0080	0.0350	
5	0.0259	0.0068	0.0191	0.0004	0.0000	-0.0147	0.0283	
10	0.0000	0.0002	-0.0002	0.0000	0.0007	-0.0213	0.0218	
15	0.0000	0.0000	0.0000	0.0000	0.0007	-0.0215	0.0215	
30	0.0000	0.0000	0.0000	0.0000	0.0007	-0.0215	0.0215	
45	0.0000	0.0000	0.0000	0.0000	0.0007	-0.0215	0.0215	
60	0.0000	0.0000	0.0000	0.0000	0.0007	-0.0215	0.0215	
90	0.0000	0.0000	0.0000	0.0000	0.0007	-0.0215	0.0215	
120	0.0000	0.0000	0.0000	0.0000	0.0007	-0.0215	0.0215	
\bar{Y}	$\sum (Y - \hat{Y})^2$	$\sum (Y - \bar{Y})^2$	df	S.E. of Y	Critical t	CI	R ²	k_2 (min ⁻¹)
0.0267	0.0012	0.0278	12	0.0099	2.1788	0.0215	0.9578	10.2887

APPENDIX I

Kinetics reaction and optimization condition for enzyme identification

The enzyme identification study for CDD in HLS9, MLS9, DLS9 and RLS9 were set to zero-order reaction.

$$[A] = kt$$

Where $[A]$ is the concentration of CDD at time t , k is degradation rate constant of CDD

The continuous product formation was investigated before choosing the one single time point in the linear time-dependent product for observing the rate of zero-order reaction of CDD with LS9. The excess CDD substrate incubated with catalyst LS9 and consequence converted to curcumin. CDD less than 30% depletion was found at the end of the incubation. In Zero order, the rate is independent of substrate concentration and remains constant over time. The formation of curcumin proceeds at a rate which is linear over a specified period ($R^2 = 0.9$). Any changing in amount of curcumin formation will be depended upon the level of enzyme present in a reaction.

In this study, CDD concentration at $3 \mu\text{M}$ and various LS9 concentrations of each species (0.01, 0.02, 0.05 and 0.1 mg/mL) are used to find suitable enzyme concentration with specified time. The data of CDD hydrolysis by HLS9, MLS9, DLS9 and RLS9 was justified to zero-order reaction as described below.

1. Zero-order reaction of CDD with HLS9

1.1 Excess reactant CDD with catalyst

CDD present excess amount, < 30% substrate depletion, in HLS9 of 0.01 and 0.02 mg/mL at 1 min, while that in HLS9 of 0.05 and 0.1 mg/mL at 0.5 min.

- HLS9 0.01 mg/mL, $[CDD] = 300 \times [HLS9]$

Time (min)	% Curcumin formation	% CDD remaining	% CDD changing	R ²
0	0	100.00	0	-
0.5	0.00	81.03	-18.97	-
1	0.68	76.81	-23.19	0.7500
2	1.39	69.26	-30.74	0.9386
3	2.01	63.65	-36.35	0.9726
4	2.74	56.04	-43.96	0.9863
5	3.96	50.81	-49.19	0.9843
10	7.09	33.43	-66.57	0.9931
15	12.17	23.28	-76.72	0.9936
30	17.27	6.06	-93.94	0.9657
45	17.55	1.70	-98.30	0.8963
60	15.98	0.36	-99.64	0.8030

- HLS9 0.02 mg/mL, $[CDD] = 150 \times [HLS9]$

Time (min)	% Curcumin formation	% CDD remaining	% CDD changing	R ²
0	0	100.00	0.00	-
0.5	1.45	82.88	-17.12	-
1	3.26	80.95	-19.05	0.9958
2	7.70	68.18	-31.82	0.9914
3	12.67	57.46	-42.54	0.9927
4	15.55	43.15	-56.85	0.9940
5	19.41	36.37	-63.63	0.9958
10	32.77	15.39	-84.61	0.9843
15	31.95	6.05	-93.95	0.8869
30	28.36	1.21	-98.79	0.5739
45	24.26	0.00	-100.00	0.3937
60	21.45	0.00	-100.00	0.2774

- HLS9 0.05 mg/mL, [CDD] = 60 x [HLS9]

Time (min)	% Curcumin formation	% CDD remaining	% CDD changing	R ²
0	0	100.00	0.00	-
0.5	2.94	70.96	-29.04	-
1	7.20	67.96	-32.04	0.9891
2	16.02	50.15	-49.85	0.9941
3	24.15	38.80	-61.20	0.9977
4	31.64	31.11	-68.89	0.9986
5	37.27	25.47	-74.53	0.9963
10	44.13	8.64	-91.36	0.8541
15	40.92	3.91	-96.09	0.7007
30	33.32	0.26	-99.74	0.3485
45	26.52	0.00	-100.00	0.1626
60	23.51	0.00	-100.00	0.0745

- HLS9 0.1 mg/mL, [CDD] = 30 x [HLS9]

Time (min)	% Curcumin formation	% CDD remaining	% CDD changing	R ²
0	0.00	100.00	0.00	-
0.5	6.15	71.69	-28.31	-
1	15.18	61.93	-38.07	0.9882
2	25.28	38.95	-61.05	0.9863
3	33.10	27.89	-72.11	0.9794
4	40.52	20.12	-79.88	0.9780
5	42.13	15.15	-84.85	0.9500
10	46.24	4.73	-95.27	0.7304
15	48.83	2.39	-97.61	0.6525
30	36.32	0.00	-100.00	0.2760
45	31.73	0.00	-100.00	0.1265
60	26.83	0.00	-100.00	0.0440

1.2 Curcumin formation upon the time and the amount of enzyme

The formation of curcumin presented the linear time-dependent product after CDD incubated with HLS9 concentration of 0.01, 0.02, 0.05 and 0.1 mg/mL at range 0 - 5 min ($R^2 = 0.9$).

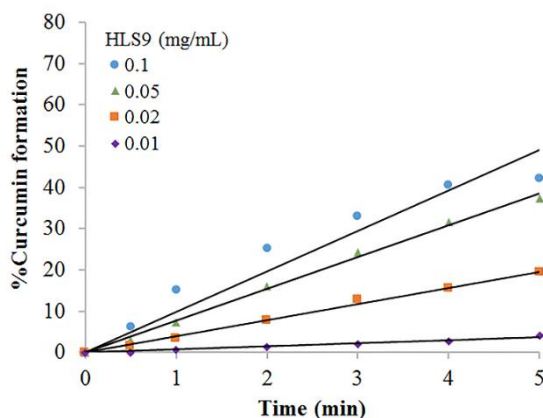


Figure 41. Formation of curcumin in HLS9 plotted against time. CDD at 3 μ M were incubated in duplicate with various concentration of each LS9 (0.01, 0.02, 0.05 and 0.1 mg/mL)

The curcumin formation incubated with HLS9 at 1 min depended upon the enzyme present of 0.01, 0.02, 0.05 and 0.1 mg/mL, respectively ($R^2 = 0.9954$).

จุฬาลงกรณ์มหาวิทยาลัย
CHULALONGKORN UNIVERSITY

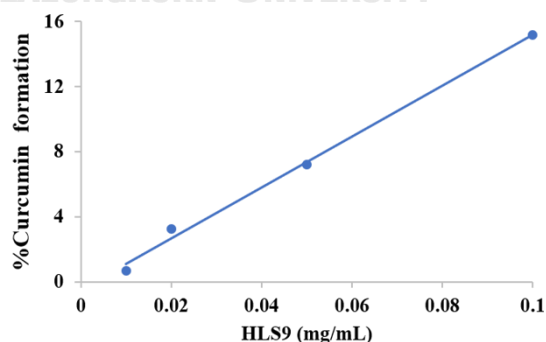


Figure 42. Formation of curcumin in HLS9 plotted against enzyme concentration. CDD at 3 μ M were incubated in duplicate with various concentration of HLS9 (0.01, 0.02, 0.05 and 0.1 mg/mL) at 1 min.

Zero-order reaction of CDD with MLS9

1.3 Excess reactant CDD with catalyst

CDD present exceeded amount in MLS9 of 0.01 and 0.02 mg/mL at 1 and 0.5 min, respectively, while CDD concentration was no saturated in MLS9 of 0.05 and 0.1 mg/mL.

- MLS9 0.01 mg/mL, $[CDD] = 300 \times [MLS9]$

Time (min)	% Curcumin formation	% CDD remaining	% CDD changing	R ²
0	0.00	100.00	0	-
0.5	1.57	79.15	-20.85	-
1	2.02	73.70	-26.30	0.9077
2	5.19	64.16	-35.84	0.9743
3	8.36	55.39	-44.61	0.9873
4	11.38	47.27	-52.73	0.9931
5	15.14	42.89	-57.11	0.9933
10	22.38	21.05	-78.95	0.9659
15	23.97	8.83	-91.17	0.9042
30	20.72	0.53	-99.47	0.5873
45	17.43	0.00	-100.00	0.3964
60	15.50	0.00	-100.00	0.2785

- MLS9 0.02 mg/mL, $[CDD] = 150 \times [MLS9]$

Time (min)	% Curcumin formation	% CDD remaining	% CDD changing	R ²
0	0.00	100.00	0.00	-
0.5	4.55	75.32	-24.68	-
1	8.30	63.90	-36.10	0.9969
2	15.56	49.34	-50.66	0.9974
3	21.97	37.51	-62.49	0.9967
4	26.70	28.36	-71.64	0.9914
5	29.52	21.92	-78.08	0.9778
10	32.21	7.57	-92.43	0.7681
15	29.09	3.71	-96.29	0.5847
30	22.20	0.44	-99.56	0.2190
45	17.50	0.00	-100.00	0.0638
60	15.40	0.00	-100.00	0.0110

- MLS9 0.05 mg/mL, [CDD] = 60 x [MLS9]

Time (min)	% Curcumin formation	% CDD remaining	% CDD changing	R ²
0	0.00	100.00	0.00	-
0.5	9.34	69.01	-30.99	-
1	16.63	56.56	-43.44	0.9950
2	28.51	38.27	-61.73	0.9881
3	35.09	27.03	-72.97	0.9676
4	39.26	19.78	-80.22	0.9442
5	40.09	14.56	-85.44	0.9008
10	42.59	5.24	-94.76	0.6518
15	36.22	2.14	-97.86	0.4240
30	25.56	0.00	-100.00	0.0839
45	19.57	0.00	-100.00	0.0017
60	15.01	0.00	-100.00	0.0223

- MLS9 0.1 mg/mL, [CDD] = 30 x [MLS9]

Time (min)	% Curcumin formation	% CDD remaining	% CDD changing	R ²
0	0.00	100.00	0.00	-
0.5	13.86	69.10	-30.90	-
1	24.72	52.86	-47.14	0.9951
2	40.25	34.42	-65.58	0.9798
3	49.09	21.83	-78.17	0.9582
4	52.22	14.63	-85.37	0.9168
5	56.14	11.40	-88.60	0.8904
10	55.41	3.73	-96.27	0.5989
15	47.79	1.36	-98.64	0.3754
30	33.10	0.27	-99.73	0.0581
45	23.02	0.00	-100.00	0.0015
60	19.06	0.00	-100.00	0.0470

1.4 Curcumin formation upon the time and the amount of enzyme

The formation of curcumin presented the linear time-dependent product after CDD incubated with MLS9 concentration of 0.01, 0.02, 0.05 and 0.1 mg/mL at range 0 - 4 min ($R^2 > 0.9$).

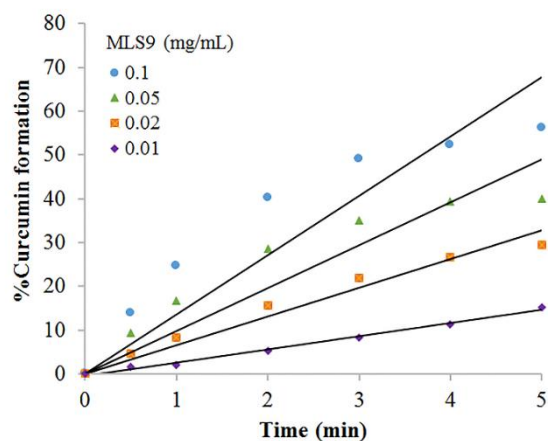


Figure 43. Formation of curcumin in MLS9 plotted against time. CDD at 3 μ M were incubated in duplicate with various concentration of each LS9 (0.01, 0.02, 0.05 and 0.1 mg/mL).

The curcumin formation incubated with MLS9 at 0.5 min depended upon the enzyme present of 0.01, 0.02, 0.05 and 0.1 mg/mL, respectively ($R^2 = 0.9952$).

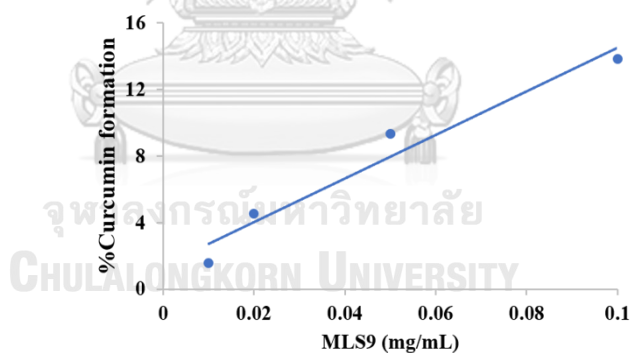


Figure 44. Formation of curcumin in MLS9 plotted against enzyme concentration. CDD at 3 μ M were incubated in duplicate with various concentration of MLS9 (0.01, 0.02, 0.05 and 0.1 mg/mL) at 0.5 min.

2. Zero-order reaction of CDD with DLS9

2.1 Excess reactant CDD with catalyst

CDD present exceeded amount in DLS9 of 0.01 and 0.02 mg/mL at 0.5 min, while CDD concentration was no saturated in DLS9 of 0.05 and 0.1 mg/mL.

- DLS9 0.01 mg/mL, [CDD] = 300 x [DLS9]

Time (min)	% Curcumin formation	% CDD remaining	% CDD changing	R ²
0	0.00	100.00	0.00	-
0.5	3.35	74.44	-25.56	-
1	6.52	62.93	-37.07	0.9997
2	12.77	50.22	-49.78	0.9998
3	18.14	40.11	-59.89	0.9984
4	23.17	32.65	-67.35	0.9973
5	26.20	26.62	-73.38	0.9894
10	28.47	10.15	-89.85	0.7859
15	24.73	4.56	-95.44	0.5783
30	21.39	0.39	-99.61	0.2739
45	17.94	0.00	-100.00	0.1267
60	16.58	0.00	-100.00	0.0608

- DLS9 0.02 mg/mL, [CDD] = 150 x [DLS9]

Time (min)	% Curcumin formation	% CDD remaining	% CDD changing	R ²
0	0.00	100.00	0.00	-
0.5	5.88	76.77	-23.23	-
1	10.51	66.99	-33.01	0.9954
2	19.45	49.79	-50.21	0.9960
3	26.54	42.26	-57.74	0.9929
4	31.49	31.30	-68.70	0.9840
5	34.24	25.06	-74.94	0.9655
10	36.13	10.12	-89.88	0.7269
15	31.02	4.25	-95.75	0.5047
30	25.85	0.33	-99.67	0.1981
45	21.45	0.00	-100.00	0.0671
60	17.05	0.00	-100.00	0.0078

- DLS9 0.05 mg/mL, [CDD] = 60 x [DLS9]

Time (min)	% Curcumin formation	% CDD remaining	% CDD changing	R ²
0	0.00	100.00	0.00	-
0.5	8.22	67.62	-32.38	-
1	15.41	59.46	-40.54	0.9985
2	25.16	42.33	-57.67	0.9825
3	30.57	32.23	-67.77	0.9587
4	34.07	23.78	-76.22	0.9346
5	38.34	18.99	-81.01	0.9279
10	41.25	7.60	-92.40	0.7184
15	36.50	3.51	-96.49	0.5209
30	29.22	0.58	-99.42	0.1897
45	22.23	0.00	-100.00	0.0396
60	18.24	0.00	-100.00	0.0003

- DLS9 0.1 mg/mL, [CDD] = 30 x [DLS9]

Time (min)	% Curcumin formation	% CDD remaining	% CDD changing	R ²
0	0.00	100.00	0.00	-
0.5	11.98	63.14	-36.86	-
1	20.87	48.74	-51.26	0.9928
2	32.48	29.84	-70.16	0.9683
3	41.63	20.17	-79.83	0.9637
4	42.37	13.33	-86.67	0.9080
5	44.40	9.94	-90.06	0.8660
10	44.61	3.17	-96.83	0.5799
15	43.18	1.40	-98.60	0.4382
30	28.08	0.28	-99.72	0.0762
45	24.64	0.00	-100.00	0.0044
60	18.12	0.00	-100.00	0.0166

2.2 Curcumin formation upon the time and the amount of enzyme

The formation of curcumin presented the linear time-dependent product after CDD incubated with DLS9 concentration of 0.01, 0.02, 0.05 and 0.1 mg/mL at range 0 - 4 min ($R^2 > 0.9$).

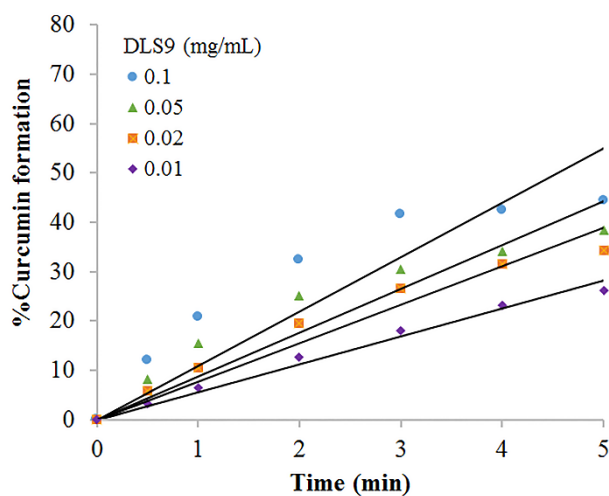


Figure 45. Formation of curcumin in DLS9 plotted against time. CDD at 3 μ M were incubated in duplicate with various concentration of each LS9 (0.01, 0.02, 0.05 and 0.1 mg/mL).

The curcumin formation incubated with DLS9 at 0.5 min depended upon the enzyme present of 0.01, 0.02, 0.05 and 0.1 mg/mL, respectively ($R^2 = 0.9605$).

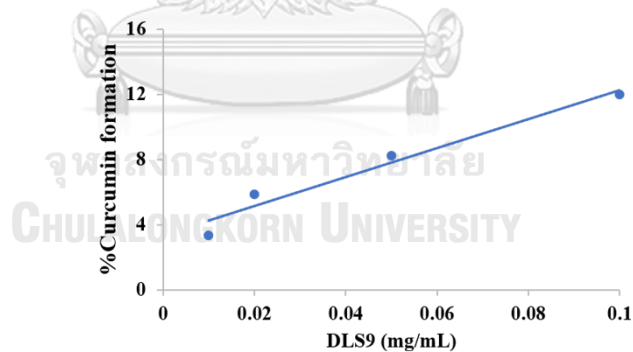


Figure 46. Formation of curcumin in DLS9 plotted against enzyme concentration. CDD at 3 μ M were incubated in duplicate with various concentration of DLS9 (0.01, 0.02, 0.05 and 0.1 mg/mL) at 0.5 min

3. Zero-order reaction of CDD with RLS9

3.1 Excess reactant CDD with catalyst

CDD present exceeded amount in RLS9 of 0.01, 0.02 and 0.05 mg/mL at 1 min, while that in RLS9 of 0.1 mg/mL at 0.5 min.

- RLS9 0.01 mg/mL, [CDD] = 300 x [RLS9]

Time (min)	% Curcumin formation	% CDD remaining	% CDD changing	R ²
0	0.00	100.00	0.00	-
0.5	0.64	79.48	-20.52	-
1	1.42	72.89	-27.11	0.9969
2	3.89	66.49	-33.51	0.9766
3	6.37	58.64	-41.36	0.9874
4	8.77	52.50	-47.50	0.9930
5	10.15	40.60	-59.40	0.9933
10	17.82	26.68	-73.32	0.9856
15	21.00	13.66	-86.34	0.9568
30	18.13	1.63	-98.37	0.6543
45	13.85	0.00	-100.00	0.4143
60	12.62	0.00	-100.00	0.2903

- RLS9 0.02 mg/mL, [CDD] = 150 x [RLS9]

Time (min)	% Curcumin formation	% CDD remaining	% CDD changing	R ²
0	0	100.00	0.00	-
0.5	1.28	82.81	-17.19	-
1	3.25	78.14	-21.86	0.9853
2	6.93	62.71	-37.29	0.9953
3	10.94	56.54	-43.46	0.9971
4	12.25	46.44	-53.56	0.9829
5	17.72	40.58	-59.42	0.9880
10	22.48	19.07	-80.93	0.9157
15	24.38	8.96	-91.04	0.8577
30	21.94	1.99	-98.01	0.5725
45	18.66	0.89	-99.11	0.3924
60	14.99	0.00	-100.00	0.2392

- RLS9 0.05 mg/mL, [CDD] = 60 x [RLS9]

Time (min)	% Curcumin formation	% CDD remaining	% CDD changing	R ²
0	0	100.00	0.00	-
0.5	4.24	78.87	-21.13	-
1	8.29	70.44	-29.56	0.9998
2	17.61	56.81	-43.19	0.9990
3	23.63	42.65	-57.35	0.9941
4	28.14	34.27	-65.73	0.9845
5	29.59	25.96	-74.04	0.9559
10	32.81	9.07	-90.93	0.7413
15	27.71	3.83	-96.17	0.5148
30	19.56	0.70	-99.30	0.1379
45	15.54	0.00	-100.00	0.0216
60	12.98	0.00	-100.00	0.0002

- RLS9 0.1 mg/mL, [CDD] = 30 x [RLS9]

Time (min)	% Curcumin formation	% CDD remaining	% CDD changing	R ²
0	0.00	100.00	0.00	-
0.5	4.62	73.91	-26.09	-
1	9.97	56.82	-43.18	0.9982
2	22.63	40.53	-59.47	0.9950
3	25.94	27.41	-72.59	0.9626
4	27.60	19.44	-80.56	0.9161
5	29.86	14.25	-85.75	0.8886
10	28.74	4.62	-95.38	0.5778
15	23.55	2.00	-98.00	0.3293
30	17.18	0.00	-100.00	0.0556
45	11.39	0.00	-100.00	0.0012
60	10.40	0.00	-100.00	0.0344

3.2 Curcumin formation upon the time and the amount of enzyme

The formation of curcumin presented the linear time-dependent product after CDD incubated with RLS9 concentration of 0.01, 0.02, 0.05 and 0.1 mg/mL at range 0 - 4 min ($R^2 > 0.9$).

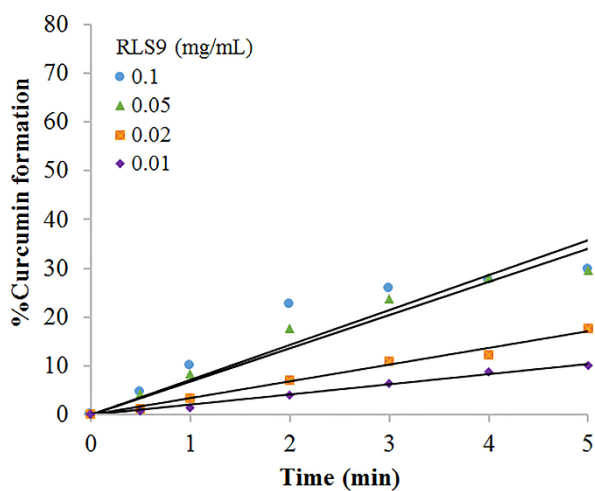


Figure 47. Formation of curcumin in RLS9 plotted against time. CDD at 3 μ M were incubated in duplicate with various concentration of each LS9 (0.01, 0.02, 0.05 and 0.1 mg/mL)

The curcumin formation incubated with RLS9 at 1 min depended upon the enzyme present of range 0.01 - 0.1 mg/mL ($R^2 = 0.8725$), while that with RLS9 range 0.01 - 0.05 show better relationship ($R^2 = 0.9997$).

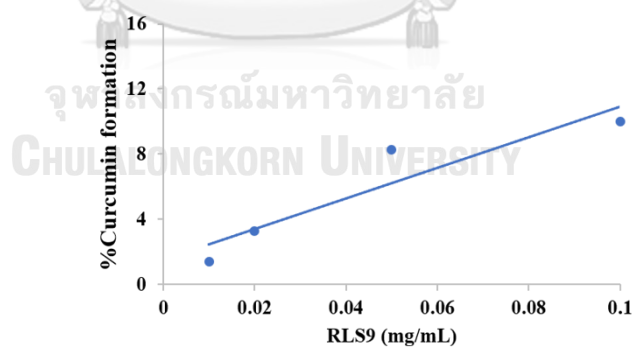


Figure 48. Formation of curcumin in RLS9 plotted against enzyme concentration. CDD at 3 μ M were incubated in duplicate with various concentration of each LS9 (0.01, 0.02, 0.05 and 0.1 mg/mL) at 1 min.

In this study, the saturating substrate occurred when incubated with 0.02 mg/mL of HLS9 and RLS9 at 1 min, while that when incubate with MLS9 and RLS9 at 0.5 min. This time point is suitable for observing the rate of reaction in enzyme identification study. Curcumin content could be investigated after CDD reacted with LS9 at 0.02 mg/mL in all test species. The linear time-dependent formation of curcumin in rage 0-4 min were observed in LS9 of all test species. The curcumin formation in HLS9, MLS9 and DLS9 depended upon the range enzyme present of 0.01- 0.1 mg/mL, excepted RLS9 range 0.01 – 0.05 mg/mL.



APPENDIX J

Esterase inhibitor structure

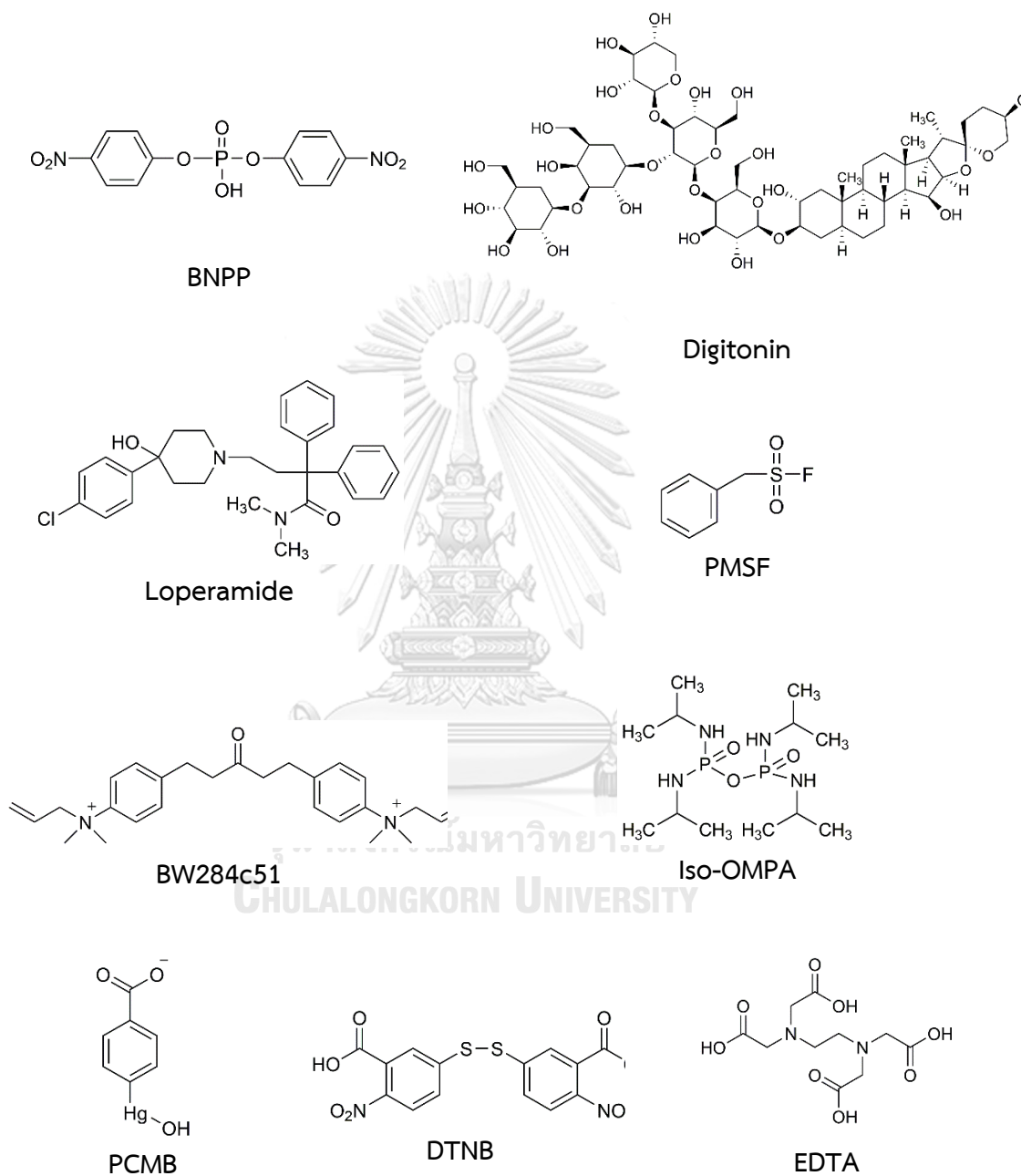


Figure 49. Structure of esterase inhibitors.

APPENDIX K

Esterase Activity in LS9

The common method to determine the activities of esterase is by performing continuous spectrophotometric assays using *p*-nitrophenyl acetate or *p*-nitrophenyl caprylate 500 μ M in 50mM phosphate buffer (pH 7.4) as substrate in LS9 5 μ g/mL in 50 mM phosphate buffer (pH 7.4) at 37°C after a 5-minute preincubation. Hydrolysis of *p*-nitrophenyl acyl esters to generate *p*-nitrophenol, which produces a yellow coloration. The UV spectrum of *p*-nitrophenolate show maximum wavelength at 405 nm

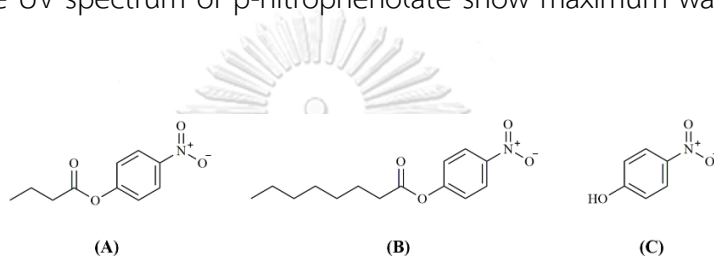


Figure 50. Structure of (A) *p*-nitrophenyl acetate, (B) *p*-nitrophenyl caprylate and (C) *p*-nitrophenol

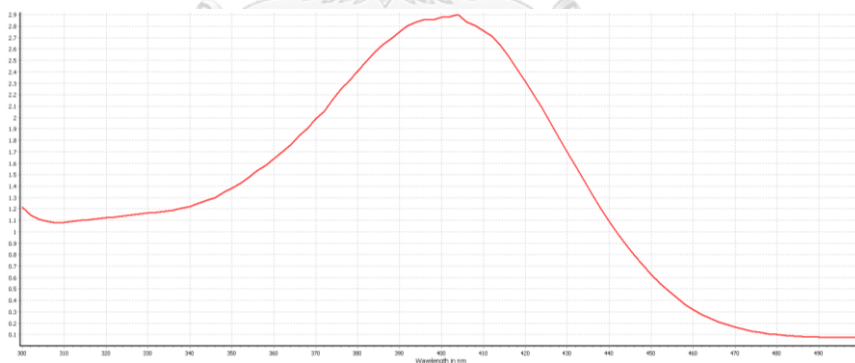


Figure 51. UV spectrum of *p*-nitrophenol

The time-dependent rate of formation of this hydrolysis product was monitored spectrometrically by Microplate reader with following parameter.

Microplate reader parameter for one-point measurement of standard curve

Parameters	Conditions
- Microplate:	COSTAR 96
- Wavelength settings:	Discrete wavelengths
Wavelength:	405 nm
- Path length correction	On
Volume	200 μ L
Length	6.31 mm
- General setting	0.5 s
- No. of flashes per well	22
Temperature control	37°C

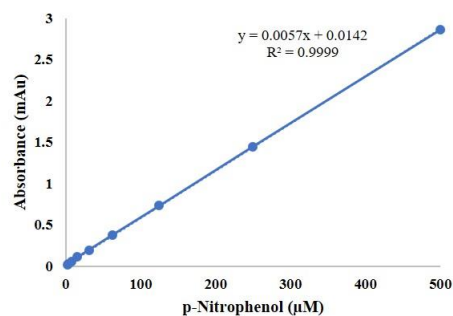
Microplate reader parameter for continuous kinetics measurement of sample

Parameters	Conditions
- Microplate:	COSTAR 96
- Wavelength settings:	Discrete wavelengths
Wavelength:	405 nm
- Path length correction	On
Volume	200 μ L
Length	6.31 mm
- General setting	
Setting time	0.1 s
No. of kinetic windows	1
- Kinetic window 1	
No. of cycles	31
No. of flashes per well and cycle	22
Cycle time	10
- Minim cycle time 1:	2 s
- Temperature control	37°C
- Shaking options	
Mode	Double orbital
Shaking frequency	500 rpm
Additional shaking	Before first cycle
Shaking time	4 s

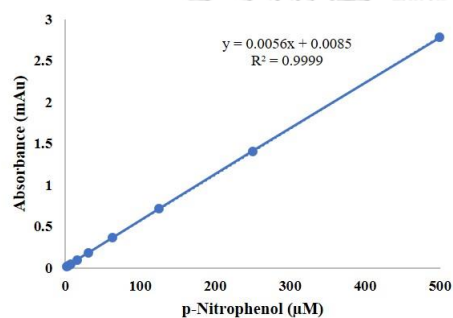
The standard curve of absorbance versus *p*-nitrophenol concentration (1.95-500 μM) in phosphate buffer pH 7.4, HLS9, MLS9 and RLS9 were plotted.

Standard curve of *p*-nitrophenol solution

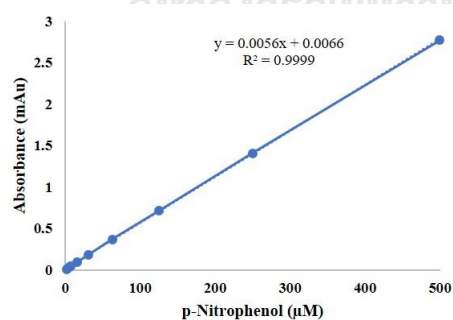
- In phosphate buffer pH 7.4



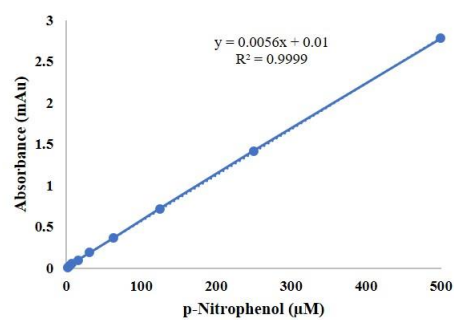
- In HLS9



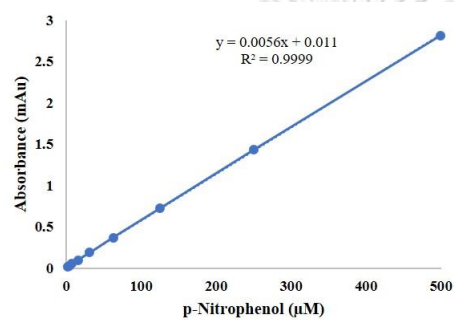
- In MLS9



- In DLS9



- In RLS9



The concentration of *p*-nitrophenolate ion from *p*-nitrophenyl acetate and *p*-nitrophenyl caprylate in phosphate buffer pH 7.4, HLS9, MLS9, DLS9 and RLS9 were measured every at 405 nm every 10 sec for 5 min.

- Concentration of *p*-nitrophenol after incubated *p*-nitrophenyl acetate with phosphate buffer pH 7.4

Time	N1	N2	N3
0	9.781	8.730	9.431
10	9.956	9.080	9.781
20	9.956	9.080	9.606
30	10.307	9.781	10.131
40	10.131	9.256	10.131
50	11.007	9.956	10.657
60	11.183	10.131	10.832
70	11.183	10.307	10.657
80	11.533	10.307	11.007
90	11.883	10.657	11.533
100	11.883	10.482	11.358
110	12.059	10.832	11.533
120	12.059	10.832	11.708
130	12.409	11.007	11.883
140	12.759	11.183	12.234
150	12.759	11.533	12.409
160	12.934	11.533	12.584
170	13.110	11.708	12.759
180	13.285	12.409	13.110
190	13.635	12.584	13.460
200	13.810	12.584	13.635
210	13.810	12.934	13.635
220	13.986	12.759	13.635
230	14.336	13.110	13.986
240	14.336	13.110	14.161
250	14.686	13.635	14.336
260	14.686	13.810	14.511
270	14.686	13.810	14.862
280	15.212	14.161	14.862
290	15.212	14.336	15.037
300	15.387	14.336	15.562
R ²	0.9902	0.9877	0.9939

- Concentration of *p*-nitrophenol after incubated *p*-nitrophenyl caprylate with phosphate buffer pH 7.4

Time	N1	N2	N3
0	28.001	26.424	28.526
10	27.825	26.424	28.351
20	28.001	26.424	28.701
30	27.825	26.074	28.526
40	28.176	26.424	28.526
50	28.526	25.723	28.176
60	28.526	25.723	27.825
70	28.877	26.074	28.176
80	28.001	26.249	28.526
90	28.176	25.898	28.351
100	28.001	25.548	28.526
110	28.701	25.898	28.351
120	27.825	26.074	28.351
130	27.825	25.723	28.176
140	27.825	25.723	28.001
150	28.351	25.898	28.176
160	28.176	26.074	28.526
170	28.526	25.898	26.950
180	27.300	25.022	27.125
190	27.125	25.548	27.300
200	26.950	25.373	27.475
210	27.300	25.548	27.475
220	27.650	25.198	27.125
230	27.650	25.548	27.300
240	27.300	25.548	27.300
250	27.125	25.198	27.650
260	27.300	25.373	27.475
270	28.001	26.424	28.526
280	27.825	26.424	28.351
290	28.001	26.424	28.701
300	27.825	26.074	28.526
R ²	0.4390	0.6016	0.6263

- Concentration of *p*-nitrophenol after incubated *p*-nitrophenyl acetate with HLS9

Time	N1	N2	N3
0	16.460	15.921	13.583
10	18.438	17.539	15.381
20	20.596	20.057	17.539
30	22.394	22.214	19.337
40	24.732	24.013	21.495
50	26.710	26.170	23.653
60	28.508	27.969	25.271
70	30.666	30.306	27.609
80	32.464	32.464	29.587
90	33.723	34.083	31.565
100	35.341	36.061	33.363
110	36.960	38.398	35.521
120	38.578	40.376	37.319
130	40.376	42.175	38.938
140	42.534	44.692	41.275
150	44.153	46.850	42.894
160	46.310	48.828	44.872
170	48.468	50.626	47.030
180	50.806	52.964	49.547
190	52.604	55.122	51.885
200	54.762	57.100	53.683
210	56.740	59.258	55.841
220	58.359	61.236	58.179
230	60.516	63.394	59.977
240	62.854	65.372	62.315
250	65.372	67.529	64.293
260	67.889	69.867	66.271
270	69.867	71.845	68.608
280	71.845	74.003	70.586
290	73.464	76.161	72.924
300	75.801	78.678	74.902
R ²	0.9981	0.9998	0.9995

- Concentration of *p*-nitrophenol after incubated *p*-nitrophenyl caprylate with HLS9

Time	N1	N2	N3
0	29.227	28.328	28.868
10	29.767	29.227	29.767
20	30.306	29.767	29.767
30	30.846	30.306	30.486
40	31.205	30.306	30.666
50	31.565	30.846	31.026
60	32.284	30.846	31.565
70	33.004	31.745	32.284
80	33.184	32.105	31.925
90	33.363	32.464	32.464
100	33.903	32.284	33.363
110	34.083	33.004	33.903
120	34.982	34.262	34.442
130	35.162	34.262	34.442
140	35.521	34.442	34.802
150	35.701	34.622	35.162
160	36.420	35.162	35.341
170	36.420	35.341	36.061
180	36.780	35.701	36.780
190	37.499	36.061	36.960
200	37.859	36.600	37.319
210	38.578	37.140	37.679
220	38.758	37.499	38.398
230	39.477	38.039	38.578
240	39.657	38.578	39.477
250	40.376	38.938	39.837
260	40.556	38.758	39.837
270	40.916	39.837	40.197
280	41.635	40.556	41.096
290	41.995	40.916	41.995
300	42.714	41.275	43.433
R²	0.9970	0.9937	0.9906

- Concentration of *p*-nitrophenol after incubated *p*-nitrophenyl acetate with MLS9

Time	N1	N2	N3
0	13.752	15.012	11.593
10	15.372	16.811	13.932
20	17.171	18.790	15.372
30	19.150	20.229	17.171
40	20.409	21.129	18.790
50	22.208	23.288	20.229
60	23.828	25.267	21.669
70	25.807	26.886	23.468
80	27.246	28.865	24.727
90	28.865	30.304	26.346
100	30.125	31.924	28.145
110	31.744	34.083	30.125
120	33.183	35.882	31.744
130	35.522	37.861	33.723
140	36.961	39.480	35.162
150	38.581	41.459	36.601
160	39.840	42.899	37.861
170	41.819	44.698	39.840
180	43.078	46.137	41.099
190	44.698	48.116	42.719
200	46.857	50.095	45.057
210	48.476	51.894	46.677
220	49.915	53.513	48.116
230	51.894	55.313	49.915
240	53.154	56.932	51.355
250	54.953	58.911	53.513
260	56.392	60.350	54.593
270	58.371	62.509	56.752
280	59.990	64.308	58.371
290	61.610	65.928	59.990
300	63.409	67.547	61.610
R²	0.9998	0.9998	0.9997

- Concentration of *p*-nitrophenol after incubated *p*-nitrophenyl caprylate with MLS9

Time	N1	N2	N3
0	33.723	32.463	34.802
10	33.543	33.903	35.702
20	33.903	35.162	36.242
30	34.443	36.422	36.961
40	35.162	36.242	37.681
50	36.242	37.321	38.760
60	36.781	37.681	39.480
70	36.961	39.120	40.200
80	38.401	39.840	41.459
90	39.120	40.020	42.899
100	40.380	40.740	43.438
110	41.099	41.819	43.258
120	41.999	42.359	44.158
130	41.999	42.899	44.878
140	42.539	43.978	45.597
150	43.078	45.057	45.957
160	44.338	45.237	47.216
170	44.698	45.417	48.296
180	46.317	46.317	48.476
190	45.777	47.396	49.196
200	46.677	47.756	49.915
210	47.576	49.016	51.175
220	48.296	49.555	51.714
230	48.656	50.635	52.614
240	49.555	50.995	53.693
250	50.095	51.355	54.233
260	51.175	52.434	55.493
270	51.894	53.513	56.392
280	52.254	53.513	56.212
290	52.974	53.873	57.112
300	53.873	54.953	58.011
R²	0.9962	0.9965	0.9974

- Concentration of *p*-nitrophenol after incubated *p*-nitrophenyl acetate with DLS9

Time	N1	N2	N3
0	26.386	24.591	19.744
10	30.875	28.720	24.232
20	35.183	33.029	28.361
30	39.133	37.158	32.490
40	43.442	40.928	36.440
50	47.392	45.237	40.390
60	52.059	49.366	44.519
70	55.830	53.496	48.110
80	59.779	58.702	53.137
90	64.088	62.472	56.548
100	67.320	66.781	60.318
110	71.090	70.910	64.986
120	74.860	75.399	69.654
130	78.630	80.066	73.603
140	82.400	84.734	77.733
150	86.709	89.402	81.682
160	91.557	94.070	86.350
170	96.224	98.558	90.120
180	101.072	102.508	95.147
190	105.381	106.817	99.636
200	110.048	110.946	104.483
210	114.178	114.896	109.151
220	118.666	120.102	113.819
230	122.795	125.668	118.127
240	127.822	130.874	122.795
250	133.388	135.183	128.002
260	138.235	138.774	132.849
270	141.107	143.621	137.517
280	146.134	148.468	142.364
290	150.264	153.316	147.212
300	155.291	158.163	152.059
R²	0.9988	0.9995	0.9987

- Concentration of *p*-nitrophenol after incubated *p*-nitrophenyl caprylate with DLS9

Time	N1	N2	N3
0	39.133	41.288	42.724
10	40.210	42.724	43.262
20	42.006	43.981	45.237
30	43.801	45.058	47.033
40	45.596	47.571	48.648
50	46.494	48.648	49.905
60	48.110	50.444	51.341
70	49.546	51.700	53.137
80	52.419	53.496	54.752
90	52.419	55.112	56.189
100	54.393	56.727	57.625
110	56.009	57.445	59.061
120	57.266	59.420	60.857
130	58.523	60.318	62.831
140	60.318	62.293	64.627
150	61.754	63.729	65.524
160	63.190	65.345	67.320
170	64.627	66.422	68.397
180	66.602	68.397	70.372
190	67.679	69.654	71.808
200	69.654	71.090	73.244
210	71.269	72.526	74.501
220	72.347	74.142	75.937
230	73.962	75.040	77.912
240	75.219	77.553	79.169
250	76.835	78.092	80.785
260	78.271	78.989	81.862
270	78.989	80.246	82.939
280	80.426	82.041	84.196
290	81.862	83.478	85.812
300	83.478	84.734	86.530
R²	0.9991	0.9989	0.9988

- Concentration of *p*-nitrophenol after incubated *p*-nitrophenyl acetate with RLS9

Time	N1	N2	N3
0	36.041	34.443	28.406
10	40.834	41.544	34.443
20	46.871	47.048	40.302
30	52.907	53.973	47.048
40	59.121	59.832	52.907
50	64.803	65.513	58.944
60	71.727	71.017	64.980
70	76.343	76.876	70.662
80	81.669	82.912	77.053
90	87.528	88.416	83.800
100	92.855	93.565	89.481
110	98.004	99.069	95.518
120	103.685	104.750	100.844
130	109.189	110.964	107.413
140	114.693	116.113	112.917
150	119.664	121.084	117.888
160	124.813	127.298	121.972
170	129.961	133.157	127.476
180	134.755	139.194	133.690
190	139.371	144.343	139.549
200	145.230	150.379	146.651
210	151.444	154.995	152.332
220	156.948	159.611	158.546
230	162.630	164.227	163.695
240	168.133	171.152	169.909
250	173.815	176.478	175.058
260	179.851	182.692	180.384
270	186.065	187.841	184.645
280	191.569	193.877	189.794
290	195.830	198.671	195.653
300	201.867	204.175	202.222
R²	0.9997	0.9997	0.9994

- Concentration of *p*-nitrophenol after incubated *p*-nitrophenyl caprylate with RLS9

Time	N1	N2	N3
0	39.236	41.367	42.787
10	40.302	42.787	43.320
20	42.077	44.030	45.273
30	43.853	45.095	47.048
40	45.628	47.581	48.646
50	46.516	48.646	49.889
60	48.114	50.422	51.309
70	49.534	51.664	53.085
80	52.375	53.440	54.683
90	52.375	55.038	56.103
100	54.328	56.636	57.523
110	55.926	57.346	58.944
120	57.168	59.299	60.719
130	58.411	60.187	62.672
140	60.187	62.140	64.448
150	61.607	63.560	65.335
160	63.027	65.158	67.111
170	64.448	66.223	68.176
180	66.401	68.176	70.129
190	67.466	69.419	71.549
200	69.419	70.839	72.970
210	71.017	72.260	74.213
220	72.082	73.857	75.633
230	73.680	74.745	77.586
240	74.923	77.231	78.829
250	76.521	77.763	80.427
260	77.941	78.651	81.492
270	78.651	79.894	82.557
280	80.072	81.669	83.800
290	81.492	83.090	85.398
300	83.090	84.333	86.108
R²	0.9991	0.9989	0.9988

The formation of p-nitrophenolate from p-nitrophenyl acetate and p-nitrophenyl caprylate in HLS9, MLS9, DLS9 and RLS9 were linear over this time period ($r^2 > 0.99$). The slope and specified activity of hydrolysis of p-nitrophenyl acetate and p-nitrophenyl caprylate were investigated as showing below.

Slope of hydrolysis of p-nitrophenyl acetate and p-nitrophenyl caprylate in 50 mM phosphate buffer pH (7.4) and LS9 of different animal species ($\mu\text{M sec}^{-1}$)

No.	p-Nitrophenyl acetate					p-Nitrophenyl caprylate				
	PBS pH7.4	HLS9	MLS9	DLS9	RLS9	PBS pH7.4	HLS9	MLS9	DLS9	RLS9
N1	0.0189	0.1952	0.1642	0.4265	0.5482	-0.0038	0.0429	0.0700	0.1488	0.1472
N2	0.0187	0.2081	0.1763	0.4455	0.5598	-0.0033	0.0409	0.0721	0.1460	0.1444
N3	0.0197	0.2043	0.1652	0.4382	0.5767	-0.0048	0.0437	0.0773	0.1509	0.1492
X	0.0191	0.2026	0.1686	0.4368	0.5616	-0.0040	0.0425	0.0731	0.1486	0.1469
SD	0.0005	0.0066	0.0067	0.0096	0.0143	0.0007	0.0015	0.0038	0.0024	0.0024

Specific activities of enzyme for each substrate were expressed as $\mu\text{mol min}^{-1} \text{mg}^{-1}$ protein (mean \pm SD) as following equation.

$$\text{Specific activity} = (\text{Slope}_{\text{LS9}} - \text{Slope}_{\text{control}}) (\mu\text{M sec}^{-1}) \times 60 (\text{sec min}^{-1}) \times \frac{1}{1000} (\text{L ml}^{-1}) \times \frac{1}{0.005} (\text{mg mL}^{-1})$$

(Eq. 1)

Specific activity of HLS9, MLS9, DLS9 and RLS9 ($\mu\text{mole min}^{-1} \text{mg}^{-1}$).

No.	p-Nitrophenyl acetate				p-Nitrophenyl caprylate			
	HLS9	MLS9	DLS9	RLS9	HLS9	MLS9	DLS9	RLS9
N1	2.1134	1.7414	4.8892	6.3491	0.5620	0.8874	1.8334	1.8136
N2	2.2684	1.8862	5.1173	6.4882	0.5377	0.9129	1.8001	1.7806
N3	2.2226	1.7538	5.0296	6.6912	0.5718	0.9754	1.8584	1.8384
X	2.20	1.79	5.01	6.51	0.56	0.93	1.83	1.81
SD	0.08	0.08	0.12	0.17	0.02	0.05	0.03	0.03

APPENDIX L

Effect of nine esterase inhibitors on CDD metabolism in LS9

Table 12. Effect of esterase inhibitors on CDD metabolism in LS9 of human monkey, dog and rat

Control/ Inhibitor	Target	Curcumin formation rate (nmol min ⁻¹ mg protein ⁻¹)									% of Control			
		Human	Monkey	Dog	Rat	Human	Monkey	Dog	Rat	Human	Monkey	Dog	Rat	
Inhibitor-free control		10.77 ± 0.82	14.60 ± 1.51	26.79 ± 2.43	12.71 ± 0.25	100 ± 7.66	100 ± 10.37	100 ± 9.07	100 ± 1.98					
Enzyme-free control		ND	ND	ND	ND	ND	ND	ND	ND				ND	
Solvent-free control		9.60 ± 0.77	14.05 ± 1.11	24.68 ± 0.89	11.29 ± 1.54	89.11 ± 7.12 ^{NS}	96.24 ± 7.60 ^{NS}	92.13 ± 3.30 ^{NS}	88.83 ± 12.13 ^{NS}					
BNPP	CES	ND	ND	ND	ND	ND	ND	ND	ND				ND	
Digitonin	CES1	ND	9.37 ± 0.70	8.84 ± 0.36	6.21 ± 0.66	ND	64.15 ± 4.78 ^{***}	33.00 ± 1.33 ^{***}	48.85 ± 5.16 ^{***}					
Loperamide	CES2	ND	6.29 ± 0.77	16.73 ± 0.30	4.86 ± 0.25	ND	43.05 ± 5.28 ^{***}	62.45 ± 1.13 ^{***}	38.24 ± 1.99 ^{***}					
PMSF	Serine hydrolase	4.19 ± 0.86	6.15 ± 0.17	ND	ND	38.93 ± 7.96 ^{***}	42.12 ± 1.18 ^{***}	ND	ND				ND	
BW284c51	ACHE	9.93 ± 0.95	14.13 ± 1.86	24.06 ± 1.61	5.59 ± 0.78	92.22 ± 8.81 ^{NS}	96.81 ± 12.72 ^{NS}	89.83 ± 6.02 ^{NS}	43.99 ± 6.14 ^{***}					
Iso-OMPA	BChE	3.40 ± 0.76	6.32 ± 0.69	8.38 ± 0.35	4.29 ± 0.17	31.54 ± 7.03 ^{***}	43.26 ± 4.71 ^{***}	31.28 ± 1.30 ^{***}	33.75 ± 1.34 ^{***}					
PCMB	CMBL	ND	12.15 ± 1.26	16.06 ± 0.53	ND	ND	83.24 ± 8.62 ^{NS}	59.96 ± 1.99 ^{***}	ND					
DTNB	Cysteine hydrolase	7.60 ± 1.03	14.77 ± 1.51	23.92 ± 2.18	12.36 ± 1.19	70.62 ± 9.61 ^{***}	101.17 ± 10.31 ^{NS}	89.28 ± 8.16 ^{NS}	97.28 ± 9.35 ^{NS}					
EDTA	PON	8.74 ± 0.54	13.58 ± 0.74	23.44 ± 1.50	11.12 ± 1.36	81.14 ± 4.98 ^{NS}	93.03 ± 5.07 ^{NS}	87.48 ± 5.58 ^{NS}	87.50 ± 10.68 ^{***}					

Data are presented as the mean ± SD (n=3). One-way ANOVA analysis with Dunnett's post hoc test was used to indicate statistical difference. ND = not determined since the curcumin concentration was below the lower limit of quantification; NS = not statistically significant vs. control; *** p < 0.001 (vs. control). The classification of enzymatic inhibition as strong, moderate, weak or no inhibition was reflected by relative curcumin formation rate of < 20%, 20-49 %, 50-80 %, and > 80%, respectively

APPENDIX M

Acceptance on an analytical run criterion

In this study, the *in vitro* metabolism profiles and enzymatic identification of CDD were investigated by UHPLC. The Acceptance of an analytical run criterion was set based on three parameter which are system suitability, IS response plot and standard curve. The analytical data of sample were observed and processed after these parameters met the criteria

In bioanalytical analysis by liquid chromatography, system suitability test is one of the most important and integral parts of HPLC process during the routine analysis of analysts. System suitability test is performed to determine the suitability and effectiveness of the entire chromatographic system prior to use on each run. Repeatability relative standard deviations (RSD) of retention time and peak response, resolution (R), tailing factor (T), theoretical plate (N), capacity factor (k) are possessing as the indicate system precision. System suitability criteria for HPLC chromatogram was %RSD < 2.0%, R > 1.5, Tailing factor < 2.0, N > 2000 and k > 2 (168, 169).

Monitoring of Internal standard (IS) response across a run of analysis and evaluation of irregularity is now expectation. Internal standard is crucial to ensure the accuracy and precision in bioanalysis by compensating the variations in analytical procedure including sample preparation, injection volume and instrument response. The monitoring IS response for all assay provide complementary information regarding assay, run and result acceptance. In this study, visual inspection of IS response of standard and sample was evaluated.

Visual inspection of IS response plot identify in individual samples or groups of samples for any irregularity. The lowest IS response in the standard curve (Ref_{low}) with apply the criteria of individual anomalies and system variability described below (170):

In individual anomalies:

Assign as an analytical repeat if IS response is $> 2x \text{Ref}_{\text{low}}$ or $< 10\%$ of Ref_{low} or if IS response is $< 50\%$ of Ref_{low} and $<$ lowest lower limit of quantitation standard response.

Systematic variability:

Assign as an analytical repeat if IS response across a group of samples is $> 2x \text{Ref}_{\text{low}}$ or $< 50\%$ of Ref_{low} . The acceptance window for the IS response variability varies range $50\% \text{Ref}_{\text{Low}}$ to $2x \text{Ref}_{\text{Low}}$.

Standard curve in bioanalytical method is a linear relationship between concentration and peak area using a linear least squares method. The standard curves were evaluated with a correlation coefficient value, R^2 , greater than 0.99 being considered as acceptable.

Moreover, the acceptance of an analytical run for optimization for enzyme assay condition in LS9 consider two parameter including system suitability and monitoring of Internal standard (IS) response reference to lowest IS response in the test sample (Test_{low}) instead and justifies the processing data as previously described.

The system suitability, visual inspection of IS response plot and standard curve of all analytical runs are showed below. The results demonstrated that all analytical run of *in vitro* metabolism, optimization of enzyme assay condition and enzymatic identification met the criteria. The system suitability parameters are within permitted limits, indicating the HPLC system is suitable for analysis. The IS response of all samples are between 50% to 200% of Ref_{low} , indicating the bioanalytical runs are acceptable and had no abnormal IS in term of individual and systemic variability. The standard curve in each run demonstrated R^2 value greater than 0.99 and could be used to determine the concentration of samples.

1. *In vitro* metabolic stability of CDD in LS9

Sequential injection

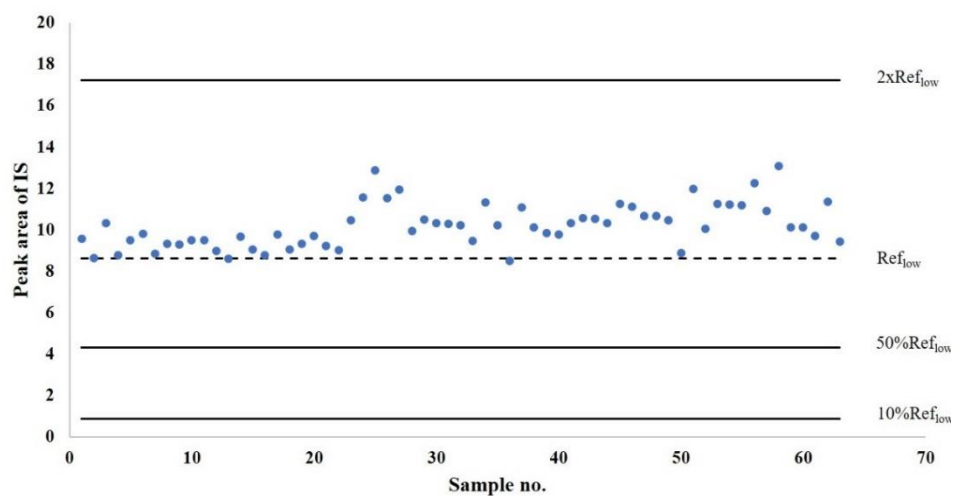
No.	Name	No.	Name	No.	Name
-	System suitability N1	18	STD CDD_1.5 μ M	41	Sample N2_T4 min
-	System suitability N2	19	STD CDD_2.5 μ M	42	Sample N2_T5 min
-	System suitability N3	20	STD CDD_3.5 μ M	43	Sample N2_T10 min
-	System suitability N4	21	STD CDD_4.5 μ M	44	Sample N2_T15 min
-	System suitability N5	22	Sample N1_T0 min	45	Sample N2_T30 min
-	Blank_LS9	23	Sample N1_T0.5 min	46	Sample N2_T45 min
1	STD Curcumin_0.025 μ M	24	Sample N1_T1 min	47	Sample N2_T60 min
2	STD Curcumin_0.25 μ M	25	Sample N1_T2 min	48	Sample N2_T90 min
3	STD Curcumin_0.50 μ M	26	Sample N1_T3 min	49	Sample N2_T120 min
4	STD Curcumin_1.5 μ M	27	Sample N1_T4 min	50	Sample N3_T0 min
5	STD Curcumin_2.5 μ M	28	Sample N1_T5 min	51	Sample N3_T0.5 min
6	STD Curcumin_3.5 μ M	29	Sample N1_T10 min	52	Sample N3_T1 min
7	STD Curcumin_4.5 μ M	30	Sample N1_T15 min	53	Sample N3_T2 min
8	STD MSCUR_0.0125 μ M	31	Sample N1_T30 min	54	Sample N3_T3 min
9	STD MSCUR_0.025 μ M	32	Sample N1_T45 min	55	Sample N3_T4 min
10	STD MSCUR_0.05 μ M	33	Sample N1_T60 min	56	Sample N3_T5 min
11	STD MSCUR_0.1 μ M	34	Sample N1_T90 min	57	Sample N3_T10 min
12	STD MSCUR_0.25 μ M	35	Sample N1_T120 min	58	Sample N3_T15 min
13	STD MSCUR_0.5 μ M	36	Sample N1_T0 min	59	Sample N3_T30 min
14	STD MSCUR_0.75 μ M	37	Sample N2_T0.5 min	60	Sample N3_T45 min
15	STD CDD_0.025 μ M	38	Sample N2_T1 min	61	Sample N3_T60 min
16	STD CDD_0.25 μ M	39	Sample N2_T2 min	62	Sample N3_T90 min
17	STD CDD_0.5 μ M	40	Sample N2_T3 min	63	Sample N3_T120 min

- HLS9

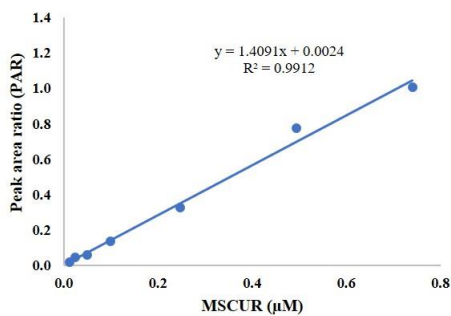
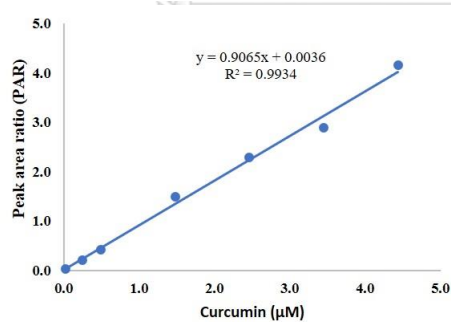
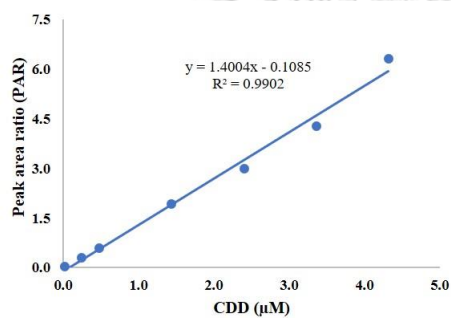
System suitability

System suitability parameters	Acceptance criteria	Result
Precision of retention time (n = 5)	RSD < 2%	
- Curcumin		0.070
- DMC		0.015
- MSCUR		0.030
- CDD		0.020
Precision of peak area (n = 5)	RSD < 2%	
- Curcumin		1.593
- DMC		1.587
- MSCUR		0.766
- CDD		1.074
Resolution (R)	$R \geq 1.5$	
- Curcumin		19.14
- DMC		22.22
- MSCUR		4.64
- CDD		2.52
Tailing factor (T)	$T \leq 2.0$	
- Curcumin		0.87
- DMC		1.07
- MSCUR		0.97
- CDD		1.00
Theoretical plates (N)	$N \geq 2000$	
- Curcumin		4418
- DMC		30607
- MSCUR		31563
- CDD		95544
Capacity factor (k')	$k' \geq 2.0$	
- Curcumin		28.59
- DMC		65.24
- MSCUR		72.61
- CDD		113.12

Visual inspection of IS response plot



Standard curve

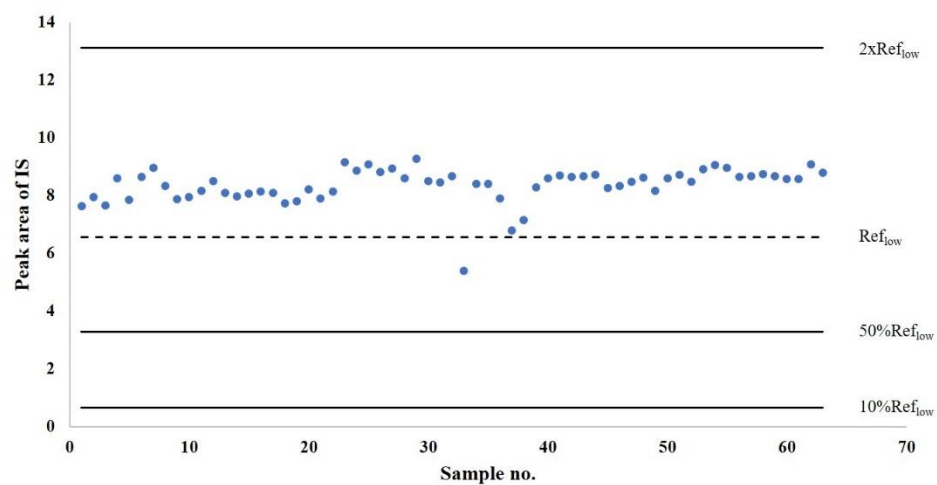


- MLS9

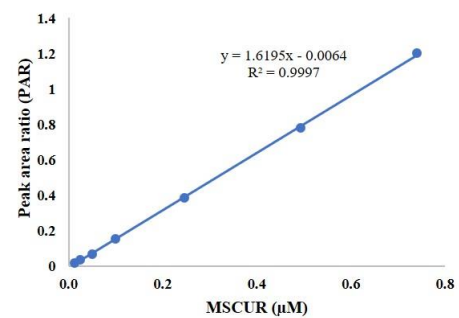
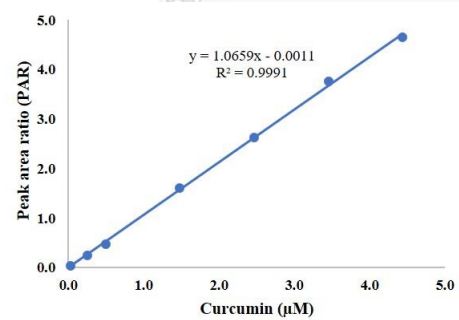
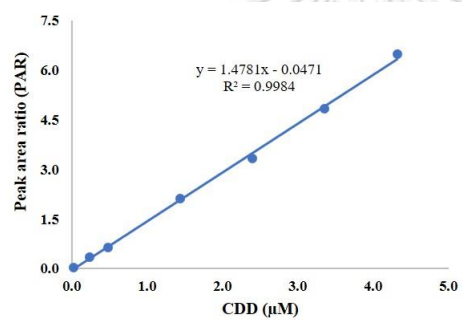
System suitability

System suitability parameters	Acceptance criteria	Result
Precision of retention time (n = 5)	RSD < 2%	
- Curcumin		0.078
- DMC		0.015
- MSCUR		0.032
- CDD		0.013
Precision of peak area (n = 5)	RSD < 2%	
- Curcumin		1.251
- DMC		1.097
- MSCUR		1.272
- CDD		1.647
Resolution (R)	$R \geq 1.5$	
- Curcumin		16.44
- DMC		19.03
- MSCUR		3.71
- CDD		1.88
Tailing factor (T)	$T \leq 2.0$	
- Curcumin		0.91
- DMC		1.01
- MSCUR		0.93
- CDD		1.29
Theoretical plates (N)	$N \geq 2000$	
- Curcumin		3413
- DMC		20132
- MSCUR		20464
- CDD		61325
Capacity factor (k')	$k' \geq 2.0$	
- Curcumin		28.06
- DMC		64.64
- MSCUR		71.87
- CDD		112.40

Visual inspection of IS response plot



Standard curve

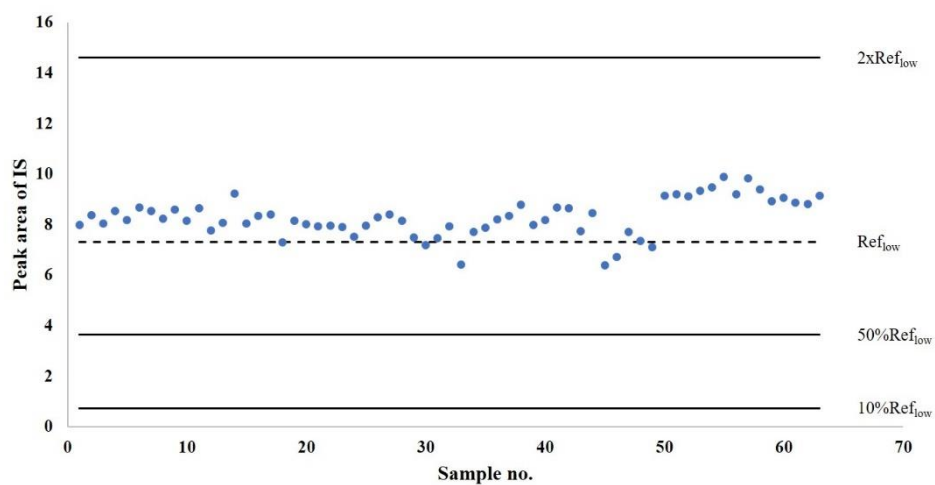


- DLS9

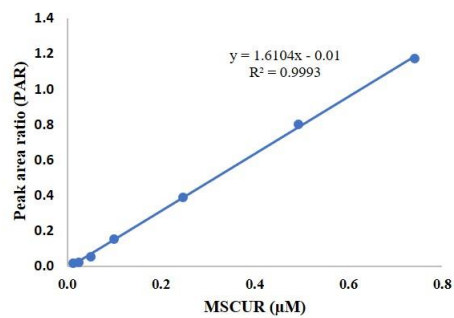
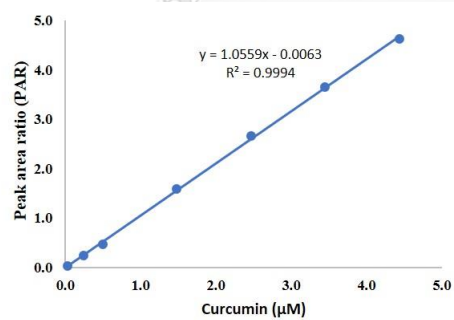
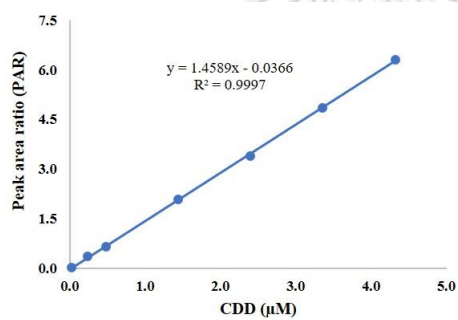
System suitability

System suitability parameters	Acceptance criteria	Result
Precision of retention time (n = 5)	RSD < 2%	
- Curcumin		0.218
- DMC		0.089
- MSCUR		0.099
- CDD		0.061
Precision of peak area (n = 5)	RSD < 2%	
- Curcumin		1.826
- DMC		1.403
- MSCUR		0.716
- CDD		1.254
Resolution (R)	$R \geq 1.5$	
- Curcumin		15.86
- DMC		16.51
- MSCUR		3.26
- CDD		1.66
Tailing factor (T)	$T \leq 2.0$	
- Curcumin		1.06
- DMC		1.41
- MSCUR		1.34
- CDD		1.33
Theoretical plates (N)	$N \geq 2000$	
- Curcumin		2612
- DMC		15328
- MSCUR		15918
- CDD		49382
Capacity factor (k')	$k' \geq 2.0$	
- Curcumin		28.43
- DMC		65.13
- MSCUR		72.43
- CDD		112.91

Visual inspection of IS response plot



Standard curve

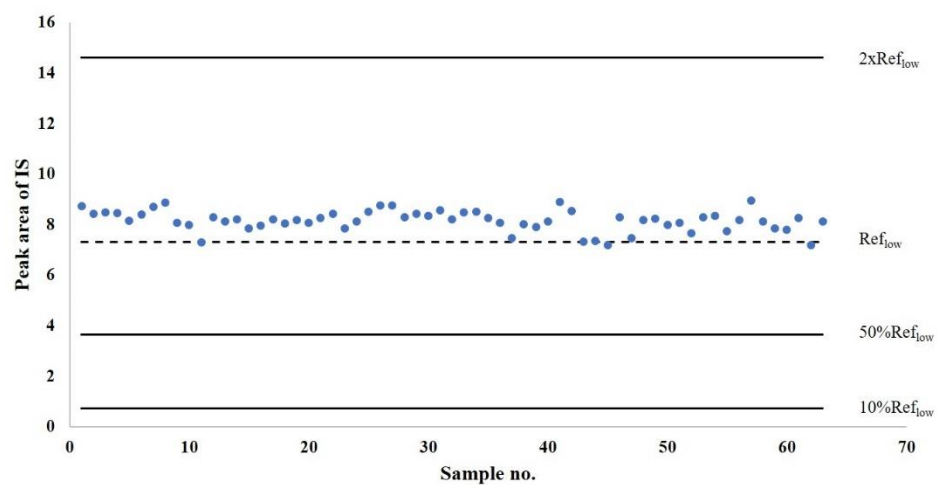


- RLS9

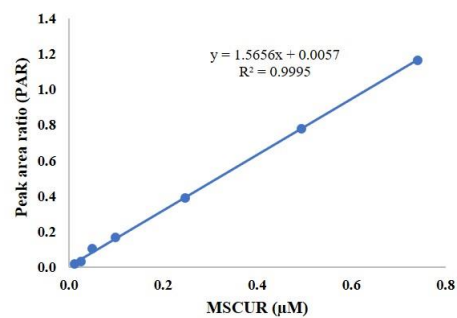
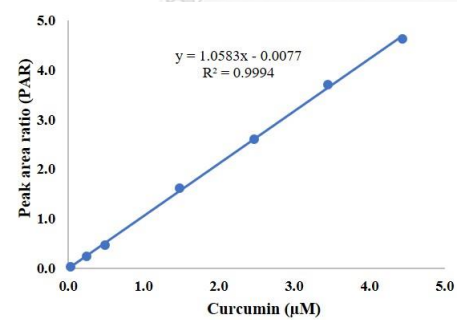
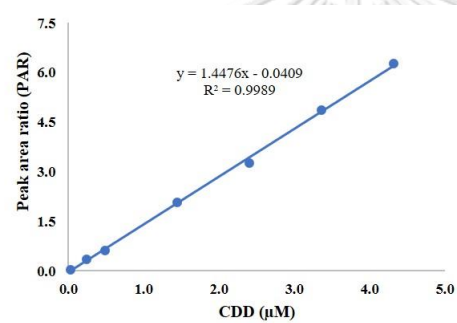
System suitability

System suitability parameters	Acceptance criteria	Result
Precision of retention time (n = 5)	RSD < 2%	
- Curcumin		0.124
- DMC		0.064
- MSCUR		0.074
- CDD		0.042
Precision of peak area (n = 5)	RSD < 2%	
- Curcumin		1.078
- DMC		1.150
- MSCUR		1.362
- CDD		1.972
Resolution (R)	$R \geq 1.5$	
- Curcumin		17.46
- DMC		21.18
- MSCUR		4.24
- CDD		2.27
Tailing factor (T)	$T \leq 2.0$	
- Curcumin		0.94
- DMC		1.13
- MSCUR		1.04
- CDD		1.08
Theoretical plates (N)	$N \geq 2000$	
- Curcumin		3977
- DMC		25979
- MSCUR		27775
- CDD		79431
Capacity factor (k')	$k' \geq 2.0$	
- Curcumin		27.87
- DMC		64.54
- MSCUR		71.69
- CDD		112.28

Visual inspection of IS response plot



Standard curve



2. Enzyme identification of CDD hydrolysis in LS9

2.1. Optimization of enzyme assay condition in LS9

Sequential injection

No.	Name	No.	Name
-	System suitability N1	47	Sample N2_LS9 0.05 mg/mL_T45 min
-	System suitability N2	48	Sample N2_LS9 0.05 mg/mL_T60 min
-	System suitability N3	49	Sample N1_LS9 0.02 mg/mL_T 0 min
-	System suitability N4	50	Sample N1_LS9 0.02 mg/mL_T 0.5 min
-	System suitability N5	51	Sample N1_LS9 0.02 mg/mL_T 1 min
1	Sample N1_LS9 0.1 mg/mL_T 0 min	52	Sample N1_LS9 0.02 mg/mL_T 2 min
2	Sample N1_LS9 0.1 mg/mL_T 0.5 min	53	Sample N1_LS9 0.02 mg/mL_T 3 min
3	Sample N1_LS9 0.1 mg/mL_T 1 min	54	Sample N1_LS9 0.02 mg/mL_T 4 min
4	Sample N1_LS9 0.1 mg/mL_T 2 min	55	Sample N1_LS9 0.02 mg/mL_T 5 min
5	Sample N1_LS9 0.1 mg/mL_T 3 min	56	Sample N1_LS9 0.02 mg/mL_T10 min
6	Sample N1_LS9 0.1 mg/mL_T 4 min	57	Sample N1_LS9 0.02 mg/mL_T15 min
7	Sample N1_LS9 0.1 mg/mL_T 5 min	58	Sample N1_LS9 0.02 mg/mL_T30 min
8	Sample N1_LS9 0.1 mg/mL_T10 min	59	Sample N1_LS9 0.02 mg/mL_T45 min
9	Sample N1_LS9 0.1 mg/mL_T15 min	60	Sample N1_LS9 0.02 mg/mL_T60 min
10	Sample N1_LS9 0.1 mg/mL_T30 min	61	Sample N2_LS9 0.02 mg/mL_T 0 min
11	Sample N1_LS9 0.1 mg/mL_T45 min	62	Sample N2_LS9 0.02 mg/mL_T 0.5 min
12	Sample N1_LS9 0.1 mg/mL_T60 min	63	Sample N2_LS9 0.02 mg/mL_T 1 min
13	Sample N2_LS9 0.1 mg/mL_T 0 min	64	Sample N2_LS9 0.02 mg/mL_T 2 min
14	Sample N2_LS9 0.1 mg/mL_T 0.5 min	65	Sample N2_LS9 0.02 mg/mL_T 3 min
15	Sample N2_LS9 0.1 mg/mL_T 1 min	66	Sample N2_LS9 0.02 mg/mL_T 4 min
16	Sample N2_LS9 0.1 mg/mL_T 2 min	67	Sample N2_LS9 0.02 mg/mL_T 5 min
17	Sample N2_LS9 0.1 mg/mL_T 3 min	68	Sample N2_LS9 0.02 mg/mL_T10 min
18	Sample N2_LS9 0.1 mg/mL_T 4 min	69	Sample N2_LS9 0.02 mg/mL_T15 min
19	Sample N2_LS9 0.1 mg/mL_T 5 min	70	Sample N2_LS9 0.02 mg/mL_T30 min
20	Sample N2_LS9 0.1 mg/mL_T10 min	71	Sample N2_LS9 0.02 mg/mL_T45 min
21	Sample N2_LS9 0.1 mg/mL_T15 min	72	Sample N2_LS9 0.02 mg/mL_T60 min
22	Sample N2_LS9 0.1 mg/mL_T30 min	73	Sample N1_LS9 0.01 mg/mL_T 0 min
23	Sample N2_LS9 0.1 mg/mL_T45 min	74	Sample N1_LS9 0.01 mg/mL_T 0.5 min
24	Sample N2_LS9 0.1 mg/mL_T60 min	75	Sample N1_LS9 0.01 mg/mL_T 1 min
25	Sample N1_LS9 0.05 mg/mL_T 0 min	76	Sample N1_LS9 0.01 mg/mL_T 2 min
26	Sample N1_LS9 0.05 mg/mL_T 0.5 min	77	Sample N1_LS9 0.01 mg/mL_T 3 min
27	Sample N1_LS9 0.05 mg/mL_T 1 min	78	Sample N1_LS9 0.01 mg/mL_T 4 min
28	Sample N1_LS9 0.05 mg/mL_T 2 min	79	Sample N1_LS9 0.01 mg/mL_T 5 min
29	Sample N1_LS9 0.05 mg/mL_T 3 min	80	Sample N1_LS9 0.01 mg/mL_T10 min
30	Sample N1_LS9 0.05 mg/mL_T 4 min	81	Sample N1_LS9 0.01 mg/mL_T15 min
31	Sample N1_LS9 0.05 mg/mL_T 5 min	82	Sample N1_LS9 0.01 mg/mL_T30 min
32	Sample N1_LS9 0.05 mg/mL_T 10 min	83	Sample N1_LS9 0.01 mg/mL_T45 min
33	Sample N1_LS9 0.05 mg/mL_T15 min	84	Sample N1_LS9 0.01 mg/mL_T60 min
34	Sample N1_LS9 0.05 mg/mL_T30 min	85	Sample N2_LS9 0.01 mg/mL_T 0 min

No.	Name	No.	Name
35	Sample N1_LS9 0.05 mg/mL_T45 min	86	Sample N2_LS9 0.01 mg/mL_T 0.5 min
36	Sample N1_LS9 0.05 mg/mL_T60 min	87	Sample N2_LS9 0.01 mg/mL_T 1 min
37	Sample N2_LS9 0.05 mg/mL_T 0 min	88	Sample N2_LS9 0.01 mg/mL_T 2 min
38	Sample N2_LS9 0.05 mg/mL_T 0.5 min	89	Sample N2_LS9 0.01 mg/mL_T 3 min
39	Sample N2_LS9 0.05 mg/mL_T 1 min	90	Sample N2_LS9 0.01 mg/mL_T 4 min
40	Sample N2_LS9 0.05 mg/mL_T 2 min	91	Sample N2_LS9 0.01 mg/mL_T 5 min
41	Sample N2_LS9 0.05 mg/mL_T 3 min	92	Sample N2_LS9 0.01 mg/mL_T10 min
42	Sample N2_LS9 0.05 mg/mL_T 4 min	93	Sample N2_LS9 0.01 mg/mL_T15 min
43	Sample N2_LS9 0.05 mg/mL_T 5 min	94	Sample N2_LS9 0.01 mg/mL_T30 min
44	Sample N2_LS9 0.05 mg/mL_T 10 min	95	Sample N2_LS9 0.01 mg/mL_T45 min
45	Sample N2_LS9 0.05 mg/mL_T15 min	96	Sample N2_LS9 0.01 mg/mL_T60 min
46	Sample N2_LS9 0.05 mg/mL_T30 min	-	-

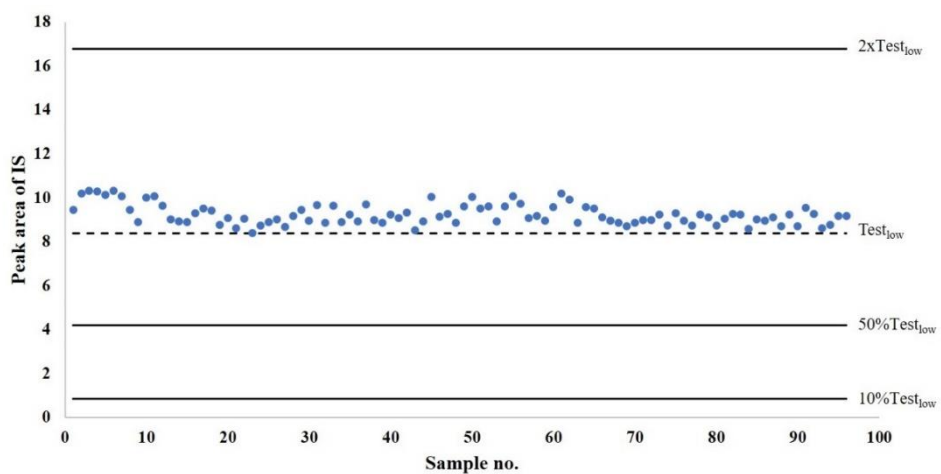


- HLS9

System suitability

System suitability parameters	Acceptance criteria	Result
Precision of retention time (n = 5)	RSD < 2%	
- Curcumin		0.146
- DMC		0.044
- MSCUR		0.052
- CDD		0.020
Precision of peak area (n = 5)	RSD < 2%	
- Curcumin		1.058
- DMC		0.858
- MSCUR		0.881
- CDD		0.664
Resolution (R)	$R \geq 1.5$	
- Curcumin		21.45
- DMC		22.57
- MSCUR		4.31
- CDD		2.13
Tailing factor (T)	$T \leq 2.0$	
- Curcumin		0.95
- DMC		1.10
- MSCUR		1.01
- CDD		0.81
Theoretical plates (N)	$N \geq 2000$	
- Curcumin		5126
- DMC		29828
- MSCUR		31586
- CDD		93037
Capacity factor (k')	$k' \geq 2.0$	
- Curcumin		29.31
- DMC		66.00
- MSCUR		72.95
- CDD		113.02

Visual inspection of IS response plot

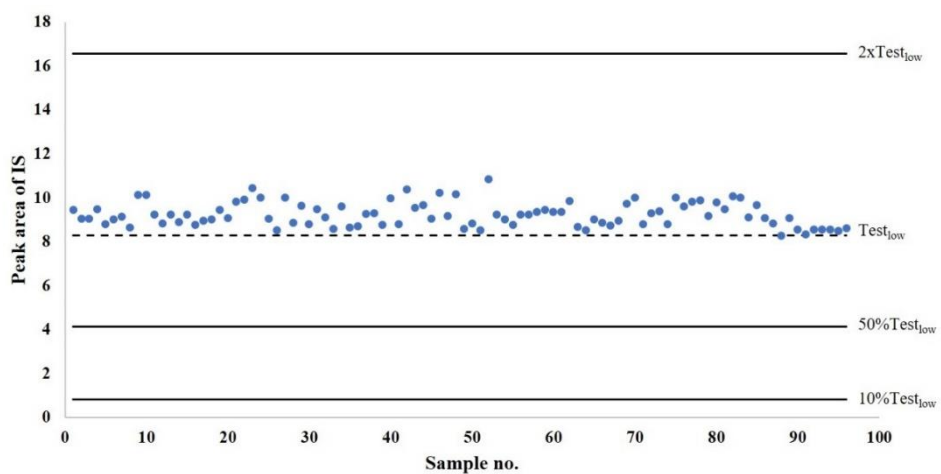


- MLS9

System suitability

System suitability parameters	Acceptance criteria	Result
Precision of retention time (n = 5)	RSD < 2%	
- Curcumin		0.676
- DMC		0.233
- MSCUR		0.232
- CDD		0.078
Precision of peak area (n = 5)	RSD < 2%	
- Curcumin		1.964
- DMC		0.833
- MSCUR		0.882
- CDD		1.415
Resolution (R)	$R \geq 1.5$	
- Curcumin		10.96
- DMC		23.65
- MSCUR		4.51
- CDD		2.47
Tailing factor (T)	$T \leq 2.0$	
- Curcumin		0.95
- DMC		1.04
- MSCUR		1.01
- CDD		1.02
Theoretical plates (N)	$N \geq 2000$	
- Curcumin		5745
- DMC		32298
- MSCUR		33372
- CDD		96000
Capacity factor (k')	$k' \geq 2.0$	
- Curcumin		29.46
- DMC		66.21
- MSCUR		73.25
- CDD		113.39

Visual inspection of IS response plot

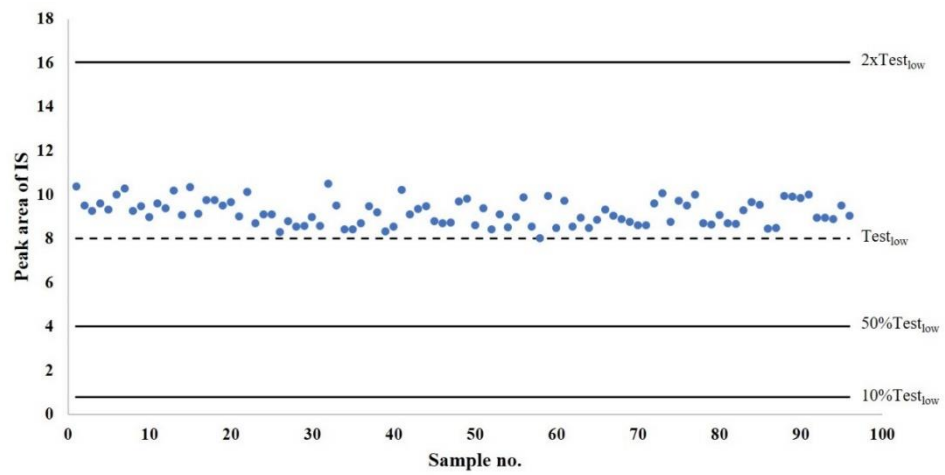


- DLS9

System suitability

System suitability parameters	Acceptance criteria	Result
Precision of retention time (n = 5)	RSD < 2%	
- Curcumin		0.321
- DMC		0.109
- MSCUR		0.119
- CDD		0.042
Precision of peak area (n = 5)	RSD < 2%	
- Curcumin		1.125
- DMC		1.301
- MSCUR		0.961
- CDD		1.231
Resolution (R)	$R \geq 1.5$	
- Curcumin		20.91
- DMC		23.24
- MSCUR		4.43
- CDD		2.42
Tailing factor (T)	$T \leq 2.0$	
- Curcumin		0.97
- DMC		1.06
- MSCUR		1.01
- CDD		1.01
Theoretical plates (N)	$N \geq 2000$	
- Curcumin		5482
- DMC		32507
- MSCUR		31418
- CDD		91417
Capacity factor (k')	$k' \geq 2.0$	
- Curcumin		29.69
- DMC		66.37
- MSCUR		73.42
- CDD		113.46

Visual inspection of IS response plot

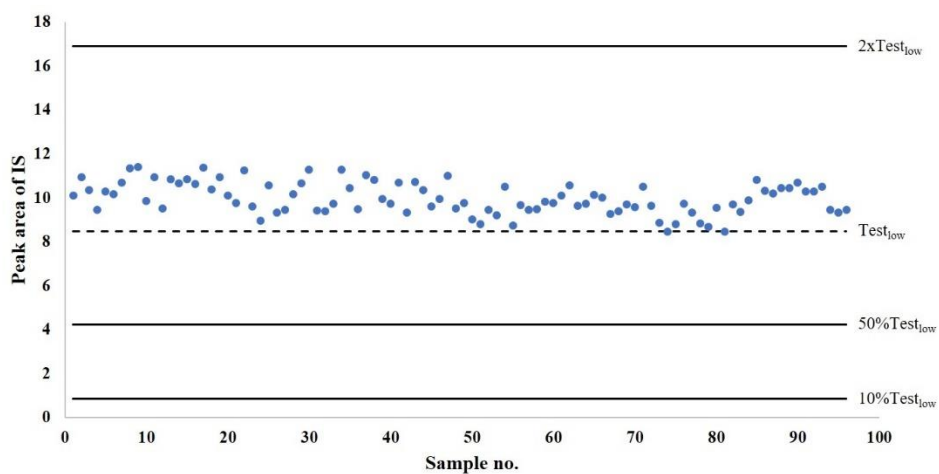


- RLS9

System suitability

System suitability parameters	Acceptance criteria	Result
Precision of retention time (n = 5)	RSD < 2%	
- Curcumin		0.188
- DMC		0.051
- MSCUR		0.056
- CDD		0.021
Precision of peak area (n = 5)	RSD < 2%	
- Curcumin		1.865
- DMC		1.129
- MSCUR		1.607
- CDD		0.841
Resolution (R)	$R \geq 1.5$	
- Curcumin		23.12
- DMC		23.42
- MSCUR		4.48
- CDD		2.45
Tailing factor (T)	$T \leq 2.0$	
- Curcumin		0.94
- DMC		1.06
- MSCUR		0.99
- CDD		1.00
Theoretical plates (N)	$N \geq 2000$	
- Curcumin		5809
- DMC		32656
- MSCUR		32451
- CDD		96234
Capacity factor (k')	$k' \geq 2.0$	
- Curcumin		29.96
- DMC		66.58
- MSCUR		73.65
- CDD		113.53

Visual inspection of IS response plot



2.2. Effect of esterase inhibitors on CDD hydrolysis in LS9

Sequential injection

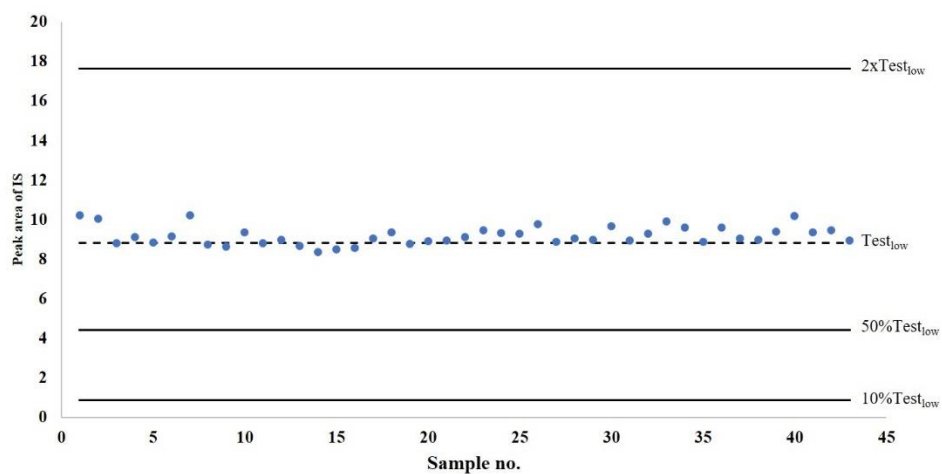
No.	Name	No.	Name
-	System suitability N1	20	Sample N1_Digitonin
-	System suitability N2	21	Sample N2_Digitonin
-	System suitability N3	22	Sample N3_Digitonin
-	System suitability N4	23	Sample N1_Loperamide
-	System suitability N5	24	Sample N2_Loperamide
-	Blank_LS9	25	Sample N3_Loperamide
1	STD Curcumin_0.025 μ M	26	Sample N1_PMSF
2	STD Curcumin_0.25 μ M	27	Sample N2_PMSF
3	STD Curcumin_0.50 μ M	28	Sample N3_PMSF
4	STD Curcumin_1.5 μ M	29	Sample N1_BW284c51
5	STD Curcumin_2.5 μ M	30	Sample N2_BW284c51
6	STD Curcumin_3.5 μ M	31	Sample N3_BW284c51
7	STD Curcumin_4.5 μ M	32	Sample N1_Iso-OMPA
8	Sample N1_Control	33	Sample N2_Iso-OMPA
9	Sample N2_Control	34	Sample N3_Iso-OMPA
10	Sample N3_Control	35	Sample N1_PCMB
11	Sample N1_Non-enzymatic control	36	Sample N2_PCMB
12	Sample N2_Non-enzymatic control	37	Sample N3_PCMB
13	Sample N3_Non-enzymatic control	38	Sample N1_DTNB
14	Sample N1_Non-solvent control	39	Sample N2_DTNB
15	Sample N2_Non-solvent control	40	Sample N3_DTNB
16	Sample N3_Non-solvent control	41	Sample N1_EDTA
17	Sample N1_BNPP	42	Sample N2_EDTA
18	Sample N2_BNPP	43	Sample N3_EDTA
19	Sample N3_BNPP	-	-

- HLS9

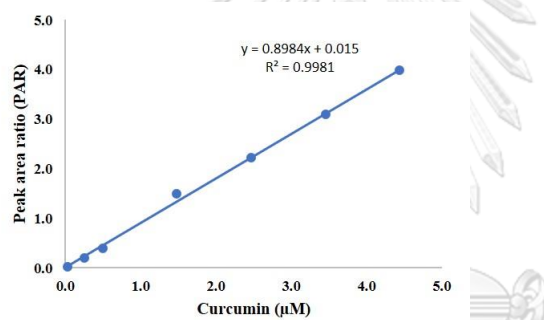
System suitability

System suitability parameters	Acceptance criteria	Result
Precision of retention time (n = 5)	RSD < 2%	
- Curcumin		0.054
- DMC		0.012
- MSCUR		0.030
- CDD		0.008
Precision of peak area (n = 5)	RSD < 2%	
- Curcumin		1.199
- DMC		0.973
- MSCUR		1.442
- CDD		1.137
Resolution (R)	$R \geq 1.5$	
- Curcumin		20.45
- DMC		22.64
- MSCUR		4.36
- CDD		2.36
Tailing factor (T)	$T \leq 2.0$	
- Curcumin		0.97
- DMC		1.10
- MSCUR		1.03
- CDD		1.02
Theoretical plates (N)	$N \geq 2000$	
- Curcumin		5189
- DMC		29860
- MSCUR		32710
- CDD		93096
Capacity factor (k')	$k' \geq 2.0$	
- Curcumin		29.34
- DMC		66.00
- MSCUR		72.96
- CDD		113.03

Visual inspection of IS response plot



Standard curve



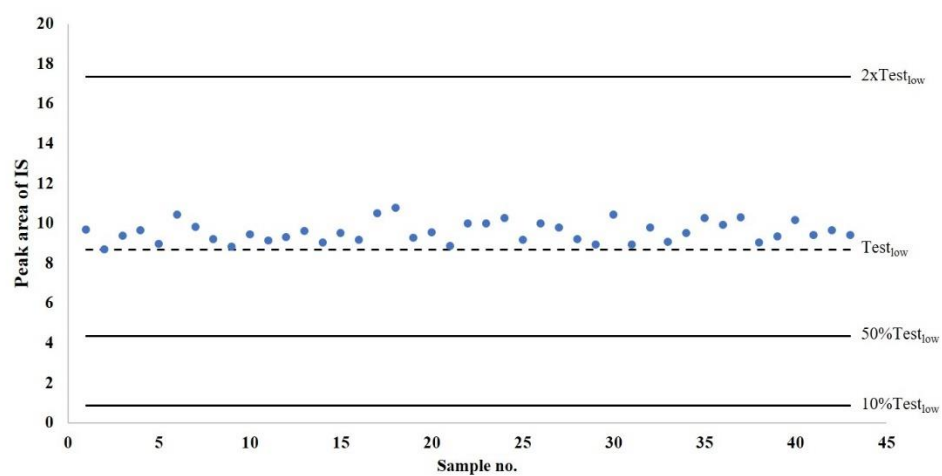
จุฬาลงกรณ์มหาวิทยาลัย
CHULALONGKORN UNIVERSITY

- MLS9

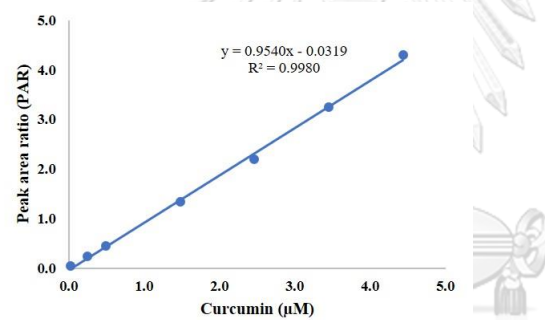
System suitability

System suitability parameters	Acceptance criteria	Result
Precision of retention time (n = 5)	RSD < 2%	
- Curcumin		0.097
- DMC		0.053
- MSCUR		0.057
- CDD		0.028
Precision of peak area (n = 5)	RSD < 2%	
- Curcumin		1.688
- DMC		1.045
- MSCUR		0.956
- CDD		1.406
Resolution (R)	$R \geq 1.5$	
- Curcumin		21.51
- DMC		22.78
- MSCUR		4.43
- CDD		25.57
Tailing factor (T)	$T \leq 2.0$	
- Curcumin		0.92
- DMC		1.05
- MSCUR		1.01
- CDD		0.99
Theoretical plates (N)	$N \geq 2000$	
- Curcumin		5353
- DMC		30904
- MSCUR		33461
- CDD		93524
Capacity factor (k')	$k' \geq 2.0$	
- Curcumin		29.69
- DMC		66.33
- MSCUR		73.34
- CDD		113.32

Visual inspection of IS response plot



Standard curve



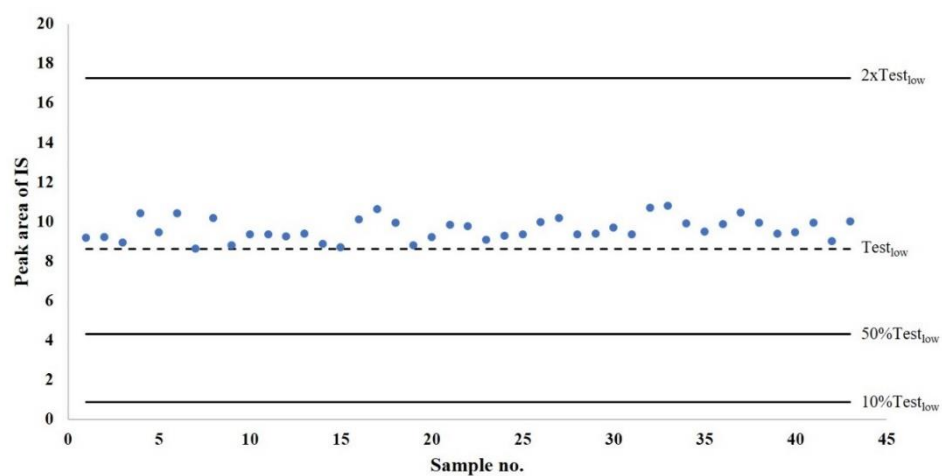
จุฬาลงกรณ์มหาวิทยาลัย
CHULALONGKORN UNIVERSITY

- DLS9

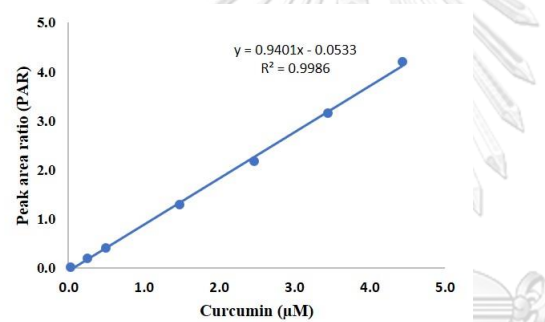
System suitability

System suitability parameters	Acceptance criteria	Result
Precision of retention time (n = 5)	RSD < 2%	
- Curcumin		0.062
- DMC		0.031
- MSCUR		0.033
- CDD		0.023
Precision of peak area (n = 5)	RSD < 2%	
- Curcumin		1.782
- DMC		0.700
- MSCUR		0.731
- CDD		0.439
Resolution (R)	$R \geq 1.5$	22.06
- Curcumin		22.61
- DMC		4.37
- MSCUR		25.46
- CDD		
Tailing factor (T)	$T \leq 2.0$	
- Curcumin		0.94
- DMC		1.04
- MSCUR		1.00
- CDD		
Theoretical plates (N)	$N \geq 2000$	
- Curcumin		5199
- DMC		30786
- MSCUR		32104
- CDD		95693
Capacity factor (k')	$k' \geq 2.0$	
- Curcumin		29.65
- DMC		66.26
- MSCUR		73.24
- CDD		113.21

Visual inspection of IS response plot



Standard curve



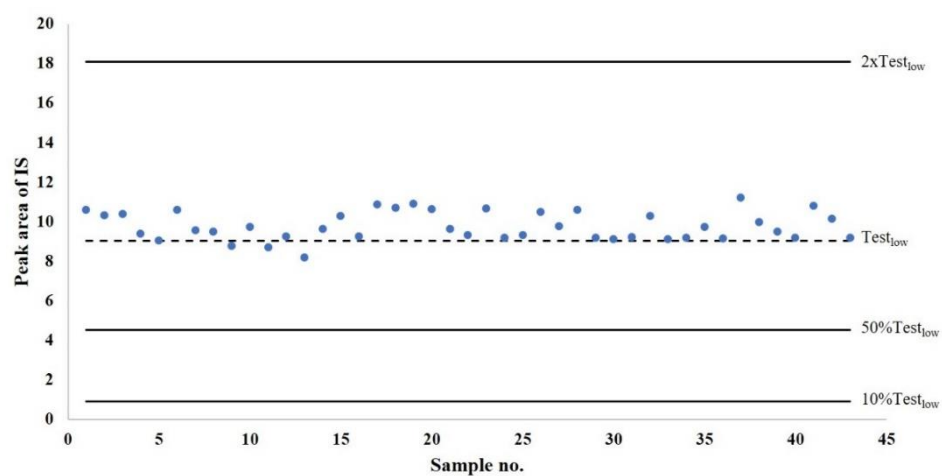
จุฬาลงกรณ์มหาวิทยาลัย
CHULALONGKORN UNIVERSITY

- RLS9

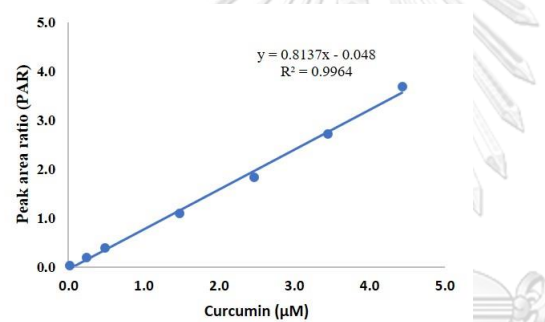
System suitability

System suitability parameters	Acceptance criteria	Result
Precision of retention time (n = 5)	RSD < 2%	
- Curcumin		0.067
- DMC		0.049
- MSCUR		0.047
- CDD		0.012
Precision of peak area (n = 5)	RSD < 2%	
- Curcumin		1.281
- DMC		1.303
- MSCUR		1.003
- CDD		0.819
Resolution (R)	$R \geq 1.5$	
- Curcumin		20.46
- DMC		22.62
- MSCUR		4.44
- CDD		25.85
Tailing factor (T)	$T \leq 2.0$	
- Curcumin		0.94
- DMC		1.06
- MSCUR		0.98
- CDD		0.97
Theoretical plates (N)	$N \geq 2000$	
- Curcumin		5229
- DMC		30936
- MSCUR		33493
- CDD		98444
Capacity factor (k')	$k' \geq 2.0$	
- Curcumin		29.76
- DMC		66.40
- MSCUR		73.42
- CDD		113.34

Visual inspection of IS response plot



Standard curve



VITA

NAME Ponsiree Jithavech

DATE OF BIRTH 25 May 1976

PLACE OF BIRTH Bangkok

INSTITUTIONS ATTENDED 2002-2005 M.Sc. (Pharm) in Pharmaceuticals,
Chulalongkorn University, Bangkok, Thailand.
1994-1999 B.Sc. in Pharmacy, Chulalongkorn University,
Bangkok, Thailand.

HOME ADDRESS 125/8 Soi Suwansawat, Rama 4 Road, Thung Maha Mek,
Sathon, Bangkok, 10120.

PUBLICATION Jithavech P, Ratnatilaka Na Bhuket P, Supasena W, Qiu G,
Ye S, Wong TW and Rojsitthisak P. In vitro hepatic
metabolism of curcumin diethyl disuccinate by liver S9
from different animal species. Front Pharmacol (In Press).

AWARD RECEIVED

1. Outstanding Poster Presentation: The 5th International
Conference on Pharmaceuticals, Nutraceuticals and
Cosmetic Science, Bangkok, Thailand, August 3-4. Title:
Metabolomics on antioxidant effect of curcumin in HepG2
cells induced oxidative stress.
2. Outstanding Poster Presentation: The 24th International
Annual Meeting in Pharmaceutical Sciences, Bangkok,
Thailand, December 12. Title: Sensitive and specific
method for the determination of meropenem in human
plasma using high-performance liquid chromatography.